# Progress Toward Elucidating the Mechanisms of Energy Transduction in Cytochrome c Oxidase

Thesis by

David Francis Blair

In Partial Fulfillment of the Requirements

for the Degree of

Doctor of Philosophy

California Institute of Technology

Pasadena, California

1986

(Submitted September 10, 1985)

There is a theory which states that if ever anyone discovers exactly what the oxidase is for and why it is here, it will instantly disappear and be replaced by something even more bizarre and inexplicable.

There is another theory which states that this has already happened.

-Adapted (with apologies) from Douglas Adams' The Restaurant at the End of the Universe

"The pump don't work 'cuz the vandals took the handle."

-Bob Dylan, "Subterranean Homesick Blues"

ACKNOWLEDGEMENTS

Interactions are important to this thesis, both with respect to its content and its creation. Without a great deal of interaction among many people, most of the work which it contains would have been impossible. It is a pleasure to thank the friends whose contributions of ideas, enthusiasm, and muscle have been equal to my own. These include especially Jeff Gelles, Hsin Wang, Steve Witt, and Walther Ellis. I am very grateful to Hsin and Walther for their determination in finishing so many graveyard shifts. Through hundreds of "equilibrium vigils," the three of us have achieved an enduring esprit de corpse.

I would like to thank Harry Gray for fostering the interaction between our groups which permitted this research to be carried out, and for his patience in awaiting its fruits. I would also like to thank the members of his group, who have been very helpful and generous with their time and their expertise.

It could be unpleasant working for six years at a small desk in a clammy windowless basement office. For making it otherwise, I thank Craig, Joel, Joey, Larry, Utpal, Tim, and the many visitors who have passed through the lab, including Tan, Jin, Maggie, Wilson, Bob, and anyone else I may have forgotten. I hope we all have windows in future jobs.

I would like to thank Diana Barnes for teaching me how to swim and for pointing out the importance of goggles.

My family has been loving and supporting throughout my life, and I thank them. They have demonstrated, by example, the value of dedication. At the same time, they have always encouraged curiosity and a questioning attitude, which must have taken all of their patience at times. When they read this, I hope they remember the billion questions that they answered when I was a child.

I would like to thank Pat for her encouragement and advice before and during the preparation of this thesis. I hope that I will be as helpful to her when her time comes.

Finally, I would like to thank Sunney, who has likewise allowed curiosity a free reign to set new directions, while retaining a sound physical chemical perspective. I would also like to thank him for his friendship and counsel through years that have witnessed many changes for us both.

ABSTRACT

The exothermic transfer of four electrons from cytochrome c to dioxygen is catalyzed in eucaryotes by mitochondrial cytochrome c oxidase. A large fraction of the energy made available from these electron transfers is conserved in the form of a proton electrochemical gradient across the mitochondrial inner membrane. Two energy-conserving mechanisms operate in cytochrome c oxidase: First, the electron transfers to dioxygen are themselves electrogenic, since the electrons originate from the outer side of the membrane while the protons required to produce water originate from the inner side. Second, the electron transfers are coupled to the active transport across the membrane of additional protons, perhaps as many as one for every electron transferred. In this work, investigations which are intended to contribute to a detailed understanding of the mechanisms of energy transduction in cytochrome c oxidase are described.

Cytochrome c oxidase performs its catalytic functions with the assistance of four metal ion sites. The redox thermodynamic properties of three of these sites have been extensively characterized by spectroelectrochemical methods. A fairly complex interactive scheme involving all four metal centers is required to account for the observed thermodynamic behavior. Via measurements of reduction potential temperature dependences, it is found that the standard entropies of reduction of the two sites which have been suggested to play a role in proton pumping (cytochrome a and $Cu_A$) are unusually large and negative, suggesting that a substantial protein-ordering conformational change accompanies their reduction. The reduction potential of cytochrome a is only moderately pH-dependent, indicating that its reduction is not stoichiometrically coupled to proton uptake.

The energy made available for transduction by the oxidase comes primarily from the exothermic transfer of electrons from the metal centers to dioxygen. The mechanism of these electron transfers has been examined in a detailed kinetic study of the reaction of the

enzyme with dioxygen at low temperatures. Two different reaction intermediates have been found in which dioxygen is reduced to the same, namely, the three-electron level. The conversion between these two intermediates is rather highly activated but is promoted by entropic factors. It is suggested that this step corresponds to the breaking of the oxygen-oxygen bond. Earlier suggestions that electrons may be transferred via multiple pathways through the enzyme have been confirmed and extended. An examinination of the reaction of partially reduced samples of the oxidase with dioxygen indicates that the rates of internal electron transfer within the oxidase are different at different steps in dioxygen reduction. Multiple pathways and step-dependent rates are expected to have important implications for the mechanisms of energy conservation by the oxidase.

The steady-state kinetics of a simple model for redox-linked proton pumping has been examined in a final chapter. In this analysis, special emphasis was given to the importance of controlling electron flows through the transducing site. The consideration of electron flows results in some novel conclusions which assist in rationalizing the results of the redox thermodynamic study. It is expected that the analysis should also contribute to the design and interpretation of further experiments intended to reveal the mechanisms of proton pumping.

# TABLE OF CONTENTS

LIST OF TABLES AND FIGURES

CHAPTER II

CHAPTER III

CHAPTER IV

CHAPTER V.

CHAPTER VI.

# CHAPTER I. INTRODUCTION

Mitochondrial cytochrome *c* oxidase is found in eucaryotic organisms as diverse as wheat and the roseate spoonbill, and is vital to them all. The enzyme, which is situated across the mitochondrial inner membrane, catalyzes the terminal electron transfer steps in respiration and thus plays a crucial role in the conversion of food into adenosine triphosphate (ATP), the energy currency of the cell.

The overall reaction catalyzed by cytochrome oxidase is given by the equation:

$$4\ e^-_C + 4\ H^+_M + n\ H^+_M + O_2 \longrightarrow 2\ H_2O + n\ H^+_C\ . \quad (1)$$

In this equation, the subscripts M and C denote the mitochondrial matrix (the inside) and the mitochondrial cytosol (the outside), respectively. The electrons are derived from ferrocytochrome *c* in the cytosol and the protons from the matrix, so the electron transfers to dioxygen are electrogenic; i.e., they create an electrical potential across the hydrophobic barrier of the membrane in which the enzyme is imbedded. Additionally, the enzyme catalyzes the electrogenic active transport of n protons from the matrix to the cytosol (the precise value of n is currently debated, but under ideal conditions approaches four). The $O_2$ in equation 1 accounts for most of the oxygen consumed in the biosphere, and the membrane potential-generating steps for a large fraction of all biological energy transduction. The details of the mechanisms of energy transduction by cytochrome oxidase, as well as by other members of the respiratory chain, are unsolved problems of central importance in biochemistry.

Since the oxidase was discovered almost fifty years ago (1), its study has engendered thousands of scientific publications. As will be detailed in the following chapters, the enzyme performs its catalytic functions with the assistance of four metal ions coordinated to the protein. These are two iron ions in heme A porphyrins, called cytochrome *a* and cytochrome $a_3$, and two

copper ions called $Cu_A$ and $Cu_B$. The last decade has witnessed steady progress toward understanding the structures of these metal sites and deducing structure-function relationships (2-4). A number of kinetic studies have partially clarified the mechanisms of dioxygen reduction and of the inter- and intramolecular electron transfers. Current proposals regarding the mechanism of active proton transport ("proton pumping") are at best speculative, since most experiments to date have been intended only to demonstrate its occurrence conclusively and to measure its stoichiometry, usually under artificial conditions (5). In the near future, most mechanistic studies of the enzyme are likely to be directed toward understanding proton pumping.

In this thesis, the mechanisms of electron transfer and dioxygen reduction by cytochrome oxidase are examined from a physical chemical point of view, using absorbance and electron paramagnetic resonance (EPR) spectroscopies as probes of the metal centers. Most of the studies described are intended to provide a sound framework in which to conduct future investigations of the mechanisms of proton pumping, and most of the results will be discussed from this point of view.

Detailed knowledge of the redox thermodynamic properties of the metal sites of cytochrome oxidase is prerequisite to understanding its mechanisms of energy transduction. Toward this goal, the redox thermodynamic properties of three of the metal centers have been extensively characterized. Via measurements of the temperature dependences of reduction potentials, it has been found that the sites suggested to be involved in proton pumping exhibit unprecedentedly large and negative standard entropies of reduction. At the same time, their reduction potentials exhibit unexpectedly small pH dependences which indicate that protonation is not stoichiometrically coupled to reduction of the sites. Both of these observations have implications for the mechanism of proton pumping by the enzyme. The latter is especially important, because it is not readily rationalized within current frameworks for understanding proton pumping.

The free energy made available for transduction by cytochrome *c* oxidase comes primarily from exothermic electron transfers from the oxidase metal centers to dioxygen. In order to better understand these electron transfers, the mechanism of the reaction of the enzyme with dioxygen has been studied at low temperatures, where individual electron transfer steps are readily resolved. The results of this study indicate that electrons may be transferred through the enzyme via more than one pathway, with important consequences for its mechanisms of energy transduction. Additionally, this investigation has furnished new and detailed insights into the basis of the enzyme's catalytic potency.

A recurrent theme of this thesis, and the central topic of Chapter II, is the occurrence of various interactions among the four metal sites. Optical, magnetic, and thermodynamic site-site interactions have been demonstrated. The thermodynamically manifested interactions have been accorded the most consideration, since they are expected to influence function significantly. The interaction scheme which emerges from the present studies is fairly complex, and emphasizes the need to approach mechanistic questions from an integrated point of view which recognizes these interactive properties. At the same time, it is found that several of the observed interactions may be understood in terms of a conceptually simple model which assigns a central role to cytochrome *a*.

In a concluding chapter, a formal kinetic analysis of a simple model for redox-linked proton pumping is presented. Special emphasis is given to the importance of controlling electron flows so that the energy available from electron transfers is conserved rather than dissipated as heat. A consideration of the importance of controlled electron flow furnishes a natural explanation of some otherwise problematic results of earlier chapters. This analysis is intended primarily as a background to assist in the design and in the quantitative interpretation of future studies of proton pumping, but it should also be helpful in understanding other biological transducers with which a formal analogy can be made.

REFERENCES

1. Keilin, D., and Hartree, E.F. (1939). Proc. R. Soc. London, Ser. B 127, 167-191.

2. Wikstrom, M., Krab, K., & Saraste, M. (1981). Cytochrome Oxidase: A Synthesis, Academic Press, London.

3. Blair, D.F., Martin, C.T., Gelles, J., Wang, H., Brudvig, G.W., Stevens, T.H., and Chan, S.I. (1983). Chemica Scripta 21, 43-53.

4. Malmstrom, B.G. (1980). In Metal Ion Activation of Dioxygen (Spiro, T.G., Ed.), pp. 181-207, Wiley, New York.

5. Wikstrom, M., and Krab, K. (1979). Biochim. Biophys. Acta 549, 177-222.

# CHAPTER II. SPECTROSCOPIC INTERACTIONS AMONG THE METAL SITES OF CYTOCHROME *c* OXIDASE

## INTRODUCTION

In its role as the terminal electron acceptor in mitochondrial respiration, cytochrome *c* oxidase catalyzes two reactions of central metabolic importance: the four electron reduction of dioxygen to water, using electrons donated by ferrocytochrome *c* on the cytosol (outer) site of the inner mitochondrial membrane and protons derived from the matrix (inner) side, and the active transport of protons from the matrix to the cytosol. These two reactions are linked, so that the free energy made available in the electron transfers is used to drive the endergonic transport of protons against a proton electrochemical gradient across the mitochondrial inner membrane. Both of the cytochrome *c* oxidase-catalyzed reactions contribute to the maintenance of this gradient, which is used by another mitochondrial membrane protein, the ATP synthase, to drive the synthesis of ATP (1).

Cytochrome oxidase employs four metal ion sites to accomplish its complex catalytic functions: two iron ions contained in the heme A porphyrin, called cytochromes *a* and $a_3$, and two copper ions called copper A ($Cu_A$) and copper B ($Cu_B$). Cytochrome *a* and $Cu_A$ are able to accept electrons from cytochrome *c* rapidly, and subsequently they transfer these electrons to cytochrome $a_3$ and $Cu_B$, which are situated close to each other and together constitute the site of dioxygen reduction (for recent reviews, see Refs. 2-4).

In recent years, impressive progress has been made toward understanding the structures of the four metal centers. A variety of spectroscopic methods, notably magnetic resonance (5), MCD (6,7), and resonance Raman (8) have been used to study the structures of the four metal sites. The axial ligands to cytochrome *a* are almost certainly two histidyl imidazoles (9,10), and cytochrome *a* is low-spin in both the fully reduced and fully oxidized states of the enzyme. Cytochrome $a_3$ is axially coordinated by one histidyl

imidazole (11) and is high-spin in both the fully reduced and fully oxidized resting enzyme. The second axial position of cytochrome $a_3$ is probably occupied by a water molecule or hydroxide ion in the resting enzyme (12), although cysteinyl thiolate has also been suggested (13). During turnover of the enzyme the iron of cytochrome $\underline{a}_3$ is presumably coordinated by intermediates of dioxygen reduction. $Cu_A$ is coordinated by at least one cysteinyl thiolate and one histidyl imidazole (5) and in the oxidized state exhibits EPR and ENDOR properties which indicate a substantial delocalization of its unpaired spin onto coordinated sulfur, and perhaps coordination by a second cysteinyl thiolate (14). $Cu_B$ exhibits no EPR signals under most conditions, owing to magnetic coupling between $Cu_B$ and its nearby neighbor cytochrome $\underline{a}_3$ (15), and no strong optical or near-infrared absorbances. The structure of $Cu_B$ is presently the least well understood among the metal centers.

Absorbance spectrophotometry was the earliest (16), and is still the most routinely applied spectroscopic probe of cytochrome oxidase. Both cytochromes $\underline{a}$ and $\underline{a}_3$ exhibit strong visible and near-ultraviolet absorbances associated with electronic transitions within their hemes; these absorbances are typical of hemoproteins but are somewhat red-shifted relative to most by the presence of a formyl group on the periphery of the heme A porphyrin. Absorbance spectra of reduced and oxidized cytochrome oxidase in the 700 nm-350 nm range are shown in Figure 1. The strong visible absorbances give the enzyme an attractive green color in its reduced state and a drab brown-green color in its oxidized state. The large spectral changes which accompany reduction of the enzyme have been used to monitor the oxidation states of the cytochromes in several potentiometric (17,18), oxidative (19,20), and reductive (21,22) titrations. The oxidase also has a moderately strong near-infrared absorbance centered near 830 nm (23). The precise origin of this band has been debated, but most workers agree that it is due to the copper(s) rather than to the cytochromes. This absorbance has also been used to monitor electrochemical titrations of the enzyme.

**Figure 1. Absorbance spectra of 15 μM cytochrome c oxidase. Trace A, ascorbate reduced; trace B, native oxidized; trace C, reduced minus oxidized trace A minus trace B).**

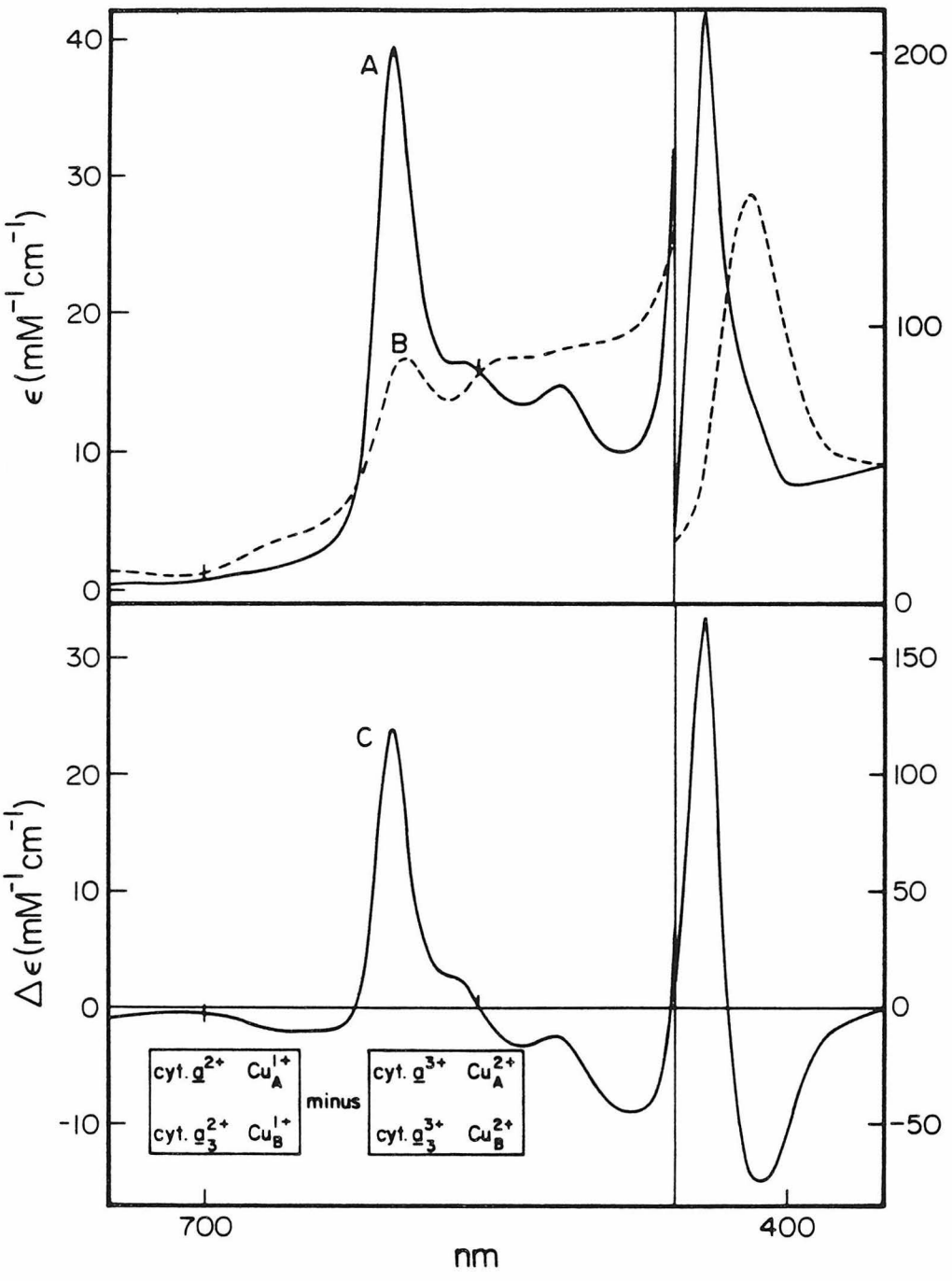
A
B
C
ε (mM⁻¹cm⁻¹)
Δε (mM⁻¹cm⁻¹)
nm
700
400
cyt. a2+ CuA1+
cyt. a32+ CuB1+
minus
cyt. a3+ CuA2+
cyt. a33+ CuB2+

In order to interpret spectrophotometrically monitored electrochemical titrations of the oxidase, it is necessary to know the extent to which each titrating site contributes to the various absorbance changes. Estimates of the individual cytochrome contributions to the strong visible and near-UV absorbances have been made in numerous studies based upon ligand inhibition of cytochrome $\underline{a}_3$ (16,24-26). Cytochrome $\underline{a}_3$ binds exogenous ligands such as cyanide, formate, carbon monoxide (CO), and nitric oxide (NO), while cytochrome $\underline{a}$ does not (27). These ligands may be used to stabilize cytochrome $\underline{a}_3$ in either its ferrous state (using CO or NO) or ferric state (using cyanide or formate, for example), since they bind preferentially to one or the other. Oxidoreduction of cytochrome $\underline{a}$ in these liganded species allows reduced minus oxidized difference spectra of cytochrome $\underline{a}$ to be recorded, presumably in the absence of contributions from cytochrome $\underline{a}_3$. The consensus from these studies is that cytochrome $\underline{a}$ is responsible for most (70-80%) of the absorbance changes in the band near 600 nm, called the alpha band, and somewhat less than 50% of the absorbance changes near 443 nm, called the Soret band.

The individual contributions of the copper ions to the near-infrared absorbance near 830 nm have been estimated using an analogous ligand-inhibition method in conjunction with reflectance spectrophotometry at low temperatures (28). The results of this study suggested that the two copper ions make comparable contributions to the 830 nm absorbance. However, the correlation of optical and EPR spectra in a large number of samples led Beinert et al. (29) to suggest that only $Cu_A$ contributes significantly to this band.

Spectrum deconvolution methods which are based upon ligand inhibition rely on the implicit assumption that the different metal sites do not interact so that the spectroscopic properties of one site are influenced by the ligation or oxidation state of the others. Because of the possibility of such spectroscopically manifested interactions, the interpretation of spectroelectrochemical titrations is ambiguous: The same data may be interpreted either in

terms of spectroscopic interactions (30) or in terms of thermodynamic interactions which cause the electron affinity of one site to be influenced by the oxidation state of the others (31).

A systematic examination of the effects of the ligation and oxidation state of the cytochrome $\underline{a}_3/Cu_B$ site upon the spectroscopic properties of the cytochrome $\underline{a}$ and $Cu_A$ sites would provide a more solid foundation for the interpretation of spectroelectrochemical titrations. As a prelude to spectroelectrochemical studies of the oxidase, such a systematic examination has been carried out. Four different methods based upon ligand inhibition of cytochrome $\underline{a}_3$ have been used to estimate the reduced-minus-oxidized absorbance difference spectrum of cytochrome $\underline{a}$. Cytochrome $\underline{a}_3$ has been stabilized in the ferric low-spin state with cyanide, the ferric high-spin state with formate, and the ferrous low-spin state with NO. Two different partially reduced complexes of NO were used to obtain reference spectra in which cytochrome $\underline{a}$ was oxidized; in one of these complexes only cytochrome $\underline{a}_3$ was reduced while in the other both cytochrome $\underline{a}_3$ and $Cu_B$ were reduced. The four methods yield somewhat different results, especially with respect to the intensity of the reduced minus oxidized alpha band of cytochrome $\underline{a}$ near 604 nm. Comparison of the two different methods employing NO indicates that the oxidation state of $Cu_B$ can influence the absorbance properties of the nearby cytochrome $\underline{a}_3$. Spectroscopically manifested interaction between the '$\underline{a}$ sites' (cytochrome $\underline{a}$ and $Cu_A$) and the '$\underline{a}_3$ sites' (cytochrome $\underline{a}_3$ and $Cu_B$) takes place but is evidently not very strong, especially at the wavelengths typically used in spectroelectrochemical titrations.

A similar study was carried out on the near-infrared absorbance of the enzyme. The results of two different deconvolution methods, employing either formate or CO, are presented; the results indicate that the spin- and oxidation state of the cytochrome $\underline{a}_3/Cu_B$ site may be changed without significantly influencing the near-infrared absorbance. A comparison of the near-infrared difference spectra obtained using inhibitors with that obtained from the native enzyme

indicates that the absorbance near 830 nm is due to $Cu_A$, in agreement with the conclusions of Beinert et al. (29).

Besides those manifested in the optical properties, other spectroscopic interactions among the oxidase metal centers have been proposed previously. Magnetic interaction between $Cu_A$ and other paramagnetic sites in the protein has been suggested in order to explain the unusually rapid relaxation of the electron spin on $Cu_A$ (32) or its EPR signal intensity, which is somewhat lower than expected (33). In a further elaboration of the theme of site-site interactions, this possibility has been explored in partially reduced CO-inhibited species of the enzyme. In these enzyme species, the oxidation and spin states of the other metal centers were manipulated while the EPR properties of $Cu_A$ were monitored. The results indicate that $Cu_A$ participates in an interaction with cytochrome *a* which influences its electron spin relaxation, and that reduction of cytochrome *a* causes a small structural change at the $Cu_A$ site. Using the assumption that the $Cu_A$-cytochrome *a* interaction is magnetic dipolar in nature, a rough estimate of the distance between cytochrome *a* and $Cu_A$ is presented.

## MATERIALS AND METHODS

Enzyme and Inhibitor Complexes. Cytochrome c oxidase was isolated by the method of Hartzell & Beinert (34). The enzyme concentration was determined by using a reduced minus oxidized extinction coefficient of 24 $mM^{-1}$ $cm^{-1}$ at 605 nm (35). The purified oxidase contained 7 nmol of heme a per mg. protein, indicating a satisfactorily pure preparation. Optical absorbance and EPR spectra indicated that the preparation was essentially free of contaminants which interfere with the important spectroscopic signatures of the enzyme. The enzyme was solubilized in 0.5% Tween-20 and 50 mM tris(hydroxymethyl) aminomethane hydrochloride (Tris-HCl) pH 7.4 or 50 mM phosphate pH 7.4. Concentrations used in optical absorbance and EPR experiments are indicated in the figure legends.

The cyanide derivative of the oxidized enzyme was prepared by adding solid KCN, to a final concentration of 0.1 M, to an aerobic enzyme sample contained in an airtight cuvette. Solid $KH_2PO_4$ was added simultaneously to a final concentration of 0.2 M in order to maintain the solution pH and to produce HCN, which is the species which reacts with the oxidase (36). The solution was then incubated for 4 hours or longer at 4°C to ensure that complexation was complete before optical spectra were recorded. The partially reduced cyanide complex was prepared by adding sodium ascorbate (6 mM) and tetramethylphenylenediamine (TMPD, 60 μM) to the cyanide complex. Optical spectra were recorded after 30 minutes. In the cyanide derivative, cytochrome $a_3$ is stabilized in its oxidized, low-spin state. With the high cyanide concentration and mild reductant employed, $Cu_B$ also remains oxidized, as verified by EPR spectra which did not exhibit an EPR signal from cyanocytochrome $a_3$ in proximity to cuprous $Cu_B$.

The formate complex of cytochrome oxidase was prepared by adding 1.0 M NaHCOO to an aerobic enzyme sample to a final concentration of 0.1 M. The solution was incubated at 4°C for at least 6 hours prior to recording absorbance spectra. The

partially reduced formate complex was produced by adding ascorbate (6 mM) and TMPD (60 μM) to the oxidized formate complex; absorbance spectra were recorded after 30 minutes. In the aerobic formate complex, cytochrome $\underline{a}_3$ is stabilized in the ferric high-spin state (37) and $Cu_B$ also remains oxidized, as verified by EPR spectra which did not show a significant high-spin iron signal from ferricytochrome $\underline{a}_3$ adjacent to cuprous $Cu_B$.

The partially reduced nitric oxide (NO) complex of the oxidase was prepared by degassing the enzyme by at least 3 cycles of evacuation and flushing with argon followed by reduction of the enzyme with a small excess of NADH in the presence of phenazine methosulfate (PMS, 0.01 equivalent) and the addition of NO to a pressure of 0.1 atmosphere. After 5 minutes of incubation at 4°C, the cytochrome $\underline{a}$ and $Cu_A$ sites were reoxidized by the addition of ferricyanide (8 equivalents). Absorbance spectra were recorded immediately. In this species, cytochrome $\underline{a}_3$ is ferrous low-spin, $Cu_B$ is reduced, and both cytochrome $\underline{a}$ and $Cu_A$ are oxidized, as verified by EPR. The fully reduced NO complex was prepared by vacuum degassing, reduction of the enzyme with ascorbate (6 mM) and TMPD (60 μM), and the addition of NO to a pressure of 0.1 atm. Absorbance spectra were recorded after 30 minutes at 4°C.

The one equivalent-reduced, NO-associated enzyme was prepared by incubating the enzyme with sodium azide (100 mM) for 6 hours followed by vacuum degassing and addition of NO to a pressure of 0.9 atm, as described by Stevens et al. (38). Azide and nitric oxide together react with the enzyme to produce nitrogen, nitrous oxide, and a one equivalent-reduced, NO-associated enzyme species. The formation of this species was verified by the presence of the triplet EPR signal due to nitrosylferrocytochrome $\underline{a}_3$ in proximity to cupric $Cu_B$ (38). Absorbance spectra were recorded after 20 minutes; subsequent incubation for 16 hours at 4°C caused only minor changes in the spectrum.

Carbon monoxide (CO) complexes for EPR study were prepared by vacuum degassing followed by the addition of the appropriate number of equivalents of NADH, and CO to a pressure of 1.0 atmosphere. PMS

(2 μM) was included as a mediator, and 0.01 equivalent cytochrome c was included to ensure intermolecular redox equilibrium. Samples were incubated for 90 minutes at 4°C prior to recording EPR spectra. CO complexes for absorbance spectrophotometry were prepared as described above for the NO complexes, except that 1.0 atmosphere of CO was used. In the CO complexes, cytochrome $\underline{a}_3$ is ferrous low-spin.

Spectroscopy. Absorbance spectra were recorded at room temperature with a Cary 219 spectrophotometer for near-infrared measurements or a Beckman Acta CIII interfaced to a microcomputer for visible wavelength measurements. Visible wavelength spectra were stored on magnetic disk so that difference spectra and difference-of-difference spectra could be obtained by computer subtraction. Near-infrared difference spectra were calculated by manually digitizing and subtracting the reference spectra. The spectral bandwidth was 1.0 nm (visible) or 3.0 nm (near-IR).

EPR spectra were obtained with a Varian E-Line Century Series X-band spectrometer employing 100 kHz field modulation. The sample temperature was regulated with an Air Products Heli-Tran temperature controller. The temperature was measured immediately before and after spectrum acquisition using a Au(0.07% Fe) chromel thermocouple placed in an oil-filled EPR tube, and data were rejected if significant (> 0.5 K) temperature changes had occurred. Samples were contained in 5 mm O.D. (3.4 mm ID) EPR tubes. For microwave power saturation measurements on $Cu_A$, the signal intensity was measured as the peak-to-trough amplitude at $g_y$. EPR spectra of inhibitor complexes prepared in the same manner as those used in visible absorbance experiments were recorded, and verified that the cytochrome $\underline{a}$ and $Cu_A$ oxidation states were as expected, and as prescribed in the figures below.

Data analysis. For $Cu_A$ at the temperatures examined here, the EPR line width is largely determined by inhomogeneous broadening, specifically 'g-strain' (inhomogeneity in the g-values

of paramagnets in slightly different environments). At higher temperatures or at very high microwave powers, homogeneous broadening can also contribute to the observed linewidth. For situations where both inhomogeneous and homogeneous broadening may contribute to the observed linewidth, Rupp et al. (39) have shown that the EPR absorption derivative amplitude may be fitted empirically to the function

$$Y = \frac{Y_o P^{1/2}}{(1 + \alpha P)^{b/2}} \qquad (1)$$

where $\alpha$ is a saturation parameter proportional to the product of $T_1$ and $T_2$, and b is an inhomogeneity parameter which may vary from 1.0 in the inhomogeneous to 4.0 in the homogeneous limit.

The EPR saturation data in this work were fitted to equation 1 by a nonlinear least-squares routine. Initially, $Y_o$, $\alpha$, and b were all allowed to vary. In all cases presented here, b was not significantly different from 1, so it was fixed at 1.0 (inhomogeneous limit) in a second fit to the data which improved the determinations of $\alpha$. In all cases, a satisfactory fit to the data was obtained by this procedure.

The product of $T_1$ and $T_2$ was obtained from the parameter $\alpha$ by the equation

$$T_1 T_2 = 2.1\ \alpha \qquad (2)$$

which was obtained using $\alpha,\alpha'$-diphenyl $\beta$-picrylhydrazyl (DPPH) as a standard. At room temperature, $T_1 = T_2 = 2 \times 10^{-8}\ s^{-1}$ for solid DPPH (2).

## RESULTS

Visible Absorbance Spectra. Absorbance spectra of oxidized and reduced cytochrome c oxidase are displayed above in Figure 1. The composite difference spectrum, representing both reduced minus oxidized cytochrome a and reduced minus oxidized cytochrome $a_3$, is shown in the lower panel. The composite difference spectrum has peaks at 604 nm ($\Delta\varepsilon$ = 24 $mM^{-1}$ $cm^{-1}$, ref. 35) and 444 nm ($\Delta\varepsilon$ = 168 $mM^{-1}$ $cm^{-1}$), and crosses zero at 622, 559, 462, and 431 nm.

Four different methods of fixing the oxidation state of cytochrome $a_3$ with inhibitor ligands were employed in order to measure the reduced minus oxidized difference spectrum of cytochrome a. The results of these experiments are displayed in Figures 2-5. Alpha and Soret band positions and intensities for the various inhibitor derivatives and for the cytochrome a difference spectra are compiled in Tables I and II, respectively.

The cytochrome a difference spectra obtained by the four methods exhibited differences which were characterized by subtracting them from each other pairwise (i.e., calculating difference-of difference spectra). The largest differences which resulted involved the one equivalent-reduced NO complex. The difference (of cytochrome a difference spectra) spectrum which compares this method with the most nearly similar method, which involves the two equivalent-reduced NO complex, is shown in Figure 6. The spectra obtained from the other five possible pairwise subtractions are displayed in Figure 7. The strongest features in the difference-of-difference spectra appear in the 600 nm region and the 400-450 nm region, which is consistent with assignment to one or both of the cytochromes. Noteworthy features include a fairly strong, asymmetric peak near 606 nm in the spectrum of Figure 6, which compares the one equivalent-reduced and two equivalent-reduced nitric oxide methods of obtaining the cytochrome a difference spectrum, and fairly strong features near 415 nm in all spectra which involve the formate method.

**Figure 2. Absorbance spectra of 15 μM cyanide-inhibited cytochrome c oxidase. Trace A, enzyme inhibited with 100 mM cyanide and partially reduced with ascorbate/TMPD; trace B, enzyme inhibited with cyanide; trace C, reduced minus oxidized cytochrome *a*, obtained as the difference of traces A and B.**

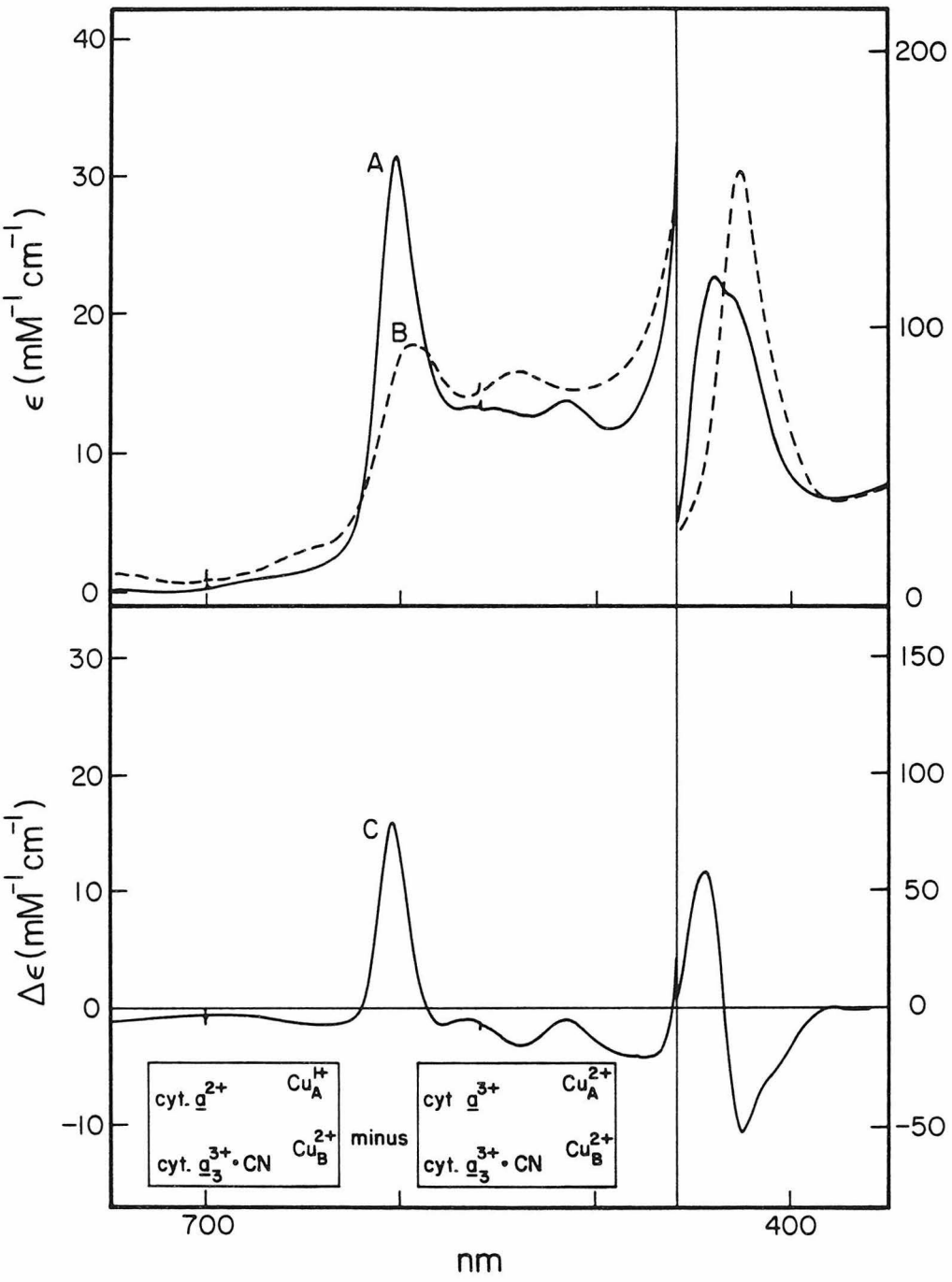
40
30
20
10
0
200
100
0
A
B
ε (mM⁻¹cm⁻¹)
30
20
10
0
−10
150
100
50
0
−50
C
Δε (mM⁻¹cm⁻¹)
cyt. g2+ CuA1+
cyt. g33+ • CN CuB2+
minus
cyt g3+ CuA2+
cyt. g33+ • CN CuB2+
700
400
nm

Figure 3. Absorbance spectra of 13.6 μM formate-inhibited cytochrome oxidase. Trace A, enzyme inhibited with formate and partially reduced with ascorbate/TMPD; trace B, enzyme inhibited with formate; trace C, reduced minus oxidized cytochrome a, obtained as the difference of traces A and B.

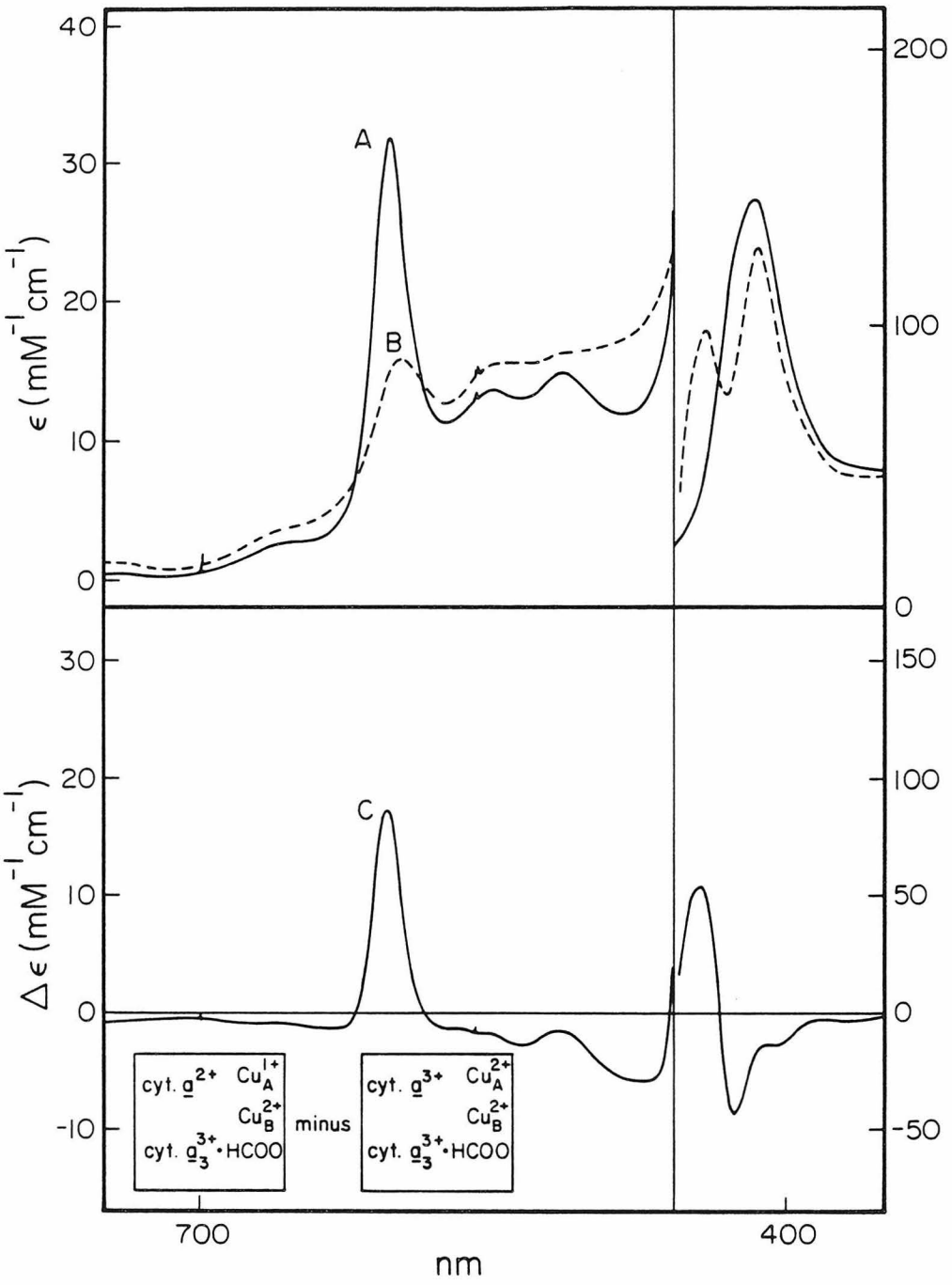
40
30
20
10
0
200
100
0
A
B
ε (mM⁻¹cm⁻¹)
30
20
10
0
-10
150
100
50
0
-50
C
Δε (mM⁻¹cm⁻¹)
cyt. g 2+ Cu A 1+
Cu B 2+
cyt. g 3 3+ • HCOO
minus
cyt. g 3+ Cu A 2+
Cu B 2+
cyt. g 3 3+ • HCOO
700
400
nm

Figure 4. Absorbance spectra of 12 μM nitric oxide-inhibited cytochrome oxidase. Trace A, enzyme reduced with NADH/PMS and exposed to NO; trace B, enzyme reduced and exposed to NO and then partially reoxidized with ferricyanide; trace C, reduced minus oxidized cytochrome a, obtained as the difference of traces A and B.

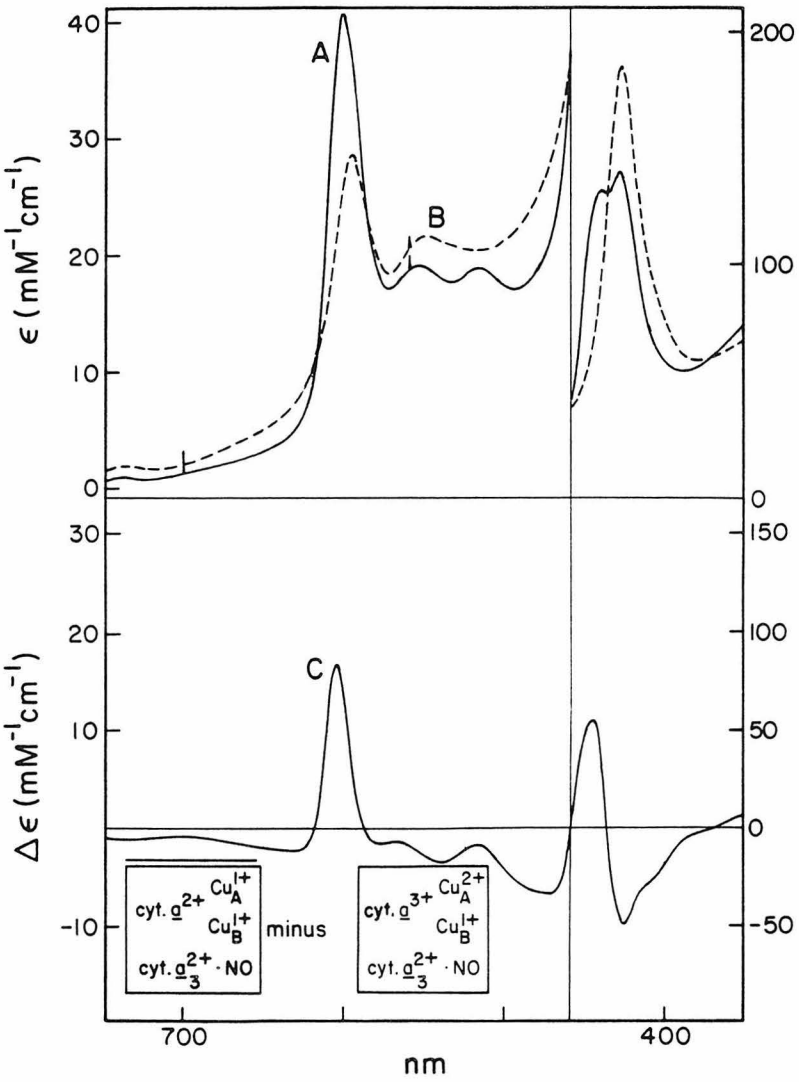
A
B
C
ε (mM⁻¹cm⁻¹)
Δε (mM⁻¹cm⁻¹)
cyt. a2+ CuA1+ CuB1+ cyt. a3 2+ · NO
minus
cyt. a3+ CuA2+ CuB1+ cyt. a3 2+ · NO
700
400
nm

**Figure 5. Absorbance spectra of 11 μM nitric oxide–inhibited cytochrome oxidase. Trace A, enzyme reduced with ascorbate/TMPD and exposed to NO; trace B, enzyme incubated with azide followed by exposure to NO for 20 min.; trace C, reduced minus oxidized cytochrome *a*, obtained as the difference of traces A and B.**

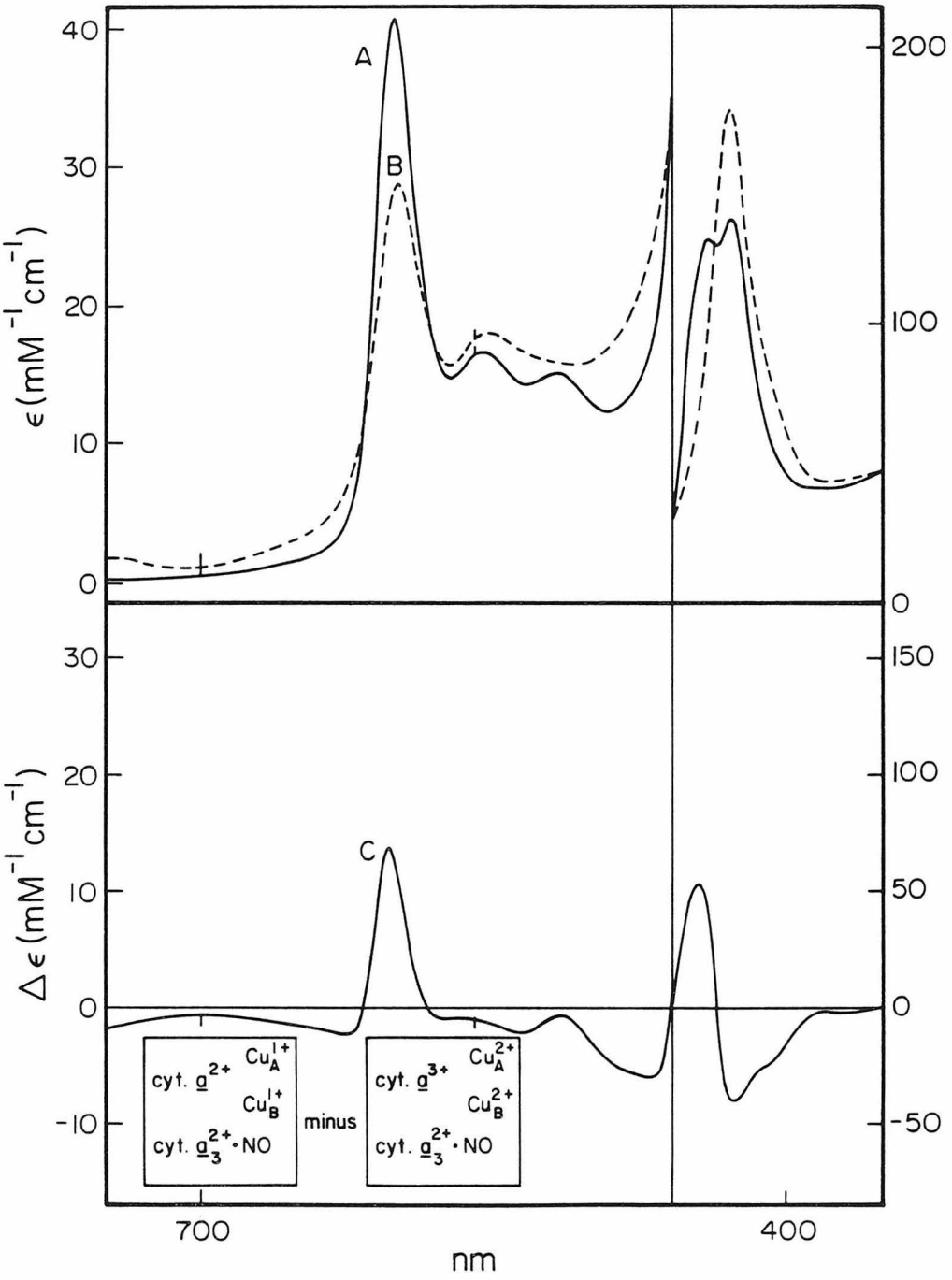
A
B
C
ε (mM⁻¹cm⁻¹)
Δε (mM⁻¹cm⁻¹)
nm
700
400
cyt. a2+ CuA1+ CuB1+ cyt. a3 2+ · NO
minus
cyt. a3+ CuA2+ CuB2+ cyt. a3 2+ · NO

Table I. Band Maxima (nm) and Extinctions ($mM^{-1}$ $cm^{-1}$) of Cytochrome Oxidase Derivatives

| enzyme derivative | α-band max | ε(α) | Soret band max | ε(Soret) |
|---|---|---|---|---|
| oxidized | 597 | 16.3 | 420 | 141 |
| reduced | 603 | 39.6 | 442 | 209 |
| oxidized + CN- | 594 | 18.1 | 427 | 156 |
| oxidized + CN- + ascorbate/TMPD | 603 | 31.8 | 440 | 118 |
| oxidized + HCOO- | 597 | 15.8 | 417 | 145 |
| oxidized + HCOO- + ascorbate/TMPD | 603 | 31.7 | 415,442 | 128,102 |
| reduced + NO | 601 | 41.3 | 428,440 | 138,130 |
| reduced + NO + ferricyanide | 595 | 27.7 | 427 | 184 |
| oxidized + N3- + NO | 598 | 28.9 | 428 | 177 |

Table II. Band Maxima (nm) and Extinctions ($mM^{-1}$ $cm^{-1}$) of Cytochrome Oxidase Difference Spectra

| difference spectrum | α-band max | ε(α) | Soret band max | ε(Soret) |
|---|---|---|---|---|
| reduced minus oxidized | 604 | 24 | 444 | 168 |
| ox. + CN- + asc./TMPD minus ox. + CN- | 605 | 16 | 444 | 59 |
| ox. + HCOO- + asc./TMPD minus ox. + HCOO- | 605 | 17 | 444 | 55 |
| red. + NO minus red. + NO + ferricyanide | 604 | 17.4 | 444 | 56 |
| red. + NO minus ox. + N3 + NO | 604 | 13.7 | 445 | 53 |

Figure 6. Difference-of-difference spectrum obtained from the cytochrome a difference spectra calculated in Figure 4 (two equivalent-reduced NO method) and Figure 5 (one equivalent-reduced NO method). This spectrum is algebraically equivalent to a one equivalent-reduced NO complex minus two equivalent-reduced NO complex difference spectrum, since these two methods employ a common reference state (fully reduced NO complex) in calculating the cytochrome a difference spectra.

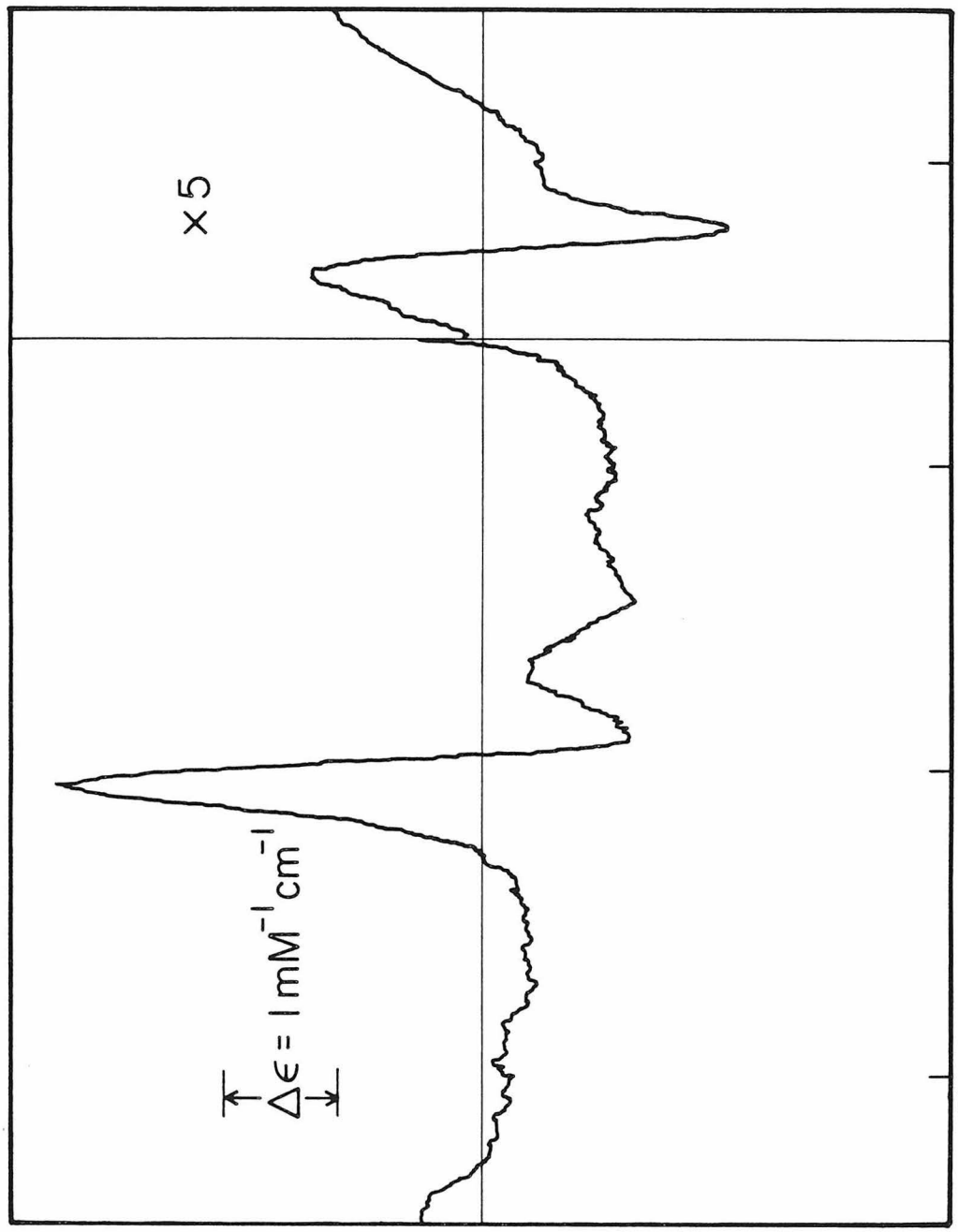
×5
Δε = 1 mM⁻¹cm⁻¹
700
600
500
400
nm

Figure 7. Difference-of-difference spectra obtained by pairwise subtraction of the cytochrome a difference spectra calculated in Figures 2-5. Trace A, two equivalent NO method minus cyanide method (4C minus 1C); trace B, two equivalent NO method minus formate method (4C minus 2C); trace C, formate method minus one equivalent NO method (2C minus 5D); trace D, formate method minus cyanide method (2C minus 1C); trace E, cyanide method minus one equivalent NO method (1C minus 5C).

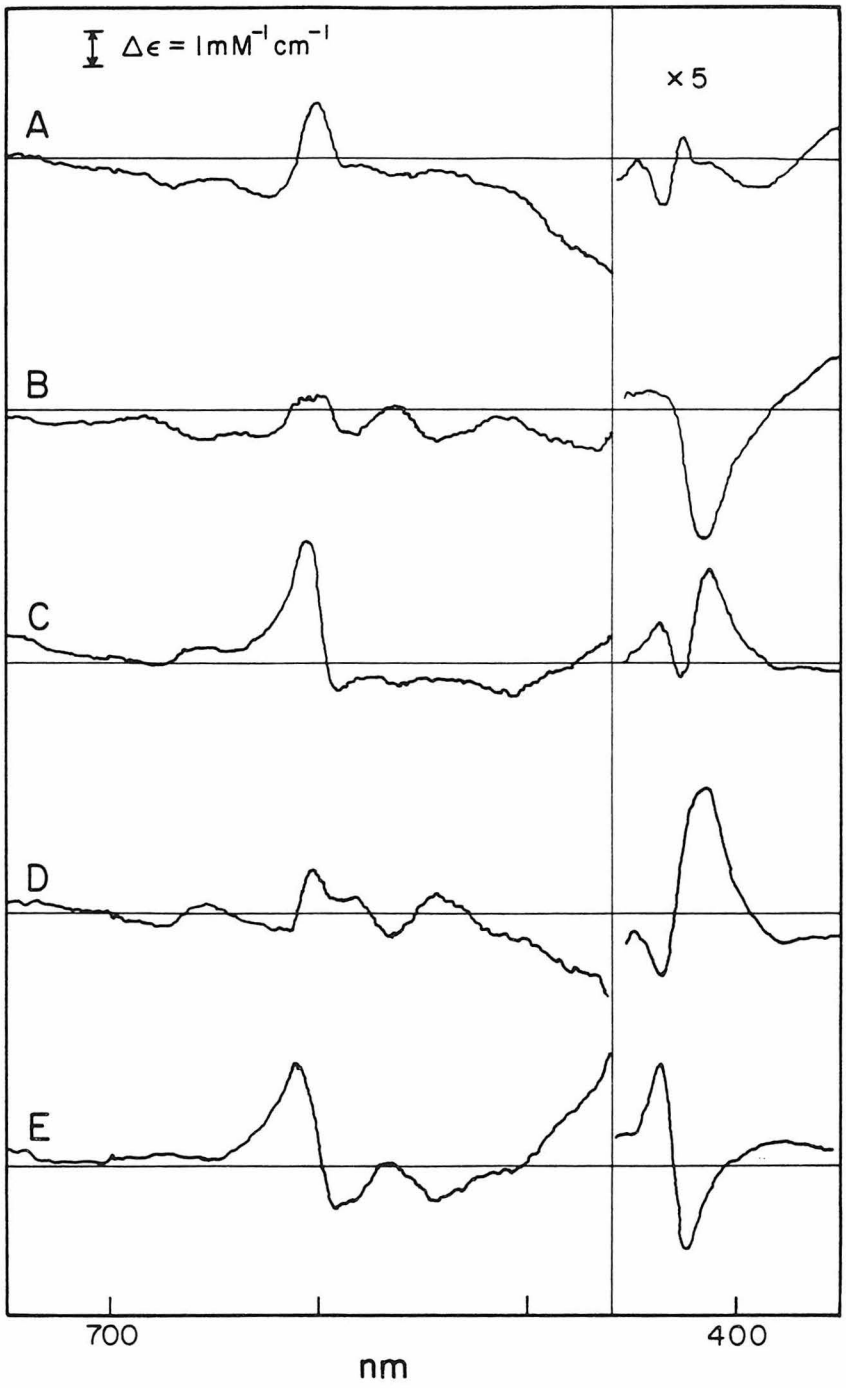
Δε = 1mM⁻¹cm⁻¹
×5
A
B
C
D
E
700
400
nm

Near-Infrared Absorbance Spectra. Available evidence indicates that the absorbance centered near 830 nm in oxidized cytochrome oxidase is due to the copper rather than to the hemes of the enzyme. It has been suggested that $Cu_A$ is the only contributor (29), or that both $Cu_A$ and $Cu_B$ make approximately equal contributions (28). Near-infrared difference spectra were obtained by two methods based on either formate or carbon monoxide inhibition of the cytochrome $\underline{a}_3/Cu_B$ site. Since in both cases the oxidation state of $Cu_B$ remains fixed (cupric in the formate derivative, as verified by EPR, and cuprous in the CO derivative, Ref. 40) while the oxidation state of $Cu_A$ is varied, these difference spectra are due entirely to $Cu_A$. The difference spectra obtained by the two methods are displayed in Figure 8. Within the uncertainty of the determinations, the peak positions and bandwidths of the near-infrared absorbances measured by the two methods are the same. Fully-oxidized minus fully-reduced near-infrared difference spectra recorded in the absence of inhibitors were negligibly different from the ones shown here with respect to the intensity of the band at 825 nm, indicating that any additional contribution due to $Cu_B$ is small.

Electron Spin Relaxation in Partially Reduced Inhibitor Complexes. Electron spin interaction among the metal sites was examined by measuring the microwave power saturation of the EPR signal from $Cu_A$ in the native and in partially reduced, CO-associated derivatives of the oxidase. The results of this comparison are displayed in Figure 9. In the native oxidized enzyme, the high-spin ferric cytochrome $\underline{a}_3$ and cupric $Cu_B$ are antiferromagnetically coupled to yield a total electron spin of 2 at the dioxygen reduction site (15). In the two equivalent-reduced, CO-associated enzyme, both cytochrome $\underline{a}_3$ and $Cu_B$ are reduced (40) and the iron is low-spin, yielding a spin of zero at the dioxygen reduction site, but the cytochrome $\underline{a}$ and $Cu_A$ sites remain oxidized. The reduction in spin of the cytochrome $\underline{a}_3/Cu_B$ site from 2 to zero has a negligible effect upon the power saturation of

the $Cu_A$ signal (Figure 9). In the ca. 3 equivalent-reduced enzyme, cytochrome *a* is approximately 75% reduced and $Cu_A$ approximately 35% reduced. Assuming that the reduction potentials of these sites are not influenced by a cooperative interaction (spectroelectrochemical titrations indicate the presence of an *anti*cooperative interaction, cf. Chapter III), this means that at least 75% of the observed $Cu_A$ signal in this sample arises from cytochrome oxidase molecules in which cytochrome *a* is reduced and therefore diamagnetic. In this sample, the $Cu_A$ electron spin relaxation was significantly slower, as evidenced by a 50% increase in $T_1T_2$ (Figure 9), which indicates that the $Cu_A$ spin is influenced by an interaction with cytochrome *a*.

The $Cu_A$ lineshape was not changed upon formation of the CO derivative from the native enzyme (data not shown), but a small lineshape change ($\Delta g_y = 0.001$) was reproducibly observed in the $Cu_A$ signal upon subsequent partial reduction of cytochrome *a* (Figure 10). This lineshape change persisted at a high temperature (62K) where a dipolar splitting of moderate strength due to cytochrome *a* is expected to be largely relaxed, so it is likely that the $Cu_A$ site undergoes a minor structural change in response to the reduction of cytochrome *a*.

Figure 8. Oxidized minus reduced near-infrared difference spectra of cytochrome oxidase obtained using two different methods of inhibiting cytochrome $\underline{a}_3$ and $Cu_B$. Top: oxidized formate complex minus partially reduced formate complex. The circles represent a Gaussian centered at 825 nm with hwhh = $1.43 \times 10^3$ $cm^{-1}$. Bottom: Two equivalent-reduced CO complex minus fully reduced CO complex. The circles represent a Gaussian centered at 823 nm with hwhh = $1.41 \times 10^3$ $cm^{-1}$. In both cases, the metals of the dioxygen reduction site (cytochrome $\underline{a}_3$ and $Cu_B$) are inhibited so that neither undergoes a change of oxidation state which will contribute to the difference spectrum.

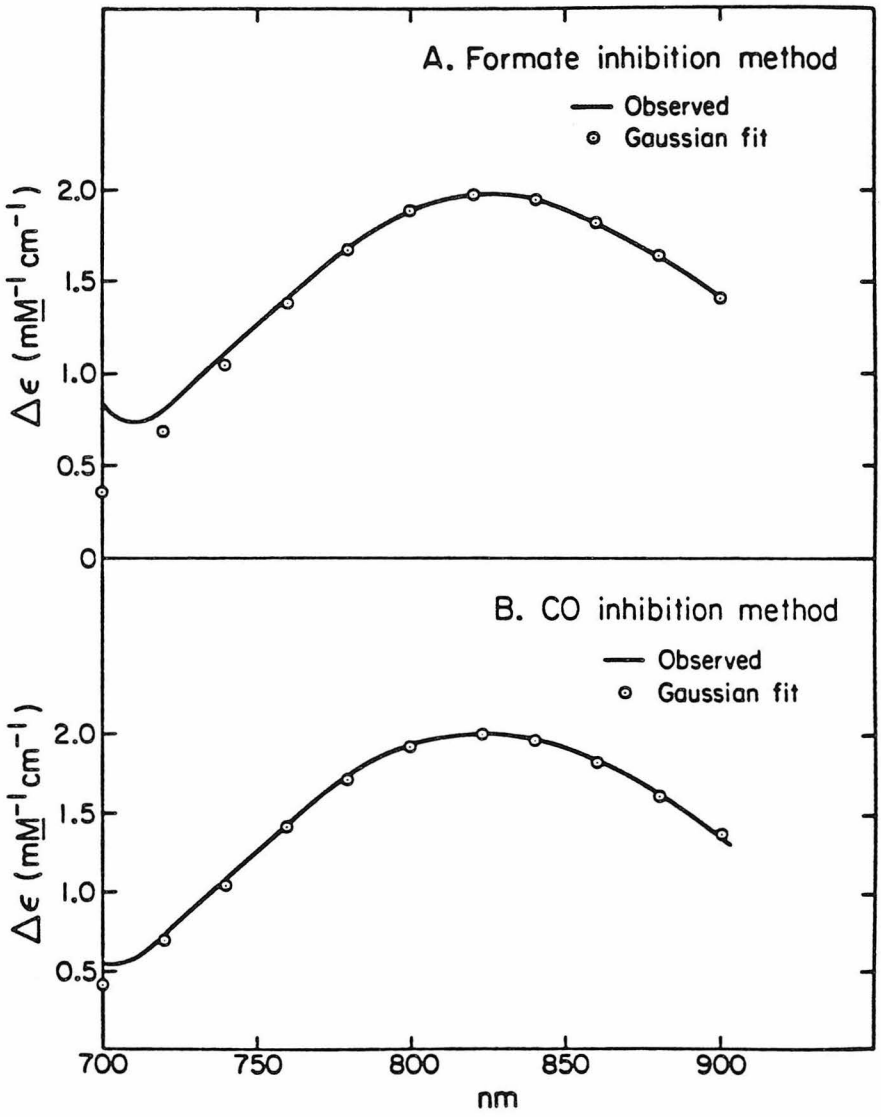
A. Formate inhibition method
Observed
Gaussian fit
Δε (mM⁻¹cm⁻¹)
2.0
1.5
1.0
0.5
0
B. CO inhibition method
Observed
Gaussian fit
Δε (mM⁻¹cm⁻¹)
2.0
1.5
1.0
0.5
700
750
800
850
900
nm

Figure 9. The product $1/T_1T_2$ for $Cu_A$ in three different cytochrome oxidase species, inferred from microwave power saturation measurements. Data obtained at three temperatures are shown. The circles denote the native, uninhibited cytochrome oxidase. The squares denote the two equivalent-reduced CO complex of the enzyme, in which cytochrome $\underline{a}_3$ and $Cu_B$ are reduced to the ferrous and cuprous states, respectively. The triangles denote the ca. three equivalent-reduced CO complex of the enzyme, in which cytochrome $\underline{a}_3$ and $Cu_B$ are fully reduced, cytochrome $\underline{a}$ is approximately 75% reduced, and $Cu_A$ is approximately 35% reduced. The EPR signal was measured at gy. Sample concentration was approximately 0.2 mM.

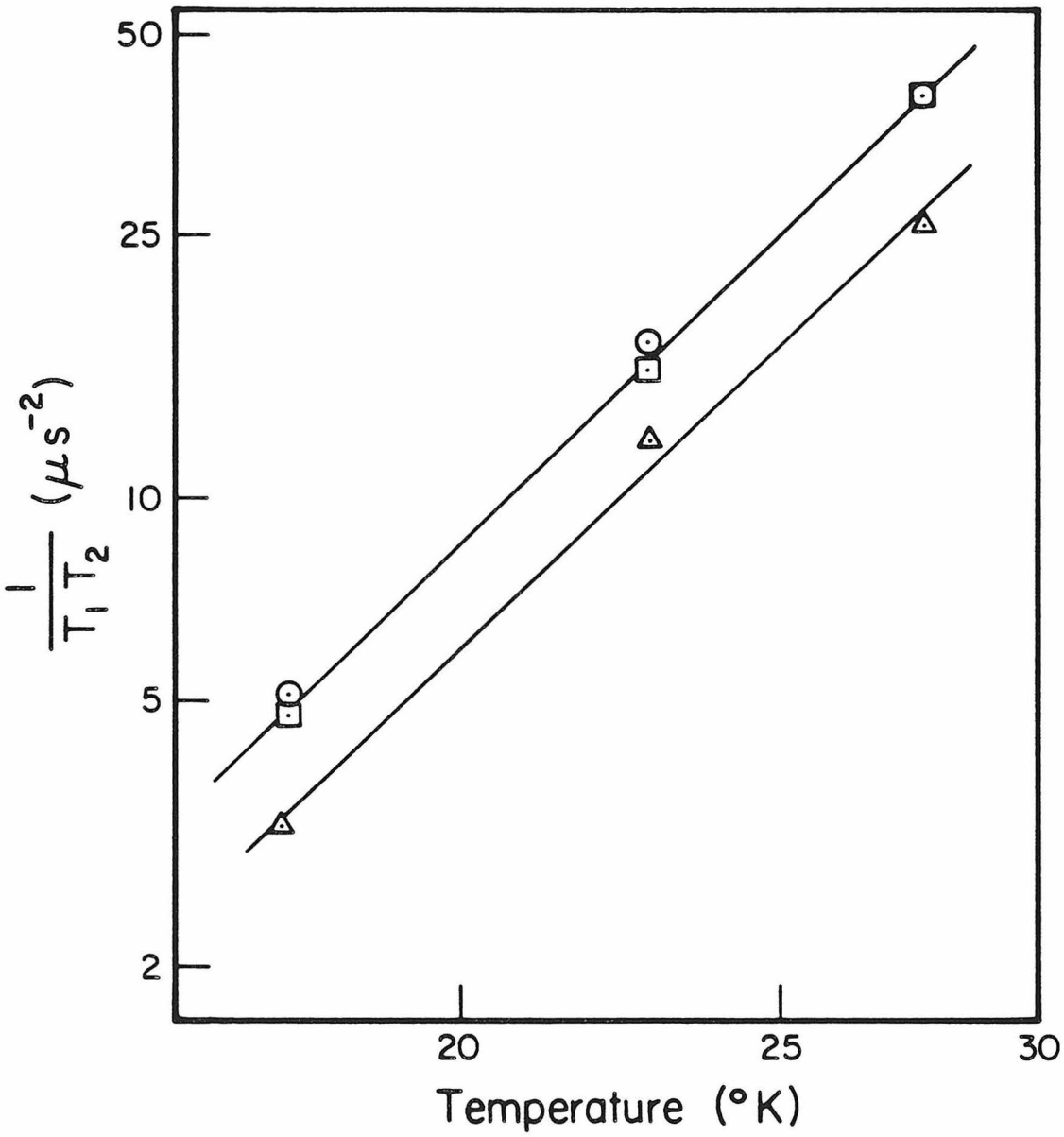
50
25
10
5
2
$\frac{1}{T_1 T_2}$ ($\mu s^{-2}$)
20
25
30
Temperature (°K)

Figure 10. EPR spectra in the g = 1.95–2.10 region of $Cu_A$ in two equivalent- (solid line) and ca. three equivalent- (dashed line) reduced CO complexes of cytochrome oxidase. The EPR spectrum of the native oxidized enzyme was not significantly different from that of the two equivalent-reduced CO complex, so for the sake of clarity it is omitted. Sample concentration was ca. 0.2 mM, temperature = 14K.

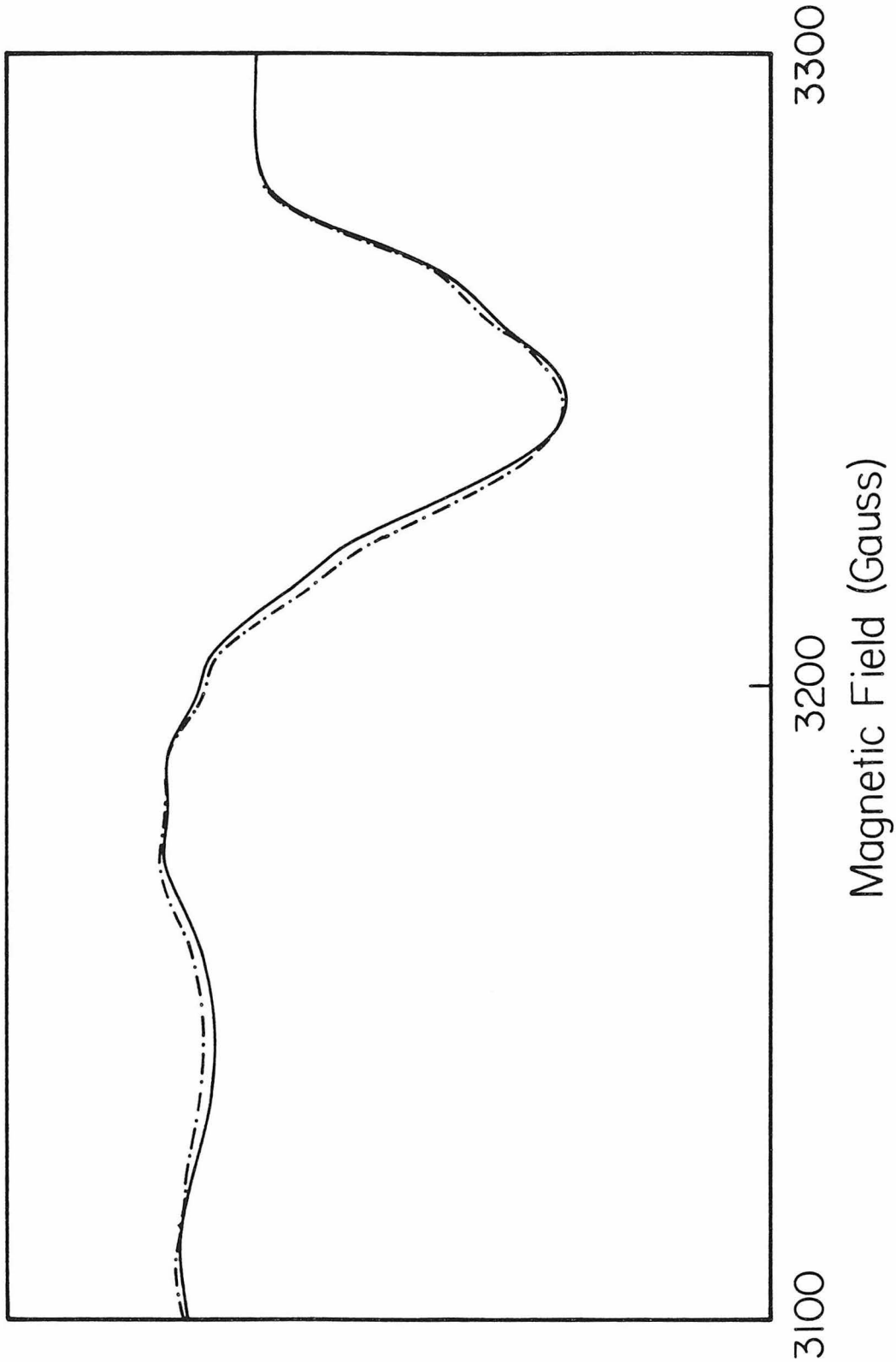
3100
3200
3300
Magnetic Field (Gauss)

## DISCUSSION

Visible Absorbance Spectra of Cytochromes a and $a_3$. In the simplest model of the cytochrome oxidase absorbance spectrum, the metal centers are assumed to be spectroscopically independent, so that the absorbance of each of the chromophores is considered to be the same regardless of the ligation or oxidation states of the other metal centers. Within this framework, the composite visible absorbance spectrum may be expressed as a sum:

$$\varepsilon(\lambda) = \varepsilon_a{}^o(\lambda) + \varepsilon_{a_3}{}^o(\lambda) + f_a\Delta\varepsilon_a(\lambda) + f_{a_3}\Delta\varepsilon_{a_3}(\lambda) \qquad (3)$$

where $\varepsilon_a{}^o(\lambda)$ and $\varepsilon_{a_3}{}^o(\lambda)$ are the extinctions of oxidized cytochromes *a* and $a_3$, respectively, $f_a$ and $f_{a_3}$ denote the fractions of cytochromes *a* and $a_3$ which are reduced, and $\Delta\varepsilon_a(\lambda)$ and $\Delta\varepsilon_{a_3}(\lambda)$ refer to the changes in extinction which accompany reduction of the two cytochromes (It has been assumed that the coppers make a negligible contribution in the spectral range between 700 and 350 nm, Ref. 41). Cytochrome $a_3$ may be stabilized in either the reduced ($f_{a_3} = 1.0$) or the oxidized ($f_{a_3} = 0$) state by exogenous ligands while cytochrome *a* undergoes oxidoreduction. Under these assumptions, the absorbance change accompanying reduction of cytochrome *a*, $\Delta\varepsilon_a(\lambda)$, may thus be measured without interfering contributions from cytochrome $a_3$.

If the metal centers are not spectroscopically independendent, additional terms must be incorporated in equation 3 to formally describe the effects of ligation and oxidation state of each of the metal centers upon the absorption properties of each of the cytochromes. The equation then becomes

$$\varepsilon(\lambda) = \varepsilon_a{}^o(\lambda) + \varepsilon_{a_3}{}^o(\lambda) + f_a\Delta\varepsilon_a(\lambda) + f_{a_3}\Delta\varepsilon_{a_3}(\lambda) + \Delta\varepsilon_a{}^i(\lambda,a3,A,B) + \Delta\varepsilon_{a_3}{}^i(\lambda,a3,A,B) \qquad (4)$$

where the $\Delta\varepsilon_a{}^i(\lambda,a3,A,B)$ and $\Delta\varepsilon_{a_3}{}^i(\lambda,a,A,B)$ terms describe any

site-site interactions which influence the absorbance properties of cytochromes a and $a_3$, respectively.

Four different methods, all based upon ligand inhibition of cytochrome $a_3$, were used to estimate the reduced minus oxidized difference spectrum of cytochrome a. Each method gives a different result, especially with respect to the intensity of the peak near 604 nm and the trough near 415 nm. The intensity of the 604 nm peak varied between 13.7 and 17.4 $mM^{-1}$ $cm^{-1}$, with the one-equivalent reduced NO method yielding the anomolously low value. The Soret peak near 443 nm was less variable on a percent basis, ranging in intensity between 53 and 59 $mM^{-1}$ $cm^{-1}$.

It might be argued that the variability in the cytochrome a difference spectra is caused by sample heterogeneity, for example, incomplete reduction of cytochrome a in the cyanide derivative or partial reduction of cytochrome a in the one equivalent-reduced NO derivative. These possibilities were explored, and ruled out, by parallel EPR studies on similarly treated samples. In all cases except with formate, the ligands used are expected to bind very strongly to the enzyme, so that effectively complete complexation was assured. It is conceivable that formate binds less completely or in a different manner to the oxidized enzyme than to the oxygen-pulsed (42) species which results from the addition of reductant to the aerobic formate-inhibited samples (in the presence of oxygen and a suitable reductant, the formate complex of the enzyme undergoes slow turnover, Ref. 37); this could explain the fairly intense features near 415 nm in the difference of difference spectra which are associated with the formate method (Figure 7, Traces B, C, and D). The most important conclusions to follow are not based upon the results obtained using formate inhibition, and this possibility was not explored further.

Most of the differences in the results obtained by the various methods are not like those expected if sample heterogeneity is the cause. For example, while the one equivalent-reduced NO method and the two equivalent-reduced NO method give very different results in the alpha band region, they are more nearly in agreement with

respect to the Soret band intensity, implying that a greater or lesser degree of cytochrome *a* reduction is not responsible for the differences. In most cases, the difference-of-difference spectra in the 600 nm region do not resemble the cytochrome *a* difference spectra, but instead suggest shifts in peak position as well as changes in peak intensities. In the Soret region, the difference-of-difference spectra do not resemble the reduced minus oxidized spectrum for cytochrome *a* or that expected for cytochrome $a_3$ (25) but again suggest shifts in position or changes in intensity of peaks associated with chromophores of defined oxidation state. The observed spectral variations are thus most plausibly explained as arising from interaction between the metal centers of the enzyme, implying that either or both of the formal interaction terms $\Delta\varepsilon_a{}^i$ and $\Delta\varepsilon_{a_3}{}^i$ are nonzero.

In the one equivalent-reduced NO-associated species, $Cu_B$ is oxidized while cytochrome $a_3$ is reduced and associated with NO. In the two equivalent-reduced NO-associated species, both $Cu_B$ and cytochrome $a_3$ are reduced. The oxidation state of $Cu_B$ is thus the only feature which distinguishes them, yet the two methods involving these species produce the most discrepant estimates of the intensity of the 604 nm peak in the reduced minus oxidized cytochrome *a* difference spectrum (Table II). The oxidation state of $Cu_B$ must therefore influence the absorbance properties of the enzyme. The difference-of-difference spectra comparing these methods (Figure 6), which is algebraically equal to a one equivalent-reduced minus two equivalent-reduced difference spectrum, shows a fairly strong, asymmetric peak at 606 nm. The width of this peak indicates that it is not associated with a charge transfer transition of a copper ion; blue or type 1 copper charge transfer bands are typically 3-4 times more broad (43). The shape and positions of the spectral features point instead to the involvement of one or both of the cytochromes.

The $\alpha$ band-extinction of both high-spin and low-spin heme A model compounds is known to be sensitive to solvent polarity (8,44). Since $Cu_B$ is fairly close to cytochrome $a_3$ (15,38) the oxidation state of $Cu_B$ might influence the absorbance properties of cytochrome

$\underline{a}_3$, producing the differences expressed in the spectrum of Figure 6. Davis et al. (45) have found that a charge situated on the periphery of the chlorophyll $\underline{a}$ macrocycle can induce a reversible wavelength shift of 90 $cm^{-1}$ and an increase in extinction of approximately 8 $mM^{-1}$ $cm^{-1}$ in the red absorption maximum of this chromophore. In the case of the cytochrome $\underline{a}_3$-NO complex, a red shift of comparable magnitude (70 $cm^{-1}$) is observed upon oxidation of $Cu_B$ (compare Figures 4 and 5), suggesting that the spectrum of cytochrome $\underline{a}_3$ is influenced in an analogous fashion by the additional charge on $Cu_B$. Alternatively, a change in the coordination environment of the copper, possibly the disruption of a ligand bridge between the iron and copper, may be involved. The derivative-shaped feature in the Soret region of the spectrum in figure 6 crosses zero near 430 nm, consistent with assignment to ferrocytochrome $\underline{a}_3$-NO, which absorbs maximally near 428 nm. Thus the spectrum of Figure 6 is readily explained as arising from the term $\Delta\varepsilon_{a_3}{}^{i}(\lambda,a,A,B)$, in which the important variable is B. While it cannot be excluded that the interaction term $\Delta\varepsilon_{a}{}^{i}(\lambda,a3,A,B)$ also has an effect, this term is clearly not necessary.

An interaction between $Cu_B$ and cytochrome $\underline{a}_3$ is plausible because these sites are close to each other in the enzyme. However, this proximal interaction alone will not account for all of the data. The discrepancies between the cyanide, formate, and two equivalent-reduced NO methods suggest that there may also be an interaction between the 'a-sites' (cytochrome $\underline{a}$ and $Cu_A$) and the metals of the dioxygen reduction site. In the absence of such an interaction, these methods should yield identical results.

The observed discrepancies may in principle involve either of the interactive terms, but for a variety of reasons they appear more likely to involve the term which influences cytochrome $\underline{a}_3$, $\Delta\varepsilon_{a_3}{}^{i}(\lambda)$. All spectra which involve the formate method show features near 415 nm, close to the Soret absorbance maximum of the formate complex of cytochrome $\underline{a}_3$ at 416 nm and far from the absorbance maxima of ferric cytochrome $\underline{a}$ at 427 nm (25) and ferrous cytochrome $\underline{a}$ at 442 nm (25). The spectra involving the

cyanide and the two equivalent-reduced NO methods have features near 430 nm, which is close to the Soret absorbance maxima of these complexes, so interactive effects at the cytochrome $\underline{a}_3$ site are again sufficient to explain the data without invoking effects at cytochrome $\underline{a}$ (which also absorbs maximally close to 430 nm). Finally, an interaction between the a-sites and the oxygen reduction site which influences the extinction of cytochrome $\underline{a}_3$ rather than cytochrome $\underline{a}$ is made appealing by the demonstrated sensitivity of the cytochrome $\underline{a}_3$ spectrum to its environment (specifically, the oxidation state of $Cu_B$). This sensitivity suggests a plausible mechanism whereby the extinction of cytochrome $\underline{a}_3$ might be modulated by the states of the other metal centers: Reduction of cytochrome $\underline{a}$ and/or $Cu_B$ may induce a conformational change which causes $Cu_B$ to move in relation to cytochrome $\underline{a}_3$ and thereby influence its extinction. The ligation and oxidation state of cytochrome $\underline{a}_3$, among other factors, will determine the nature and extent of this effect, causing the observed discrepancies between the cyanide, formate, and NO methods. This suggestion gains support from the recent observation that the reduction of cytochrome $\underline{a}$ increases the rate of cyanide binding to ferric cytochrome $\underline{a}_3$; these results were interpreted in terms of 'open' and 'closed' conformations of the cytochrome $\underline{a}_3/Cu_B$ site (46).

All of the visible absorbance data are thus satisfactorily explained in a model incorporating spectroscopic interaction manifested at cytochrome $\underline{a}_3$ and treating cytochrome $\underline{a}$ as spectroscopically isolated. The alpha band intensity of the reduced minus oxidized cytochrome $\underline{a}$ spectrum is thus between 16 and 17.4 $mM^{-1}$ $cm^{-1}$ (the range established by the three methods in which the oxidation of $Cu_B$ did not change), meaning that cytochrome $\underline{a}$ contributes between 67% and 73% to the total reduced minus oxidized absorbance at this wavelength. The Soret peak intensity is more closely determined on a percentage basis and is somewhere between 55 and 59 $mM^{-1}$ $cm^{-1}$, corresponding to between 33% and 35% of the composite difference spectrum intensity. It should be stressed that the interactive effects are not large except when a change in the

oxidation state of $Cu_B$ is involved. In the case where the oxidation state of $Cu_B$ was fixed and where complete complexation by the inhibitor ligand was assured (cyanide method minus two equivalent-reduced NO method, trace 7A) the effects of *a*-site/$a_3$-site interaction are minor, especially in the Soret region. The cytochrome absorbance spectra therefore retain the greater part of their utility for monitoring electrochemical titrations of the oxidase. The present results also indicate that spectroelectrochemical results which suggest the occurrence of spectroscopic interaction are likely to involve cytochrome $a_3$ rather than cytochrome *a*.

Near-Infrared Absorbance Spectrum of $Cu_A$. The close similarity of the near-infrared absorbance difference spectra in Figure 8 indicates that the ligation and oxidation state of the dioxygen reduction site do not significantly influence the shape or intensity of the 825 nm absorbance. The fully oxidized minus fully reduced near-infrared difference spectrum (not shown) was not significantly different from the spectra of Figure 8, indicating that $Cu_B$ makes a negligible contribution to the spectrum near 825 nm. The same conclusion was reached by Beinert et al. (29) in a study which correlated the near-infrared absorbance properties with the $Cu_A$ oxidation state monitored by EPR. The present result contradicts the near-infrared reflectance spectroscopy measurements of Powers et al (28). It appears likely that sample heterogeneity, specifically undesired reduction of $Cu_A$, or artifacts of the more problematical reflectance method, led to their erroneous conclusion that $Cu_B$ also makes a substantial contribution to this band.

The intensity of the 825 nm $Cu_A$ absorbance indicates that it is due to a charge transfer transition. Since the position, intensity, and bandwidth of this transition should be sensitive to the details of the $Cu_A$ coordination geometry, the similarity of the spectra in Figure 8 indicates that the structure of the $Cu_A$ site is not greatly affected by changes in the spin and oxidation state

of the dioxygen reduction site.

EPR Properties of $Cu_A$ in CO Complexes. Reduction of the dioxygen reduction site and complexation with CO had no measurable effect upon either the shape of the $Cu_A$ EPR signal or its spin relaxation (Figures 9 and 10), in agreement with the above conclusion that spin and oxidation state changes at the dioxygen reduction site do not influence the structure of $Cu_A$. The absence of magnetic dipolar splittings or incremental spin relaxation at $Cu_A$ due to cytochrome $a_3$ and $Cu_B$ is difficult to interpret in terms of direct through-space (as distinct from conformationally modulated) interactions, since the coupled iron-copper system (S=2) is quantized along the heme normal by the zero field splitting of the heme and because the electron spin-lattice relaxation of this S=2 system may be very fast. Because of the zero field splitting, the ground state of the coupled iron-copper spin system will have $m_s$ = 0; i.e., it will have no static component of magnetic moment to cause static dipolar splittings. Also, extremely rapid spin-lattice relaxation of this spin system will collapse any moderately strong dipolar splittings it might cause via its thermally excited states with $m_s$ = +/- 1,2 and will cause the cytochrome $a_3/Cu_B$ spin system to be relatively inefficient in inducing spin relaxation in slower-relaxing nearby spins. An estimate of the minimum cytochrome $a_3$-to-$Cu_A$ distance based on the absence of magnetic interaction effects at $Cu_A$ was therefore not attempted.

Reduction of cytochrome a caused a small, temperature-independent shift in one of the $Cu_A$ g-values (Figure 10), which signals a minor structural change at the $Cu_A$ site. The temperature dependences between 20 and 62K of the $Cu_A$ lineshapes were very similar (data not shown). A moderate (10-25 G) magnetic dipolar splitting by cytochrome a, which would have been manifested at 20K, would be largely collapsed at 64K given the measured spin-lattice relaxation rate of cytochrome a at the two temperatures (47). A large number of different molecular orientations was sampled in this experiment, since a fairly large

portion of the powder spectrum was examined. Only a fraction of these orientations can correspond to those for which a dipolar interaction is unfavorable due to geometric factors (i.e., close to the magic angle), so it may be concluded that substantial (> 10 G) magnetic dipolar splitting due to cytochrome a does not contribute to the $Cu_A$ lineshape. Using the equation

$$\Delta H = \frac{\mu_e (3\cos^2\theta - 1)}{R^3} \qquad (5)$$

which relates dipolar splittings to distance, and assuming a spherically averaged value for the geometric factor $(3\cos^2\theta - 1)$ (justified by the fact that many molecular orientations contribute to the region of the spectrum which was examined) this result indicates that cytochrome a and $Cu_A$ are more than 13 Å away from each other. This first-order estimate must be considered approximate; a closer specification of the minimum intersite distance would require simulations of the $Cu_A$ lineshape under various assumptions regarding the geometric relationship between the intersite vector and the $Cu_A$ g-tensor, and a more quantitative consideration of the orientational averaging of the factor $(3\cos^2\theta - 1)$. Given the nature of the observations, viz. no positive evidence for dipolar splittings, this detailed analysis was not undertaken. We note, however, that because of the inverse third-power dependence of the dipolar splitting, the present estimate is not expected to be greatly in error: if the data are taken as consistent with up to a 22 G rather than a 10 G dipolar coupling, the minimum distance estimate is decreased by only 3Å.

The data in Figure 9 imply an incremental relaxation of the $Cu_A$ electron spin caused by interaction with cytochrome a. This effect probably involves magnetic dipolar interaction between the sites, and using well-known equations (48) it may also be used to place

limits on the cytochrome *a*-$Cu_A$ distance. The analysis, which is discussed in detail in Reference 48, is complicated by the possibility of interaction-induced increments to both $1/T_1$ and $1/T_2$. The resulting distance estimates are least constrained if it is assumed that increments to $1/T_2$ dominate the observed effect. Under this assumption, the upper limit on the cytochrome *a*-$Cu_A$ distance which is implied by the relaxation data is 26 Å.

A similar experimental result, namely, a ca. twofold reduction in $T_1T_2$ ($Cu_A$) accompanying cytochrome *a* reduction in CO derivatives of the enzyme, has since been obtained by Goodman and Leigh (49). Goodman and Leigh obtained estimates of $T_2$ for cytochrome *a* by extrapolating the cytochrome *a* linewidth from relatively high temperatures (40–60K) to the temperature of their experiments (15K) and obtained estimates of $T_2$ for $Cu_A$ from computer fits to the power saturation curves ($T_2$ may in principle be deduced from the inhomogeneity parameter b in equation 1). Using these $T_2$ values, they then obtained estimates of the individual increments to $1/T_1(Cu_A)$ and $1/T_2(Cu_A)$ caused by dipolar interaction with cytochrome *a*. Their analysis leads to a $Cu_A$-cytochrome *a* distance estimate of less than 13 Å. In view of the large difference between their conclusions and those of the present analysis, it is appropriate to discuss the pertinent assumptions which underpin each.

The conclusions of Goodman and Leigh are based on the assumption that $1/T_2$ exhibits a power dependence upon temperature over a broad range,

$$1/T_2 = c\,T^n \qquad (6)$$

so that a log-log plot of $T_2$ vs. temperature may be extrapolated from high temperatures, where $T_2$ may be deduced from the observed linewidth, to lower temperatures where the linewidth is dominated by inhomogeneous broadening. There is presently no theoretical or experimental justification for this assumption. It is expected to be true at temperatures sufficiently high that $T_1 = T_2$, since $T_1$

obeys an equation analogous to equation 6 over a fairly broad temperature range (50). Since the mechanisms of transverse and longitudinal relaxation are different, there is no reason to expect that $1/T_2$ and $1/T_1$ will exhibit similar temperature dependences, so at lower temperatures $T_2$ is likely to diverge from $T_1$. The value of $T_2$ which Goodman and Leigh obtained by extrapolation was used in conjunction with their measured value of $1/T_1T_2$ ($Fe_a$) to estimate $T_1(Fe_a)$. Direct measurements of $T_1(Fe_a)$ have been made by pulsed saturation-recovery methods (47); these measurements disagree with the extrapolation-based estimates of $T_1(Fe_a)$ by a factor of more than 50.

Goodman and Leigh used values of the saturation parameter b obtained from computer fits to equation 1 to obtain estimates of $T_2(Cu_A)$ in the partially reduced CO derivatives. They found that the homogeneous linewidth of $Cu_A$ was only 0.4% +/- 0.1% of the observed inhomogeneous linewidth, in both their two equivalent and ca. three equivalent-reduced samples. The evidently small contribution of lifetime broadening to the observed linewidth limits the precision of $T_2$ estimates based on such a procedure. Within the reported error limits, the ratio of the $T_2$ values in the two samples may be as high as 1.67 or as low as 0.6. The results of unpublished spin-echo measurements of $T_2(Cu_A)$ in the same samples are described by Goodman and Leigh but are not employed in their calculations; the directly measured values of $T_2(Cu_A)$ indicate that $T_2$ is increased approximately twofold upon reduction of cytochrome a. This increment in $T_2$ is just sufficient to explain their observations (a ca. twofold increase in $T_1T_2(Cu_A)$) without involving any $T_1$ effect at all, but a significant $T_1$ effect is the basis of their distance estimate.

In the present analysis, it was assumed that $T_2$ effects are dominant, which constrains the resulting distance estimate the least, and which is just what the spin-echo measurements imply. A larger distance estimated is obtained, because the $T_2$ effect can be more efficient at long range (48). Because a magnetic dipolar-induced increment to $1/T_1$ requires the participating sites

to be closer to each other, the direct measurement of $T_1$ in similar samples by the pulsed saturation-recovery method of Scholes et al. (47) would immediately lead to a more precise distance estimate.

REFERENCES

1. Wikstrom, M., Krab, K., and Saraste, M. (1981). Cytochrome Oxidase: A Synthesis, Academic Press, New York.

2. Malmstrom, B.G. (1980). In Metal Ion Activation of Dioxygen (Spiro, T.G., Ed.), pp. 181-207, Wiley, New York.

3. Brunori, M., Antonini, E., and Wilson, M.T. (1981). Metal Ions in Biological Systems 13, 187-228.

4. Blair, D.F., Martin, C.T., Gelles, J., Wang, H., Brudvig, G.W., Stevens, T.H., and Chan, S.I. (1983). Chemica Scripta 21, 43-53.

5. Stevens, T.H., Martin, C.T., Wang, H., Brudvig, G.W., Scholes, C.P., and Chan, S.I. (1982). J. Biol. Chem. 257, 12106-12113.

6. Babcock, G.T., Vickery, L.E., and Palmer, G. (1976). J. Biol. Chem. 251, 7907-7919.

7. Thomson, A.J., Brittain, T., Greenwood, C., and Springall, J.P. (1976). FEBS Lett. 67, 94-98.

8. Babcock, G.T., Callahan, P.M., Ondrias, M.R., and Salmeen, I. (1981). Biochemistry 20, 959-966.

9. Peisach, J. (1978). In Frontiers of Biological Energetics (Dutton, P.L., Leigh, J.S., and Scarpa, A., Eds.), Vol. 2, pp. 873-881, Academic Press, New York.

10. Martin, C.T., Scholes, C.P., and Chan, S.I. (1985). J. Biol. Chem. 260, 2857-2861.

11. Stevens, T.H., and Chan, S.I. (1981). J. Biol. Chem. 256, 1069-1071.

12. Brudvig, G.W., Stevens, T.H., Morse, R.H., and Chan, S.I. (1981). Biochemistry 20, 3912-3921.

13. Powers, L., Chance, B., Ching, Y., and Angiolillo, P. (1981). Biophys. J. 34, 465-498.

14. Martin, C.T., Scholes, C.P., and Chan, S.I. (1985). J. Biol. Chem., in press.

15. Tweedle, M.F., Wilson, L.J., Garcia-Iniguez, L., Babcock, G.T., and Palmer, G. (1978). J. Biol. Chem. 253, 8065-8071.

16. Keilin, D., and Hartree, E.F. (1939). Proc. R. Soc. London Ser. B 127, 167-191.

17. Tiesjema, R.H., Muijsers, A.O., and Van Gelder, B.F. (1973). Biochim. Biophys. Acta 305, 19-28.

18. Leigh, J.S., Wilson, D.F., Owen, C.S., and King, T.E. (1974). Arch. Biochem. Biophys. 160, 476-487.

19. Mackay, L.N., Kuwana, T., and Hartzell, C.R. (1973). FEBS Lett. 36, 326-329.

20. Babcock, G.T., Vickery, L.E., and Palmer, G. (1978). J. Biol. Chem. 253, 2400-2411.

21. Schroedl, N.A., and Hartzell, C.R. (1977). Biochemistry 16, 4961-4965.

22. Schroedl, N.A., and Hartzell, C.R. (1977). Biochemistry 16, 4966-4971.

23. Gibson, Q.H., and Greenwood, C. (1965). J. Biol. Chem. 240, 2694-2698.

24. Horie, S., and Morrison, M. (1963). J. Biol. Chem. 238, 2859-2868.

25. Vanneste, W.H., and Vanneste, M.-T. (1965). Biochem. Biophys. Res. Commun. 19, 182-186.

26. Blair, D.F., Bocian, D.F., Babcock, G.T., and Chan, S.I. (1982). Biochemistry 21, 6928-6935.

27. Lemberg, M.R. (1969). Physiol. Revs. 49, 48-121.

28. Powers, L., Blumberg, W.E., Chance, B., Barlow, C.H., Leigh, J.S., Jr., Smith, J., Yonetani, T., Vik, S., and Peisach, J. (1979). Biochim. Biophys. Acta 546, 520-538.

29. Beinert, H., Shaw, R.W., Hansen, R.E., and Hartzell, C.R. (1980). Biochim. Biophys. Acta 591, 458-470.

30. Wilson, D.F., and Leigh, J.S. (1974). Ann. N.Y. Acad. Sci. 227, 630-635.

31. Wikstrom, M.K.F., harmon, H.J., Ingledew, W.J., and Chance, B. (1976). FEBS Lett. 65, 259-277.

32. Chan, S.I., Brudvig, G.W., Martin, C.T., and Stevens, T.H. (1982). In Electron Transport and Oxygen Utilization (Ho, C., Ed.), pp. 171-177, Elsevier, Amsterdam.

33. Beinert, H., Griffiths, D.E., Wharton, D.C., and Sands, R.H. (1962). J. Biol. Chem. 237, 2337-2346.

34. Hartzell, C.R., and Beinert, H. (1974). Biochim. Biophys.

Acta 369, 318-338.

35. Van Gelder, B.F. (1966). Biochim. Biophys. Acta 118, 36-46.

36. Stannard, J.N., and Horecker, B.L. (1948). J. Biol. Chem. 172, 599-608.

37. Brittain, T., Greenwood, C., and Johnson, A. (1977). Biochem. J. 167, 531-534.

38. Stevens, T.H., Brudvig, G.W., Bocian, D.F., and Chan, S.I. (1979). Proc. Natl. Acad. Sci. USA 76, 3320-3324.

39. Rupp, H., Rao, K.K., Hall, D.O., and Cammack, R. (1978). Biochim. Biophys. Acta 537, 255-269.

40. Wilson, D.F., and Nelson, D. (1982). Biochim. Biophys. Acta 680, 233-241.

41. Bocian, D.F., Lemley, A.T., Peterson, N.O., Brudvig, G.W., and Chan, S.I. (1979). Biochemistry 18, 4396-4402.

42. Antonini, E., Brunori, M., Colosimo, A., Greenwood, C., and Wilson, M.T. (1977). Proc. Natl. Acad. Sci. USA 74, 3128-3132.

43. Gray, H.B., and Solomon, E.I. (1981). In Copper Proteins (Spiro, T.G., Ed.), Chapter 1, Wiley-Interscience, New York.

44. Babcock, G.T., Ondrias, M.R., Gobeli, D.A., van Steelandt, J., and Leroi, G.E. (1979). FEBS Lett. 108, 147-151.

45. Davis, R.C., Ditson, S.L., Fentiman, A.F., and Pearlstein, R.M. (1981). J. Am. Chem. Soc. 103, 6823-6826.

46. Jensen, P., Wilson, M.T., Aasa, R., and Malmstrom, B.G. (1984). Biochem. J. 224, 829-837.

47. Scholes, C.P., Janakiraman, R., Taylor, H., and King, T.E. (1984). Biophys. J. 45, 1027-1030.

48. Brudvig, G.W., Blair, D.F., and Chan, S.I. (1984). J. Biol. Chem. 259, 11001-11009.

49. Goodman, G., and Leigh, J.S., Jr. (1985). Biochemistry 24, 2310-2317.

50. Stapleton, H.J., Allen, J.P., Flynn, C.P., Stinson, D.G., and Kurtz, S.R. (1980). Phys. Rev. Lett. 45, 1456-1459.

# CHAPTER III. SPECTROELECTROCHEMICAL STUDY OF CYTOCHROME *a* AND $Cu_A$ IN CARBON MONOXIDE-INHIBITED CYTOCHROME *c* OXIDASE

## INTRODUCTION

During mitochondrial electron transport, cytochrome *c* shuttles reducing equivalents from the membrane-bound cytochrome $bc_1$ complex to a binding site (1,2) or sites (3) on cytochrome *c* oxidase. Electrons transfer rapidly from bound cytochrome *c* to cytochrome *a* of the oxidase. The apparent first-order rate constant for this electron transfer is greater than 1000 $s^{-1}$ under some conditions (2), indicating that these sites are fairly close to each other in the bimolecular complex. The $Cu_A$ site in the oxidase is also reduced by cytochrome *c* fairly rapidly (ca. 100 $s^{-1}$, 4); it is not known with certainty whether this electron transfer is direct or takes place via cytochrome *a*.

While details of the electron pathways are debated, it is generally agreed that $Cu_A$ and cytochrome *a* catalyze electron transfer between cytochrome *c* and the metals of the dioxygen reduction site of the enzyme. $Cu_A$ exhibits unusual spectroscopic properties which have made it the subject of many chemical (5) and spectroscopic (6) investigations. The unusual spectroscopic parameters of the $Cu_A$ site (7,8), which must reflect a structure different from those of other metalloprotein copper sites, have led Chan and co-workers (9) to suggest that $Cu_A$ is also important in the energy-transducing functions of cytochrome oxidase, specifically as the site of redox-coupled proton pumping. A variety of circumstantial evidence has led Wikstrom and co-workers (10,11) and Babcock and co-workers (12) to suggest instead that cytochrome *a* is the proton pump.

The oxidase contains two other prosthetic groups which together constitute the site of dioxygen reduction: A high-spin iron in another heme A, called cytochrome $a_3$, and another copper ion called $Cu_B$. These ions are situated close (ca. 5Å) to each other, presumably in an optimal configuration for stabilizing the intermediates of dioxygen reduction. (For reviews of the oxidase structure and metal centers, see Refs. 13-17). Each of the four

metal centers of the oxidase is known to undergo oxidoreduction, as evidenced by optical and EPR measurements at various stages during enzymatic turnover with solution oxidoreductants and dioxygen (2,18-21). An electrochemical titration has demonstrated that the enzyme accepts four electrons upon complete reduction (22).

In an early spectrophotometrically monitored titration of cyanide-inhibited cytochrome oxidase with cytochrome c, Minnaert (23) measured the midpoint potential of cytochrome a to be 278 mV vs. NHE. However, the titration behavior of cytochrome a was not that expected for a Nernstian n=1 (one-electron acceptor) site; the observed Nernst plot slope was closer to n=0.5. It was subsequently proposed that the metal sites of the enzyme possess similar (within 100 mV) reduction potentials and interact anticooperatively (24-27). In such a situation, a departure from simple Nernstian behavior is predicted (24,28).

The nature and magnitude of the thermodynamically manifested intersite interactions have been the subject of many recent investigations. In all but one of these studies, the dominant interaction was postulated to be between cytochrome a and cytochrome $a_3$ (25,26,29,30). However, published optically-monitored titrations (23,31), as well as recent EPR studies (27), suggest that interaction between cytochrome a and $Cu_B$ is also important. The possibility of interactions involving $Cu_A$ has not previously been explored. A consideration of all of the possible intersite interactions requires a complex scheme in which the enzyme may take on any of 16 different states (2). This complexity, together with the problem of deconvolving the spectral contributions of each of the chromophores (25, 32 and references therein), has made it difficult to elucidate the redox properties of cytochrome oxidase in detail.

The redox behavior of the oxidase is simpler in the presence of ligands which bind to cytochrome $a_3$ and stabilize this site in one redox state. For example, cyanide stabilizes cytochrome $a_3$ in the oxidized state (31), while evidently allowing $Cu_B$ to undergo oxidoreduction if suitably low cyanide concentrations or long

equilibration times are employed (27). Carbon monoxide evidently stabilizes both cytochrome $\underline{a}_3$ and $Cu_B$ in their reduced states (33). Ligand binding thus decreases the number of overall redox states accessible to the enzyme, and simplifies the interaction problem accordingly.

In order to more completely characterize the thermodynamic properties of the metal centers of cytochrome c oxidase, a series of spectroelectrochemical experiments have been carried out under a variety of conditions of temperature, ionic strength, and pH. The initial studies have employed the carbon monoxide derivative of the enzyme, in which only cytochrome a and $Cu_A$ undergo oxidoreduction. By treating this relatively simple problem first, it has proven possible to characterize the thermodynamic properties of cytochrome a in detail, and to measure the temperature dependence of the reduction potential of $Cu_A$.

The measurements show that the reduction potential of cytochrome a is only weakly (-9 mV/pH unit) dependent upon pH in the physiological range, indicating that reduction of this site is not stoichiometrically linked to protonation. A negligible dependence upon ionic strength was observed. The temperature dependence of the reduction potential of cytochrome a is steeper, and its standard entropy of reduction more negative, than those of other cytochromes, suggesting that a substantial conformational change accompanies cytochrome a reduction. Complexation by cytochrome c (2 equivalents) has no measurable effect upon either the reduction potential of cytochrome a or upon its temperature dependence. The temperature dependence of the $Cu_A$ reduction potential indicates that the standard entropy of reduction of this site is also relatively large and negative.

Even in the carbon monoxide-inhibited enzyme, markedly non-Nernstian behavior was observed for both the cytochrome a and $Cu_A$ sites. This behavior is most readily interpreted in terms of an anticooperative interaction between cytochrome a and $Cu_A$, which causes the reduction potential for one to be decreased by 20-40 mV upon reduction of the other. Analysis of data from experiments in

which the iron and copper sites were monitored simultaneously shows that these data are in all respects consistent with this interaction model. An interaction of this kind, which has not previously been suggested, is expected to influence the steady-state electron transfer properties of the enzyme.

## MATERIALS AND METHODS

Materials. Cytochrome c oxidase was purified from beef heart mitochondria by the method of Hartzell and Beinert (34) and was stored frozen at -80 °C. Protein concentration was determined by the method of Lowry, et al. (35) and heme concentration by the reduced minus oxidized extinction of the uninhibited enzyme at 604 nm using an extinction coefficient of 24 $mM^{-1}$ $cm^{-1}$ (36). The purified enzyme contained 8 nmol heme a per mg. protein and its activity in a polaragraphic assay was 90 (+/- 11) electrons transferred to oxygen per oxidase molecule per second. Just prior to use, the enzyme was thawed and dialyzed into potassium phosphate buffer containing 0.5% Tween-20. Phosphate buffer was used because the pH of phosphate, unlike that of Tris, is relatively insensitive to temperature. Following dialysis, samples were centrifuged at 35,000xg for 30 minutes to remove insoluble material. Enzyme concentrations were typically 0.10-0.15 mM in thin-layer experiments and 0.04 mM in experiments using the long pathlength cell. Horse heart cytochrome c (Sigma Type VI) was chromatographically purified on Whatman CM-52 cellulose prior to use (37).

All buffer solutions were prepared using glass-distilled water and research grade reagents. Hexammineruthenium trichloride was obtained from Alfa and purified by the method of Pladziewicz et al. (38). Hydroxymethylferrocene (Strem Chemicals) and 1,1'-Bis(hydroxymethyl)ferrocene (Research Organic/Inorganic Chemical Corp.) were used as received. Pentamminepyridineruthenium perchlorate was prepared as previously described (39). The above redox mediators (see Table 1) were selected because they have a negligible absorbance in the 400-700 nm region at the concentrations used and have reduction potentials that allow the solution potential to be poised from -50 to +550 mV vs. NHE. Equilibrium dialysis experiments indicated that these mediators do not bind strongly to the enzyme.

Apparatus. Reduction potential measurements were made using

Table I. Redox Mediators Employed in This Study

| Mediator | $E^{o\prime}$ (mV vs. NHE) | No. of Equiv. Used | |
|---|---|---|---|
| | | thin-layer | long path |
| $[(NH_3)_6Ru]Cl_3$ | +51 | 1 | 5 |
| $[(NH_3)_5pyRu](ClO_4)_3$ | +260 | 1 | 5 |
| Hydroxymethylferrocene | +405 | 0.5 | 2.5 |
| 1,1'-Bis(hydroxymethyl)ferrocene | +465 | 0.5 | 2.5 |

an Optically Transparent Thin-Layer Electrode (OTTLE) cell similar to that described by Taniguchi et al. (40) for studies in which the relatively strong cytochrome absorptions were monitored, or a 2 cm pathlength cell designed by W.R. Ellis at Caltech for experiments in which the much weaker ($\Delta\varepsilon$ = 2000 $M^{-1}$ $cm^{-1}$) near infrared $Cu_A$ absorption was monitored. The OTTLE cell was machined from lucite and employed quartz windows (path length ca. 0.47mm). The working electrode material consisted of two pieces of 500 line/in. electroformed gold mesh soldered to a copper wire. The long pathlength cell was machined from lucite and had quartz windows; its working electrode was a thin gold foil which lined the bottom and the sides of the cell. The long pathlength cell contained approximately 0.7 ml of sample which was stirred during equilibration periods (but not during spectrum acquisition) by a small magnetic stirring bar. A Sargent-Welch S-30080-17 miniature calomel reference electrode was used along with a platinum wire counter electrode. The spectroelectrochemical cell/electrode assemblies were contained in a gas-tight stainless steel shroud in order to maintain strict anaerobicity.

Cell temperatures were varied using a Forma Model 2095 constant temperature bath and measured directly (+/- 0.2 $^{o}C$) with an Omega Engineering, Inc. miniature copper-constantan thermocouple placed in the protein solution in close proximity to the sample. A Princeton Applied Research Model 174A potentiostat was used to control the potentials applied across the protein solutions. The potentials were measured (+/- 0.1 mV) with a digital multimeter. UV-visible spectra were obtained with a Cary 219 spectrophotometer interfaced to a Spex Industries SCAMP SC-31 data processor. The spectral bandwidth was 0.55 nm for OTTLE experiments and 3 nm for long pathlength experiments.

Methods. After the addition of redox mediators, enzyme and buffer solutions were thoroughly degassed on a vacuum apparatus and subsequently allowed to stir under one atmosphere of CO (99.99%, Matheson) for at least thirty minutes. The CO-saturated solutions, spectroelectrochemical cell, electrodes, and shroud were then

transferred into an inert atmosphere box where the spectroelectrochemical cells were loaded, fitted with the reference and auxiliary electrodes, and placed into the air-tight container.

Enzyme/mediator solutions were poised at -50 mV vs. NHE for at least two hours in order to reduce the enzyme fully and form the CO-associated derivative (verified by a change in the Soret $\lambda_{max}$ from 443 to 430 nm or the formation of the characteristic spectral features in the 580-610 nm region, Ref. 41). Reduction potentials were determined by sequentially applying a series of potentials across the cell. Each potential was maintained, typically for 1 hour (thin-layer experiments) or 2 hours (long path experiments), until electrolysis ceased, as verified by cessation of spectral changes. At equilibrium, the value of the ratio of concentrations of oxidized to reduced forms, (Oxid/Red), of all redox couples in solution is established by the Nernst equation:

$$E(\text{applied}) = E^{o\prime} + 2.303RT/nF \quad \log\ (\text{Oxid/Red}) \qquad (1)$$

where $E^{o\prime}$ is the reduction potential of the redox couple (the prime signifies that the present measurements were made near neutral pH). Redox couples were converted in increments from one oxidation state to the other by the series of applied potentials, for which each value of (Oxid/Red) was determined from the corresponding overlay spectra. Care was taken to insure that oxidations were reversible: Re-reduction led to data closely superimposable with oxidative data (cf. Figs. 3,4). Absorption spectra were stored on magnetic disk; difference spectra were obtained by computer subtraction. At least 10 points were included in each Nernst plot.

In thin-layer experiments, the level of cytochrome a reduction was measured using the strong Soret absorbance of ferrous cytochrome a at 443 nm. The state of $Cu_A$ was monitored by the intensity of the absorption band centered at 830nm. The bulk of available evidence indicates that this band is due almost entirely to $Cu_A$ (Chapter II,16,42). The intensity of the $Cu_A$ absorbance was measured as the area under the spectrum and above a straight line connecting

the data at 740nm and 900nm. This area was taken as a measure of the concentration of oxidized $Cu_A$ in calculating values of log(ox/red) at each potential. In long pathlength experiments, the level of reduction of cytochrome a was monitored simultaneously by the absorbance change at 604nm, which is due entirely to cytochrome a in the carbon monoxide-inhibited enzyme (41).

The measured absorbance changes for both $Cu_A$ and cytochrome a did not show the behavior expected of single-electron acceptors. However, the behaviors of both cytochrome a and $Cu_A$ were well accounted for by postulating an interaction between these sites which causes the reduction potential for one to be decreased by approximately 40 mV upon reduction of the other. The reaction scheme appropriate to this situation is:

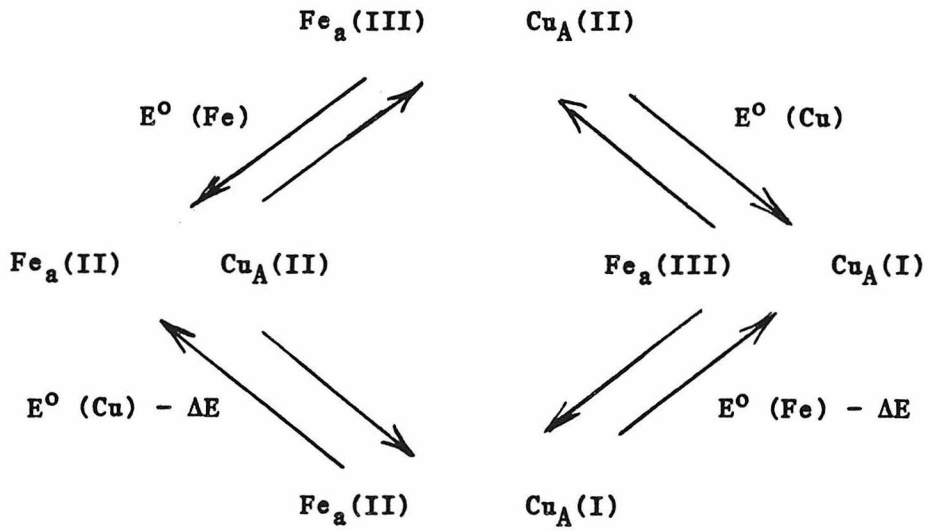


Scheme 1

In this scheme, $E^o$ (Fe) and $E^o$ (Cu) are the reduction potentials of the iron and copper sites when their respective interaction partners are oxidized, and $\Delta E$ is an interaction

potential which measures the decrease in reduction potential of one site which accompanies the reduction of the other site.

The equilibrium equations which describe Scheme 1 were used in a nonlinear least-squares fitting program to calculate the best-fit values for $E^o$, $\Delta E$, and the potential of the hypothetical site which interacts with the site under observation. In long pathlength experiments where both the cytochrome _a_ and $Cu_A$ sites were monitored simultaneously, the optimal values of these parameters were calculated using both the $Cu_A$ data and the cytochrome _a_ data. Finally, in long pathlength experiments the values of $E^o$(Fe) estimated using the 604 nm data were used as fixed parameters in refitting the $Cu_A$ data at each temperature, thus improving the determinations of $E^o$(Cu) and $\Delta E$.

It should be noted that in the present interactive situation, the conventionally defined midpoint potential is no longer useful as a measure of the intrinsic properties of the site, since it is sensitive not only to the properties of the site but to the potential of its interaction partner and the strength of the interaction. The potentials reported here are those which pertain when the interacting partner is <u>oxidized</u>; in the present situation, where the interaction is anticooperative, this is the higher of the two potentials which may be defined. Potentials defined in this way are meaningful measures of the intrinsic thermodynamic properties of the sites, because they pertain under a single, specific set of conditions with regard to the interaction(s) which influence the potentials.

To avoid oxidation of the $Fe_{a_3}/Cu_B$-CO site, potentials above 420 mV (vs. NHE) were not applied to the sample solutions. (Higher potentials caused irreversible changes which probably involve the depletion of the carbon monoxide by oxidation to carbon dioxide (43,44)). Oxidation of the cytochrome _a_ and $Cu_A$ sites was thus not complete at the highest potentials used. A correction for this incomplete oxidation was applied in the following manner: The values for $E^{o\prime}$ which were estimated from the initial computer fits were used to calculate the fractions of cytochrome _a_ and $Cu_A$ which

remained reduced at the highest potentials applied. The corresponding predicted absorbance difference was then added to the observed absorbance changes, to obtain a corrected fully oxidized endpoint. Using the corrected absorbance differences, new values of log (Oxid/Red) were calculated, and new estimates of $E^{o\prime}$ were obtained from computer fits. The refined estimates of $E^{o\prime}$ were sufficiently close (within 3 mV) to those employed in the initial correction to verify the self-consistency of this treatment, and the Nernst plots obtained adhered more closely to the predicted high-potential asymptotic behavior.

Standard entropies of reduction were obtained from the slopes of plots of reduction potential vs. temperature, essentially as described by Taniguchi et al. (40). In previous metalloprotein titrations using the OTTLE cell (40,45), the reference electrode was maintained at a constant (room) temperature while the sample temperature was varied. This so-called nonisothermal electrode arrangement substantially simplifies the measurement of standard entropies of reduction if, as has been demonstrated previously (40,45), the various thermal junction potentials may be neglected. Because of the need for strict anaerobicity, the sample cell and reference electrode were placed together inside a stainless steel chamber in the present experiments, which resulted in partial thermostatting of the reference electrode along with the sample. Control experiments using two thermocouples were carried out to measure the extent of this partial thermostatting of the reference electrode, and the measured potentials were corrected accordingly for the temperature dependence of the potential (vs. NHE) of the saturated calomel electrode. In order to obtain standard entropies of reduction on a meaningful absolute scale, the reaction entropy of the normal hydrogen electrode half-cell (15.6 e.u., 46) is ordinarily substracted from the reaction entropies measured for the overall redox reaction involving both the NHE and the redox half-reaction of interest (40). In the present situation, in which the SCE reference electrode is partially thermostatted, the NHE (which is formally, if not actually, used to obtain standard

entropies of reduction from the measurements) is in effect also partially thermostatted, so that the entire reaction entropy for the NHE half-cell is not expressed in the measured overall reaction entropy. Thus, only a fraction of the NHE reaction entropy, equal to the fractional nonisothermal character of the electrode arrangement, should be subtracted from the measured entropy of the overall reaction. The deviation of the reference electrode temperature from room temperature was found to be linearly related to the difference between the sample temperature and room temperature, so that the fractional nonisothermal character of the electrode arrangement could be simply defined:

$$FNC = \frac{\Delta T_s - \Delta T_r}{\Delta T_s} \qquad (2)$$

where $\Delta T_s$ is the difference between the sample temperature and room temperature and $\Delta T_r$ is the difference between the reference electrode temperature and room temperature. Standard entropies of reduction have therefore been corrected according to the following formula:

$$\delta(\Delta S^o) = (1 - FNC)* \Delta S_{rc}\ (SCE) + (1 - FNC)*(15.6) \qquad (3)$$

where $\Delta S_{rc}$ is the entropy of reduction of the SCE obtained directly from a plot of the temperature dependence of the potential of the SCE, measured relative to the NHE. Since $\Delta S_{rc}$ (SCE) is -15.3 e.u., the two terms in the correction very nearly cancel each other (i.e., to within 2%), and the net correction to $\Delta S^o$ is very small. The smallness of the correction reflects the fact that the <u>standard</u> entropy of reduction of the SCE is very small (ca. 0.3 e.u.) in the convention where the NHE is assigned a reduction entropy of 15.6 units. The reported error estimates in the thermodynamic parameters are the standard errors of determination in the relevant parameters

obtained from linear least-squares computer fits of the reduction potential vs. temperature data.

RESULTS

Overlay difference spectra obtained in a typical thin-layer experiment are displayed in Figure 1. A linear relation between $\Delta A_{605}$ and $\Delta A_{443}$, with a slope consistent with measurements of the reduced minus oxidized spectrum of cytochrome a (32,47) was observed (plot not shown), indicating that only cytochrome a is titrated at the potentials used. At potentials above 420 mV, similar plots showed departures from linearity which indicate that the ferrocytochrome $a_3$-CO complex is partially oxidized at these high potentials.

Near-infrared absorbance difference spectra obtained during a spectroelectrochemical titration using the long-pathlength cell are shown in Figure 2. The spectra indicate that the titration is very nearly reversible, except for minor baseline drift. The difference spectrum obtained during the high-potential half of the titration (140mV - 35mV) was not significantly different from that obtained during the low-potential half of the titration (35mV - (-200mV)) (spectra not shown), indicating that the absorbance properties of $Cu_A$ did not change during the course of the titration. A change in the shape of the spectrum would be expected, for example, if reduction of cytochrome a (whose reduction potential is close to that of $Cu_A$ under these conditions) caused a large change in the structure of the $Cu_A$ site (cf. the minor structural change implied by EPR data, Chapter II).

Nernst plots of the spectral data of Figures 1 and 2 are shown in Figures 3 and 4. The plots are not as expected for simple n = 1 Nernstian processes (which, from equation 1, is a straight line with slope 56 mV/decade at 9.8 °C). The slope of the observed Nernst plots is a strong indication of anticooperative interaction among the metal sites in the enzyme (24,28). The line through the data points in Figure 3 is the computer-generated best fit to a model in which cytochrome a participates in an anticooperative interaction of magnitude 24mV with another site whose potential is 256mV vs. NHE. The line through the data points in Figure 4 is the

Figure 1. Representative set of absorbance difference spectra of cytochrome a at different applied potentials in a thin-layer spectroelectrochemical titration of carbon monoxide-inhibited cytochrome oxidase. Sample conditions: Temperature = 9.8 °C, pH = 7.0, ionic strength = 0.220 M. Applied potentials (mV vs. NHE): (A) 29.8, (B) 149.8, (C) 179.8, (D) 209.8, (E) 224.8, (F) 239.8, (G) 254.8, (H), 269.8, (I) 284.8, (J) 299.8, (K) 314.8, (L) 329.8, (M) 344.8, (N) 359.8, (O) 389.8. The most oxidized spectrum (measured at 389.8 mV vs. NHE) has been subtracted from the spectra recorded at each potential to yield the difference spectra shown.

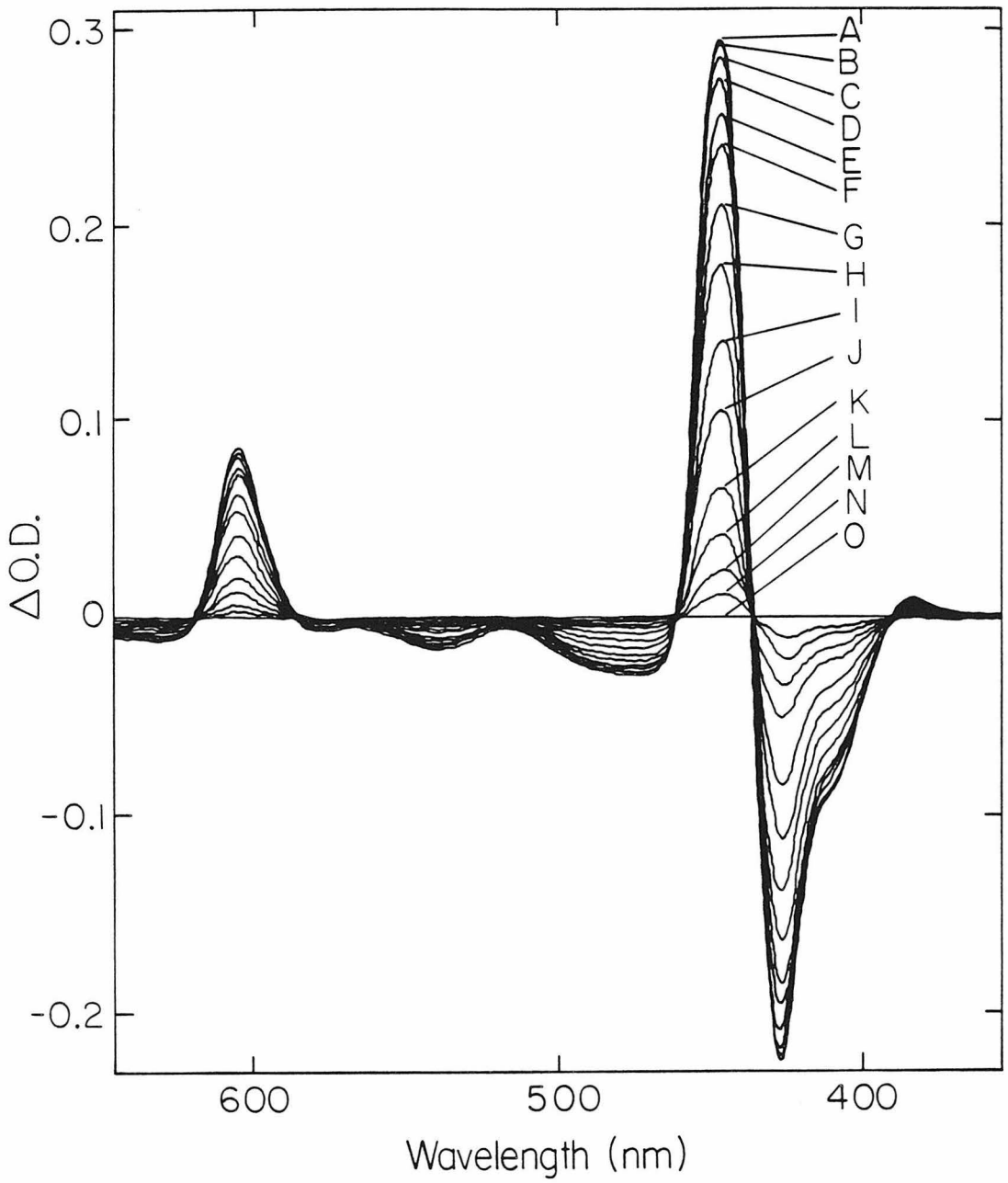
0.3
0.2
0.1
0
-0.1
-0.2
ΔO.D.
600
500
400
Wavelength (nm)
A
B
C
D
E
F
G
H
I
J
K
L
M
N
O

Figure 2. Near-infrared absorbance difference spectra obtained during a titration of carbon monoxide-inhibited cytochrome c oxidase at pH 7.0, 8 °C. The indicated potentials are relative to SCE (to obtain mV vs. NHE, add approximately 255 mV at this temperature); all spectra are referenced to the spectrum of the fully reduced enzyme obtained at a potential of -200 mV vs. SCE. The enzyme concentration was approximately 40 μM. The redox mediators employed are not expected to make a significant contribution to the absorbance changes observed in this region of the spectrum.

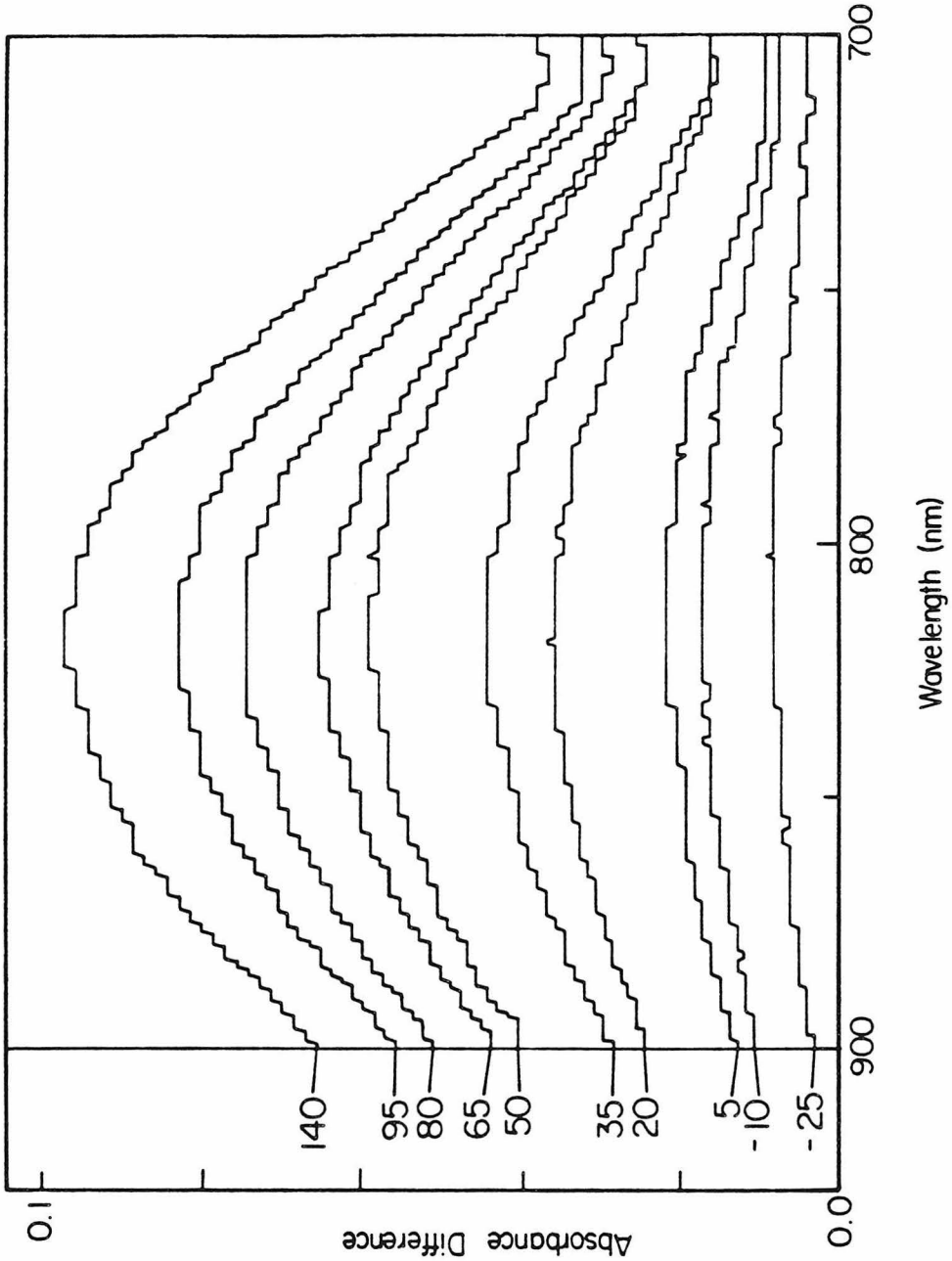
0.1
0.0
Absorbance Difference
140
95
80
65
50
35
20
5
-10
-25
900
800
700
Wavelength (nm)

Figure 3. Nernst plot calculated from the spectra shown in Figure 1 by using $\Delta A_{443}$. The solid line is the computer-generated best fit to a model in which the cytochrome a site participates in an anticooperative interaction of magnitude 24 mV with another site whose potential is 256 mV vs. NHE. (■) and (□) were obtained on oxidation and re-reduction, respectively.

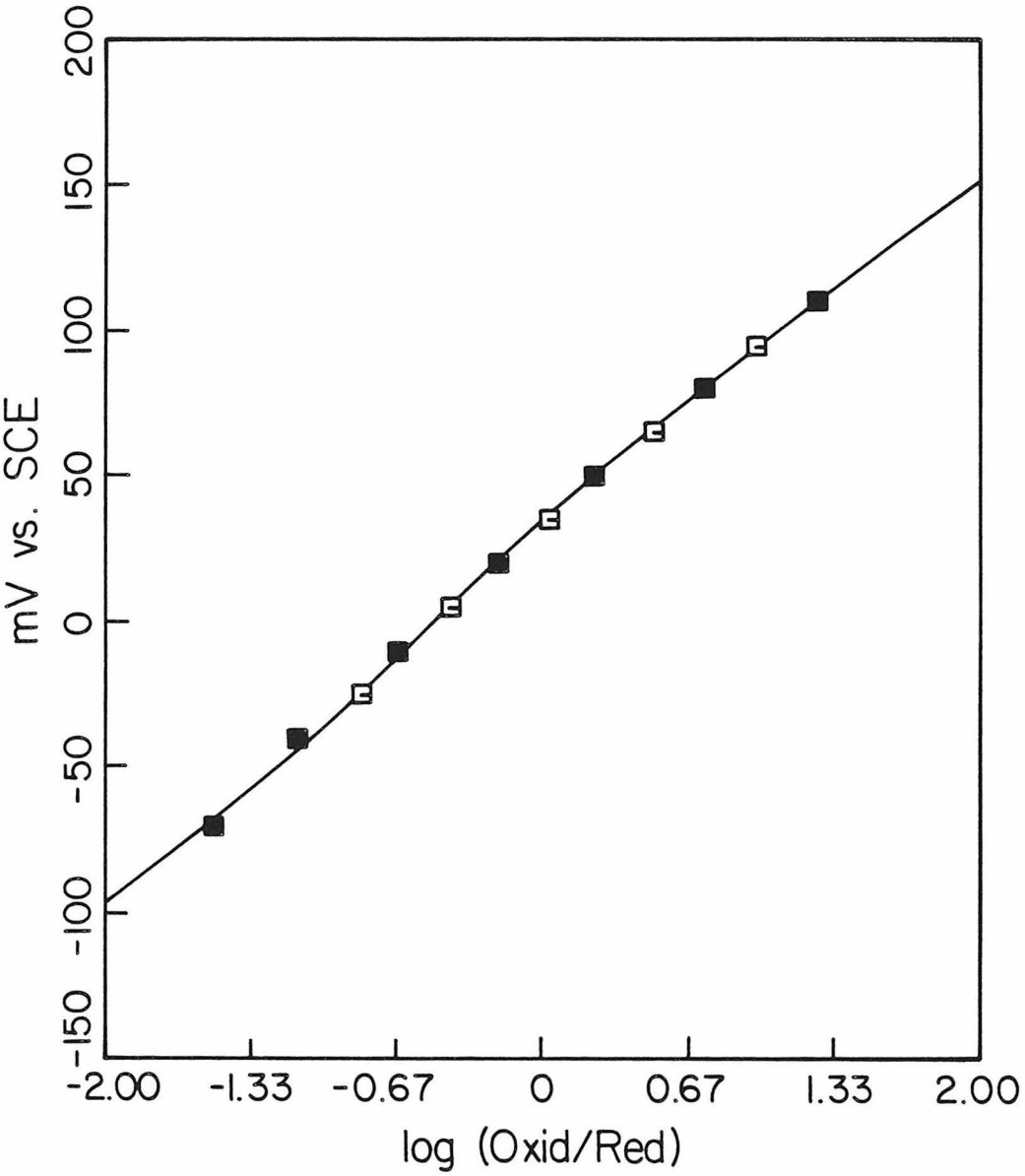
200
150
100
50
0
-50
-100
-150
mV vs. SCE
-2.00
-1.33
-0.67
0
0.67
1.33
2.00
log (Oxid/Red)

**Figure 4. Nernst plot of the near-infrared absorbance changes measured during the titration of Figure 2. The line through the data points is the computer-generated best fit appropriate to the interaction model described in the text. Open circles: oxidation. Filled circles: re-reduction.**

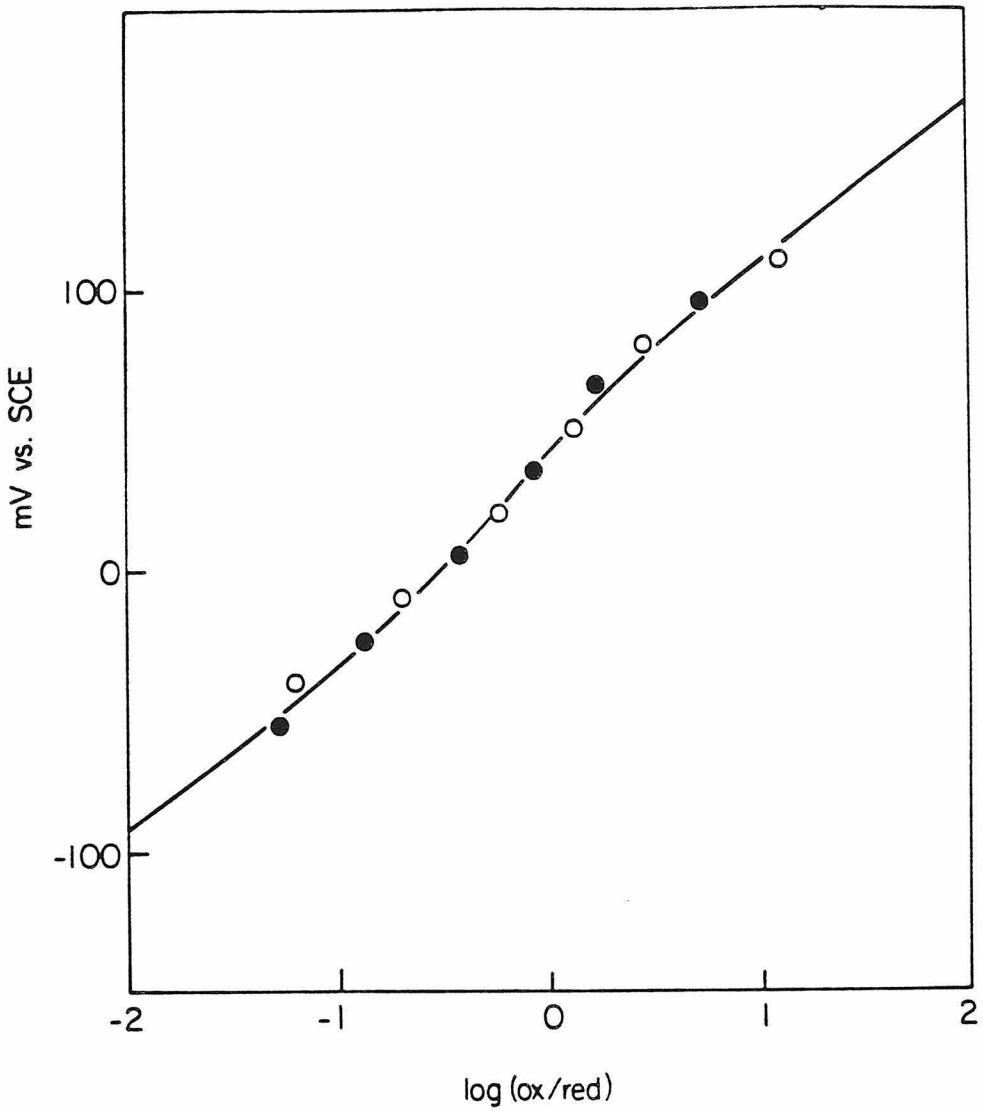
100
0
-100
mV vs. SCE
-2
-1
0
1
2
log (ox/red)

computer-generated best fit appropriate to a model in which $Cu_A$ participates in an anticooperative interaction of magnitude 42 mV with another site whose reduction potential is 298 mV vs. NHE. The data of Figures 3 and 4 were obtained on different enzyme batches. In thin-layer experiments where only cytochrome a was monitored, the interaction potential varied between 20 and 40 mV among different enzyme batches. When the two sites were monitored simultaneously, the interaction potential deduced from the $Cu_A$ data (39 +/- 2 mV) was in agreement with that deduced from the cytochrome a data (42 +/- 6 mV).

The temperature dependence of the cytochrome a reduction potential at pH 7.0 is shown in Figure 5. The thermodynamic parameters deduced from a linear least-squares fit to the data are: $\Delta G^{o\prime}$(25 °C) = -6.37 +/- 0.05 kcal $mol^{-1}$, $\Delta H^{o\prime}$ = -18.7 +/- 0.8 kcal $mol^{-1}$, and $\Delta S^{o\prime}$ = -41.4 +/- 2.8 cal $mol^{-1}$. The temperature dependence of the cytochrome a reduction potential in the cytochrome oxidase:cytochrome c complex (2 equivalents of cytochrome c) is also displayed. At 25 °C, $E^{o\prime}$ is not significantly different in the complex with cytochrome c than in the uncomplexed enzyme (274 mV vs. NHE in the complex; 276 mV vs. NHE in the uncomplexed enzyme). The temperature dependence is also the same within experimental uncertainty, leading to the following estimates for the thermodynamic parameters: $\Delta G^{o\prime}$(25 °C) = -6.32 +/- 0.05 kcal $mol^{-1}$, $\Delta H^{o\prime}$ = -17.5 +/- 1.2 kcal $mol^{-1}$, and $\Delta S^{o\prime}$ = -37.5 +/- 3.9 cal $mol^{-1}$ $K^{-1}$. The thermodynamic parameters for reduction of cytochrome a are compiled in Table II.

The temperature dependence of the $Cu_A$ reduction potential is shown in Figure 6. The thermodynamic quantities deduced from a straight-line fit to the data are $\Delta G^{o\prime}$(25 °C) = -6.64 +/- 0.08 kcal $mol^{-1}$, $\Delta H^{o\prime}$ = -17.1 +/- 1.0 kcal $mol^{-1}$, and $\Delta S^{o\prime}$ = -35 +/- 2.5 cal $mol^{-1}$ $K^{-1}$.

The reduction potential of cytochrome c, and its temperature dependence, were also measured in the complex with cytochrome oxidase (data not shown). The thermodynamic parameters for reduction of oxidase-complexed cytochrome c deduced from the data are: $\Delta G^{o\prime}$(25 °C) = -5.77 +/- 0.05 kcal $mol^{-1}$; $\Delta H^{o\prime}$ = -14.2 +/- 0.35

kcal $mol^{-1}$; and $\Delta S^{o\prime}$ = -28.4 +/- 1.1 e.u.. For comparison, the values measured for uncomplexed cytochrome c are $\Delta G^{o\prime}$(25 °C) = -6.00 +/- 0.05 kcal $mol^{-1}$, $\Delta H^{o\prime}$ = -14.5 +/- 0.4 kcal $mol^{-1}$, and $\Delta S^{o\prime}$ = -28.5 +/- 1.2 cal $mol^{-1}$ $K^{-1}$ (40). Thus, $\Delta G^{o\prime}$(25 °C) is slightly different from that measured in uncomplexed cytochrome c, but the data are not of sufficient precision to apportion the effect between enthalpic and entropic components.

The effect of pH on the reduction potential of cytochrome a is shown in Figure 7. A linear least-squares fit to the data yields a slope of -9 mV/pH unit. Significant degradation of the enzyme took place at pH values outside the extremes shown.

The cytochrome a reduction potential was measured at different ionic strengths between 0.05 M and 0.42 M (phosphate buffer, supplemented with KCl at the high ionic strengths). Within experimental uncertainty, no ionic strength dependence was observed (Figure 8).

Figure 5. Temperature dependence of the cytochrome a reduction potential in CO-inhibited cytochrome c oxidase (pH 7.0, ionic strength 0.220 M), in the uncomplexed oxidase (○) and in the presence of two equivalents of cytochrome c (●). The error bars shown represent the standard error of determination of $E^{o\prime}$ in nonlinear least-squares computer fits to the interaction model described in the text. The lines (solid = uncomplexed; dashed = complex with cytochrome c) are linear least-squares fits to the data, corresponding to the following thermodynamic parameters: Uncomplexed enzyme, $E^{o\prime}$(25 °C) = 276 +/- 3 mV vs. NHE; $\Delta G^{o\prime}$(25 °C) = -6.37 +/- 0.08 kcal $mol^{-1}$; $\Delta H^{o\prime}$ = -18.7 +/- 0.8 kcal $mol^{-1}$; $\Delta S^{o\prime}$ = -41.4 +/- 2.8 cal $mol^{-1}$ $K^{-1}$. Complex with cytochrome c, $E^{o\prime}$(25 °C) = 274 +/- 3 mV vs. NHE; $\Delta G^{o\prime}$(25 °C) = -6.32 +/- 0.08 kcal $mol^{-1}$; $\Delta H^{o\prime}$ = -17.5 +/- 1.2 kcal $mol^{-1}$; $\Delta S^{o\prime}$ = -37.5 +/- 3.9 cal mol-1 $K^{-1}$.

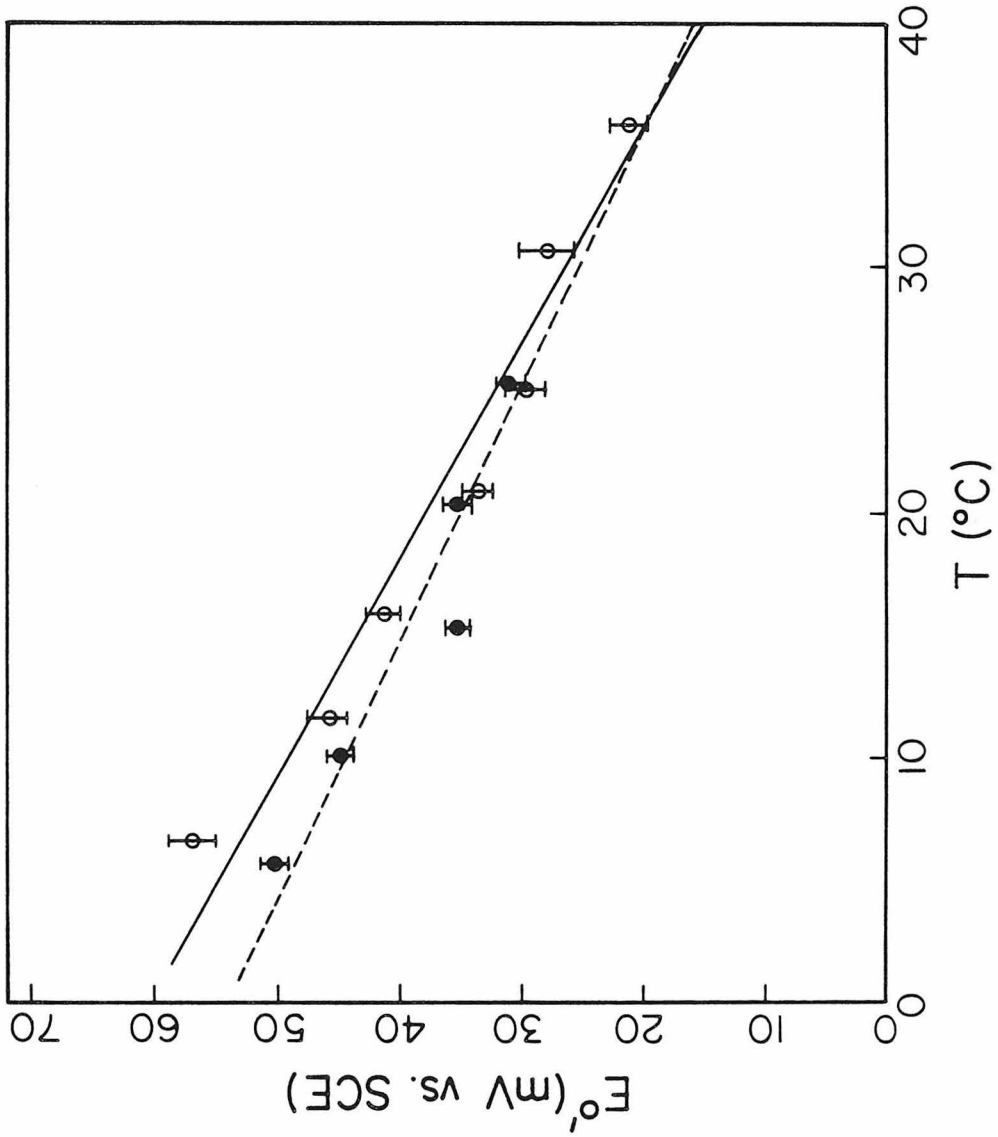
E°' (mV vs. SCE)
0
10
20
30
40
50
60
70
T (°C)
0
10
20
30
40

Figure 6. Temperature dependence of the reduction potential of $Cu_A$ in CO-inhibited cytochrome *c* oxidase. The straight line through the data points is the linear least-squares best fit and leads to the following estimates of the thermodynamic parameters for the reduction of $Cu_A$: $\Delta G^{o\prime}$(25 °C) = -6.62 +/- 0.08 kcal $mol^{-1}$, $\Delta S^{o\prime}$ = -35 +/- 2.5 cal $mol^{-1}$ $K^{-1}$, and $\Delta H^{o\prime}$ = -17.1 +/- 1.0 kcal $mol^{-1}$.

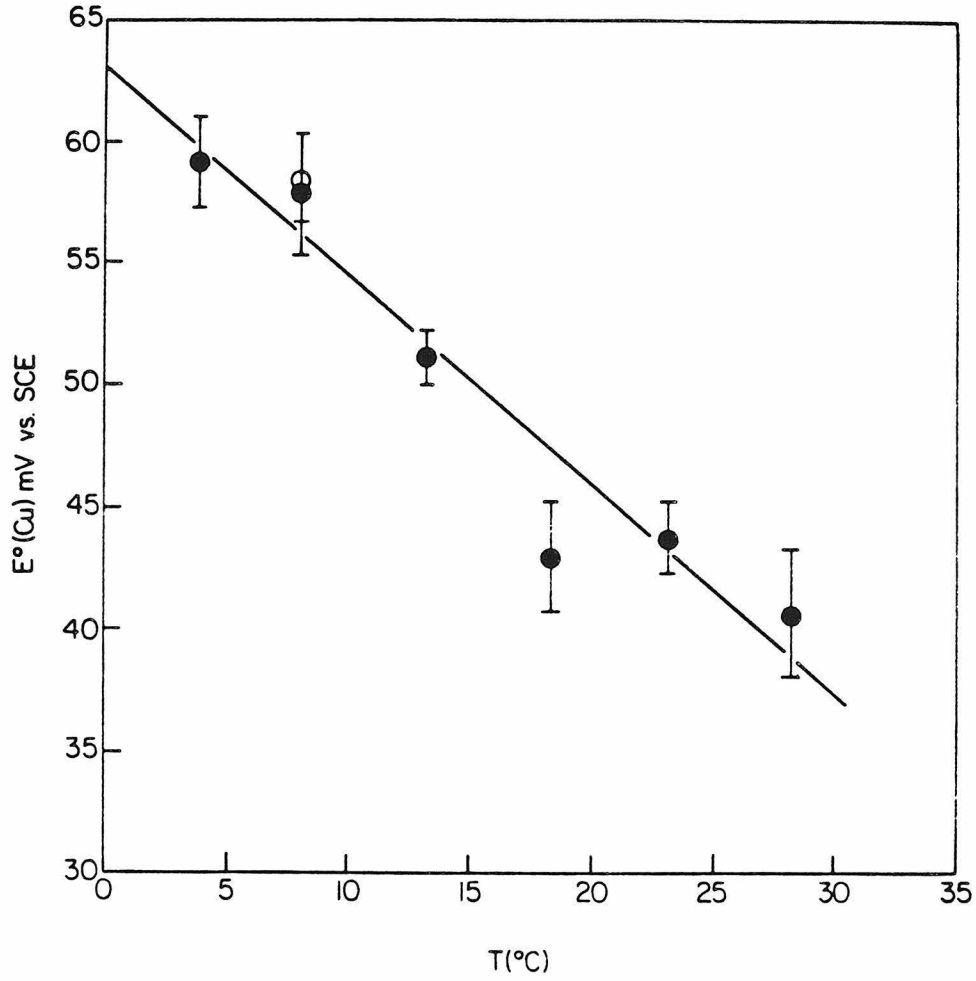
65
60
55
50
45
40
35
30
0
5
10
15
20
25
30
35
E°(Cu) mV vs. SCE
T(°C)

Table II. Thermodynamic Parameters for the Reduction of Cytochrome a in CO-inhibited Cytochrome Oxidase

| Parameter | Uncomplexed | + 2 Equiv. Cyt. c |
|---|---|---|
| $E^{o\prime}$ (mV vs. NHE) | 276 +/- 3 | 274 +/- 3 |
| $\Delta G^{o\prime}$ (kcal $mol^{-1}$) | -6.37 +/- 0.08 | -6.32 +/- 0.08 |
| $\Delta H^{o\prime}$ (kcal $mol^{-1}$) | -18.7 +/- 0.8 | -17.5 +/- 1.2 |
| $\Delta S^{o\prime}$ (cal $mol^{-1}$ $K^{-1}$) | -41.4 +/- 2.8 | -37.5 +/- 3.9 |

Figure 7. pH dependence of the cytochrome a reduction potential in CO-inhibited cytochrome c oxidase (9.8 °C, ionic strength 0.220 M). The solid line is a linear least-squares fit to the data, with slope -9mV/pH unit.

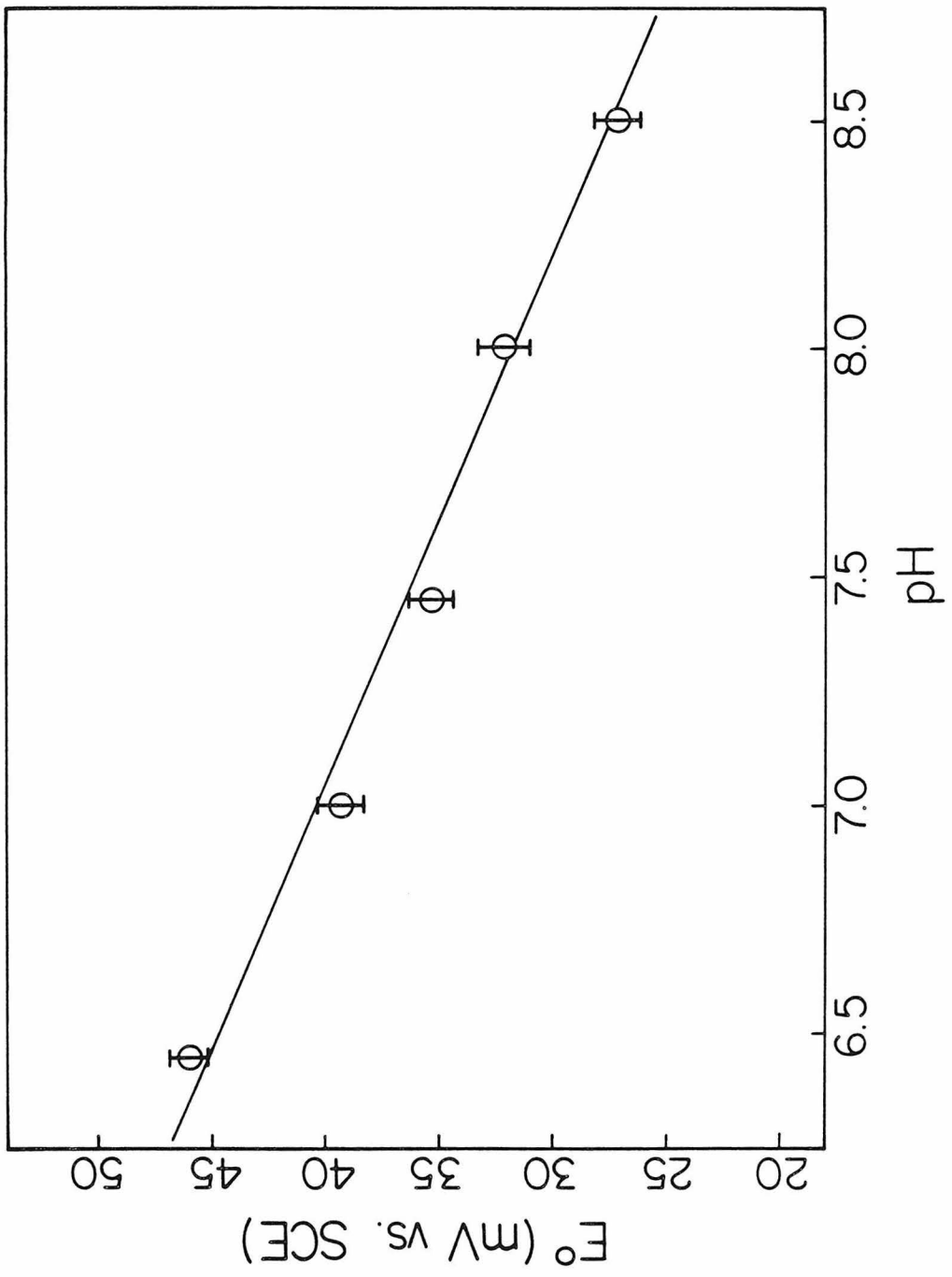
E° (mV vs. SCE)
20
25
30
35
40
45
50
pH
6.5
7.0
7.5
8.0
8.5

Figure 8. Ionic strength dependence of the cytochrome a reduction potential in CO-inhibited cytochrome c oxidase (9.8 °C, pH 7.0).

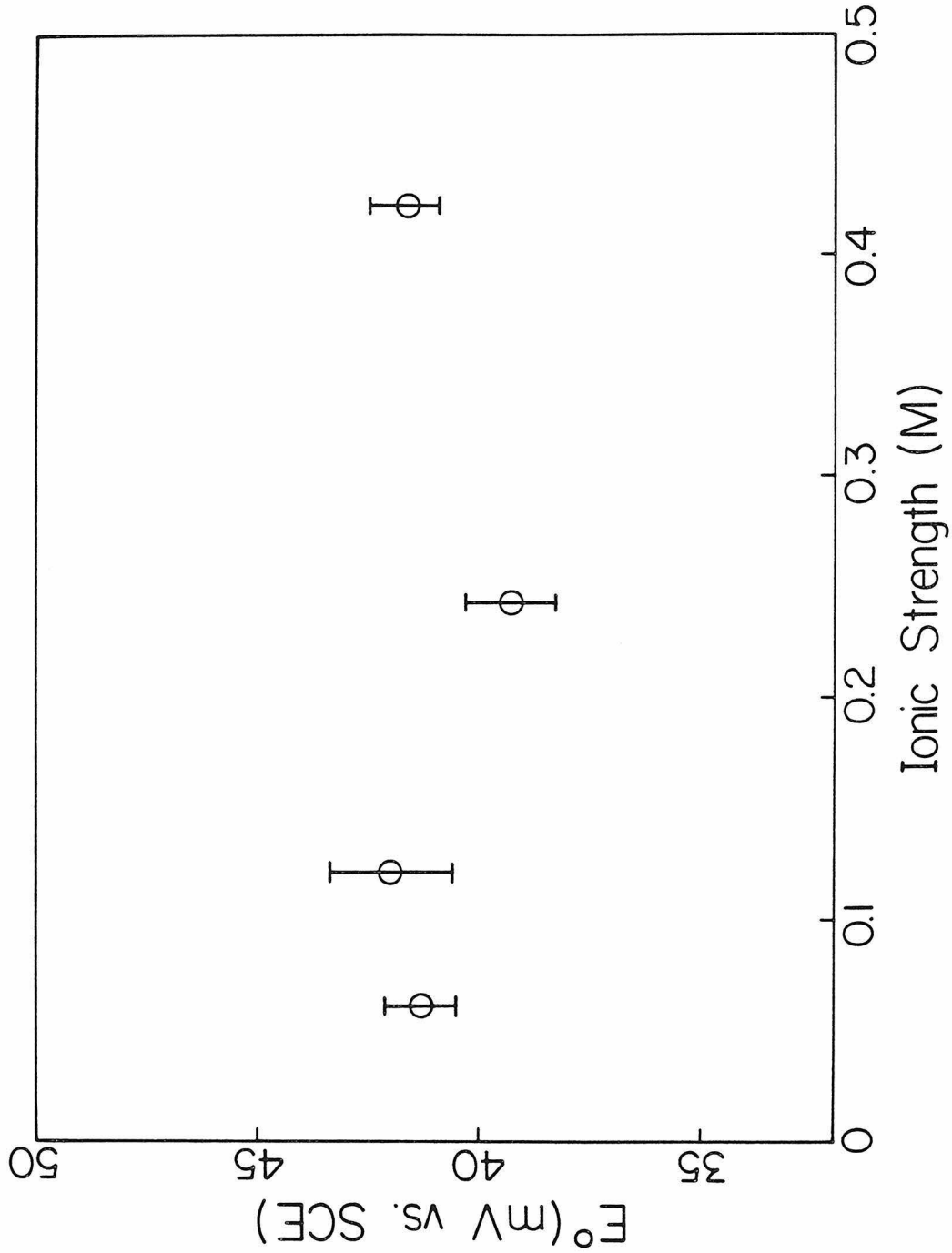
E°(mV vs. SCE)
50
45
40
35
0
0.1
0.2
0.3
0.4
0.5
Ionic Strength (M)

## DISCUSSION

Although several measurements of the cytochrome *a* reduction potential have been reported (25,48-50) for the CO derivative of cytochrome oxidase, none has carefully evaluated the effects of pH, ionic strength, and temperature. The available measurements (E(midpoint) = 250-255 mV vs. NHE at 24-25 °C) are in agreement with the values determined here.

Unlike previous studies, the present results are of sufficiently high precision to detect deviations from simple Nernstian behavior in both cytochrome *a* and $Cu_A$. Since cytochrome $a_3$ and $Cu_B$ remain reduced during the course of these experiments (33), the slightly sigmoidal appearance and non-integral slope of the data in Figures 3 and 4, if caused by intersite interaction, indicate that there is a previously unsuspected interaction between cytochrome *a* and $Cu_A$. The potentials of these sites are matched closely enough to allow such an interaction to be expressed. In the course of the various experiments on cytochrome *a*, some batch-to-batch variation in the interaction behavior was observed: The interaction potential, which measures the decrease in electron affinity of one site accompanying reduction of the other site, varied between ca. 20 and 40 mV in different enzyme batches. It should be stressed, however, that when cytochrome *a* and $Cu_A$ were monitored in the same batch, their interaction potentials were in agreement.

Various alternatives to intersite interactions may be proposed to explain non-Nernstian behavior, including electrostatic effects within a membrane-like aggregate (51) or intradimeric interactions (11). The present two-site system is the simplest interactive system which can be examined, and is thus ideally suited to the systematic study of the detailed aspects of the interaction. The data obtained from this system, in conjunction with the pertinent equilibrium analysis, furnish strong evidence for a thermodynamic interaction between cytochrome *a* and $Cu_A$, since they are consistent with this model in two key respects: First, the interaction potential

inferred from the data on the iron site is the same, within experimental error, as that inferred from the data on the copper site, and second, the potentials of the copper site which are inferred from the computer fits to the iron data, while less well determined by the fits and hence subject to some variation from one experiment to another, are in agreement with the copper potentials determined directly.

The anticooperative interaction between $Cu_A$ and cytochrome _a_ could take place via either an electrostatic mechanism or a conformational mechanism. The electron spin relaxation of $Cu_A$ in the CO-inhibited enzyme is made slower upon reduction of cytochrome _a_ (52), which suggests that these sites interact magnetically. However, magnetic dipolar broadening of the $Cu_A$ resonance by the spin on cytochrome _a_ has not been detected. The absence of any detectable dipolar splittings suggests an intersite distance greater than 13 Å (52, Chapter II). A 40 mV electrostatic interaction at this distance is unlikely.

Close examination of the lineshape of the $Cu_A$ EPR resonance shows that one of its g-values shifts slightly (by approximately 3 Gauss at X-band) upon reduction of cytochrome _a_ (52, Chapter II). This indicates that cytochrome _a_ reduction induces a minor structural change at the $Cu_A$ site. It is reasonable to associate this structural change with a change in the reduction potential of the copper: The EPR spectra of the blue copper protein azurin from two different species (_Alcaligenes faecalis_ and _Pseudomonas aeruginosa_) are also only slightly different, yet the reduction potentials of these proteins differ by 42 mV (Table I). The anticooperative redox interaction between cytochrome _a_ and $Cu_A$ is thus most plausibly explained by a mechanism in which these sites communicate via a conformational change.

The proposed redox interaction is likely to have implications for the behavior of the oxidase during turnover. Because of this interaction, $Cu_A$ and cytochrome _a_ will tend to accept only one electron between them and it will be thermodynamically less likely for both sites to be reduced simultaneously. The reduction potential

of cytochrome a is substantially increased upon oxidation of the $Fe_{a_3}/Cu_B$ site (25-27, cf. Chapter IV), so the effective reduction potential of cytochrome a is likely to be significantly more positive than that of $Cu_A$ under turnover conditions (where the $Fe_{a_3}/Cu_B$ site is mostly oxidized). If electron transfer between $Cu_A$ and cytochrome a is very rapid, so that these sites are at redox equilibrium with each other, this would mean that the $Cu_A$/cytochrome a redox interaction will not be manifested as a splitting of their reduction potentials as is observed in the present experiments. The first electron into these sites would transfer rapidly to cytochrome a and would reside on cytochrome a most of the time. The $Cu_A$ site would not be significantly reduced until the transfer of a second electron into these sites; in this case the pertinent reduction potential of the $Cu_A$ site would be the lower of the two measured here. However, the electron transfer between $Cu_A$ and cytochrome a is not necessarily as rapid as is sometimes suggested (2,4). The available kinetic data may be interpreted as well if it is postulated instead that $Cu_A$ can accept electrons directly from cytochrome c. The presence of two different functional cytochrome c binding sites on the oxidase (3,53) and the proximity of $Cu_A$ to residues which are involved in binding cytochrome c (54) are consistent with this proposal. In this case, the cytochrome a and $Cu_A$ sites could each take on one of two different effective reduction potentials, depending upon the oxidation state of their respective interaction partners. Since cytochrome a is mostly oxidized in the mitochondrial steady state, the higher of the $Cu_A$ potentials measured here will most often be the pertinent potential.

The large, negative values of $\Delta S^{o\prime}$ obtained from analyses of the $E^{o\prime}$ vs. temperature data for cytochrome a (Figure 5) suggest that reduction of cytochrome a is accompanied by a significant conformational change. It is known that reduction of the enzyme causes ORD spectral changes (55) and an increase in the volume of the protein (56); in the latter case, the change is known to involve cytochrome a and/or $Cu_A$ rather than the metals of the

dioxygen reduction site.

The $\Delta H^{o\prime}$ values for cytochrome *a* are negative, most likely as a result of favorable metal-to-ligand pi-backbonding, which tends to stabilize iron(II). The redox thermodynamic parameters reported here are substantially more negative than those for smaller low-spin cytochromes (40,45,57,58). An entropy-enthalpy compensation effect has been noted (59) for cytochromes *c*. This situation also holds for cytochrome *a*: The $\Delta H^{o\prime}$ and $\Delta S^{o\prime}$ values deduced from Figure 5 correlate well with a plot of $\Delta S^{o\prime}$ vs. $\Delta H^{o\prime}$ for c-type cytochromes.

The standard entropy of reduction of the $Cu_A$ site deduced from the data in Figure 6 is also relatively large and negative. The thermodynamic parameters for reduction of $Cu_A$ are compared with those of several other metalloprotein copper sites in Table III. All of the thermodynamic data available for comparison are for the type 1 or blue coppers (for a review of the properties of type 1 coppers see Ref. 60). These sites are known to function as efficient catalysts of electron transfer reactions, but they are not involved in energy conservation or transduction. Compared to the blue coppers, the $Cu_A$ site has a relatively large negative entropy of reduction. Only that of *P. aeruginosa* azurin is comparable, and at the pH employed for the azurin study (45) it is expected that reduction is partially linked to protonation of an ionizable group in the protein, probably His-35 (61,62), so that a component of the observed entropy of reduction may be due to protonation rather than to reduction per se. The reduction potential of $Cu_A$ is weakly if at all pH-dependent near pH 7 (63), so protolysis is not expected to contribute to its measured entropy of reduction.

The relatively large entropy change which occurs upon reduction of $Cu_A$, like that of cytochrome *a*, is likely to reflect a substantial protein conformational change. This conformational change may be related to a role of the copper site in energy transduction, i.e., proton pumping (9). Alternatively, it may be caused by the large overall negative charge of the oxidase, or by a relatively buried disposition of the copper site which shields it

Table III. Thermodynamic Parameters for the Reduction of Metalloprotein Copper Sites

| Protein | $\Delta^{o\prime}G$ [a] (kcal $mol^{-1}$) | $\Delta S^{o\prime}$ (e.u.) | $\Delta H^{o\prime}$ (kcal $mol^{-1}$) |
|---|---|---|---|
| Azurin (*Pseudomonas aeruginosa*)[b,e] | -7.10 | -31.7 | -16.6 |
| Azurin (*Alcaligenes denitrificans*)[b,f] | -6.37 | -23.2 | -13.3 |
| Azurin (*Alcaligenes faecalis*)[b,g] | -6.14 | | |
| Plastocyanin (*P. vulgaris*)[b,e] | -8.30 | -18.0 | -13.7 |
| Stellacyanin (*R. vernicifera*)[b,e] | -4.41 | -19.8 | -10.3 |
| Laccase type 1 (*P. versicolor*)[c,h] | -17.99 | -13.9 | -22.1 |
| Cytochrome *c* Oxidase $Cu_A$ (*Bos taurus* heart)[d] | -6.6 | -35 | -17.1 |

a. at 25 °C.

b. phosphate buffer, ionic strength 0.1 M, pH 7.0

c. 0.2 M phosphate buffer, pH 5.4

d. 0.1 M phosphate buffer, pH 7.0

e. Reference 45

f. Reference 68

g. Reference 69

h. Reference 70

from interaction with the solvent, thus necessitating more extensive tightening of the protein structure upon reduction (40). Further spectroscopic studies of the structure of the reduced $Cu_A$ site are needed to test the suggestion that significant structural changes accompany oxidoreduction of this site.

The thermodynamic parameters deduced for cytochrome _a_ and $Cu_A$ indicate that electron transfer from cytochrome _c_ to these sites is enthalpically driven but entropically unfavorable. The enthalpy and entropy changes accompanying these electron transfers are: $\Delta H = -4.2$ kcal $mol^{-1}$, $\Delta S = +12.9$ cal $mol^{-1}$ $K^{-1}$ (cytochrome _c_ to cytochrome _a_), and $\Delta H = -2.0$ kcal $mol^{-1}$, $\Delta S = +4.6$ cal $mol^{-1}$ $K^{-1}$ (cytochrome _c_ to $Cu_A$).

The absence of a measurable ionic strength dependence (Figure 8) suggests that charge solvation does not play a large direct role (as opposed to an indirect role via its effect upon the overall conformation of the protein) in determining the reduction potential of cytochrome _a_. Spin label-spin probe studies employing compounds of dysprosium (64) suggest that the heme of cytochrome _a_ is less accessible to the solvent than the heme of cytochrome _c_. The absence of any significant effect of complex formation upon the reduction potential of cytochrome _a_ is consistent with the suggestion that the solvent plays a relatively small direct role in tuning the cytochrome potential, and may in fact be the physiologically desirable consequence of 'designing' the protein so that the cytochrome _a_ reduction potential is not very sensitive to the immediate solvent environment. Another beneficial consequence of shielding the metal site from the solvent is that the outer-sphere reorganizational barrier to electron transfer will be smaller, and the rates of electron transfer to and from cytochrome _a_ correspondingly greater. The cytochrome _c_ reduction potential is only slightly affected ($E^{o\prime}$ changes by ca. 6 mV) by complexation with cytochrome oxidase in our experiments, but since cytochrome _c_ was present in excess, only a fraction of the cytochrome _c_ was complexed with the oxidase. In experiments using an excess of the oxidase, Vanderkooi and Erecinska (65) saw a somewhat larger effect

($E^{o\prime}$ changed by ca. 30 mV). The reduction potential of cytochrome c is only very weakly dependent upon ionic strength in the 0.01M - 0.23M range, but the enthalpy and entropy of reduction change considerably (58), consistent with a somewhat greater power of the solvent in influencing the cytochrome c potential.

The observed pH-dependence of the cytochrome a reduction potential (-9 mV /pH unit, on average) is similar to that observed by Hinkle and Mitchell (66). If the protein took up one proton upon reduction of the cytochrome a site, the pH dependence would be much greater, i.e., -56 mV per pH unit at 10 $^{o}$C. The present results imply that the protein takes up, on the average, only 0.16 proton on reduction of cytochrome a. The site of redox-linked proton translocation in cytochrome oxidase is still unclear, but either cytochrome a or $Cu_A$ is implicated on energetic grounds. Babcock and Callahan (12) suggest, on the basis of resonance Raman data, that the heme a formyl group of cytochrome a is involved in a redox-coupled hydrogen bonding interaction with a proton donor supplied by the enzyme. They further suggest that the redox-coupled modulation of the strength of this hydrogen bond might lead to proton pumping. However, the present data indicate that substantial net proton uptake or release is not coupled to oxidoreduction of cytochrome a. It should be stressed that the lack of a pronounced pH dependence in $E^{o\prime}$, and hence of a strong redox Bohr effect, does not rule out the possibility that cytochrome a is involved in proton pumping (67, cf. Chapter VI). As noted above, the reduction potential of $Cu_A$ also appears to be only weakly pH-dependent (63). Very precise data on the pH-dependence of the $Cu_A$ potential are not yet available; the protocol developed in the present work might be fruitfully applied to obtaining such data.

REFERENCES

1. Michel, B., and Bosshard, H.R. (1984). J. Biol. Chem. 259, 10083-10091.

2. Antalis, T.M., and Palmer, G. (1982). J. Biol. Chem. 257, 6194-6206.

3. Wilms, J., Veerman, E.C.J., Konig, B.W., Dekker, H.L., and van Gelder, B.F. (1981). Biochim. Biophys. Acta 635, 13-24.

4. Wilson, M.T., Greenwood, C., Brunori, M., and Antonini, E. (1975). Biochem. J. 147, 145-153.

5. Gelles, J., and Chan, S.I. (1985). Biochemistry 24, in press.

6. Stevens, T.H., Martin, C.T., Wang, H., Brudvig, G.W., Scholes, C.P., and Chan, S.I. (1982). J. Biol. Chem. 257, 12106-12113.

7. Beinert, H., Griffiths, D.E., Wharton, D.C., and Sands, R.H. (1962). J. Biol. Chem. 237, 2337-2346.

8. Peisach, J., and Blumberg, W.E. (1974). Arch. Biochem. Biophys. 165, 691-708.

9. Chan, S.I., Bocian, D.F., Brudvig, G.W., Morse, R.H., and Stevens, T.H. (1979) in Cytochrome Oxidase (King, T.E., Orii, Y., Chance, B., and Okunuki, K., Eds.) pp. 177-188, Elsevier/North Holland, Amsterdam.

10. Wikstrom, M., Krab, K., and Saraste, M. (1981). Ann. Rev. Biochem. 50, 623-655.

11. Wikstrom, M., Krab, K., and Saraste, M. (1981). Cytochrome

Oxidase: A Synthesis, Academic Press, London.

12. Babcock, G.T., and Callahan, P.M. (1983). Biochemistry 22, 2314-2319.

13. Malmstrom, B.G. (1980). In Metal Ion Activation of Dioxygen (Spiro, T.G., Ed.), pp. 181-207, Wiley, New York.

14. Brunori, M., Antonini, E., and Wilson, M.T. (1981). Metal Ions in Biological Systems 13, 187-228.

15. Wainio, W.W. (1983). Biol. Rev. 58, 131-156.

16. Blair, D.F., Martin, C.T., Gelles, J., Wang, H., Brudvig, G.W., Stevens, T.H., and Chan, S.I. (1983). Chemica Scripta 21, 43-53.

17. Freedman, J.A., and Chan, S.H.P. (1984). J. Bioenerg. Biomembr. 16, 75-100.

18. Greenwood, C., and Gibson, Q.H. (1967). J. Biol. Chem. 242, 1782-1787.

19. Gibson, Q.H., and Greenwood, C. (1965). J. Biol. Chem. 240, 2694-2698.

20. Chance, B., Saronio, C., and Leigh, J.S., Jr. (1975). J. Biol. Chem. 250, 9226-9237.

21. Clore, G.M., Andreasson, L.E., Karlsson, B., Aasa, R., and Malmstrom, B.G. (1980). Biochem. J. 185, 139-154.

22. Heineman, W.R., Kuwana, T., and Hartzell, C.R. (1972). Biochem. Biophys. Res. Comm. 49, 1-8.

23. Minnaert, K. (1965). Biochim. Biophys. Acta 110, 42-56.

24. Malmstrom, B.G. (1974). Quart. Rev. Biophys. 6, 389-431.

25. Wikstrom, M.K.F., Harmon, H.J., Ingledew, W.J., and Chance, B. (1976). FEBS Lett. 65, 259-277.

26. Kojima, I., and Palmer, G. (1983). J. Biol. Chem. 258, 14908-14913.

27. Goodman, G. (1984). J. Biol. Chem. 259, 15094-15099.

28. Cornish-Bowden, A., and Koshland, D.E., Jr. (1975). J. Mol. Biol. 95, 201-212.

29. Babcock, G.T., Vickery, L.E., and Palmer, G. (1978). J. Biol. Chem. 253, 2400-2411.

30. Carithers, R.P., and Palmer, G. (1981). J. Biol. Chem. 256, 7967-7976.

31. Artzatbanov, V.Y., Konstantinov, A.A., and Skulachev, V.P. (1978). FEBS Lett. 87, 180-185.

32. Blair, D.F., Bocian, D.F., Babcock, G.T., and Chan, S.I. (1982). Biochemistry 21, 6928-6935.

33. Wilson, D.F., and Nelson, D. (1982). Biochim. Biophys. Acta 680, 233-241.

34. Hartzell, C.R., and Beinert, H. (1974). Biochim. Biophys. Acta 368, 318-338.

35. Lowry, O.H., Rosebrough, N.J., Farr, A.L., and Randall, R.J. (1951). J. Biol. Chem. 193, 265-275.

36. van Gelder, B.F. (1966). Biochim. Biophys. Acta 118, 36-46.

37. Brautigan, D.L., Ferguson-Miller, S., and Margoliash, E. (1978). Meth. Enzymol. 53, 128-164.

38. Pladziewicz, J.R., Meyer, T.J., Broomhead, S.A., and Taube, H. (1973). Inorg. Chem. 12, 639-643.

39. Cummins, D., and Gray, H.B. (1977). J. Am. Chem. Soc. 99, 5158-5167.

40. Taniguchi, V.T., Ellis, W.R., Jr., Cammarata, V., Webb, J., Anson, F.C., and Gray, H.B. (1982). In Electrochemical and Spectrochemical Studies of Biological Redox Components (Kadish, K.M., Ed.), pp 51-68. American Chemical Society Advances in Chemistry Series No. 201, Washington, D.C.

41. Greenwood, C., Wilson, M.T., and Brunori, M. (1974). Biochem. J. 137, 205-215.

42. Beinert, H., Shaw, R.W., Hansen, R.E., and Hartzell, C.R. (1980). Biochim. Biophys. Acta 591, 458-470.

43. Nicholls, P., and Chanady, G.A. (1981). Biochim. Biophys. Acta 634, 256-265

44. Morgan, J.E., Blair, D.F., and Chan, S.I. (1985). J. Inorg. Biochem. 23, 295-302.

45. Taniguchi, V.T., Sailasuta-Scott, N., Anson, F.C., and Gray, H.B. (1980). Pure and Applied Chemistry 52, 2275-2281.

46. Latimer, W.M. (1952). In Oxidation Potentials, 2nd ed., p. 30. Prentice-Hall, New York.

47. Vanneste, W.H., and Vanneste, M.-T. (1965). Biochem. Biophys. Res. Commun. 19, 182-186.

48. Schroedl, N.A., and Hartzell, C.R. (1977). Biochemistry 16, 4961-4965.

49. Schroedl, N.A., and Hartzell, C.R. (1977). Biochemistry 16, 4966-4971.

50. Anderson, J.L., Kuwana, T., and Hartzell, C.R. (1976). Biochemistry 15, 3847-3855.

51. Walz, D. (1979). Biochim. Biophys. Acta 505, 279-353.

52. Brudvig, G.W., Blair, D.F., and Chan, S.I. (1984) J. Biol. Chem. 259, 11001-11009.

53. Ferguson-Miller, S., Brautigan, D.L., and Margoliash, E. (1976). J. Biol. Chem. 251, 1104-1115.

54. Millett, F., Darley-Usmar, V.M., and Capaldi, R.A. (1982). Biochemistry 21, 3857-

55. Urry, D.W., Wainio, W.W., and Grebner, D. (1972). Biochem. Biophys. Res. Comm. 27, 625-631.

56. Cabral, F., and Love, B. (1972). Biochim. Biophys. Acta 283, 181-186.

57. Reid, L.S., Taniguchi, V.T., Gray, H.B., and Mauk, A.G. (1982). J. Am. Chem. Soc. 104, 7516-7519.

58. Margalit, R., and Schejter, A. (1970). FEBS Lett. 6, 278-280.

59. Huang, Y.-Y., and Kimura, T. (1984). Biochemistry 23, 2231-2236.

60. Gray, H.B., and Solomon, E.I. (1981) in Copper Proteins (Spiro, T.G., Ed.), Chap. 1, Wiley-Interscience, New York.

61. Corin, A.F., Bersohn, R., and Cole, P.E. (1983). Biochemistry 22, 2032-2038.

62. Canters, G.W., Hill, H.A.O., Kitchen, N.A., and Adman, E.T. (1984). Eur. J. Biochem. 138, 141-152.

63. van Gelder, B.F., van Rijn, J.L.M.L., Schilder, G.J.A., and Wilms, J. (1977) in Structure and Function of Energy-Transducing Membranes (van Dam, K., and van Gelder, B.F., Eds.), pp. 61-68, Elsevier/North Holland, Amsterdam.

64. Ohnishi, T., Blum, H., Leigh, J.S., Jr., and Salerno, J.C. (1979). In Membrane Bioenergetics (C.P. Lee et al., Eds.), pp. 21-30. Addison-Wesley, Reading, Mass.

65. Vanderkooi, J., and Erecinska, M. (1974). Arch. Biochem. Biophys. 162, 385-391.

66. Hinkle, P., and Mitchell, P. (1970). J. Bioenerget. 1, 45-60.

67. Blair, D.F., Gelles, J., and Chan, S.I. (1985). Biophys. J., submitted for publication.

68. Baker, E.M., Ellis, W.R., Jr., Loehr, T., and Gray, H.B., unpublished results.

69. Rosen, P., Segal, M., and Pecht, I. (1981). Eur. J. Biochem. 120, 339-344.

70. Taniguchi, V.T., Malmstrom, B.G., Anson, F.C., and Gray, H.B. (1982). Proc. Natl. Acad. Sci. USA 79, 3387-3389.

# CHAPTER IV. SPECTROELECTROCHEMICAL STUDY OF NATIVE CYTOCHROME *c* OXIDASE: pH AND TEMPERATURE DEPENDENCES OF THE CYTOCHROME POTENTIALS AND CHARACTERIZATION OF SITE-SITE INTERACTIONS

## INTRODUCTION

The metal centers of cytochrome *c* oxidase catalyze reactions which are of great biological importance and chemical interest, namely the reduction of dioxygen to water, using electrons derived from ferrocytochrome *c*, and the active transport of hydrogen ions across the mitochondrial inner membrane. These reactions account for most of the oxygen utilization in the biosphere and for a substantial fraction of all biological energy transduction. The efficient catalysis of the reduction of dioxygen to water, without the release of peroxide or other incompletely reduced products, is an important electrochemical problem. The mechanisms of the reactions catalyzed by cytochrome oxidase have therefore been the subject of intensive investigation for many years (reviewed in Refs. 1-6).

An understanding of the mechanisms of cytochrome *c* oxidase must be based upon a thorough understanding of the thermodynamic properties of its four metal centers. Many studies have been carried out in an effort to clarify the redox properties of the oxidase (7-20). In spite of a large number of investigations spanning 20 years, the present picture of the redox thermodynamics of the oxidase remains confused or incomplete in several respects. This confusion has arisen primarily from two sources: First, the metal centers of the enzyme evidently interact with each other in an anticooperative fashion (21,22) so that they do not exhibit the electrochemical titration behavior expected of isolated single-electron acceptors. Second, the optical properties of cytochromes *a* and $a_3$, and the possibility of optically manifested interactions between these sites, have been disputed (21,23,24, Chapter II), so that the interpretation of optically monitored titrations in terms of the individual cytochrome properties has been difficult.

Recent developments indicate that the redox thermodynamic properties of cytochrome *c* oxidase are influenced by more than one

intersite interaction. Reductive (14) and potentiometric (16,17) titrations monitored by MCD spectroscopy have provided strong evidence that both cytochromes *a* and $a_3$ participate in interactions which lead to anticooperative thermodynamic behavior. Titrations of the cyanide-inhibited enzyme monitored by EPR (18) or optical absorbance (15) and of the carbon monoxide-inhibited enzyme monitored by absorbance spectrophotometry (Chapter III,19,20) furnish evidence for previously unsuspected interactions which involve both of the copper ions in the protein. When the results from these studies are considered together, a complex picture of the redox thermodynamic behavior of the oxidase emerges.

The results described above in Chapters II and III should assist considerably in elucidating this complex thermodynamic behavior. Studies of the cytochrome absorbances in various ligand derivatives (Chapter II, 24), as well as analogous studies using MCD (25), have demonstrated that under many circumstances intersite interactions do not greatly influence the spectroscopic properties of cytochrome *a*, cytochrome $a_3$, or $Cu_A$. This suggests that straightforward deconvolution of the optical absorbance changes measured in electrochemical titrations, into factor spectra based upon ligand inhibition of cytochrome $a_3$ (24,26,27), can provide acceptable estimates of the redox states of the individual metal sites. The detailed characterization of the redox properties of cytochrome *a* and $Cu_A$ (Chapter III, 19,20) in the carbon monoxide derivative of the oxidase should also be helpful. The behavior of this simpler system provides a foundation for analyzing the behavior of the uninhibited enzyme. In the present work, thin-layer spectroelectrochemical titrations of the native, uninhibited enzyme have been carried out under a variety of conditions, and the observed absorbance changes have been deconvolved by simple factor analysis based on cytochrome difference spectra like those presented in Chapter II. The resulting Nernst plots for cytochrome *a* and $a_3$ have been analyzed in terms of a simple interaction model like that employed in the study of the CO-inhibited enzyme in Chapter III. In combination with the results of that study, the titrations

of the native enzyme reveal many of the important thermodynamic properties of cytochromes *a* and $a_3$.

Presently, no comprehensive scheme to account for all of the observed intersite thermodynamic interactions has been advanced. The most widely accepted scheme at present, which is called the "neoclassical" model (21), incorporates thermodynamic interaction only between cytochrome *a* and cytochrome $a_3$. In this work, several experiments are described which further clarify the nature and magnitudes of the various thermodynamically manifested intersite interactions, and a new interaction scheme is introduced to account for the available data. This scheme involves interactions of roughly comparable magnitude between cytochrome *a* and all three other redox sites in the protein.

The effects of pH, temperature, and ionic strength upon the redox thermodynamic properties intrinsic to cytochromes *a* and $a_3$ have been characterized, using the procedure described previously (Chapter III, 20) which allows these properties to be resolved from the effects of intersite interactions. A significant batch dependence was observed in the electrochemical properties of the enzyme. Some of the results may be summarized as follows: The standard entropy of reduction of cytochrome *a* deduced from the temperature dependence of its reduction potential is very large and negative ($\Delta S^{o\prime}$ = - 47 +/- 6 e.u.) in one batch (designated Batch B), and somewhat less negative (-34 +/- 7 e.u.) in the other batch (designated Batch A). The standard entropy of reduction of cytochrome $a_3$ is more positive than that of cytochrome *a* in both of the enzyme batches (-10 +/- 10 e.u. in Batch A, -28 +/- 7 e.u. in Batch B). The reduction potential of cytochrome *a* exhibits a ca. -30 mV/pH unit dependence upon pH in both batches, indicating that reduction of cytochrome *a* at near neutral pH is coupled, on the average, to the uptake of 0.5 protons by ionizable groups in the protein. The reduction potential of cytochrome $a_3$ is steeply pH-dependent (ca. 56 mV/pH unit) in Batch A, indicating that its reduction is stoichiometrically (1 H+/e-) linked to protonation. By contrast, the reduction potential of cytochrome $a_3$ is almost

independent of pH in Batch B. It is suggested that the batch differences are due to changes in the $pK_a$s of an ionizable group near cytochrome $\underline{a}_3$. The reduction potentials of cytochromes $\underline{a}$ and $\underline{a}_3$ are not measurably dependent upon the buffer ionic strength in the range 0.06 - 0.5 M, but the potential of cytochrome $\underline{a}_3$ and the shape of its Nernst plot are significantly affected by the addition of KCl, in a manner which suggests that chloride ion binds to the cytochrome $\underline{a}_3/Cu_B$ site when both metals are oxidized.

In the experiments with native cytochrome oxidase, it was noted that the approach to equilibrium at each applied potential was significantly slower than in experiments with carbon monoxide-inhibited cytochrome oxidase (19) or with small low-spin cytochromes (28-30). At relatively high (ca. 350 mV vs. NHE) potentials, the approach to equilibrium was especially slow. A comparison of the spectra obtained during oxidative titrations with those obtained during re-reductive titrations suggests that the irreversibility at high potentials involves the slow equilibrium between the pulsed (31) and resting forms of the oxidized enzyme. In agreement with earlier work (32), this result indicates that the formation of a pulsed enzyme species does not require oxidation by dioxygen. The presence of both the pulsed and resting forms of the enzyme has important implications for interpreting electrochemical titrations of the oxidase.

MATERIALS AND METHODS

Enzyme. Cytochrome c oxidase was purified from beef heart mitochondria by the method of Hartzell and Beinert (33) and was characterized as previously described (19). The enzyme was stored frozen at -80 °C. Just prior to use, the enzyme was thawed and dialyzed into potassium phosphate buffer containing 0.5% Tween-20 (phosphate buffer was used in these experiments because its pH is relatively insensitive to temperature). Following dialysis, samples were centrifuged at 35,000xg for 30 minutes to remove insoluble material. Enzyme concentrations were typically 0.10-0.15 mM. The following redox mediators were used to stabilize the solution potential: Ruthenium hexaammine, 1 equivalent; Ruthenium pentaamminepyridine, 1 equivalent; hydroxymethylferrocene, 0.5 equivalent; bis(hydroxymethyl) ferrocene, 0.5 equivalent. The mediators were prepared as described by Ellis et al. (19).

Electrochemistry. Reduction potential measurements were made using an Optically Transparent Thin-Layer Electrode (OTTLE) cell contained in a gas-tight stainless steel shroud as previously described (19). The sample temperature was controlled by a variable temperature water bath and measured directly (+/- 0.2 °C) with a miniature copper-constantan thermocouple placed in the protein solution in close proximity to the thin-layer cavity of the OTTLE cell. Control experiments using one thermocouple at the sample and one thermocouple near the reference electrode were carried out to determine the extent to which the reference electrode was thermostatted, so that appropriate corrections could be applied (19). A Princeton Applied Research Model 174A potentiostat was used to control the potentials applied across the protein solutions. UV-visible spectra were obtained with a Cary 219 spectrophotometer (0.55 nm spectral bandwidth) interfaced to a Spex Industries SCAMP SC-31 data processor.

After the addition of redox mediators, enzyme and buffer solutions were thoroughly degassed on a vacuum apparatus. The

solutions, OTTLE cell, electrodes, and shroud were then transferred into an inert atmosphere box where the spectroelectrochemical cells were loaded (ca. 0.7 ml volume), fitted with the reference and auxiliary electrodes, and placed into the gas-tight shroud.

Enzyme/mediator solutions were poised at -50 mV vs. NHE for at least two hours in order to reduce the enzyme fully. A series of potentials was then applied across the OTTLE cell; each potential was maintained, typically for between 1 and 3 hours, until the rate of spectral change at 443 nm was negligible (no measurable change in 30 minutes). Assuming that equilibrium is established at each potential, the ratio of concentrations of oxidized to reduced forms, (Oxid/Red), of all redox couples in solution is determined by the Nernst equation (Chapter III, equation 1). Redox couples were converted in increments from one oxidation state to the other by a series of applied potentials. At each potential, the absorbance spectrum between 700 nm and 350 nm was recorded. Absorption spectra were stored on magnetic disk; difference spectra were obtained by computer subtraction.

Data analysis. The absorbance difference spectra of cytochrome c oxidase between 700 and 350 nm contain substantial contributions from both cytochromes a and $a_3$, as discussed at length in Chapter II. The experiments described there show that metal-metal interactions can to some degree influence the absorption properties of the oxidase, and that these interactions are most strongly manifested in the absorbance spectrum of cytochrome $a_3$. If all of the possible intersite interactions are explicitly taken into consideration, the problem of deconvolving the absorbance difference spectra becomes extremely difficult. In view of the large number of possible interactions, the limited information available from the optical absorption spectra (which contain relatively few clearly defined features), and the weakness of the interactions which have been observed, spectroscopic interactions have not been incorporated in the present analysis of the electrochemical data. The spectra obtained in electrochemical

titrations were factored into two components which correspond to the reduced minus oxidized difference spectra of cytochromes *a* and $a_3$, as measured by a ligand inhibition method. Since two components are involved, measurements at a minimum of two wavelengths are required. The reduced minus oxidized peaks at 605 nm and 443 nm were selected for use in the factor analysis because they are the strongest signals in the spectrum and because each primarily reflects only one of the cytochromes (the 605 nm band cytochrome *a*, and the 443 nm band cytochrome $a_3$). The individual cytochrome contributions to each of the two absorption peaks were assumed to be those measured in Reference 4 using CO to stabilize cytochrome $a_3$ and $Cu_B$ in their reduced states. The possible consequences of neglecting spectroscopic interactions are discussed at greater length below.

Under all conditions, the Nernst plots for the titrations of cytochrome *a* and cytochrome $a_3$ reflected the interactive thermodynamic behavior noted above; that is, they exhibited behavior different from that expected for isolated one-electron acceptors. As noted previously, the midpoint potential (the potential at which a site is one-half reduced) is not a meaningful measure of the intrinsic thermodynamic properties of a site under these circumstances, since it depends critically upon the magnitude of the interactions and the potentials of the interacting partner(s). This is illustrated in Figure 1, which shows theoretical Nernst plots for a site which participates in various thermodynamically manifested interactions with another electron acceptor, but whose intrinsic potential is not varied. In panel C, for example, it is seen that a 1 mV change in the potential of the interactant can shift the midpoint of the site under observation by as much as 4 mV (assuming an interaction potential of 120 mV, as was done in panels A and C), without involving any change in the intrinsic thermodynamic properties of the site under observation. Since the interaction potentials manifested at cytochromes *a* and $a_3$ are evidently of this order, this effect cannot be overlooked in analyzing their titration behaviors.

Figure 1. Theoretical Nernst plots for an interactive electron acceptor. In all plots, the potential of the site is +60 mV when its interacting partner is oxidized. In panel A, the potential of the interacting partner is varied between ca. 40 and 80 mV while the magnitude of the interaction is fixed at -120 mV (the minus sign indicates that the interaction is anticooperative). The theoretical Nernst plot which is symmetrical about log (ox/red) = 0 is obtained when the interactant potential is 60 mV, i.e., equal to that of the site under examination. In panel B, the interactant potential is fixed at 60 mV while the magnitude of the interaction is varied in 30 mV increments between 30 and 120 mV. In both panels A and B, the dashed lines indicate the slope expected from a noninteractive one-electron acceptor. In panels C and D, the midpoint potentials (the point at which log (ox/red) = 0), obtained from the plots in panels A and B, are plotted as a function of the potential of the interactant (panel C) and the magnitude of the interaction (panel D). From panel C, it is seen that the measured midpoint depends critically upon the potential of the interactant, especially when the potentials of the two sites are well matched to each other. Changes in the magnitude of the interaction have a less dramatic, but nevertheless significant effect (panel D).

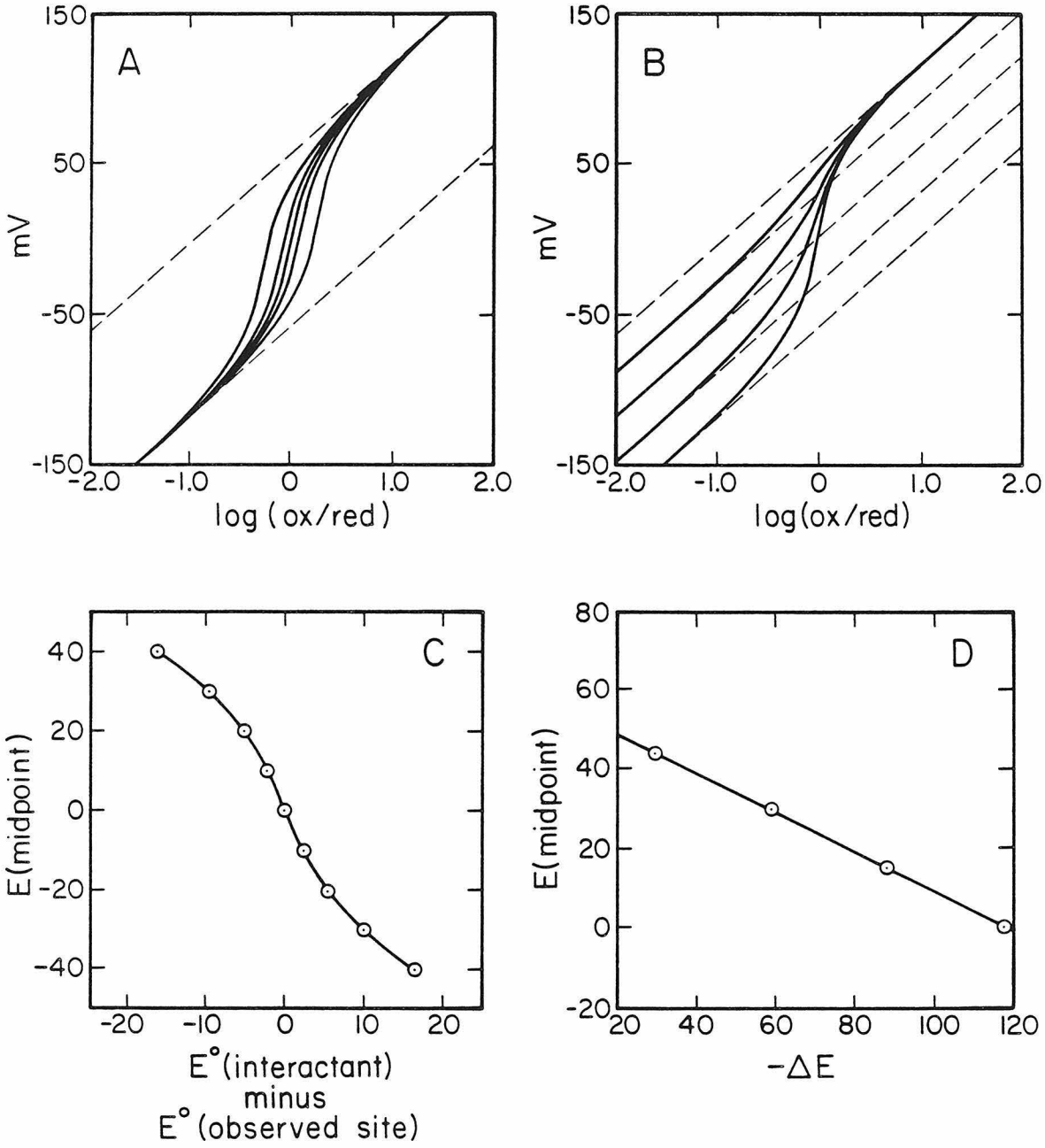
A
B
C
D
150
50
-50
-150
mV
-2.0
-1.0
0
1.0
2.0
log ( ox/red )
log(ox/red)
40
20
0
-20
-40
E(midpoint)
-20
-10
0
10
20
E°(interactant)
minus
E° (observed site)
80
60
40
20
0
-20
20
40
60
80
100
120
-ΔE

The treatment developed above (Chapter III) to describe the behaviors of cytochrome *a* and $Cu_A$ in the carbon monoxide inhibited enzyme was used to estimate the two asymptotic potentials (and thus the total interaction potentials) of the cytochrome *a* and $a_3$ sites via computer fitting of their Nernst plots. In situtations such as the present one where more than one interaction may be operative, this simple model may deviate from the observed Nernst plots in the crossover region between the two asymptotes, but it is still able to provide satisfactory estimates of the asymptotic potentials, since in all interaction schemes the asymptotic behavior is the same (i.e., a straight line corresponding to an isolated one-electron acceptor). The determination of asymptotic reduction potentials is less precise than determination of midpoints, because it involves data taken nearer the extremes of the titration. However, it should be stressed that, while plots of midpoint potentials (vs. pH, for example) will thus show less scatter, they cannot be interpreted in terms of well defined thermodynamic quantities.

Because of the way in which the titrations were carried out (oxidation followed by re-reduction), the higher asymptotic potentials, which pertain when the interacting partners are all oxidized, were more accurately determined than the lower asymptotic potentials. The time elapsing between the oxidative and reductive titrations, and the observed discrepancy between them, was greater at the lower potentials. In most cases, both of the asymptotic potentials, and thus the total interaction energy, could be satisfactorily estimated. In titrations which were fairly reversible, the simple interaction model provided a satisfactory fit to the Nernst plots at all potentials (Figure 5).

Standard entropies of reduction were calculated from measurements of reduction potential vs. temperature, using appropriate corrections for partial thermostatting of the reference electrode, as described in Chapter III. The pH-dependences of the cytochrome potentials were determined in phosphate buffer with the concentration adjusted to maintain a constant ionic strength of 0.220 M. For measurements of the effect of ionic strength, the

ionic strength was adjusted by changing the phosphate concentration.

RESULTS

Batch dependences and site-site interactions. A significant enzyme batch dependence was observed in several properties of the oxidase in spectroelectrochemical titrations. Absorbance difference spectra obtained during thin-layer electrochemical titrations of two different batches of cytochrome c oxidase at 10 °C, pH 7.66 are shown in Figure 2. In the insets to this figure, the absorbance changes at 443 nm and 605 nm are correlated. Since the two cytochromes make very different contributions to the 443 and 605 nm absorptions, a plot of $\Delta A_{443}$ vs. $\Delta A_{605}$ facilitates characterization of the behaviors of the individual cytochromes. The dashed lines in the figure insets represent the behavior expected if the two cytochromes titrate at well-resolved potentials (cytochrome a at a high potential, and cytochrome $a_3$ at a lower potential). If the two cytochromes titrate together at all potentials, the plot of $\Delta A_{443}$ vs. $\Delta A_{605}$ will be a straight line connecting the extreme data points.

For one of the enzyme batches, designated batch A, the titration follows the dashed line closely for much of the high-potential portion of the titration (inset, lower left corner). This implies that in Batch A, cytochrome a is the primary contributor to the spectral changes which occur at the highest potentials, while the spectral changes at lower potentials are caused by both cytochromes, with cytochrome $a_3$ making the larger contribution. For the other enzyme batch, designated Batch B, the plot follows the dashed line for only a small portion of the titration at the highest potentials, and then closely follows a straight line connecting the exteme data points. This behavior indicates that in Batch B the two cytochromes titrate together throughout most of the potential range examined.

A comparison of selected absorbance difference spectra of the two enzyme batches titrated under similar conditions (pH 7.66, 10 °C) is presented in Figure 3. While the fully reduced minus fully oxidized difference spectra are similar in the two batches, as

is evident in Figure 2, the spectra obtained during the low potential half of the titration, as well as the spectra obtained during the high potential half of the titration, are significantly different in the two batches. Much of the difference can be explained in terms of the different apportioning of the two cytochromes between the high and low potential parts of the titration, as was noted in the insets to Figure 2. However, the spectral differences near 415–420 nm are not as readily explained: In both enzyme batches, the absorbance changes in this region which occur at low potential do not resemble those expected for cytochrome a, cytochrome $a_3$, or any linear combination of the two. Specifically, the trough at 415 nm is not as deep as expected, relative to the peak near 443 nm, for either cytochrome a or cytochrome $a_3$.

Some degree of irreversibility was observed in the spectroelectrochemical titrations even when as many as 3 hours were allowed for equilibration at each potential. Very slow approaches to equilibrium were ordinarily observed only at relatively high (> 300 mV vs. NHE) potentials. The irreversibility was characterized by calculating the absorbance difference spectrum of the sample poised at ca. 290 mV vs. NHE during the oxidative titration minus the sample poised at ca. 290 mV during the re-reductive titration, for both enzyme batches (at pH 7.66, 10 °C). These difference spectra are displayed in Figure 4. The absorbance changes which characterize the irreversibility ($\lambda$ max near 436 nm, $\lambda$ min near 413 nm, and some evidence for a weaker peak near 595 nm, especially in Batch A) are similar to those in difference spectra comparing the pulsed and resting species of oxidized cytochrome oxidase (31,35).

Published difference spectra for reduced minus oxidized cytochromes a and $a_3$ (4,26) were used to estimate the individual contributions of cytochromes a and $a_3$ to the absorbance differences measured at each potential. Nernst plots for the titration of cytochromes a and $a_3$ are displayed in Figure 5, for both enzyme batches studied. Under most conditions, the titration behavior of both cytochromes was very different from that expected

for one-electron acceptors, which suggests that the cytochromes participate in intersite interactions which influence their reduction potentials (36,37). The average slope of the observed Nernst plots corresponds to n less than 1.0, indicating that the interactions are anticooperative. At extreme values of log (Oxid/Red), the Nernst plots approach n=1 behavior, as expected. The energy of interaction in such a situation may be estimated by the separation between the two n=1 lines which approximate the asymptotic behaviors of the Nernst plots. It is evident from the data in Figure 5 that the interaction energies for cytochromes a and $a_3$ are significantly different from each other in both enzyme batches. This result indicates that interaction between the two cytochromes is not the only source of the non-Nernstian behavior, since in this case their interaction energies would be equal.

The Nernst plots for enzyme batches A and B are very different. The largest difference involves cytochrome $a_3$, whose higher asymptotic potential is significantly (ca. 50 mV) lower in Batch A. Cytochrome a exhibits differences also: In Batch A, the Nernst plot for cytochrome a follows an n=1 line for much of the high-potential half of the titration, which indicates that the site (or sites) with which it interacts has a substantially lower reduction potential than itself. In this batch, the chromophore titrating at high potentials appears to be almost purely cytochrome a. In Batch B, the upper asymptotic potential of cytochrome a is approximately the same as that in Batch A, but its Nernst plot follows the upper asymptote for less of the titration, crossing over to the lower asymptote nearer log (Oxid/Red) = 0.

The data in Figure 5 and data from similar experiments under various conditions were fitted to a simplified interaction model which assumes that the titration behavior of each site may be satisfactorily described in terms of a single effective interaction. This interaction model, while not exact in the present situation owing to the presence of multiple interactions, nevertheless generates acceptable estimates of the asymptotic high and low potentials of the cytochromes, judging from the quality of the fits

Figure 2. Absorbance difference spectra obtained during spectroelectrochemical titration of two different batches of detergent-solubilized cytochrome c oxidase. The indicated potentials are vs. SCE. In the insets, the absorbance changes at 605 nm are plotted as functions of the absorbance changes at 443 nm. The dashed lines in the insets correspond to the behavior anticipated if cytochromes a and $a_3$ titrate at well-resolved potentials (cytochrome a at the higher potential). Sample conditions: 10 °C, pH 7.66, 90 mM phosphate buffer (ionic strength 0.22 M).

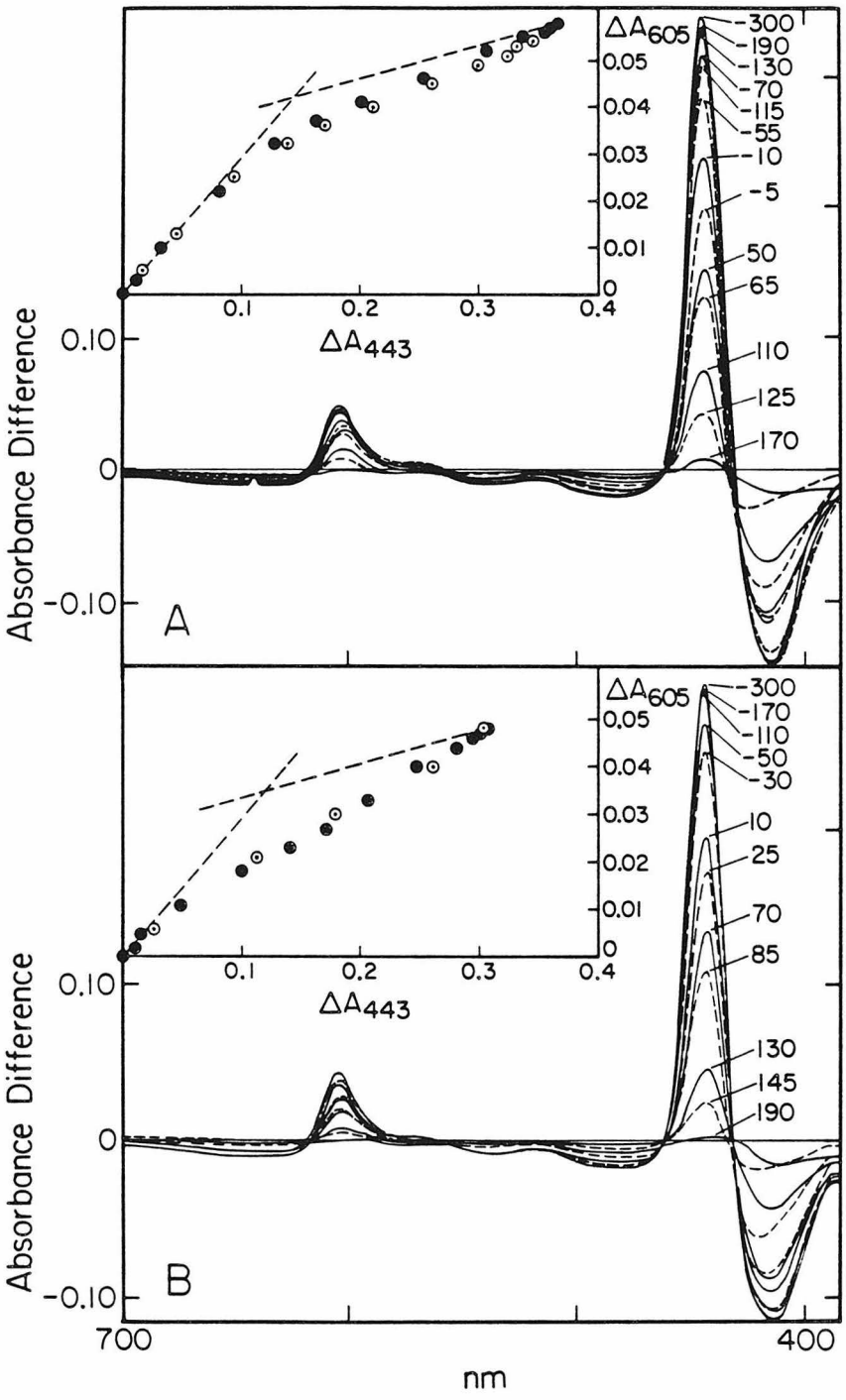
ΔA605
ΔA443
Absorbance Difference
0.10
0
-0.10
A
B
700
400
nm
-300
-190
-130
-70
-115
-55
-10
-5
50
65
110
125
170
-300
-170
-110
-50
-30
10
25
70
85
130
145
190

Figure 3. Absorbance difference spectra which describe the low (solid lines) and high (dashed lines) potential portions of spectroelectrochemical titrations of two batches of cytochrome c oxidase. Panel A, solid line, sample poised at -300 mV (vs. SCE) minus sample poised at -50 mV; dashed line, sample poised at -50 mV minus sample poised at +300 mV. Panel B, solid line, sample poised at -300 mV minus sample poised at -70 mV; dashed line, sample poised at -70 mV minus sample poised at +300 mV. Sample conditions as in Figure 2.

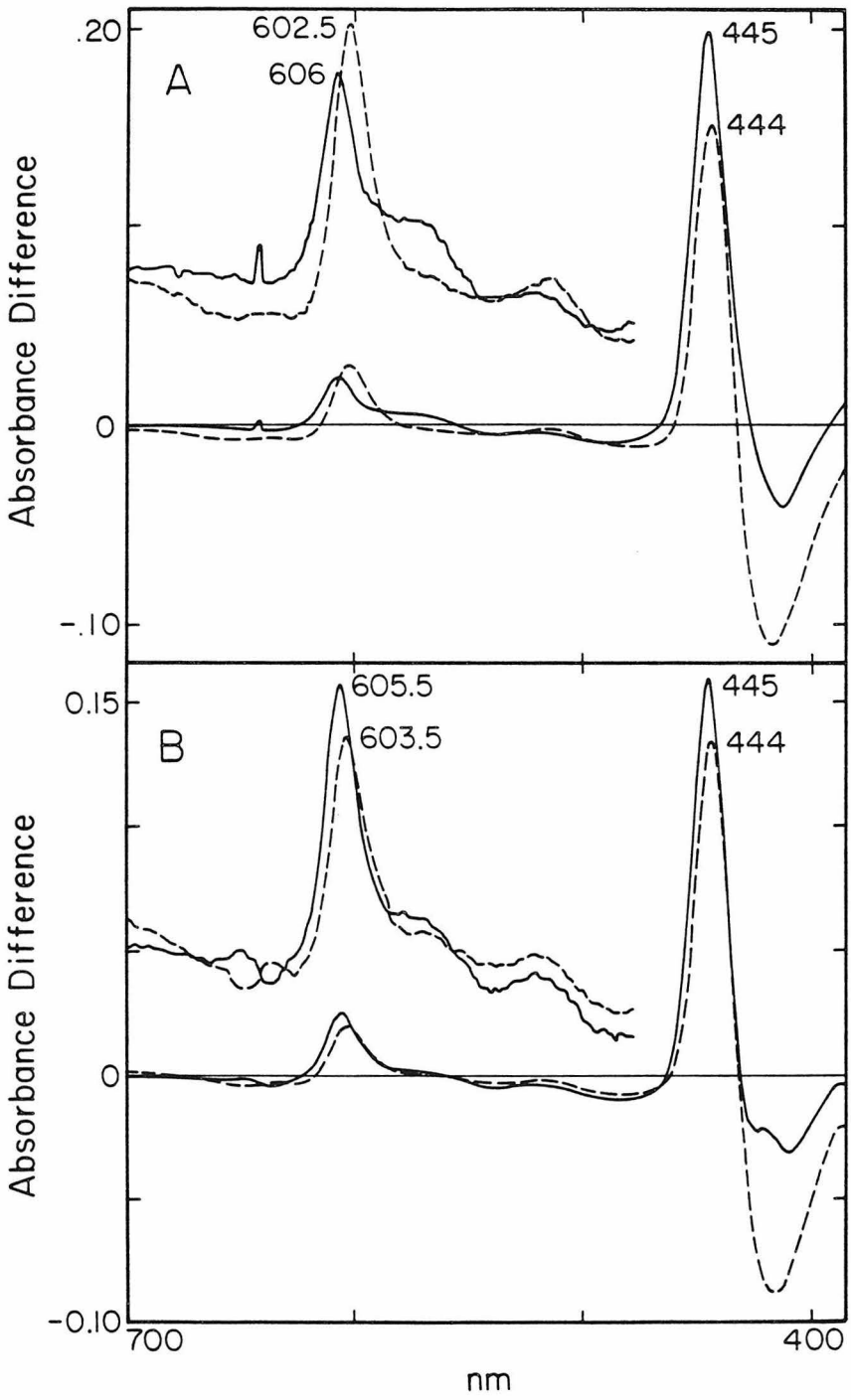
.20
602.5
606
A
445
444
0
-.10
Absorbance Difference
0.15
605.5
603.5
B
445
444
0
-0.10
Absorbance Difference
700
400
nm

**Figure 4. Absorbance difference spectra which describe the hysteresis typically observed in the high potential portion of spectroelectrochemical titrations of cytochrome c oxidase. The two spectra were obtained from the two different enzyme batches. Trace A: Spectrum of a sample of Batch A poised at 145 mV vs. SCE during the oxidative titration minus the spectrum of the same sample poised at 145 mV during the re-reductive titration. Trace B: Spectrum of a sample of Batch A poised at 140 mV during the oxidative titration minus the spectrum of the same sample poised at 140 mV during the re-reductive titration.**

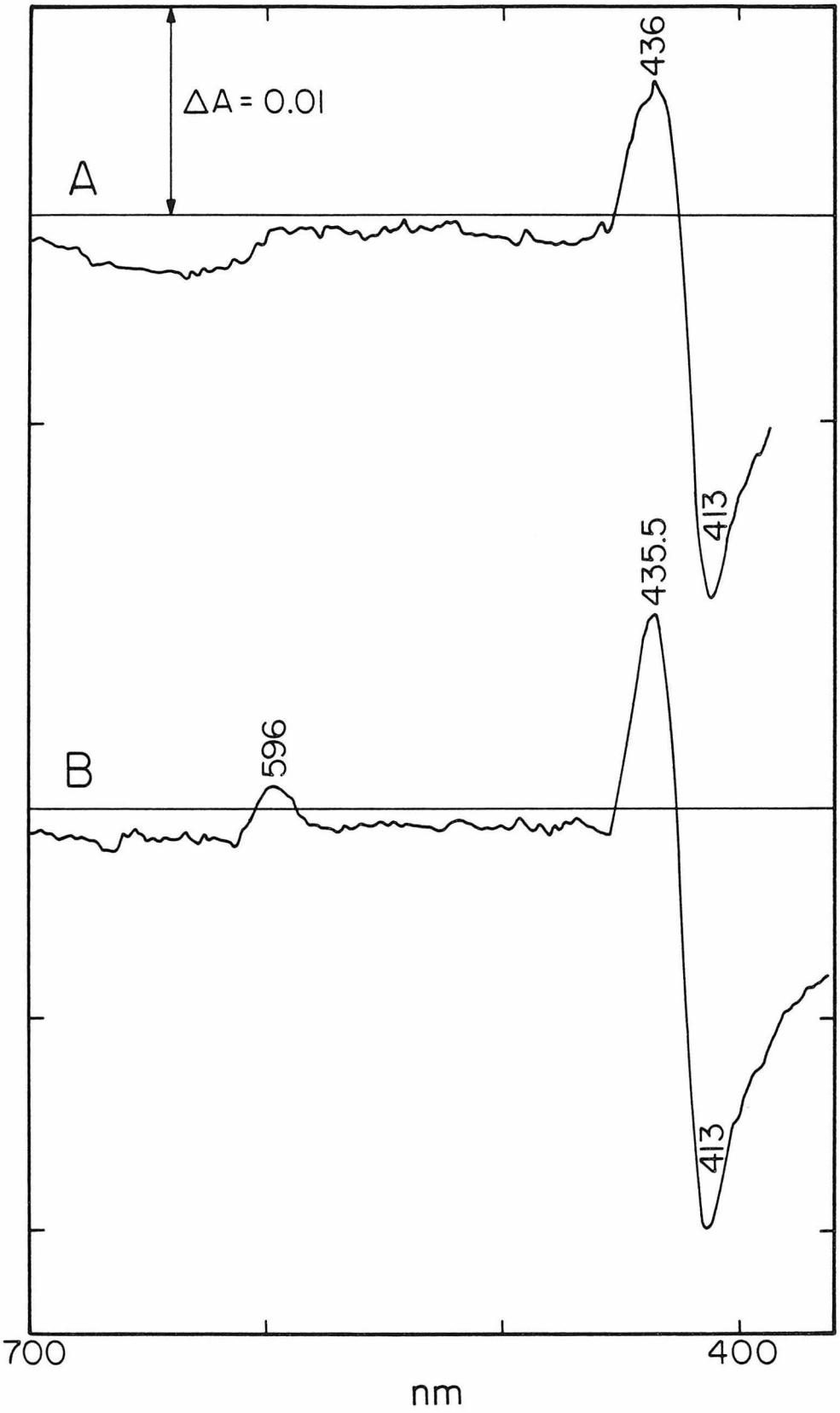
ΔA = 0.01
A
436
413
435.5
B
596
413
700
400
nm

Figure 5. Nernst plots for cytochromes a (circles) and $a_3$ (squares) obtained by deconvolving the spectral changes observed in spectroelectrochemical titrations of two batches of cytochrome c oxidase. The solid points were obtained on oxidation and the open points upon re-reduction. The solid lines are computer-generated fits of the data to the minimal interaction model described in the text.

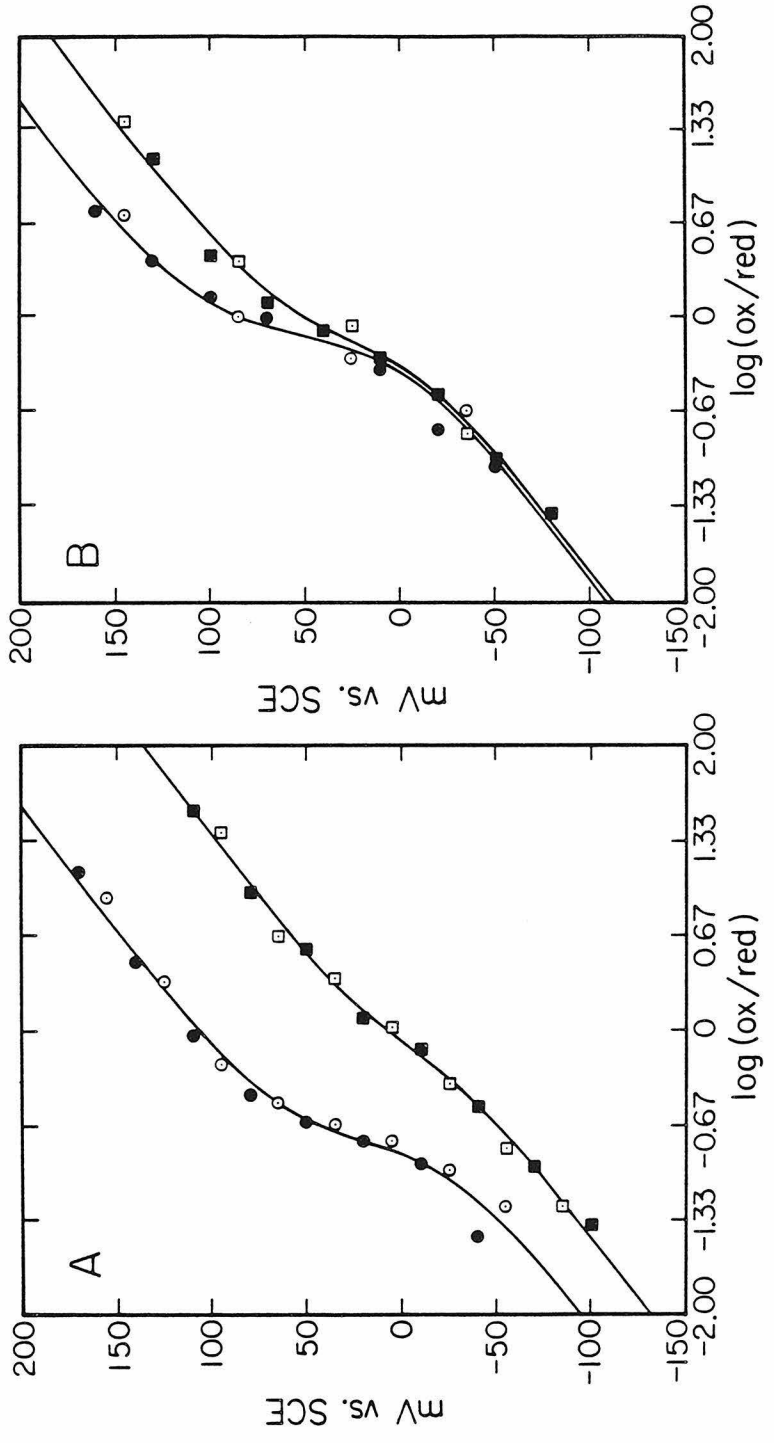
A
B
mV vs. SCE
log (ox/red)
200
150
100
50
0
-50
-100
-150
-2.00
-1.33
-0.67
0
0.67
1.33
2.00

Figure 6. Nernst plots for cytochromes *a* (circles) and $a_3$ (squares) in a spectroelectrochemical titration of Batch B (10 °C, 90 mM phosphate pH 7.66) to which 0.25 M KCl was added. The solid lines are computer-generated best fits to a minimal interaction model. The estimated values of the interaction energies are 99 mV for cytochrome *a* and 36 mV for cytochrome $a_3$.

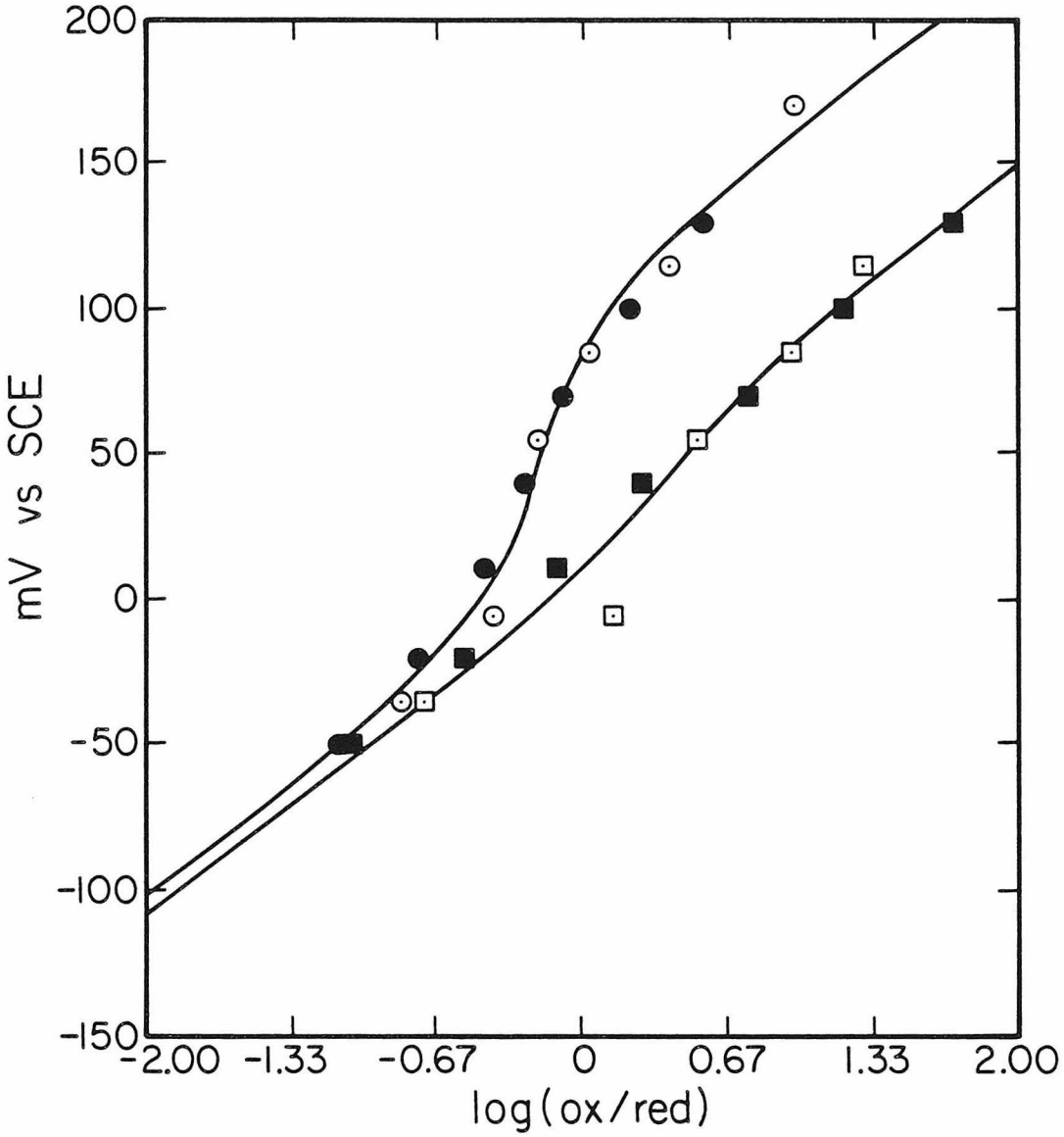
200
150
100
50
0
-50
-100
-150
mV vs SCE
-2.00
-1.33
-0.67
0
0.67
1.33
2.00
log(ox/red)

Table I. Interaction Parameters Estimated from Titrations of Native (Uninhibited) Cytochrome c Oxidase.

| Batch | pH | T (°C) | site | $E^{o}$(upper)* | Total interaction potential | Interactant potential** |
|---|---|---|---|---|---|---|
| A | 6.8 | 10 | a | 142 | 118 | 113 |
| A | 6.8 | 10 | $a_3$ | 65 | 74 | 77 |
| A | 7.3 | 10 | a | 123 | 83 | 93 |
| A | 7.3 | 10 | $a_3$ | 36 | 50 | 32 |
| A | 7.7 | 10 | a | 111 | 96 | 67 |
| A | 7.7 | 10 | $a_3$ | 24 | 43 | 17 |
| A | 7.7 | 20 | a | 116 | 92 | 100 |
| A | 7.7 | 20 | $a_3$ | 19 | 56 | 21 |
| B | 6.7 | 10 | a | 134 | 118 | 123 |
| B | 6.7 | 10 | $a_3$ | 75 | 84 | 64 |
| B | 7.4 | 10 | a | 110 | 111 | 102 |
| B | 7.4 | 10 | $a_3$ | 66 | 74 | 51 |
| B | 7.7 | 10 | a | 118 | 115 | 112 |
| B | 7.7 | 10 | $a_3$ | 72 | 72 | 63 |
| B | 7.7 | 20 | a | 104 | 119 | 103 |
| B | 7.7 | 20 | $a_3$ | 62 | 67 | 46 |

* mV vs. SCE. $E^{o}$(upper) refers to the upper asymptotic potential obtained from the fits to the Nernst plots, which is the potential which pertains when all of the partner sites are oxidized.

** The interactant potential is the potential of a single "effective" interacting site which yields the best fit to the Nernst plots. In a self-consistent 2-site interaction model, it must be equal to the directly measured upper asymptotic potential of the site which is proposed to be involved in the interaction.

(as exemplified in Figure 5). This analysis may be used to estimate the potential of the effective interaction partner, via the effect of the interactant's potential on the Nernst plot in the crossover region between the two n=1 asymptotes, and to estimate the magnitude of the total interaction expressed at a given site. The results of such an analysis of titrations carried out under a variety of conditions are given in Table I. For both enzyme batches, the interactant potentials inferred from fits to the Nernst plots for cytochrome a are very different from the directly measured potential of cytochrome $a_3$. The inferred potential of the site in interaction with cytochrome $a_3$ is also very different from the measured potential of cytochrome a. The total interaction energy expressed at cytochrome a is, on the average, 42 mV greater than that expressed at cytochrome $a_3$ in Batch A, and 39 mV greater in Batch B. These results demonstrate that interaction between cytochromes a and $a_3$ is not the only source of their unusual titration behaviors, implicating significant interactions which involve the copper ion sites in the protein.

Experiments conducted in the presence of KCL provide further indications that cytochrome-cytochrome interaction is not the only source of non-Nernstian behavior. In Batch B in buffer supplemented with 0.25 M KCl, cytochrome $a_3$ exhibits only 36 mV of interaction energy, while cytochrome a exhibits ca. 99 mV of interaction energy (Figure 6). Hence, approximately 65 mV of the interactions expressed at cytochrome a in Batch B must involve factors other than the oxidation state of cytochrome $a_3$.

pH dependences. The limiting high and low potentials of cytochromes a and $a_3$ were measured at various values of pH between ca. 6.5 and 8.5. The results are plotted in Figures 7 and 8 (Batch A) and Figures 9 and 10 (Batch B). In both enzyme batches, the upper asymptotic potential of cytochrome a exhibits a moderate (ca. -30 mV/pH unit, on the average) dependence upon pH, consistent with (but not restricted to) coupling to an ionizable group whose $pK_a$ is near 7.4 when cytochrome a is reduced and significantly

lower when it is oxidized. The lower asymptotic potential of cytochrome *a* could be satisfactorily estimated only in Batch B; this potential is less steeply dependent upon pH than the upper asymptotic potential (Figure 10). It should be stressed that neither the low nor high potential transitions of cytochrome *a* is stoichiometrically (1 $H^+/e^-$) linked to proton uptake. The behavior of cytochrome $a_3$ was more batch-dependent: In Batch A, a steep (ca. -56 mV/pH unit) pH dependence was observed, indicating that reduction of cytochrome $a_3$ is coupled to the uptake of approximately one proton. In Batch B, the upper asymptotic potential of cytochrome $a_3$ is not sensitive to pH below pH 7.5, but it drops at higher pH values in a manner which suggests the involvement of an ionizable group with a $pK_a$ near 7.8. The lower asymptotic potential of cytochrome $a_3$ showed similar behavior, but with an apparent $pK_a$ somewhat higher, evidenced by a smaller drop in potential at the higher pH values studied (Figure 10).

Temperature dependences. The temperature dependence of the cytochrome *a* potential in both enzyme batches is displayed in Figures 11 and 12. Owing to the complexities associated with deconvolving the two cytochrome spectra and analyzing this strongly interactive multisite system, the scatter in the data is greater than that obtained from single-site metalloproteins (28-30) or from CO-inhibited cytochrome oxidase (Chapter III). An apparent batch dependence was observed: In Batch A, the reduction potential of cytochrome *a* varies with temperature by ca. -.81 mV/°C, with a corresponding standard entropy of reduction of -34 (+/- 7) cal $mol^{-1}$ $K^{-1}$. In Batch B, the reduction potential of cytochrome *a* is more steeply temperature-dependent (-1.35 mV/°C), with a corresponding standard entropy of reduction of -47 (+/- 6) cal $mol^{-1}$ $K^{-1}$. For comparison, the standard entropy of reduction of cytochrome *a* in the carbon monoxide adduct of the oxidase is -41.4 (+/- 2.8) cal $mol^{-1}$ $K^{-1}$, midway between the two measured here. The standard free energy of reduction of cytochrome *a* is similar in the two batches: $\Delta G^{o\prime}$ = -8.1 (+/- 0.2) kcal $mol^{-1}$ in Batch A, and -7.7 (+/- 0.1)

kcal $mol^{-1}$ in Batch B.

The temperature dependence of the reduction potential of cytochrome $\underline{a}_3$ in the two enzyme batches is also displayed in Figures 11 and 12. In both batches, the standard entropy of reduction of cytochrome $\underline{a}_3$ is significantly more positive than that of cytochrome $\underline{a}$. The measured values are -10 (+/- 10) cal $mol^{-1}$ $K^{-1}$ in Batch A, and -28 (+/- 7) cal $mol^{-1}$ $K^{-1}$ in Batch B. The standard free energy of reduction of cytochrome $\underline{a}_3$ is -6.2 (+/- 0.2) kcal $mol^{-1}$ in Batch A, and -7.2 (+/- 0.2) kcal $mol^{-1}$ in Batch B.

Thermodynamic parameters for the reduction of cytochromes $\underline{a}$ and $\underline{a}_3$ are compiled in Table II. For comparison, results obtained with the carbon monoxide-inhibited enzyme and measured values for other heme proteins are also shown. The standard entropy of reduction of cytochrome $\underline{a}$ is relatively large and negative compared to other low-spin cytochromes which have been studied. The standard entropy of reduction of cytochrome $\underline{a}_3$ is significantly more positive than that of myoglobin, another high-spin metalloprotein heme.

The interaction energy expressed at cytochrome $\underline{a}$ at various temperatures is plotted in Figure 13. The interaction potential does not change significantly with temperature between 5 and 30 $^{o}C$.

Ionic strength dependences. The effect of ionic strength on the cytochrome potentials was measured only in Batch B. The results are displayed in Figure 14. The reduction potential of cytochrome $\underline{a}$ is not significantly affected by variations in ionic strength between 0.06 and 0.50 M, in agreement with the results on the enzyme inhibited with carbon monoxide. The potential of cytochrome $\underline{a}_3$ is also not significantly affected. As noted above, the potential of cytochrome $\underline{a}_3$ was significantly affected when KCl was used to increase the ionic strength: The upper asymptotic potential of cytochrome $\underline{a}_3$ decreased from ca. 70 mV vs. SCE to ca. 40 mV upon the addition of 0.25 KCl. At the same time, the lower asymptotic potential varies by much less, with the effect that the titration

Figure 7. pH dependence of the reduction potential of cytochrome *a* in Batch A. The potential plotted is the upper asymptotic potential obtained from the fitting method explained in the text, and pertains when the other sites in the protein are oxidized. The line drawn through the data points describes the behavior predicted for coupling to a protolyzable group whose $pK_a$ is 7.5 when cytochrome *a* is reduced and significantly lower when it is oxidized.

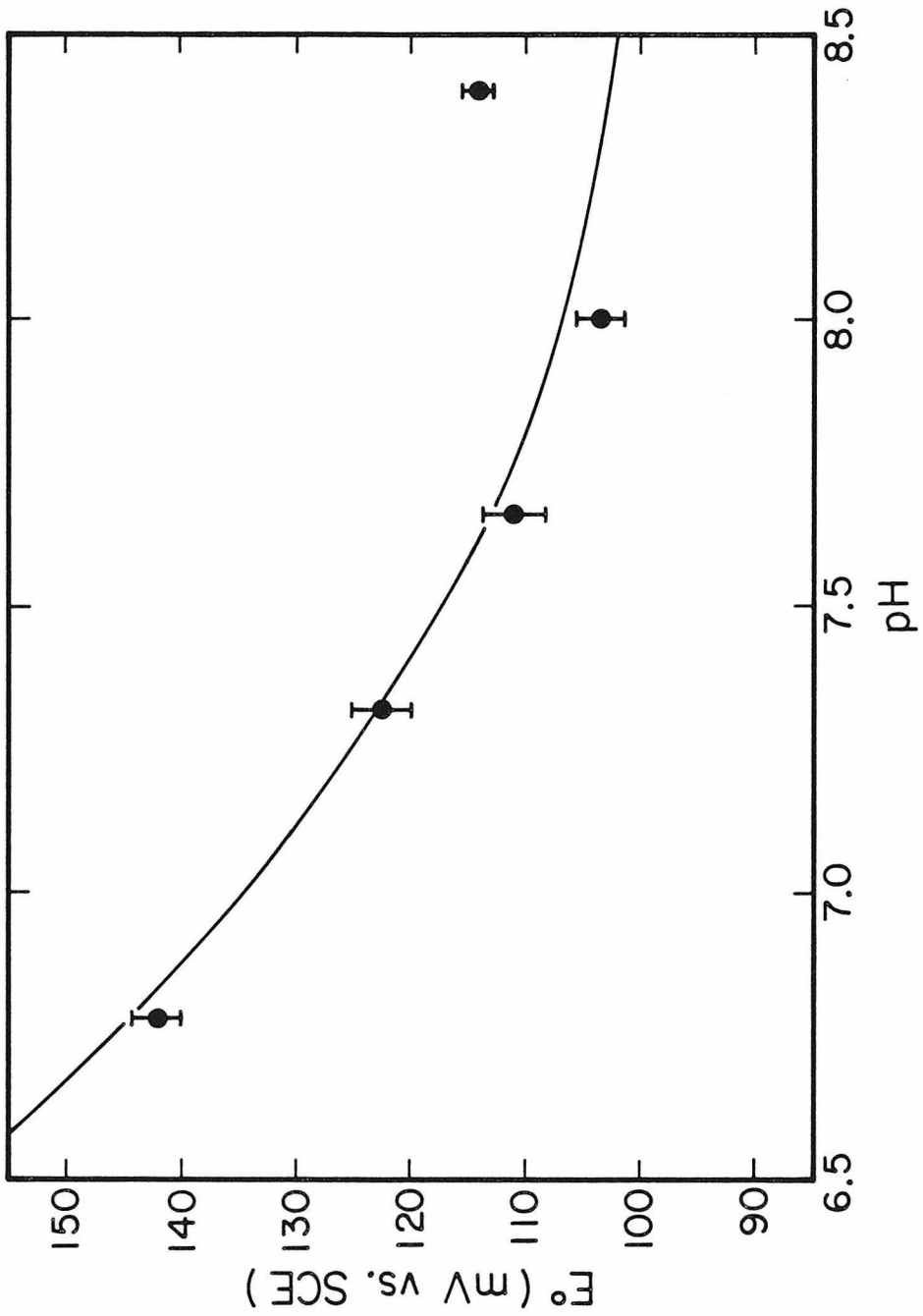
150
140
130
120
110
100
90
6.5
7.0
7.5
8.0
8.5
pH
E° (mV vs. SCE)

Figure 8. pH dependence of the reduction potential of cytochrome $\underline{a}_3$ in Batch A. The potential plotted is the upper asymptotic potential, and pertains when the other metal sites in the protein are oxidized. The line drawn through the data points has a slope of -56 mV/pH unit, corresponding to coupling to a protolyzable group whose $pK_a$s flank the middle of the pH range examined; i.e., $pK_a red < 6.7$ and $pK_a ox > 8.0$.

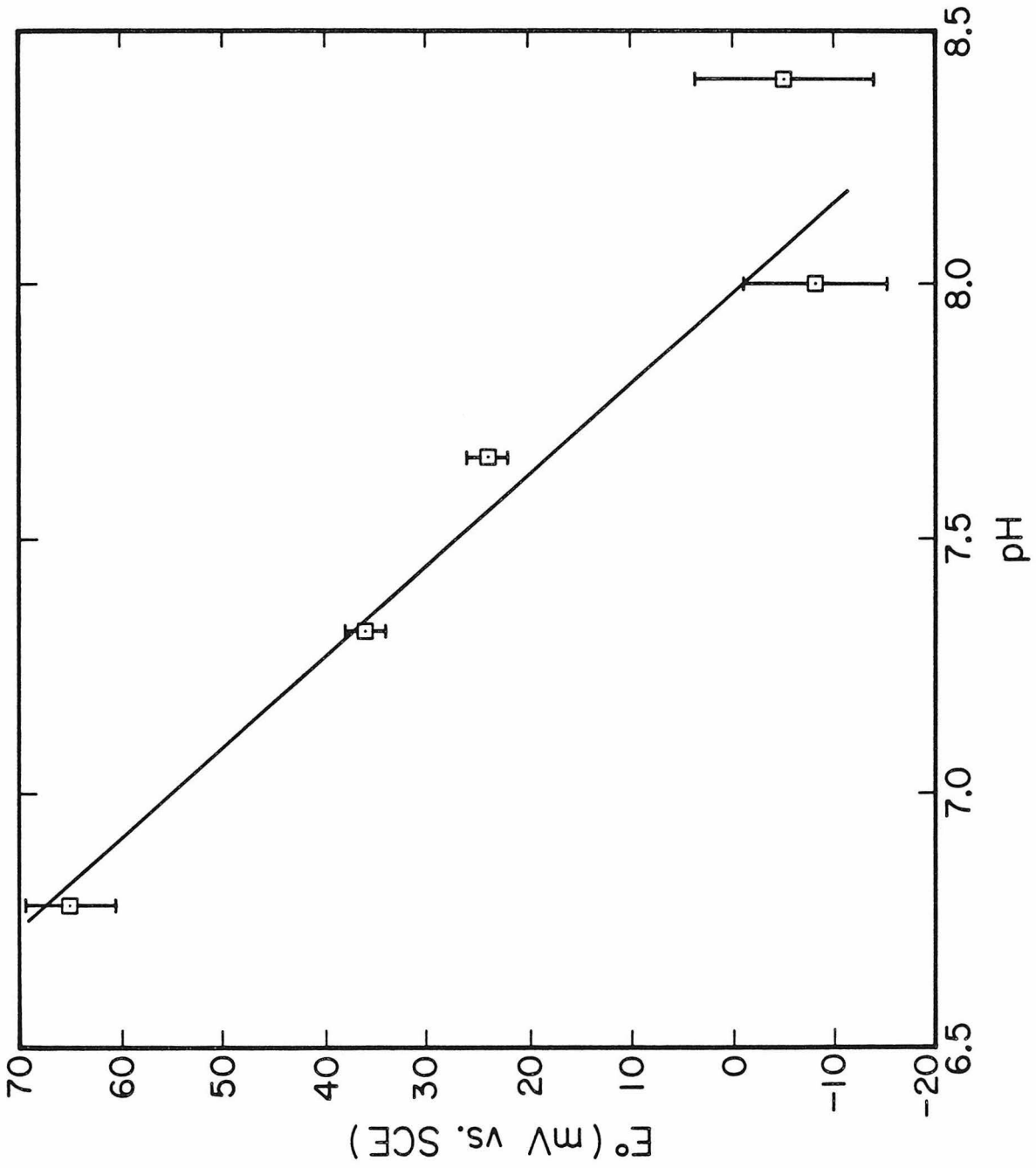
70
60
50
40
30
20
10
0
-10
-20
6.5
7.0
7.5
8.0
8.5
pH
E° (mV vs. SCE)

Figure 9. pH dependence of the upper asymptotic reduction potentials of cytochromes *a* (circles) and $a_3$ (squares) in Batch B. These potentials pertain when the other sites in the protein are oxidized. The line through the cytochrome *a* data points refers to a model like that used to describe the cytochrome *a* data from Batch A, except that $pK_a$(red) is 7.4 (cf. legend to Figure 7A). The line through the cytochrome $a_3$ data corresponds to coupling to a protolyzable group with $pK_a$ox = 7.8, and $pK_a$red significantly higher.

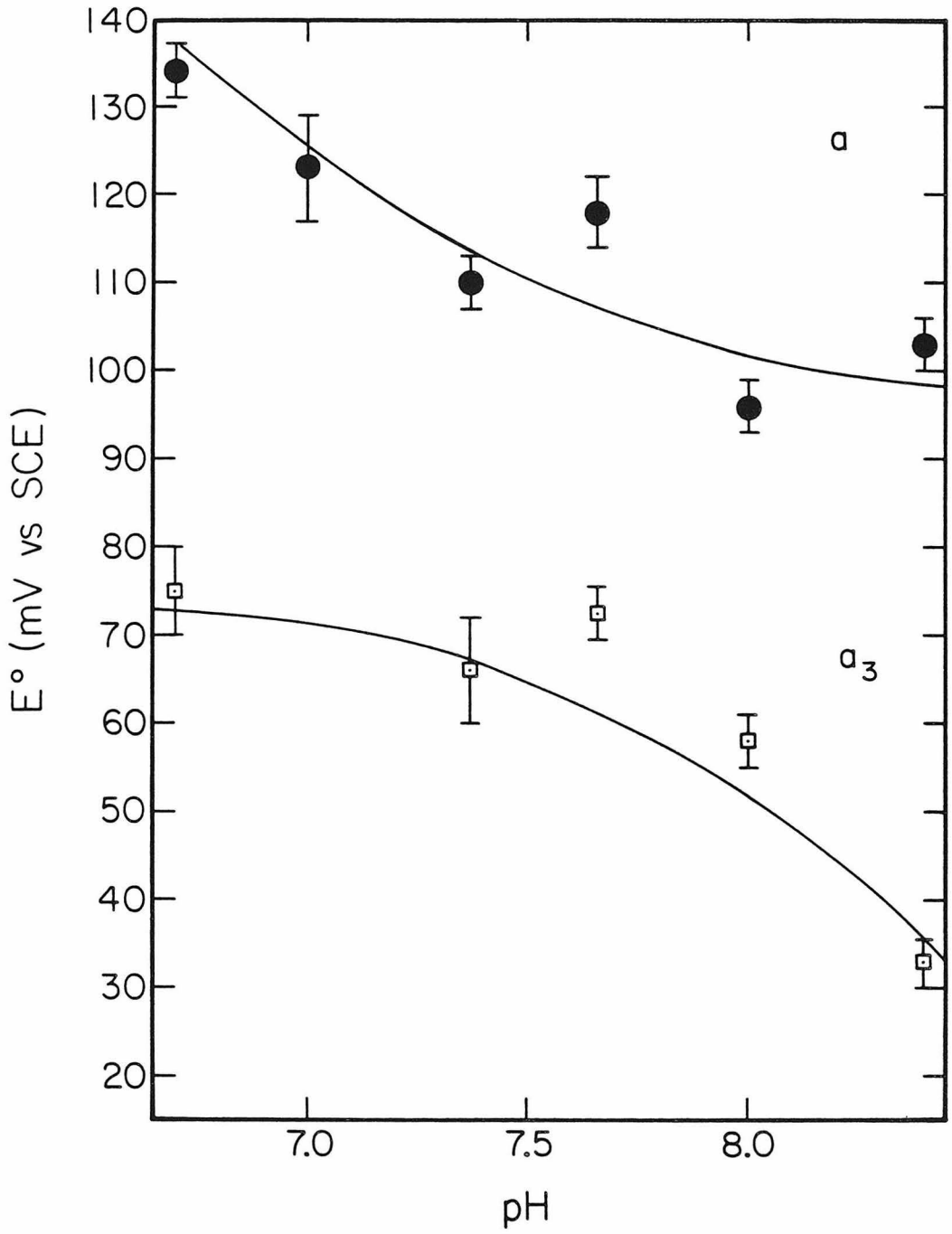
140
130
120
110
100
90
80
70
60
50
40
30
20
E° (mV vs SCE)
a
$a_3$
7.0
7.5
8.0
pH

Figure 10. pH dependence of the lower asymptotic reduction potentials of cytochromes a (circles) and $a_3$ (squares) in Batch B. These potentials pertain when the other sites in the protein are reduced. The observed pH dependences are less steep than those of the upper asymptotic potentials (Figure 9).

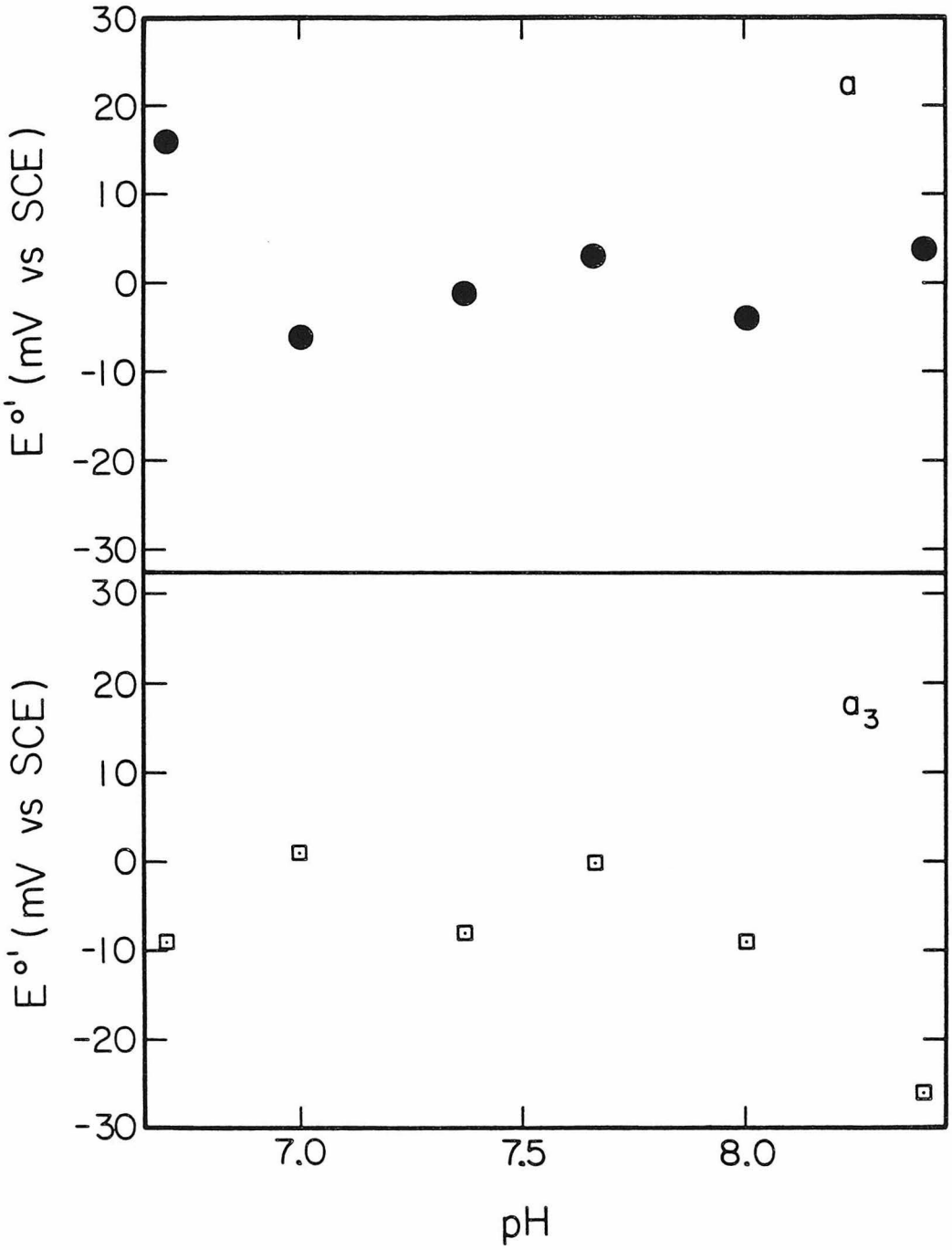
30
20
10
0
-10
-20
-30
E°' (mV vs SCE)
a
30
20
10
0
-10
-20
-30
E°' (mV vs SCE)
$a_3$
7.0
7.5
8.0
pH

Figure 11. Temperature dependence of the upper asymptotic reduction potentials of cytochromes a (circles) and $a_3$ (squares) in enzyme Batch A. The lines through the data points have slopes of −.81 mV/°C and +.23 mV/°C, corresponding to standard entropies of reduction of −34 (+/− 7) and −10 (+/− 10) entropy units, for cytochromes a and $a_3$, respectively.

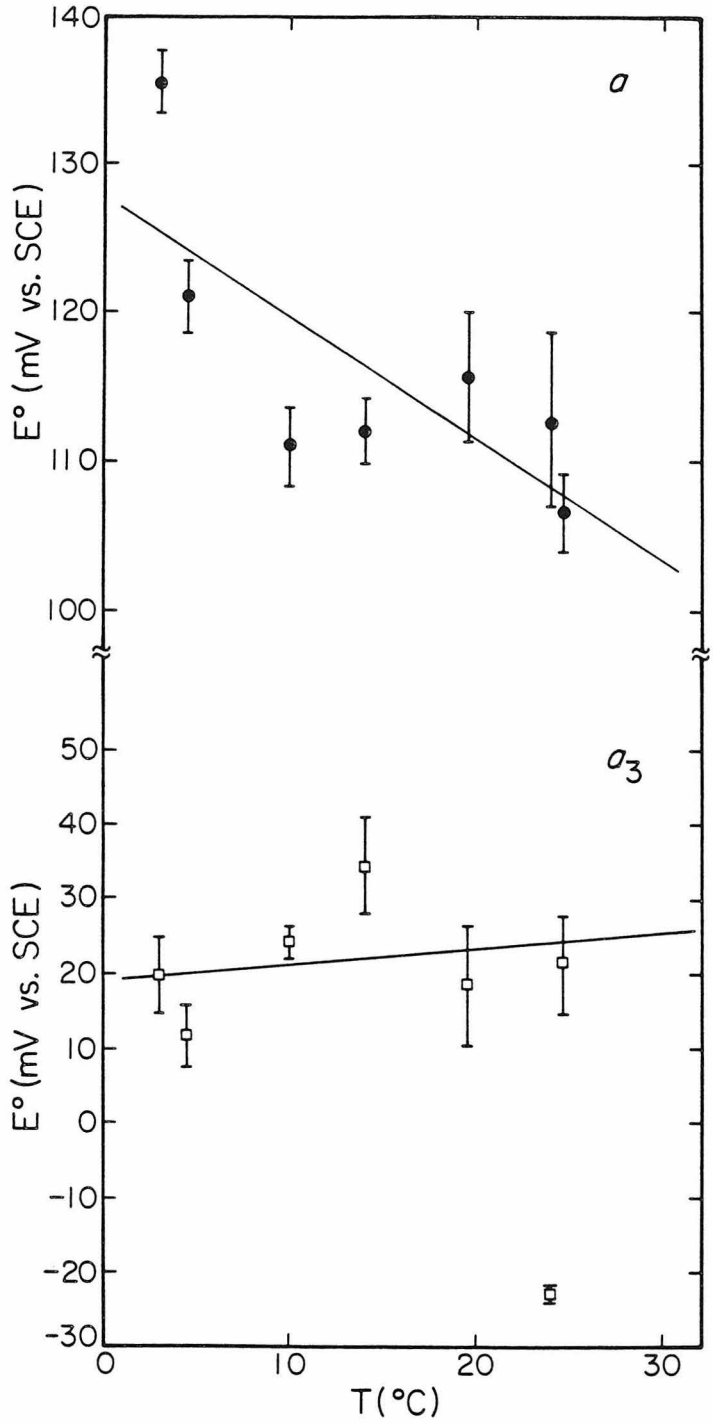
140
130
120
110
100
E° (mV vs. SCE)
a
50
40
30
20
10
0
-10
-20
-30
E° (mV vs. SCE)
$a_3$
0
10
20
30
T(°C)

Figure 12. Temperature dependence of the upper asymptotic reduction potentials of cytochromes $\underline{a}$ (circles) and $\underline{a}_3$ (squares) in enzyme Batch B. The lines through the data points have slopes of -1.35 mV/$^{o}$C and -.55 mV/$^{o}$C, corresponding to standard entropies of reduction of -47 (+/- 6) and -28 (+/- 7) entropy units, for cytochromes $\underline{a}$ and $\underline{a}_3$, respectively.

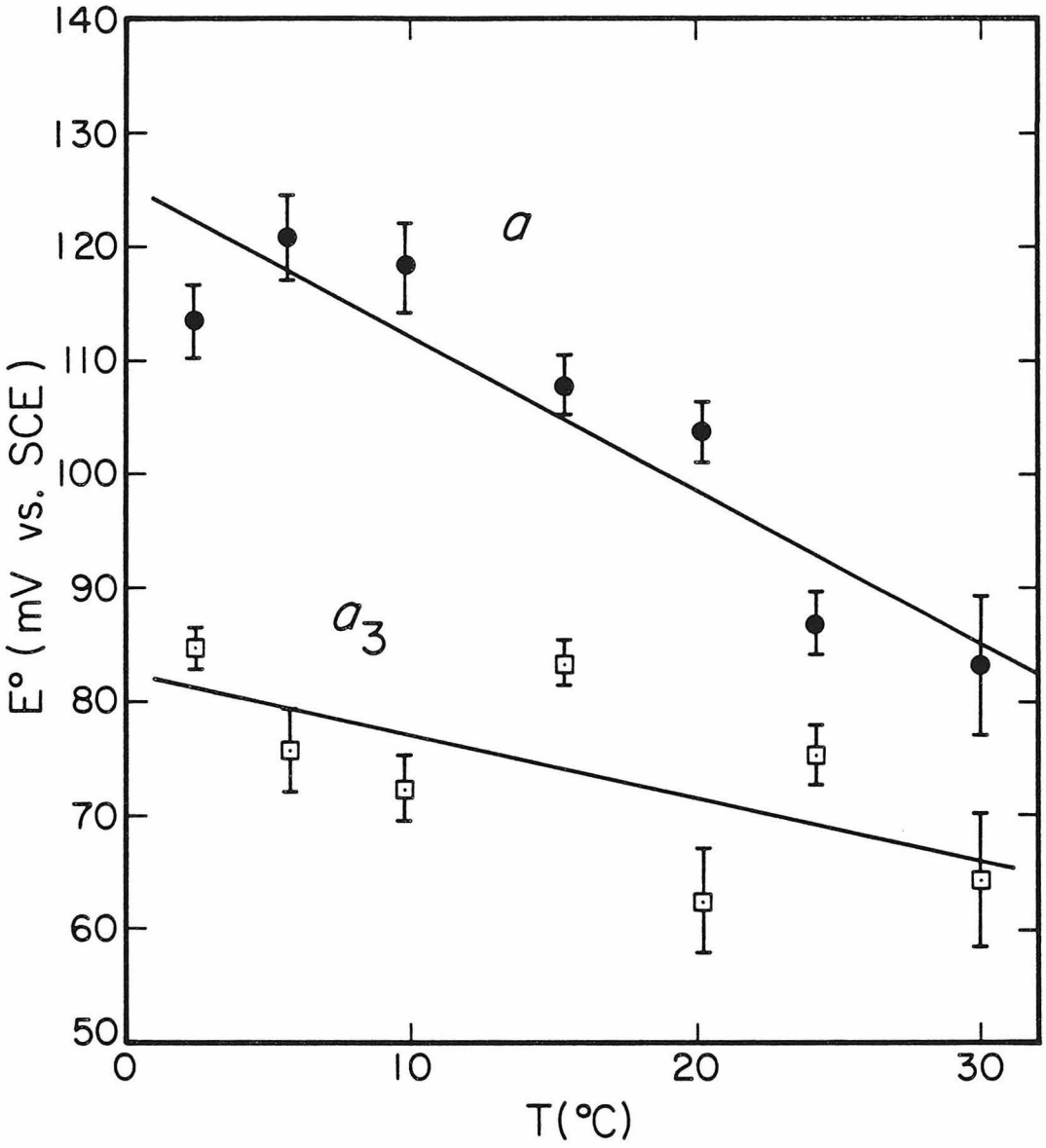
140
130
120
110
100
90
80
70
60
50
E° (mV vs. SCE)
a
$a_3$
0
10
20
30
T(°C)

Table II. Redox Thermodynamic Parameters for Heme Protein Sites

| Heme Site | $\Delta G^{o\prime}$ (kcal $mol^{-1}$, 25°C) | $\Delta S^{o\prime}$ (cal $mol^{-1}$ $K^{-1}$) | $\Delta H^{o\prime}$ (kcal $mol^{-1}$) |
|---|---|---|---|
| Cytochrome *a* (Batch A) | -8.1 +/- 0.2 | -34 +/- 7 | -18.1 +/- 2.1 |
| Cytochrome *a* (Batch B) | -7.7 +/- 0.1 | -47 +/- 6 | -21.7 +/- 1.8 |
| Cytochrome *a* (CO adduct) | -6.35 +/- 0.05 | -41.4 +/- 2.8 | -18.7 +/- 0.8 |
| Cytochrome $a_3$ (Batch A) | -6.2 +/- 0.2 | -10 +/- 10 | -9.2 +/- 3.0 |
| Cytochrome $a_3$ (Batch B) | -7.2 +/- 0.2 | -28 +/- 7 | -15.5 +/- 2.1 |
| Cytochrome *c*[a] | -6.00 +/- 0.05 | -28.5 +/- 1.2 | -14.5 +/- 0.4 |
| Cytochrome $b_5$[b] | -0.12 +/- 0.01 | -37 +/- 2.0 | -11.0 +/- 1.0 |
| Myoglobin[c] | -1.26 +/- 0.05 | -39.1 +/- 1.2 | -13.0 +/- 0.4 |

a. Reference 29

b. Reference 30

c. Reference 53

**Figure 13. Temperature dependence of the interaction energy expressed at cytochrome a in Batch B. This interaction energy is equal to the difference in the upper and lower asymptotic potentials derived from fits to the minimal interaction model described in the text.**

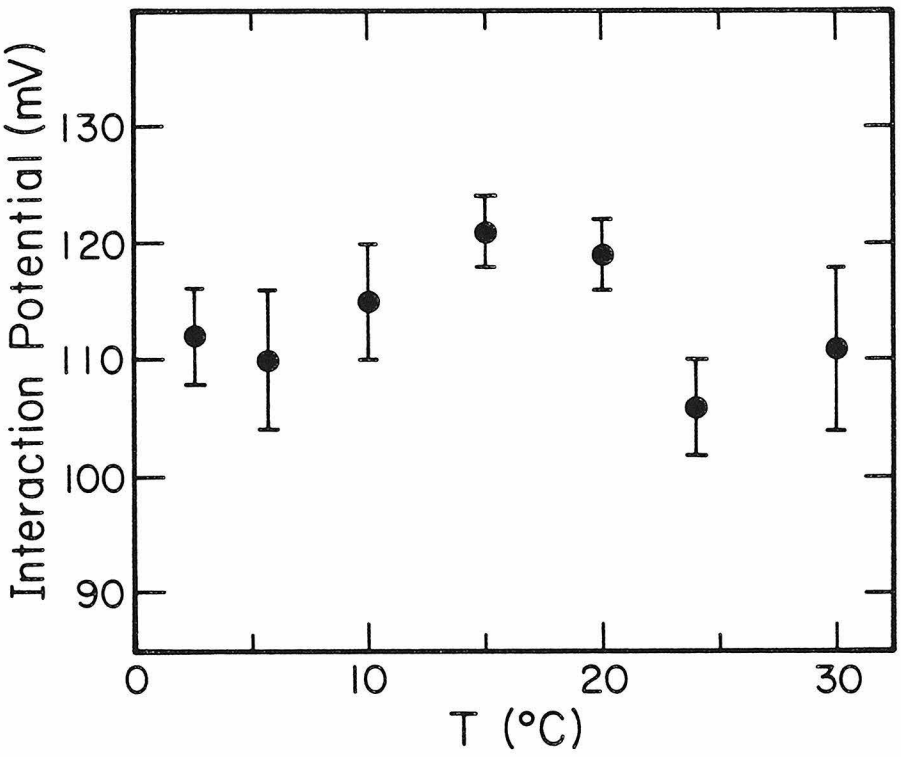
Interaction Potential (mV)
130
120
110
100
90
0
10
20
30
T (°C)

Figure 14. Ionic strength dependence of the cytochrome *a* and $a_3$ reduction potentials in enzyme Batch B. (10 °C, phosphate buffer pH 7.66) The left panel pertains to the upper asymptotic potentials, and the right panel to the lower asymptotic potentials. Circles denote cytochrome *a* and squares cytochrome $a_3$. As in other figures, the error bars shown refer to the standard error of determination of the potentials in the computer fits. Since the lower potential was not treated as an independent variable in these fits (the interaction energy was used instead), error bars are not shown for them, but would be comparable to those of the upper asymptotic potentials. The triangles refer to an experiment in which 0.25 M KCl was added to increase the ionic strength; the Nernst plots from this experiment are shown in Figure 6.

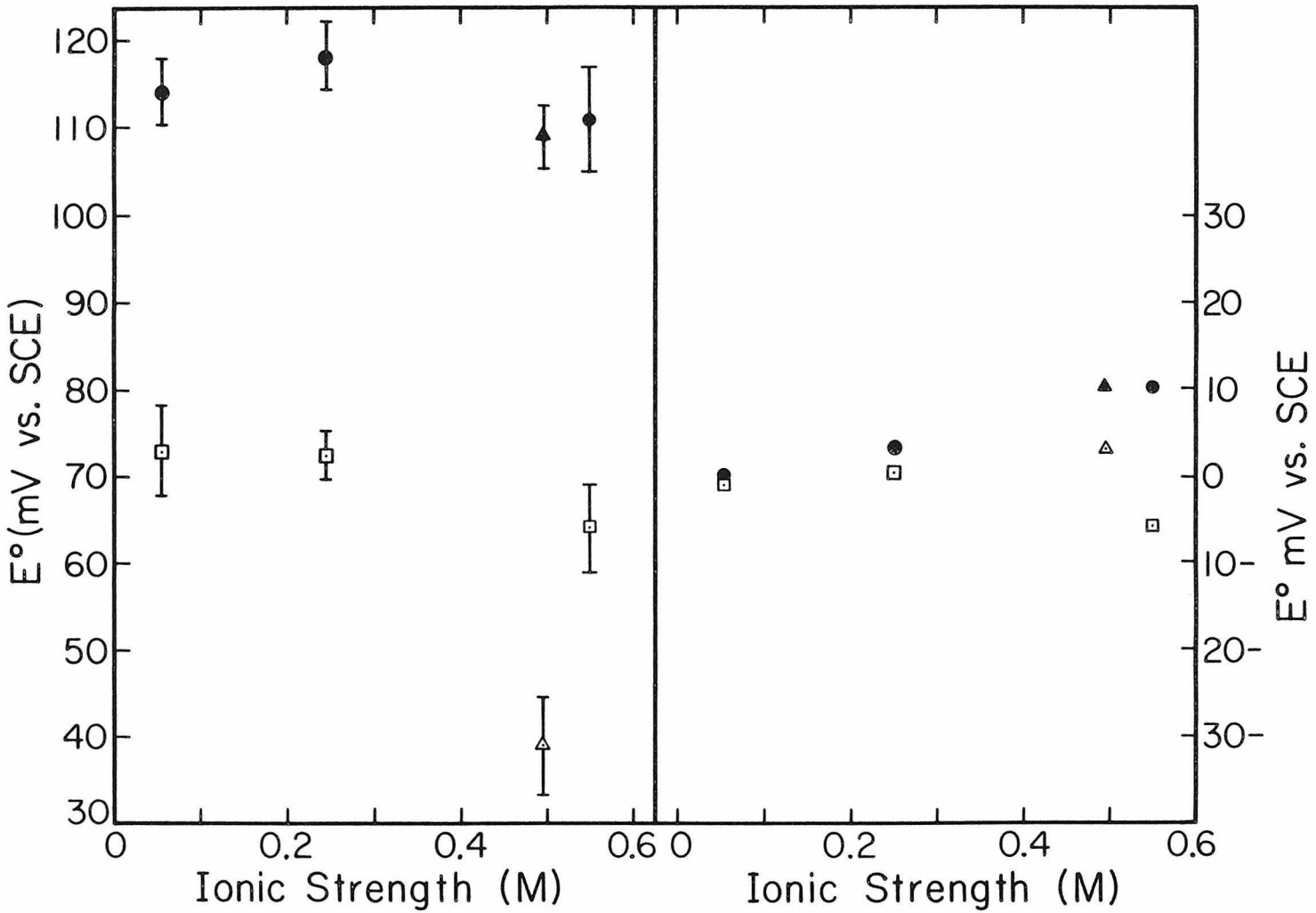
E°(mV vs. SCE)
120
110
100
90
80
70
60
50
40
30
0
0.2
0.4
0.6
Ionic Strength (M)
E° mV vs. SCE
30
20
10
0
10-
20-
30-
0
0.2
0.4
0.6
Ionic Strength (M)

behavior of cytochrome $\underline{a}_3$ approaches that expected for an isolated one-electron acceptor. The potentials measured in the presence of 0.25 M KCl are also plotted in Figure 14.

## DISCUSSION

Batch dependences. The origin of the observed batch dependences is not yet understood. Both batches were prepared in an essentially similar fashion, by the method of Hartzell and Beinert. They may nevertheless have been delipidated to different extents, since the behavior of the lipid/protein/ detergent system during the enzyme purification is likely to be complex, and subtle variations in composition or absolute concentration could concievably lead to significant differences in the final product. While their origin is poorly understood, the batch variations have proven helpful in understanding the redox behavior of the oxidase. Conversely, analysis of the titration data sheds light on the nature of the batch dependences.

The observed batch dependences involve primarily cytochrome $a_3$. The thermodynamic properties of cytochrome a (standard reduction potential, temperature and pH dependences) are more nearly batch-invariant, and are, in fact, almost the same within the uncertainty of the determinations. The pH-dependence of the upper asymptotic potential of cytochrome a is the same in the two batches (Figures 7 and 9). By contrast, both the upper asymptotic potential of cytochrome $a_3$ (at pH 7.66) and its pH-dependence are very different in the two batches (Table II, Figures 8 and 9). The probable origin of these differences will be discussed below in the context of the reduction potential pH-dependences.

Thermodynamic interactions among sites. Previous work (14,16,17,21,22) has amply demonstrated that cytochromes a and $a_3$ do not titrate as simple Nernstian n=1 electron acceptors. Previous analyses have focused upon interaction between these sites, because both of them manifest interactive behavior and because they have been more frequently studied than the coppers, being more readily monitored via their strong optical absorptions. The present work demonstrates that the copper ions must also be involved in thermodynamic interactions, in agreement with the results from the

carbon monoxide-inhibited enzyme (Chapter III,19,20) as well as results obtained using EPR at much lower temperatures (18). The evidence for this is twofold: First, the interaction manifested at cytochrome *a* (ca. 110 mV) is approximately 40 mV greater than that manifested at $a_3$ (ca. 70 mV). This result has been obtained in a large number of experiments, in two enzyme batches, and under various conditions. Second, the Nernst plots do not exhibit the shape expected if only a mutual cytochrome *a*-cytochrome $a_3$ interaction were involved. Thus the Nernst plot for cytochrome *a* (Figure 5) should follow the upper asymptote for even more of the titration before crossing over to the lower asymptote, especially in Batch A; conversely, the Nernst plot for cytochrome $a_3$ should follow the lower asymptote more closely.

In the carbon monoxide adduct of the oxidase, in which both cytochrome $a_3$ and $Cu_B$ are stabilized in their reduced states, cytochrome *a* participates in an interaction with $Cu_A$ whose magnitude is between 20 and 40 mV (Chapter III,19,20). This additional interaction is just enough to explain the difference between the total interactions expressed at cytochromes *a* and $a_3$. However, the EPR results of Goodman (18), while obtained at much lower temperature, provide strong evidence that $Cu_B$ also participates in an interaction with cytochrome *a*; the magnitude of this interaction is also approximately 40 mV. Several experiments conducted in parallel with the present work are consistent with this: Spectroelectrochemical titrations (at 10 °C) of the enzyme inhibited with ca. 1 mM cyanide showed interactive behavior in cytochrome *a* ranging between 10 and 45 mV. The origin of this variation is not presently understood but appears to involve differences in cyanide concentration in the submillimolar range. In the cyanide derivative, cytochrome $a_3$ remains oxidized, but $Cu_B$ can undergo oxidoreduction if the cyanide concentration is not very high and adequate equilibration time is allowed (18). Thus the simplest explanation of the fairly large interaction observed in some instances in titrations with the cyanide-inhibited enzyme (15,18) is that cytochrome *a* also interacts with $Cu_B$, in agreement

with the conclusions of Goodman. Given that $Cu_B$ interacts with cytochrome *a*, it is an oversimplification to assign 70 mV to a cytochrome *a*-cytochrome $a_3$ interaction, and 40 mV to a cytochrome *a*-$Cu_A$ interaction. It is evidently more correct to assign a total of 70 mV to an interaction between cytochrome *a* and the cytochrome $a_3/Cu_B$ site. Further partitioning this between the copper and iron is somewhat speculative at present, and may to some extent be artificial since the effects of the iron and copper are not necessarily simply additive. However, the results of Goodman (18), as well as the spectroelectrochemical titrations in the presence of low cyanide concentrations, suggest that approximately half of the 70 mV may be assigned to $Cu_B$.

Given that only a fraction of the 70 mV of interaction expressed at cytochrome $a_3$ is due to cytochrome *a*, a new interaction involving cytochrome $a_3$ must be proposed. An additional interaction which involves cytochrome $a_3$ is also suggested by the interaction parameters in Table I, which indicate that cytochrome $a_3$ interacts with a site whose potential is close to its own, and thus very different from that of cytochrome *a*. This interaction may in principle involve either $Cu_A$ or $Cu_B$, but owing to the proximity of these sites, it is suggested that it involves $Cu_B$. Precise titrations of the $Cu_A$ site in the native enzyme would test this proposal, since interactive behavior at $Cu_A$ in excess of that observed in the carbon monoxide derivative should be observed if $Cu_A$-cytochrome $a_3$ interaction takes place. Available titrations of $Cu_A$ in the uninhibited enzyme (38), while of limited precision, suggest that significant additional interactions are not manifested at $Cu_A$. If cytochrome $a_3$ interacts with both cytochrome *a* and $Cu_B$, the crossover region of its Nernst plot will extend over a relatively broad range of potentials, since its interacting partners will themselves have a broad range of potentials (because there are two, and because they interact with each other anticooperatively). This might explain the low apparent potential of the interactant which is derived from the analysis in Table I. Additional simulations incorporating three-site

interactions will be required to examine this question. Regardless of the details which eventually emerge, it is already clear that $\underline{a}$-$\underline{a}_3$ interaction alone cannot explain the behavior of cytochrome $\underline{a}_3$.

An interaction scheme to account for all of the available data is displayed in Figure 15. Again, the salient features of this scheme are interaction between cytochrome $\underline{a}$ and <u>all three</u> of the other sites in the protein, and interaction between cytochrome $\underline{a}_3$ and $Cu_B$. Of these, the interaction between cytochrome $\underline{a}_3$ and $Cu_B$ is the least solidly established. All of the proposed interactions are anticooperative, and will thus have the effect of buffering the redox state of the protein, so that the number of electrons which it contains will depend less sensitively on the potential of its environment than would otherwise be the case. The mechanism of the thermodynamic interaction among sites is not clear at present. Because cytochrome $\underline{a}$ is involved in interaction with every other site, and because a significant conformational change is evidently associated with its reduction (39,40, cf. below), it is tempting to assign a central role to cytochrome $\underline{a}$: A cytochrome $\underline{a}$-linked conformational change could cause the observed changes in the potentials of the other three sites, via perturbations to their structures.

<u>pH dependences</u>. The pH dependences of the cytochrome $\underline{a}$ and $\underline{a}_3$ potentials have previously been inferred from models, since proven incorrect, in which the two cytochromes were both assumed to titrate as n=1 acceptors (38,41), or from models in which the cytochromes were constrained to interact only with one another (3). More reliable estimates of the pH dependence of the cytochrome $\underline{a}$ reduction potential have been obtained from studies of the enzyme inhibited with cyanide (15) or with carbon monoxide (Chapter III); in these experiments cytochrome $\underline{a}_3$ does not titrate and thus does not complicate the observed spectral changes. Since the reduction potential of cytochrome $\underline{a}$ evidently depends upon the ligation and/or redox state of the cytochrome $\underline{a}_3/Cu_B$ site, it is important

**Figure 15. Interaction scheme to account for the thermodynamic behaviors of cytochrome *a* and cytochrome $a_3$.**

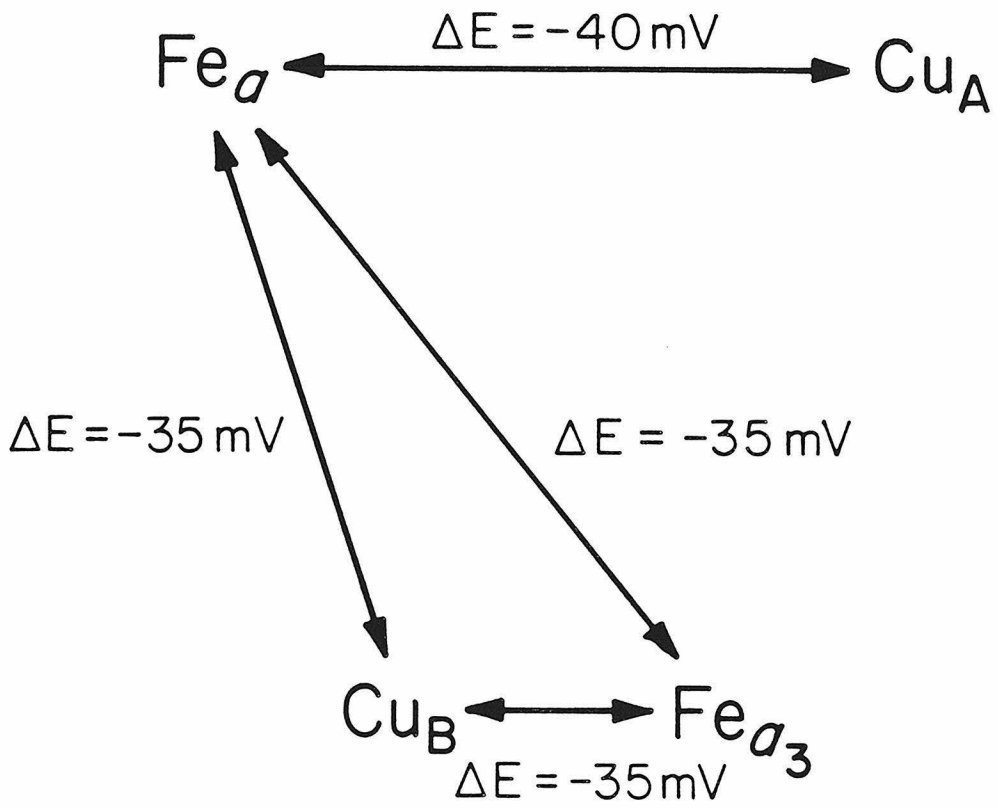
ΔE = -40 mV
Fe$_a$
Cu$_A$
ΔE = -35 mV
ΔE = -35 mV
Cu$_B$
Fe$_{a_3}$
ΔE = -35 mV

to obtain reliable measurements of pH dependences in the native enzyme. The present work represents the first attempt to deduce pH dependences from systematic deconvolution of the spectra observed in titrations of the native enzyme in conjuction with fitting the Nernst plots obtained to an interaction model in which both the intrinsic potential and the total interaction energy are treated as independent variables.

The present results for cytochrome _a_ are in accord with the results from the inhibitor derivatives: The upper asymptotic potential of cytochrome _a_, which pertains when the other sites in the protein are oxidized, displays a ca. 30 mV/pH unit dependence in the neighborhood of pH 7. This is very close to the result obtained with the cyanide-inhibited enzyme (15), in which cytochrome $\underline{a}_3$ is stabilized in its oxidized state. The lower asymptotic potential of cytochrome _a_ (Figure 10), which pertains when the other protein sites are reduced, is more weakly dependent upon pH (less than 10 mV/pH unit, on average). This is similar to the weak pH dependence of the cytochrome _a_ potential measured in the carbon monoxide adduct (ca. -9 mV/pH unit, Chapter III) in which cytochrome $\underline{a}_3$ and $Cu_B$ are maintained in their reduced states. Hence, the oxidation state of the cytochrome $\underline{a}_3/Cu_B$ site, rather than its ligation, appears to be important in determining the pH dependence of the cytochrome _a_ potential. The pronounced effect of the cytochrome $\underline{a}_3/Cu_B$ site raises the possibility that the proton taken up upon cytochrome _a_ reduction does not bind close to cytochrome _a_ but to a site in the vicinity of the cytochrome $\underline{a}_3/Cu_B$ site. Regardless of the location of proton binding, it is clear that proton uptake is not stoichiometricllly linked to reduction of cytochrome _a_. The $H^+/e^-$ quotient is maximally only 0.6 in our experiments. At pH values relevant to the mitochondrial matrix (42), i.e., well above 7, this quotient is even less. This result has important implications for the mechanism of proton pumping by the oxidase, which has been suggested to involve cytochrome _a_ (43,44).

The pH dependence of the cytochrome $\underline{a}_3$ potential in Batch A indicates that the $pK_a$ of a protolyzable group is strongly coupled to oxidoreduction of this site. This coupling, defined as $pK_a$(red) minus $pK_a$(ox), must be at least 1.5 pH units, since the data in Figure 8 indicate that the relevant $pK_a$s nearly flank the pH range examined. It has previously been suggested (45) that the axial ligand to cytochrome $\underline{a}_3$ is derived from water (when other intermediates of dioxygen reduction are not bound). If this is true, then the observed pH dependence may involve the conversion between cytochrome $\underline{a}_3$-coordinated hydroxide and a water molecule which may be either bound or free. In batch B, the pH dependence is less pronounced, but it becomes steeper at high pH in a manner which suggests an ionization with $pK_a$ near 7.8. At higher pH values, which are not accessible to study because of enzyme denaturation, this curve may continue to drop until it parallels that observed in Batch A at lower pH values. EPR experiments on partially reduced states of the oxidase (46) suggest that water coordinated to ferric cytochrome $\underline{a}_3$ deprotonates to produce hydroxide at approximately pH 8, in agreement with the $pK_a$ inferred from the reduction potential measurements on Batch B. It is interesting to note that all of the batch-dependent differences in cytochrome $\underline{a}_3$ may be explained if it is postulated that the $pK_a$(ox) of the protolyzable group coupled to cytochrome $\underline{a}_3$ has shifted from ca. 6.7 in Batch A to ca. 7.8 in Batch B, while the reduction potential of <u>protonated</u> cytochrome $\underline{a}_3$ remains the same. Such a $pK_a$ shift would cause both the increase in the cytochrome $\underline{a}_3$ reduction potential at pH 7.66 and the change in pH-dependence which is observed.

If the differences between enzyme batches reflect a shift in the $pK_a$ of the protolyzable group linked to cytochrome $\underline{a}_3$, there must exist some mechanism for modulating this $pK_a$. The stability of the iron-coordinated hydroxide is likely to depend upon the disposition of the nearby copper ion, and may, in fact, depend upon the formation of a bridged Fe-OH-Cu structure. If this is the case, then any conformational differences which influence the iron-copper distance could modulate the $pK_a$ of the hydroxide. Batch dependences

in EPR properties have previously been suggested to arise from differences of this kind at the cytochrome $\underline{a}_3/Cu_B$ site (45).

Temperature dependences and entropies of reduction. The temperature dependence of the cytochrome a reduction potential appears to be different in the two enzyme batches, but this cannot be stated with certainty given the considerable standard error in the determinations. The corresponding measurements on the carbon monoxide-inhibited enzyme yield a temperature dependence midway between the two measured here. In all cases, the observed temperature dependence is unusually steep and corresponds to a standard entropy of reduction more negative than those of most other low-spin cytochromes. This suggests that a substantial protein-ordering conformational change accompanies reduction of cytochrome a. As noted above, this conformational change may be responsible for the accompanying changes in reduction potential observed at the other three sites in the protein. It has been suggested (47) that significant protein conformational changes are likely to be involved in redox-linked proton pumping; by this criterion, cytochrome a is a suitable candidate for the proton pumping function. The total interaction expressed at cytochrome a (upper asymptotic potential minus lower asymptotic potential) is not significantly dependent upon temperature. Thus, the standard entropy of reduction of cytochrome a does not measurably depend upon the redox states of the other metal sites in the protein. Stated another way, this means that the interaction term itself has no measurable entropic component.

The temperature dependence of the cytochrome $\underline{a}_3$ reduction potential in the two enzyme batches correspond to standard entropies of reduction which are not remarkably positive or negative. The measured values are much more positive than that measured for the high-spin heme of myoglobin. Since there is no reason to expect that all high-spin hemes will have similar redox thermodynamic parameters, this result is not surprising. The enthalpy and entropy values determined here indicate that the

electron transfer from cytochrome *a* to cytochrome $a_3$ (in the absence of dioxygen) is endoenthalpic by 5–10 kcal $mol^{-1}$. Most of this is compensated by entropic factors, so that the equilibrium constant for the reaction is not very different from unity. The enthalpic cost of this electron transfer is expected to make it a relatively activated process, and the rate of electron transfer from cytochrome *a* to cytochrome $a_3$ has been shown to be steeply temperature dependent (48). The difference in the standard entropies of reduction of cytochrome $a_3$ in the two batches is probably caused by the protonation coupled to $a_3$ reduction in Batch A, but not Batch B, at pH 7.66. A study of the temperature dependence of the reduction potential of cytochrome $a_3$ at higher pH (ca. 8.4) in an enzyme sample with Batch B-like properties would test this suggestion.

Ionic strength dependence. The weak dependence of the cytochrome reduction potentials upon ionic strength suggests that these sites are effectively shielded from the solvent by the protein, as has been discussed previously for cytochrome *a* in the carbon monoxide-inhibited enzyme. Other experiments, notably resonance Raman (49) and infrared absorbance (50) studies, have shown that cytochrome $a_3$ is in a relatively hydrophobic environment. The present experiments further show that any global effects of ionic strength upon the protein structure are not manifested in the reduction potentials of cytochomes *a* or $a_3$. However, nothing is yet known of the possible effects of ionic strength upon the reduction enthalpies and entropies considered individually. In cytochrome *c*, significant compensating enthalpy–entropy effects have been seen (51), and this may also be true in cytochrome oxidase.

Chloride effect. Initially, the ionic strength was increased in our experiments by the addition of KCl (cf. triangular data points in Figure 14). The results obtained suggested that the reduction potential of cytochrome $a_3$ is significantly influenced

by ionic strength, but in an unusual way (no significant change between 0.05 and .22 M ionic strength, and a ca. 30 mV decrease between .22 and .47 M). Also, the upper and lower asymptotic potentials were affected differently, so that the interactive behavior of cytochrome $\underline{a}_3$ was diminished. Similar results were previously obtained when 0.1 M KCl was added to the oxidase in potentiometric titrations monitored by MCD (17), and were attributed to an effect of ionic strength upon the cytochrome $\underline{a}_3$ potential. By using phosphate buffer instead to raise the ionic strength, it has been shown that a specific chloride effect, rather than ionic strength, is likely to be the cause of the changes caused by KCl.

The effect of chloride upon the interactive behavior of cytochrome $\underline{a}_3$ is especially interesting. The observed effect, a ca. 30 mV reduction of $E^o$(high) with no accompanying change in $E^o$(low), is comparable to that seen in the MCD-monitored titrations, and is similar to that seen upon addition of 0.1 M fluoride (17), but somewhat smaller. The effects of chloride and fluoride are readily rationalized if it is postulated that these fairly weak ligands bind to the cytochrome $\underline{a}_3/Cu_B$ site only when <u>both</u> of these metals are oxidized. The upper asymptotic potential of cytochrome $\underline{a}_3$ pertains when its neighbor $Cu_B$ is oxidized, so the corresponding redox couple involves the totally oxidized site and will thus be subject to the chloride or fluoride effect. The lower asymptotic potential pertains when $Cu_B$ is reduced, so neither of the chemical species in the corresponding redox couple is able to bind the anions. Chloride and fluoride will therefore not affect the lower asymptotic potential. Assuming that the anions bind to the partially or fully reduced site much (ca. 100-fold) more weakly than to the oxidized site, the observed potential change of ca. 30 mV indicates that chloride binds to the fully oxidized site with a dissociation constant of approximately 0.1 M.

<u>The pulsed-resting phenomenon</u>. Attempts to obtain closely reversible titrations were frustrated, even when as many as 3 hours were allowed for equilibration at each potential. This slow

equilibration may be explained in part by the presence of interactions among the redox sites, and by the likelihood that equilibration with the electrochemical mediators occurs via only one or two of the sites (cytochrome *a* and/or $Cu_A$) in the protein, whose potentials may not be well matched to those of the other sites (cytochrome $a_3$ and $Cu_B$). However, the difference spectra which describe the hysteresis (Figure 4) indicate that multiple chemical forms of the oxidized enzyme, most likely the so-called pulsed and resting states, are involved. The equilibration between these states is known to be fairly slow (31). This problem was most pronounced at high potentials, which indicates that partial reduction of the enzyme, probably by just a single reducing equivalent, is sufficient to produce the pulsed state. The spectroscopic differences between these two states, and probably the largest structural differences, involve the cytochrome $a_3/Cu_B$ site (31,34,35,45). Since MCD is comparatively insensitive to ferric high-spin hemes, this phenomenon should not be observed in titrations monitored by MCD, and it has not been (17). While not perfectly reversible, our titrations were slow enough that they should reflect most closely the potential of the more stable resting enzyme rather than the (nonequilibrium) effective potential of the pulsed enzyme. Assuming that the reduced state of the enzyme is the same regardless of whether it is derived from pulsed or resting enzyme, the reduction potential of cytochrome $a_3$ in the resting enzyme will be lower than that of the more physiologically-relevant pulsed enzyme, and possibly much lower (no reliable estimates of the equilibrium constant of the pulsed-resting interconversion are presently available). The pertinent reduction potential of the cytochrome $a_3/Cu_B$ site during dioxygen reduction, when different intermediates are bound at every step of the reaction, may be even higher. These potentials can not be measured by equilibrium methods. These considerations should be remembered when discussing the equilibrium thermodynamic properties of cytochrome $a_3$, since these properties are of limited relevance in consequence of them.

Owing to the thermodynamic interaction between cytochrome a and $a_3$, there should be some secondary effects of the pulsed-resting phenomenon, and the associated slow equilibration of cytochrome $a_3$, at cytochrome a. In some titrations, especially at high ionic strength (and in the absence of chloride), evidence for such interaction-induced hysteresis was observed. In instances where cytochrome $a_3$ showed appreciable hysteresis of the normal kind (insufficient oxidation during the oxidative titration, and insufficient reduction during the re-reductive titration), cytochrome a showed hysteresis of the opposite kind (over-oxidation during the oxidative titration, and over-reduction during the reductive titration). Such "reversed hysteresis" is difficult to rationalize except in terms of anticooperative intersite interaction.

Spectroscopic interactions. Previous studies have found no evidence (25) or evidence for only relatively weak (Chapter II) optically manifested interactions among the sites of cytochrome oxidase under most circumstances, and it is partly on this basis that such interactions have been ignored in the present analysis. However, the spectra obtained in these titrations indicate that intersite interactions must significantly influence the absorption properties of the enzyme near 415 nm, causing the trough at this wavelength to be less deep than expected at low potentials. This wavelength suggests that ferric cytochrome $a_3$ is involved. No interactive effects at ferric cytochrome a were detected in MCD experiments (14); the optically manifested interactions described above in Chapter II were suggested to be due to cytochrome $a_3$. It is therefore likely that the unusual character of the low potential difference spectra in the 415 nm region is due to an interaction involving cytochrome $a_3$. Specifically, the results are what is expected if ferric cytochrome $a_3$ has a lower extinction when the nearby $Cu_B$ ion is reduced, so that the 415 nm trough is less deep in the low-potential portion of the titration (when $Cu_B$ is mostly reduced) than in the high-potential portion of the titration (when

$Cu_B$ is mostly oxidized). This explanation in terms of the oxidation state of $Cu_B$ is the same as that suggested in Chapter II to explain the strongest interactive effects observed there.

The present use of an interaction model to estimate the asymptotic potentials of cytochromes *a* and $a_3$ should somewhat mitigate any problems caused by spectroscopically manifested interactions. The important thermodynamic properties reported here, namely standard free energies, entropies, enthalpies, and pH- and ionic strength dependences of reduction potentials, all involve only the upper asymptotic potentials of the cytochrome *a* and $a_3$ sites. When the upper asymptotic potential of a site is measured, the other sites (including $Cu_B$) remain fixed in their oxidized states. The oxidized cytochromes absorb more weakly than the reduced cytochromes at the wavelengths employed in the factor analysis, so interactive effects involving them will be more weakly manifested in the final results. Since no evidence for significant spectroscopic interaction manifested at cytochrome *a* has ever been found, these considerations indicate that the present characterization of cytochrome *a* in particular may be accepted with a degree of confidence: The upper asymptotic potential of cytochrome *a* pertains to a particular enzyme species (viz., all other sites oxidized) in which no significant spectroscopic interaction effects are expected.

The optically manifested interaction between $Cu_B$ and cytochrome $a_3$ can evidently be significant, and requires closer consideration. In the one case where it has been measured (Chapter II), the extinction change in the alpha band associated with $Cu_B$ oxidation is ca. 3 $mM^{-1}$ $cm^{-1}$, which is a large fraction of the total extinction change in this region accompanying cytochrome $a_3$ reduction (ca. 8 $mM^{-1}$ cm.-1). The effects in the Soret region are much smaller on a percentage basis (Chapter II). An estimate of the consequences of such an effect may be made if it is assumed that the native enzyme behaves similarly, so that the alpha band reduced minus oxidized extinction is 3 $mM^{-1}$ $cm^{-1}$ too large when $Cu_B$ is oxidized, and the Soret band reduced minus oxidized extinction is

not affected. Analysis of this situation indicates that the level of reduction of cytochrome $\underline{a}_3$ will be underestimated by approximately 12%. The small value of this error is in part traceable to the great differences in alpha and Soret absorbances of the cytochromes: The factor vector ($\Delta\varepsilon(\alpha)$, $\Delta\varepsilon$(Soret)) which was used to represent cytochrome $\underline{a}$ is very different from that used to represent cytochrome $\underline{a}_3$. Furthermore, errors of this kind in measurements of the level of reduction of cytochrome $a_3$ $\underline{a}$re expected to be systematic, so that pH, temperature, and ionic strength dependences will be only secondarily affected.

More complex models for the behavior of the hemes in spectroelectrochemical titrations which take explicit account of optical interactions would necessarily introduce more adjustable parameters and assumptions into the analysis. Given the evident complexity of the system and the difficulties introduced by the pulsed-resting phenomenon, an extended analysis incorporating spectroscopically manifested interactions should await support from corollary measurements using other techniques, such as resonance Raman. In the meantime, the present study furnishes the most detailed and precise information presently available on the thermodynamic properties of cytochromes $\underline{a}$ and $\underline{a}_3$.

REFERENCES

1. Malmstrom, B.G. (1980). In Metal Ion Activation of Dioxygen (Spiro, T.G., Ed.), pp. 181-207, Wiley, New York.

2. Brunori, M., Antonini, E., and Wilson, M.T. (1981). Metal Ions in Biological Systems 13, 187-228.

3. Wikstrom, M., Krab, K., and Saraste, M. (1981a). Cytochrome Oxidase: A Synthesis, Academic Press, London.

4. Blair, D.F., Martin, C.T., Gelles, J., Wang, H., Brudvig, G.W., Stevens, T.H., and Chan, S.I. (1983). Chemica Scripta 21, 43-53.

5. Wainio, W.W. (1983). Biol. Rev. 58, 131-156.

6. Freedman, J.A., and Chan, S.H.P. (1984). J. Bioenerg. Biomembr. 16, 75-100.

7. Minnaert, K. (1965). Biochim. Biophys. Acta 110, 42-56.

8. Hinkle, P., and Mitchell, P. (1970). J. Bioenerget. 1, 45-60.

9. Heineman, W.R., Kuwana, T., and Hartzell, C.R. (1972). Biochem. Biophys. Res. Comm. 49, 1-8.

10. Vanderkooi, J., and Erecinska, M. (1974). Arch. Biochem. Biophys. 162, 385-391.

11. Anderson, J.L., Kuwana, T., and Hartzell, C.R. (1976). Biochemistry 15, 3847-3855.

12. Schroedl, N.A., and Hartzell, C.R. (1977). Biochemistry 16,

4961-4965.

13. Schroedl, N.A., and Hartzell, C.R. (1977). Biochemistry 16, 4966-4971.

14. Babcock, G.T., Vickery, L.E., and Palmer, G. (1978). J. Biol. Chem. 253, 2400-2411.

15. Artzatbanov, V.Y., Konstantinov, A.A., and Skulachev, V.P. (1978). FEBS Lett. 87, 180-185.

16. Carithers, R.P., and Palmer, G. (1981). J. Biol. Chem. 256, 7967-7976.

17. Kojima, I., and Palmer, G. (1983). J. Biol. Chem. 258, 14908-14913.

18. Goodman, G. (1984). J. Biol. Chem. 259, 15094-15099.

19. Ellis, W.R., Jr., Wang, H., Blair, D.F., Gray, H.B., and Chan, S.I. (1985) Biochemistry (in press).

20. Wang, H., Blair, D.F., Ellis, W.R., Jr., Gray, H.B., and Chan, S.I. (1985) Biochemistry, in press.

21. Wikstrom, M.K.F., Harmon, H.J., Ingledew, W.J., and Chance, B. (1976). FEBS Lett. 65, 259-277.

22. Nicholls, P., and Peterson, L.C. (1974). Biochim. Biophys. Acta 357, 462-467.

23. Wilson, D.F., and Leigh, J.S. (1974). Ann. N.Y. Acad. Sci. 227, 630-635.

24. Blair, D.F., Bocian, D.F., Babcock, G.T., and Chan, S.I.

(1982). Biochemistry 21, 6928-6935.

25. Babcock, G.T., Vickery, L.E., and Palmer, G. (1976). J. Biol. Chem. 251, 7907-7919.

26. Vanneste, W.H., and Vanneste, M.-T. (1965). Biochem. Biophys. Res. Commun. 19, 182-186.

27. Horie, S., and Morrison, M. (1963). J. Biol. Chem. 238, 2859-2868.

28. Taniguchi, V.T., Sailasuta-Scott, N., Anson, F.C., and Gray, H.B. (1980). Pure and Applied Chemistry 52, 2275-2281.

29. Taniguchi, V.T., Ellis, W.R., Jr., Cammarata, V., Webb, J., Anson, F.C., and Gray, H.B. (1982). In Electrochemical and Spectrochemical Studies of Biological Redox Components (Kadish, K.M., Ed.), pp 51-68. American Chemical Society Advances in Chemistry Series No. 201, Washington, D.C.

30. Reid, L.S., Taniguchi, V.T., Gray, H.B., and Mauk, A.G. (1982). J. Am. Chem. Soc. 104, 7516-7519.

31. Antonini, E., Brunori, M., Colosimo, A., Greenwood, C., and Wilson, M.T. (1977). Proc. Natl. Acad. Sci. USA 74, 3128-3132.

32. Brunori, M., Colosimo, A., Sarti, P., Antonini, E., and Wilson, M.T. (1981). FEBS Lett. 126, 195-198.

33. Hartzell, C.R., and Beinert, H. (1974). Biochim. Biophys. Acta 368, 318-338.

35. Orii, Y., and King, T.E. (1976). J. Biol. Chem. 251, 7487-7493.

36. Malmstrom, B.G. (1974). Quart. Rev. Biophys. 6, 389-431.

37. Cornish-Bowden, A., and Koshland, D.E., Jr. (1975). J. Mol. Biol. 95, 201-212.

38. van Gelder, B.F., van Rijn, J.L.M.L., Schilder, G.J.A., and Wilms, J. (1977) in Structure and Function of Energy-Transducing Membranes (van Dam, K., and van Gelder, B.F., Eds.), pp. 61-68, Elsevier/North Holland, Amsterdam.

39. Cabral, F., and Love, B. (1972). Biochim. Biophys. Acta 283, 181-186.

40. Urry, D.W., Wainio, W.W., and Grebner, D. (1972). Biochem. Biophys. Res. Comm. 27, 625-631.

41. Wilson, D.F., Lindsay, J.G., and Brocklehurst, E.S. (1972). Biochim. Biophys. Acta 256, 277-286.

42. Wikstrom, M., and Krab, K. (1979). Biochim. Biophys. Acta 549, 177-222.

43. Babcock, G.T., and Callahan, P.M. (1983). Biochemistry 22, 2314-2319.

44. Wikstrom, M., Krab, K., and Saraste, M. (1981b). Ann. Rev. Biochem. 50, 623-655.

45. Brudvig, G.W., Stevens, T.H., Morse, R.H., and Chan, S.I. (1981). Biochemistry 20, 3912-3921.

46. Lanne, B., Malmstrom, B.G., and Vanngard, T. (1979). Biochim. Biophys. Acta 545, 205-214.

47. Blair, D.F., Gelles, J., and Chan, S.I. (1985). Biophys. J.,

submitted for publication.

48. Scott, R.A., and Gray, H.B. (1980). J. Am. Chem. Soc. 102, 3219-3224.

49. Babcock, G.T., Callahan, P.M., Ondrias, M.R., and Salmeen, I. (1981). Biochemistry 20, 959-966.

50. Fiamingo, F.G., Altschuld, R.A., Moh, P.P., and Alben, J.O. (1982). J. Biol. Chem. 257, 1639-1650.

51. Margalit, R., and Schejter, A. (1970). FEBS Lett. 6, 278-280.

52. Morgan, J.E., Blair, D.F., and Chan, S.I. (1985). J. Inorg. Biochem. 23, 295-302.

53. Crutchley, R.J., Ellis, W.R., Jr., and Gray, H.B. (1985). J. Am. Chem. Soc. 107, in press.

# CHAPTER V. LOW TEMPERATURE KINETIC STUDY OF THE MECHANISM OF CYTOCHROME *c* OXIDASE-CATALYZED DIOXYGEN REDUCTION

## INTRODUCTION

The cytochrome oxidase-catalyzed reduction of dioxygen to water (equation 1) is rapid: Under appropriate conditions, it can be as high as 400 electrons transferred per oxidase molecule per second (2). As importantly, this reaction takes place without the release

$$4\ H^+ + O_2 + 4\ \text{ferrocyt. } \underline{c} \longrightarrow 2\ H_2O + 4\ \text{ferricyt. } \underline{c} \qquad (1)$$

of toxic partially reduced intermediates such as peroxide or hydroxyl radical.

Mitochondrial cytochrome _c_ oxidase is a large (MW = 170,000) multisubunit protein (3). As described in preceding chapters, the functional monomer contains four metal ions: two coppers, designated $Cu_A$ and $Cu_B$, and two irons contained in heme _A_ prosthetic groups, designated cytochrome _a_ ($Fe_a$) and cytochrome $\underline{a}_3$ ($Fe_{a_3}$). Two of the metal ions, $Fe_{a_3}$ and $Cu_B$, are situated close (ca. 5Å) to each other and together constitute the site of dioxygen reduction. The other two metal ions, $Fe_a$ and $Cu_A$, rapidly accept electrons from cytochrome _c_ and transfer them to the binuclear site (4).

The mechanism of dioxygen reduction by the enzyme has been the subject of several investigations (5-9). It is difficult to study the intermediates formed during the dioxygen reduction reaction under physiological conditions because the reaction is so rapid: the bimolecular rate constant for the combination of dioxygen with the reduced enzyme is $8 \times 10^6\ M^{-1}\ s^{-1}$ at room temperature and most of the ensuing intramolecular electron transfers take place within a millisecond (9,10). However, the reaction may be slowed by going to lower temperatures (160-200K). The so-called triple trapping technique, originally developed by B. Chance et al. (11), has been widely used (7,8) to follow the reaction between dioxygen and cytochrome _c_ oxidase at low temperatures. In this method, the enzyme is reduced and then inhibited by the addition of carbon

monoxide (CO), which binds tightly to ferrous $Fe_{a_3}$. Oxygen is rapidly stirred into the solution at ca. 250K, at which temperature the dissociation of CO from the enzyme is sufficiently slow that very little reoxidation of the enzyme occurs. The mixture is then frozen at a temperature at which no reaction will occur (77K) and is exposed to visible light, which causes the photodissociation of CO from $Fe_{a_3}$. The removal of CO exposes this site for reaction with dioxygen. Upon warming the sample to ca. 160K, dioxygen binds to $Fe_{a_3}$ and intramolecular electron transfer(s) occur on the time scale of minutes. These reactions can be periodically halted (by rapid cooling of the sample) and the reaction intermediates studied spectroscopically.

Clore and E. Chance (6) used this technique in conjunction with optical spectroscopy to show that at least three distinct intermediates (designated I, II, and III) form in sequence in the low-temperature reaction of dioxygen with cytochrome c oxidase. (Intermediates I and III are the same as compounds A1 and B described previously by B. Chance et al. (11).) Intermediate I is probably a species in which dioxygen is bound to ferrous $Fe_{a_3}$ and $Cu_B$ is reduced (12). Intermediate II is formed from intermediate I when one electron is transferred from one of the other oxidase metal centers ($Fe_a$ or $Cu_A$) to the dioxygen reduction site; intermediate III is produced when the last electron is transferred to this site.

Since this pioneering work, Clore et al. (8) have also followed the intermediates formed during the cytochrome c oxidase-catalyzed reduction of dioxygen using combined EPR and optical spectroscopies. EPR permits the determination of the redox states of $Cu_A$ and $Fe_a$ in intermediates I, II, and III. As a result of this more complete study, the sequential reaction scheme required refinement. The EPR experiments showed that the third electron transferred to the dioxygen molecule could originate from either $Fe_a$ or $Cu_A$, so that intermediate II is in fact a mixture of two species. In both of these species, the dioxygen reduction site may be represented formally as $[Fe_{a_3}\text{-O-O-}Cu_B]^{+2}$; the other sites may be represented by $Cu_A^{+1}/Fe_a^{+3}$ in one case or by $Cu_A^{+2}/Fe_a^{+2}$ in the other. These

species were designated IIA and IIB, respectively. At 173K, intermediate IIB is a stable product, while intermediate IIA reaches a peak concentration at 200 seconds and decays to negligible concentration after 3000 seconds. Intermediate III is formed from intermediate IIA by the transfer of an electron from $Cu_A$ to the dioxygen reduction site in the molecules in which the initial electron transfer took place from $Fe_a$.

Because both intermediates IIA and IIB contain an odd number of electrons at the dioxygen reduction site, an EPR signal might be expected from these intermediates. Although no EPR signal was reported from this site in the original work of Clore et al., Karlsson et al.(13) subsequently reported a new $Cu_B$ EPR signal associated with the 3-electron level of dioxygen reduction (intermediates IIA and IIB). (In referring to the level of dioxygen reduction, we count the electrons donated from the $Fe_{a_3}/Cu_B$ site, so that the transfer of a single electron from one of the other sites generates what will be called a 3-electron intermediate of dioxygen reduction.) The signal is unusual in that the portions of the spectrum corresponding to $g_x$ and $g_y$ are not observable, and the portion which is observable at $g_z$ is very resistant to power saturation even at 9K. This unusual EPR signal was proposed to arise from a $Cu_B$ that is coupled, via dipolar and/or exchange mechanisms, to a nearby, very rapidly relaxing species such as a ferryl $Fe_{a_3}$, which would be expected to have a total spin angular momentum of 1 (14-17).

The observation of a $Cu_B$ EPR signal from the dioxygen reduction site of a three electron-reduced intermediate is significant because it enables the direct observation of subsequent processes occurring at the dioxygen reduction site, and the elucidation of the relationship of these events to the electron transfers from the other sites. In the present work, an effort has been made to clarify the nature of the 3-electron intermediate (or intermediates) and to obtain additional insights into the mechanism of dioxygen reduction by simultaneously examining the kinetics of the electron transfers from the $Cu_A$ and $Fe_a$ sites and the behavior of the

unusual $Cu_B$ signal, over a range of temperatures. Several additional reaction steps have been resolved by incubating samples at temperatures higher than those previously used. The results indicate that there are at least two different dioxygen reduction intermediates at the 3-electron level. The temperature dependence data indicate that the conversion between these two intermediates, which is proposed to involve the breaking of the dioxygen bond, has a large enthalpy of activation but is promoted by entropic factors.

The existence of two different 3-electron intermediates of dioxygen reduction has been confirmed by conducting some experiments on partially (ca. 3 electron) reduced cytochrome c oxidase. These experiments have also proven useful in understanding the branched reaction mechanism developed by Clore et al. (8) and described above. Specifically, the results indicate that the rate of electron transfer from $Fe_a$ to the dioxygen reduction site depends significantly upon which dioxygen-reduction intermediate is present at the latter site: If the electron transferred from $Fe_a$ to the $Fe_{a_3}/Cu_B$ site is the third electron to take part in dioxygen reduction, the transfer takes place rapidly, but if it is the fourth electron the transfer is quite slow.

MATERIALS AND METHODS

Sample Preparation. Beef heart cytochrome c oxidase was isolated by the method of Hartzell and Beinert (18). The final pellet was dissolved in 0.5% Tween-20, 50 mM potassium phosphate pH 7.4 or 50 mM Tris Cl pH 7.4; ammonium sulfate and cholate were removed from the enzyme by dialysis against the same buffers. The enzyme was stored at -80 °C until ready for use. The purified enzyme contained 8 nM heme A per mg protein and its activity was 9.0 nmol $O_2$ reduced per min. per µg. protein. Heme A concentration was determined by the pyridine hemochromagen assay (19). Protein concentration was determined by a modification of the Lowry procedure which includes 1% sodium dodecyl sulfate to solubilize integral membrane proteins (20). Stock solutions used to prepare EPR samples were typically 0.2-0.3 mM in cytochrome oxidase.

EPR samples for low temperature kinetic study were prepared in 5 mm OD (3.4 mm ID) EPR tubes. They were degassed by 4-5 cycles of evacuation and flushing with argon which had been scrubbed of oxygen by passage through 0.1 M vanadous ion in 2N HCl followed by passage through 0.02M NaOH. A small excess (ca. 1.2 equivalents) of NADH (Sigma) and 0.01 equivalent of phenazine methosulfate were added to the samples under an argon atmosphere, causing complete reduction of the oxidase within 30 minutes. An equal volume of 80/20 (v/v) ethylene glycol/buffer, which had previously been degassed by 4-5 cycles of freezing, evacuation, thawing, and stirring, was mixed thoroughly with the reduced enzyme solutions at 4 °C. The argon atmosphere was then exchanged for a 25%/75% mixture of carbon monoxide (CO) (Matheson 99.99%) and scrubbed argon. The samples were cooled to -20 °C and evacuated. One atmosphere of pure oxygen was admitted to the samples in the dark and they were vigorously agitated for 15-20 s and then frozen in liquid nitrogen. It was found that the use of pure oxygen, rather than air, was important to ensure complete reaction of the oxidase with dioxygen. The frozen solution formed an optically transparent glass. Because CO is

bound to the dioxygen reduction site of the cytochrome oxidase, very little (less than 5% in most cases) oxidation of the enzyme occurs during the addition of dioxygen in the dark, as judged by the intensities of the $Fe_a$ and $Cu_A$ EPR signals prior to incubation at temperatures which allow reaction with dioxygen.

In order to remove CO from $Fe_{a_3}$, the samples were photolyzed in a finger dewar at 77K by irradiation with a 200W Hg-Xe arc lamp for 30-40 minutes, with frequent rotation of the sample so that all sides were equally exposed to the light. Following photolysis, samples were stored in liquid nitrogen until ready for use. The reaction with dioxygen was initiated by immersing the sample tubes in n-pentane baths kept at the desired temperature by immersion in methanol/ethanol solutions cooled by the addition of liquid nitrogen. It was found to be important to immerse the samples with a stirring action to accelerate thermal equilibration. The reaction was quenched by returning the samples to the liquid nitrogen bath. The n-pentane which solidified on the sample tubes was removed prior to examination of the sample by EPR.

For experiments in which the enzyme was initially only partially reduced, enough NADH was added to provide ca. 3 electrons per oxidase molecule; all other operations were identical to the preparation of the fully reduced enzyme. The extent of reduction was determined from the EPR spectrum obtained after photolysis but prior to incubation at temperatures which allow reaction with dioxygen.

EPR Spectroscopy. EPR spectra were recorded on a Varian E-line Century Series X-band spectrometer operating in the absorption mode. The modulation amplitude was 16 Gauss and the modulation frequency 100 kHz. Microwave powers used were: 0.02 mW for the $Cu_A$ signal, 0.02 mW or 0.20 mW for the $Fe_a$ signal, and 20 mW for the $Cu_B$ signal.

Sample temperature was controlled with an Air Products Heli-Tran cryostat. The temperature at the sample position was measured before and after spectra were acquired, using a

gold-chromel thermocouple in a glycerol-filled EPR tube. The temperature was typically 9K. Data were rejected if significant (>.5K) temperature changes occurred during spectrum acquisition.

For most purposes, EPR intensities were measured as peak heights ($Fe_a$ at g=3) or peak-to-trough distances ($Cu_A$). For purposes of absolute comparisons between signal intensities, the $Cu_A$ signal was double-integrated, using a baseline which was determined by the requirement that the first integral be zero, and the $Fe_a$ signal was integrated by the method of Aasa and Vanngard (21) using the peak at g=3 to estimate the total area. The $Cu_B$ signal was integrated using the lowest-field hyperfine peak to estimate the total area, using the assumption that the $g_x$ and $g_y$ values are both 1.3, as suggested by lineshape simulations (14). This integration verified that the observed $Cu_B$ signal intensity corresponded to the number of spins expected on the basis of the kinetic models postulated. For routine relative measurements of the $Cu_B$ signal, the height of the lowest-field hyperfine peak was used; the linewidth of this peak was observed to remain constant within the uncertainty of the determination.

Data Analysis. To determine the temperature dependence of the rate constant for the decay of the $Cu_B$ EPR signal, the decay was investigated over a range of temperatures. The kinetic data for the decay of the $Cu_B$ EPR signal were not well fitted by a single exponential function. It is thought that nonexponential kinetics for processes in proteins at low temperatures results from the presence of multiple conformations which have different barrier heights for the process (22-24). At low temperatures, there is insufficient thermal energy to promote interconversions among the various conformations. Thus, all of the various activation enthalpies for the process are manifested in the kinetics. Experimentally, a distribution of activation enthalpies is observed, instead of a single, well-defined value.

Austin et al. (22) first demonstrated that the nonexponential kinetics for the rebinding of CO to myoglobin at low temperatures

could be fitted to the power law given in equation 2:

$$N(t) = C(1 + t/t_0)^{-n} . \qquad (2)$$

N(t) is the fraction of unbound heme at time t. C, $t_0$, and n are constants. It should be noted that n and $t_0$ are temperature-dependent constants, so it is more accurate to write n(T) and $t_0(T)$.

Austin et al. showed that the rate of reaction which corresponds to the most probable activation enthalpy, $\Delta H_p^{\ddagger}$, is given by (22):

$$k_p = n/t_0 = \exp[\Delta S^{\ddagger}/R - \Delta H_p^{\ddagger}/RT] . \qquad (3)$$

Thus, by fitting the data from the decay of the $Cu_B$ EPR signal to equation 2, n(T) and $t_0(T)$ may be determined, from which the most probable rate constant in the distribution is obtained. A plot of log $k_p(T)$ versus 1/T then yields the activation entropy and the most probable activation enthalpy.

The $Cu_B$ kinetic data were fitted to the power law using a non-linear least-squares computer program which computes the least-squares estimates of C, n, and $t_0$. Activation enthalpies and entropies were calculated by fitting the ln $k_p$ versus 1/T data, using a linear least-squares program, to the linear form of the Arrhenius relation in Equation 3. Error bars on the graphs represent twice the sample standard deviation of the data points from the best fit line in the non-linear least-squares fit of the kinetic data at each temperature.

The same linear least-squares analysis was also applied to the Arrhenius plot of the kinetic data for $Cu_A$ oxidation. For this process, the rate was estimated by measuring the initial slope to the EPR intensity vs. time curves.

## RESULTS

The Oxidation of Fea and $Cu_A$. Following photolysis of CO from $Fe_{a_3}$ at 77K, cytochrome c oxidase samples were first incubated at temperatures between 166 and 186K to initiate the intramolecular electron transfers to dioxygen. Optically monitored low temperature kinetic studies have established that the binding of dioxygen to $Fe_{a_3}$ takes place with a bimolecular rate constant of 81 $M^{-1}$ $s^{-1}$ at 173K (8); hence, this binding step is not expected to be significantly rate-limiting in the present experiments, where the oxygen concentration is ca. 1 mM and the initial electron transfers take place with rates of approximately 2 x $10^{-3}$ $s^{-1}$ at 173K. The intermediate which is formed upon dioxygen binding, designated I by Clore et al. (8), exhibits no EPR signals. Upon incubation at temperatures between 166 and 186K, electron transfers from $Cu_A$ or $Fe_a$ to the dioxygen reduction site take place, causing the appearance of EPR signals which are characteristic of these metal ions in their oxidized states.

The magnitudes of the $Cu_A$ and $Fe_a$ EPR signals after various times of incubation at 181K are plotted in Figure 1. The oxidation of $Cu_A$ during the first 30 minutes at 181K takes place in at least two phases, as evidenced by the poor quality of a single exponential fit to the data. If the analysis is restricted to only the first 3 minutes of oxidation at 181K and if data points are taken at shorter intervals, the data are satisfactorily fitted by a single exponential (data not shown), indicating that a prior step is not partially rate-limiting. Fits to the $Fe_a$ data were not conclusive with respect to the question of whether the oxidation is monophasic or biphasic owing to the poorer signal-to-noise ratio of this signal. The ratio of the intensities of the $Cu_A$ and $Fe_a$ signals during the initial phase of oxidation is also shown in Figure 1, and demonstrates that the two sites are not oxidized in parallel. After 55 minutes at 181K, the intensity of the $Fe_a$ signal corresponded to only ca. 30% of the intensity of the $Cu_A$ signal. In samples

which had been thoroughly oxygenated prior to freezing, the intensity of the $Cu_A$ signal corresponded to nearly 100% of the enzyme molecules, as judged by the effect of thawing the samples and remeasuring the $Cu_A$ EPR signal. All of these observations agree qualitatively with the results of the combined optical/ EPR study of Clore et al. (8). Their results and ours are most satisfactorily accounted for in terms of the reaction sequence depicted in Scheme 1.

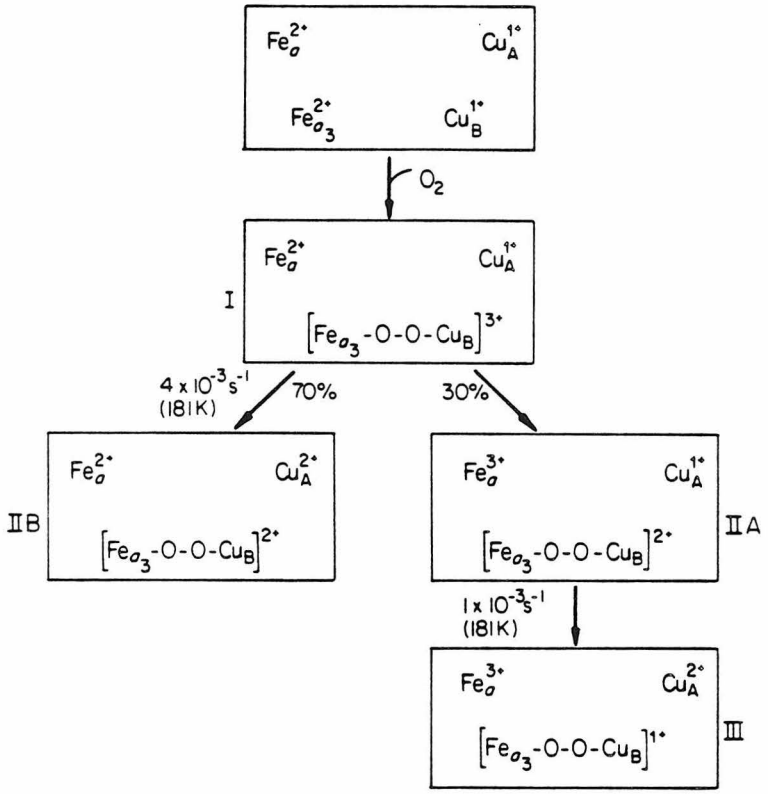


Scheme 1

The oxidation of $Cu_A$ was investigated at several temperatures between 166 and 186K. Because this process is not well fitted by a single exponential, the rate of the first oxidation step was estimated by measuring the initial slopes of the EPR intensity versus time curves. The rate constants and corresponding temperatures are presented in Table I. An Arrhenius plot of the data is linear within experimental uncertainty and gives an

Figure 1. Intensities of the EPR signals due to $Cu_A$ and $Fe_a$ during incubation of a reduced cytochrome c oxidase sample in the presence of dioxygen at 181K. Conditions of EPR spectroscopy: Temperature 9K; microwave frequency 9.172 GHz; modulation amplitude 16G; microwave power .02 mW ($Cu_A$) or .20 mW ($Fe_a$). Sample preparation, incubation methods, and quantitation of EPR signals are described in Materials and Methods. Bottom: Ratio of the intensities of the $Fe_a$ and $Cu_A$ signals during the reaction at 181K.

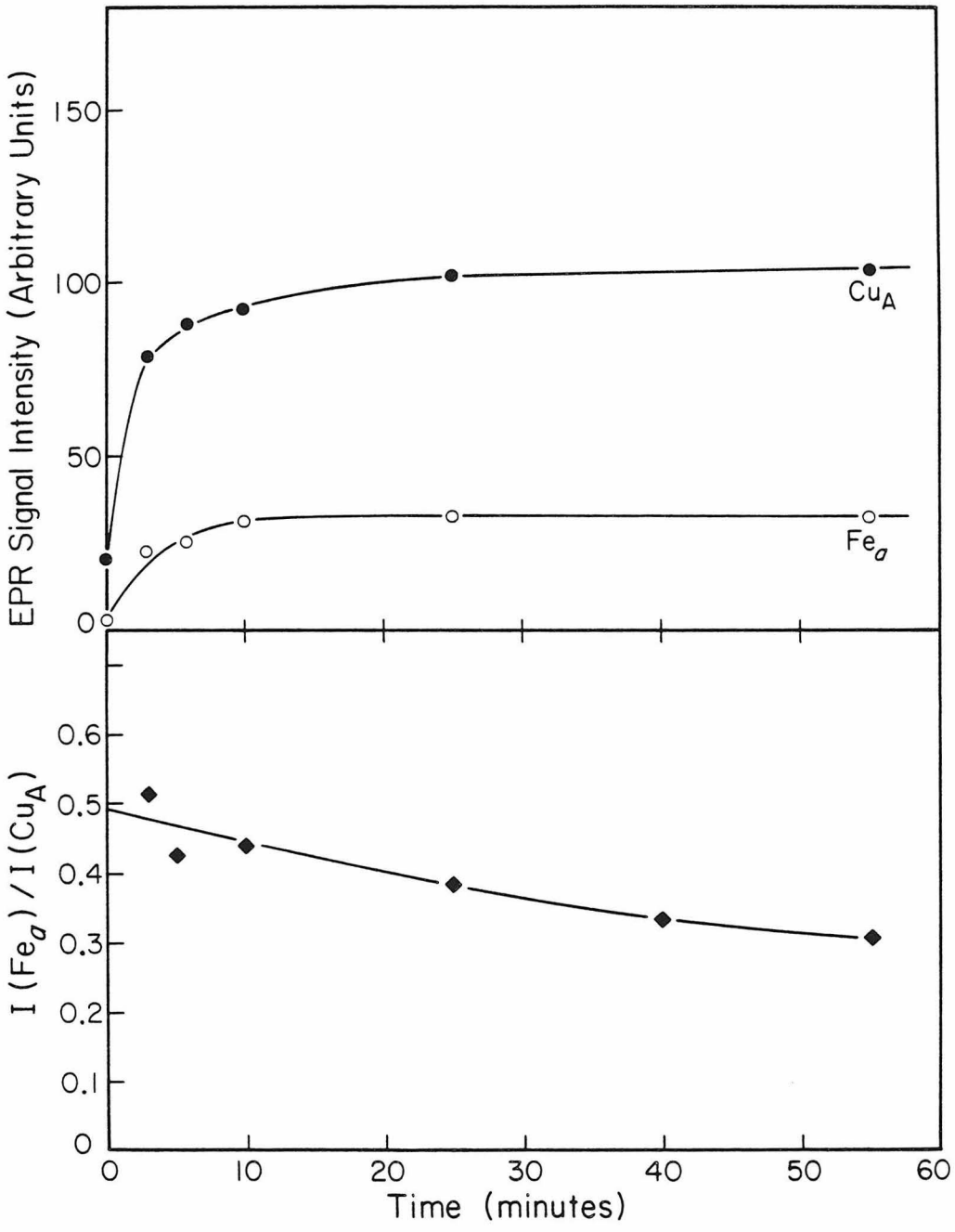
EPR Signal Intensity (Arbitrary Units)
150
100
50
0
$Cu_A$
$Fe_a$
$I(Fe_a) / I(Cu_A)$
0.6
0.5
0.4
0.3
0.2
0.1
0
0
10
20
30
40
50
60
Time (minutes)

## Table I

First-Order Rate Constants* and Corresponding Temperatures for the Formation of the $Cu_A$ EPR Signal

| Temp.(K) | k (s-1) |
|---|---|
| 186.0 | (1.7 +/- .2) x $10^{-2}$ |
| 181.0 | (4.4 +/- .2) x $10^{-3}$ |
| 180.5 | (4.6 +/- .1) x $10^{-3}$ |
| 176.0 | (1.3 +/- .1) x $10^{-3}$ |
| 173.0 | (1.9 +/- .1) x $10^{-3}$ |
| 171.0 | (5.0 +/- .2) x $10^{-4}$ |
| 166.0 | (1.9 +/- .2) x $10^{-4}$ |

* First-order rate constants were determined by measuring the initial slopes to the formation curves for the $Cu_A$ signal.

activation enthalpy and entropy of 13.2 +/- 1.4 kcal $mol^{-1}$ and 2.8 +/- 7.7 cal $mol^{-1}$ $K^{-1}$, respectively, assuming a preexponential factor of $10^{13}$ $s^{-1}$ (25). The level of $Fe_a$ oxidation which was attained in this early phase of the reaction (and therefore its rate of oxidation) relative to that of $Cu_A$ did not vary significantly over the temperature range examined, indicating that the activation enthalpies for the $Fe_a$ and $Cu_A$ oxidations are similar.

In an infrared absorption study of the photolysis of CO from cytochrome c oxidase, Fiamingo et al. (26) have shown that when CO is photolyzed from the enzyme at low (ca. 180K) temperatures, it first binds to $Cu_B$ and subsequently recombines with $Fe_{a_3}$ in a relatively slow process. While CO remains bound to $Cu_B$, the binding and reaction of dioxygen to form an electron-accepting intermediate is likely to be inhibited. These authors consequently suggested that the dissociation of CO from $Cu_B$ may be rate-limiting in the initial electron transfer step of the dioxygen-reduction reaction as studied by the triple-trapping technique. The rate of recombination of CO with $Fe_{a_3}$ (which parallels its rate of dissociation from $Cu_B$) is 7.4 x $10^{-3}$ $s^{-1}$ at 181K; the activation enthalpy for this process is 9.2 kcal $mol^{-1}$ (26). Comparison with the present measurements (Table 1) shows that the rate of $Cu_A$ oxidation at 181K is similar (within a factor of two) at this temperature whereas the activation enthalpy for $Cu_A$ oxidation is significantly greater.

Production of the Unusual $Cu_B$ EPR Signal. The initial transfer of an electron from either $Cu_A$ or $Fe_a$ to the dioxygen reduction site produces an intermediate which contains an odd number of electrons at the dioxygen reduction site. This species gives rise to a copper EPR signal which is distinguished by two unusual properties: It is very difficult to saturate, even at 9K, and only one of its g-values is evident in the spectrum (13,14). This signal has been assigned to $Cu_B$ in close proximity to another paramagnetic ion which undergoes more rapid spin relaxation (13,14). In Figure 2, the intensity of this signal after various times of incubation at 181K is shown. The $Cu_B$ EPR spectrum in the $g_z$ region is shown in

Figure 2. The intensity of the unusual $Cu_B$ EPR signal during incubation of a reduced cytochrome *c* oxidase sample in the presence of dioxygen at 181K. Conditions of EPR spectroscopy were as noted in Figure 1, except that the microwave power was 20 mW. Sample preparation, incubation methods, and EPR signal quantitation are described in Materials and Methods.

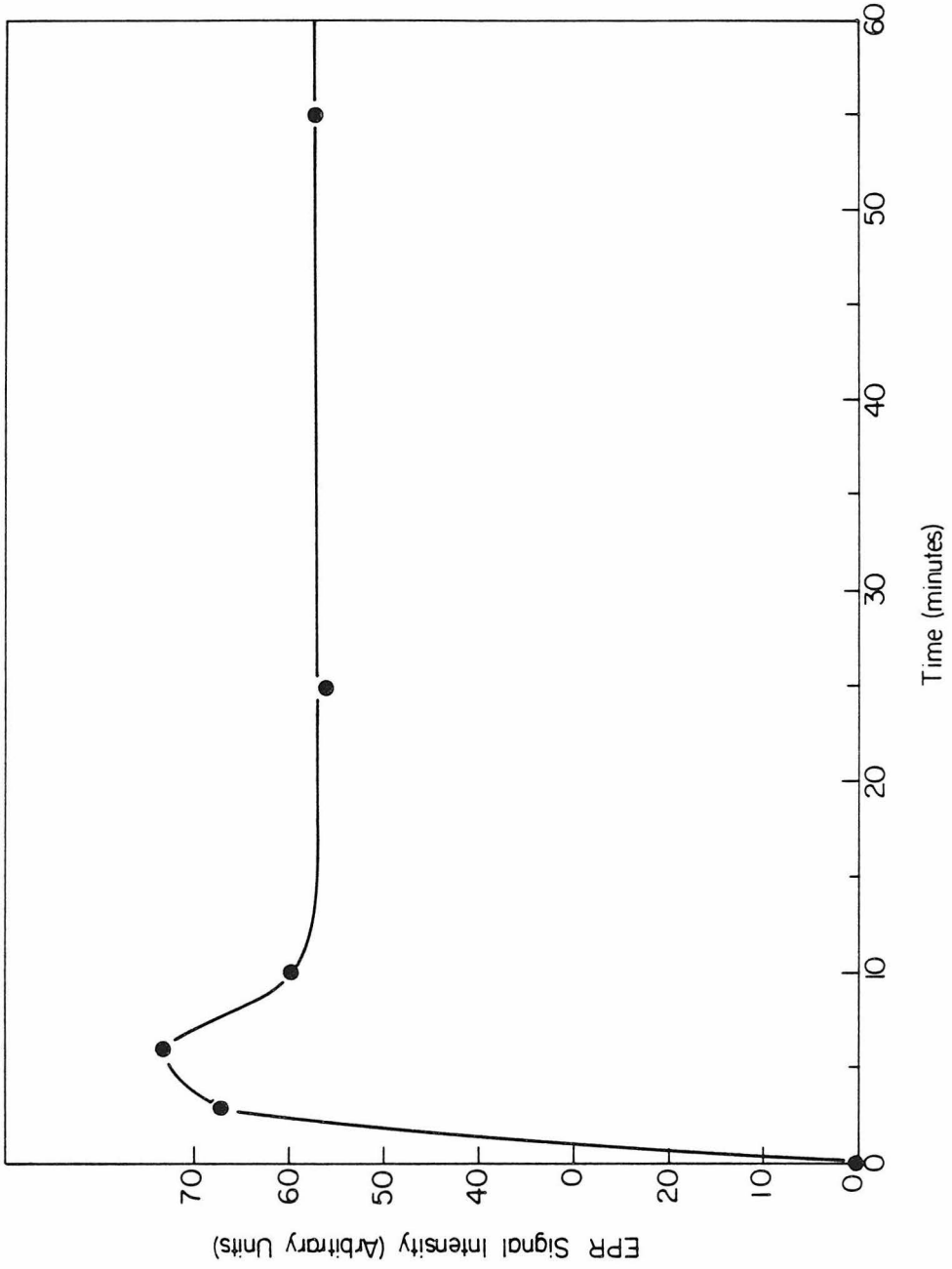
EPR Signal Intensity (Arbitrary Units)
70
60
50
40
0
20
10
0
0
10
20
30
40
50
60
Time (minutes)

Figure 3. The unusual $Cu_B$ EPR spectrum observed after incubation of a cytochrome oxidase sample (initially fully reduced) for 45 seconds at 191K. Conditions of EPR spectroscopy as in Figure 2. The observed hyperfine coupling is 137 Gauss. Only the four features indicated are associated with the $Cu_B$ signal; the remaining features are due to $Cu_A$, and to a lesser extent $Fe_a$.

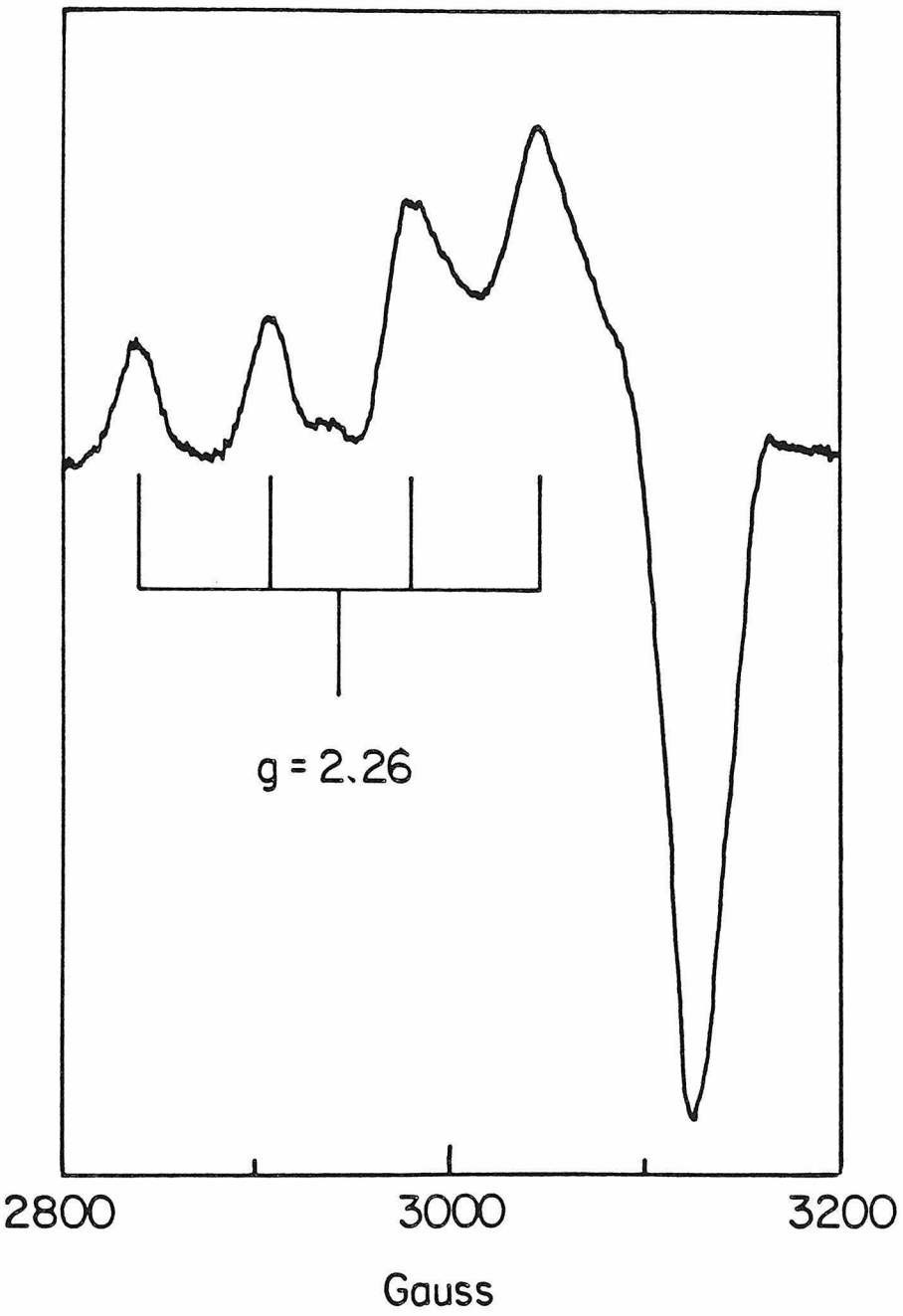
g = 2.26
2800
3000
3200
Gauss

Figure 3. In agreement with earlier findings (13), it is observed that the early growth of this signal roughly parallels the initial oxidations of $Cu_A$ and $Fe_a$. This result is consistent with the assignment of the signal to an intermediate at the $Fe_{a_3}/Cu_B$ site which is at the 3-electron level of dioxygen reduction. The intensity of this signal reaches its maximum after approximately 5 minutes at 181K; it then decays somewhat, leveling off after approximately 20 minutes. At times between 30 and 90 minutes, the signal intensity does not change appreciably; assuming $g_x$ and $g_y$ values of 1.3 (as suggested by the lineshape simulations described in reference 14) the $Cu_B$ signal intensity at this time corresponds to ca. 80% of that of $Cu_A$, consistent with Scheme 1.

Decay of the Unusual $Cu_B$ EPR Signal. Subsequent steps in the dioxygen reduction reaction, which have not been investigated previously, were studied by raising the sample incubation temperature. The intensities of the $Cu_A$, $Fe_a$, and $Cu_B$ EPR signals after various times of incubation at 191.5K are plotted in Figure 4. This sample was preincubated at a lower temperature (177K) to produce the $Cu_A$, $Fe_a$, and $Cu_B$ EPR signals. At 191.5K, the unusual $Cu_B$ signal decays to negligible intensity at a conveniently monitored rate (ca. $4.5 \times 10^{-3}$ $s^{-1}$). During the same period, the level of $Fe_a$ oxidation changes by less than 20% (in terms of the total number of oxidase molecules present) and that of $Cu_A$ by less than 10%. The changes in the $Fe_a$ and $Cu_A$ EPR signal intensities do not parallel the decay of the unusual $Cu_B$ EPR signal. After 1 hour at 198K, $Fe_a$ is still less than 50% as oxidized as is $Cu_A$, yet the unusual $Cu_B$ signal is almost completely gone. These observations imply that a process occurs at the $Fe_{a_3}/Cu_B$ site which is independent of the transfer of the fourth electron from either $Cu_A$ or $Fe_a$ and which causes the disappearance of the unusual $Cu_B$ signal. This would imply the existence of a second, EPR-silent intermediate at the 3-electron level of dioxygen reduction.

The decay of the unusual $Cu_B$ signal is clearly nonexponential at all temperatures at which it was examined. Nonexponential

Figure 4. Intensities of the EPR signals due to $Cu_A$, $Fe_a$, and $Cu_B$ during incubation of a cytochrome c oxidase sample at 191.5K. Initially reduced samples were preincubated at a lower temperature (177K) for 2 hours to produce the intermediate which exhibits the $Cu_B$ EPR signal. The lines through the $Cu_A$ and $Fe_a$ data points are drawn to guide the eye. The line through the $Cu_B$ data points is the best power law fit (explained in Materials and Methods). Conditions of EPR spectroscopy were as described in the legends to Figures 1 and 2.

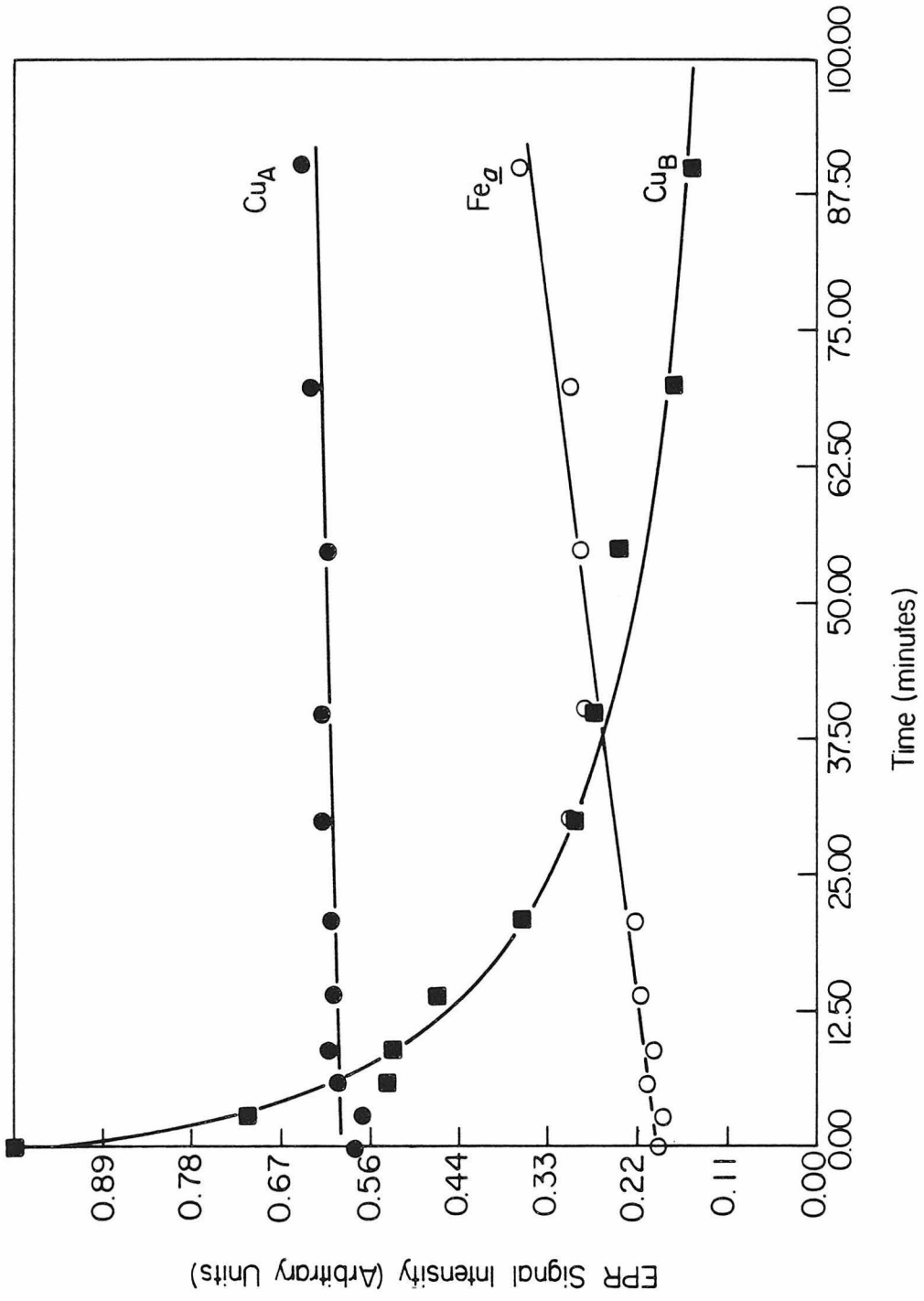
EPR Signal Intensity (Arbitrary Units)
0.89
0.78
0.67
0.56
0.44
0.33
0.22
0.11
0.00
0.00
12.50
25.00
37.50
50.00
62.50
75.00
87.50
100.00
Time (minutes)
$Cu_A$
$Fe_{\underline{g}}$
$Cu_B$

## Table II

First-Order Rate Constants* and Corresponding Temperatures for the Decay of the $Cu_B$ EPR Signal

| Temp.(K) | $k_p$ (s-1) |
|---|---|
| 207.0 | (3.4 +/- .6) x $10^{-2}$ |
| 203.0 | (1.8 +/- .4) x $10^{-2}$ |
| 203.0 | (3.4 +/- .1) x $10^{-2}$ |
| 202.5 | (6.8 +/- .3) x $10^{-3}$ |
| 197.0 | (4.5 +/- .7) x $10^{-3}$ |
| 193.0 | (1.4 +/- .3) x $10^{-3}$ |
| 191.5 | (1.8 +/- .4) x $10^{-4}$ |
| 187.0 | (5.2 +/- 1.3) x $10^{-4}$ |
| 183.0 | (8.1 +/- 2.2) x $10^{-5}$ |

* First-order rate constants were determined by a nonlinear least-squares fit to the power law expression given in equation 2. $k_p$ is the rate constant at the peak of the activation enthalpy distribution (see Experimental Section for details).

Figure 5. Arrhenius plot of the measured rate of decay of the unusual $Cu_B$ signal. The $Cu_B$ EPR signal intensities were fitted to a power law expression (Materials and Methods). The best linear least-squares fit to the data yields an activation enthalpy of 18.1 +/- 1.6 kcal $mol^{-1}$ and an activation entropy of 21.4 +/- 8.2 cal $mol^{-1}$ $K^{-1}$ (assuming a pre-exponential factor of $10^{13}$ $s^{-1}$).

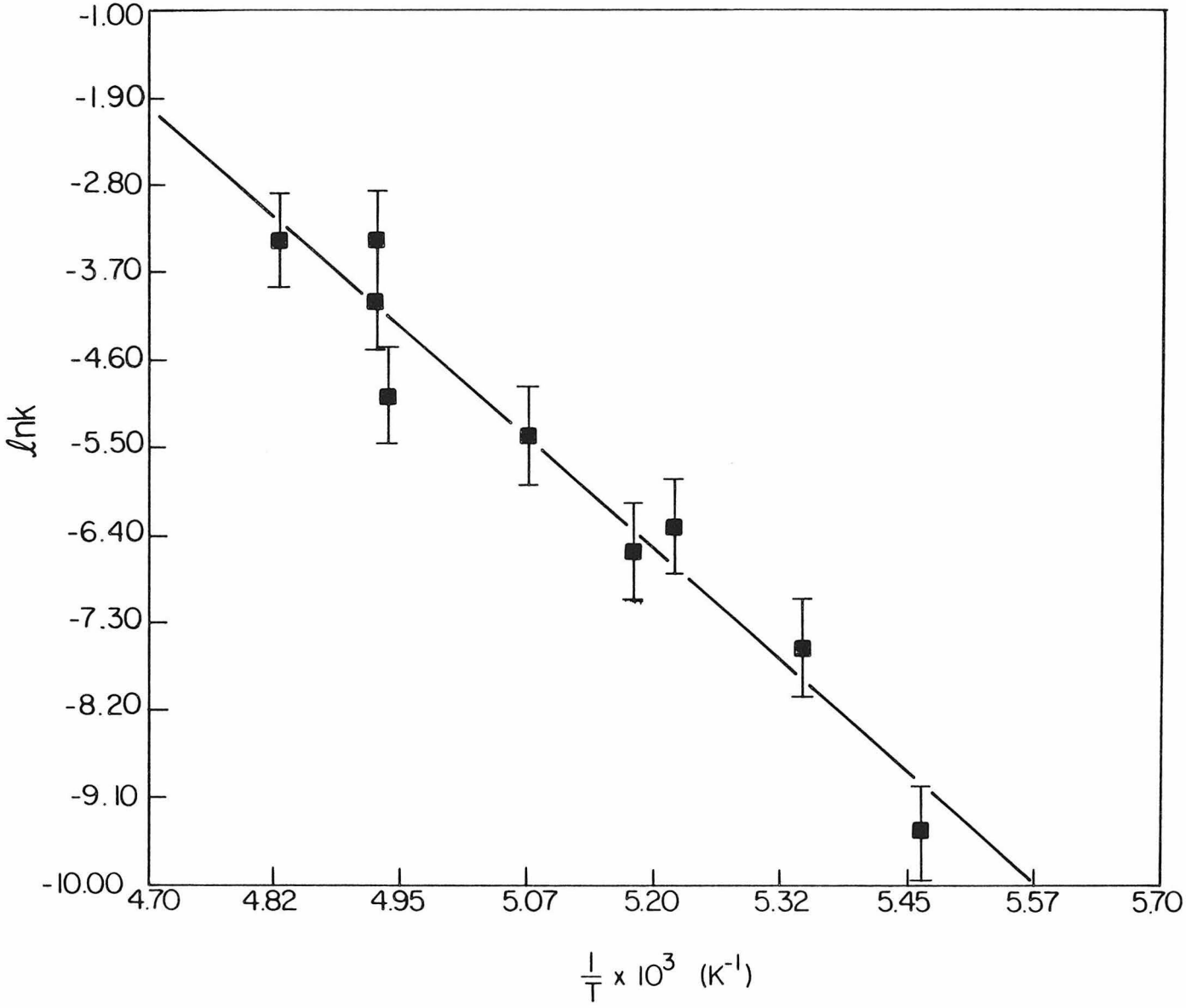
-1.00
-1.90
-2.80
-3.70
-4.60
-5.50
-6.40
-7.30
-8.20
-9.10
-10.00
lnk
4.70
4.82
4.95
5.07
5.20
5.32
5.45
5.57
5.70
1/T x 10^3 (K^-1)

processes in proteins at low temperatures have been previously attributed to the existence of multiple conformations which have different activation enthalpies for the process and which do not interconvert (22,23). The data for the decay of the unusual $Cu_B$ signal were well fitted by the power law expression (Ref. 22, cf. Materials and Methods) appropriate to such a situation. The line drawn through the $Cu_B$ points in Figure 4 is the best power-law fit.

When the activation enthalpy takes on a range of values, its most probable value may be determined from the power-law treatment if the process is examined over a range of temperatures (22). Following incubation at 181K for 90 minutes to produce the unusual $Cu_B$ signal, its decay was investigated at temperatures between 181 and 207K. The decay curve at each temperature was fitted to the power law; the best-fit kinetic parameters for the $Cu_B$ decay at various temperatures are compiled in Table II. The data in Table II were used to construct the Arrhenius plot in Figure 5. From the Arrhenius plot, a value of 18.1 +/- 1.6 kcal $mol^{-1}$ for the most probable activation enthalpy and a corresponding activation entropy of 21.4 +/- 8.2 cal $mol^{-1}$ $K^{-1}$ were obtained, assuming a preexponential factor of $10^{13}$ $s^{-1}$ (25).

Further Oxidation of Fea. As noted above, $Fe_a$ oxidation is not complete even after incubations which cause the nearly complete disappearance of the unusual $Cu_B$ signal. Continued incubation at 203K causes further oxidation of $Fe_a$ to take place at a rate of approximately $8 \times 10^{-4}$ $s^{-1}$ (Figure 6). A comparison of the $Fe_a$ oxidation with the decay of the unusual $Cu_B$ signal again shows clearly that the two processes are not correlated: Most of the increase in the $Fe_a$ signal takes place after the unusual $Cu_B$ signal has decayed. Even after prolonged (more than 1 hr.) incubation at 203K, $Fe_a$ oxidation is still not complete, however, as evidenced by a further increase in its intensity upon incubation at a somewhat higher temperature (211K). Judging from the slowness of $Fe_a$ oxidation at 193K (not shown) relative to that at 203K, this process is rather highly activated. The activation enthalpy

Figure 6. The intensity of the $Fe_a$ EPR signal during incubation of a cytochrome c oxidase sample at 203K. Prior to the 203K incubation, the sample was incubated at 177K for 2 hours. The behavior of the unusual $Cu_B$ signal during the 203K incubation is also shown. The lines through the data points are drawn to guide the eye. Conditions of EPR spectroscopy were as described in the legends to Figures 1 and 2.

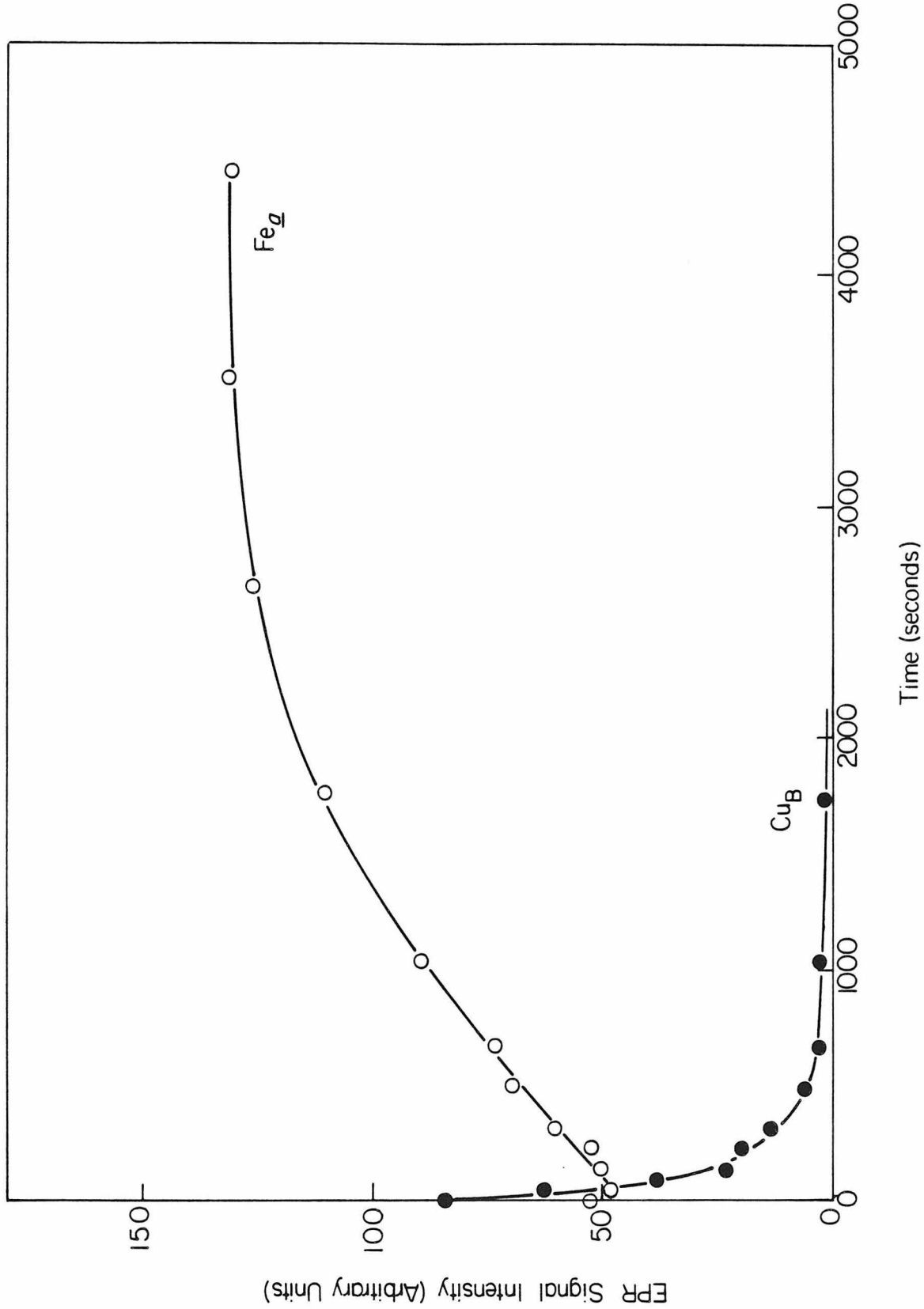
EPR Signal Intensity (Arbitrary Units)
150
100
50
0
0
1000
2000
3000
4000
5000
Time (seconds)
$Fe_g$
$Cu_B$

for this process was not determined, owing to the occurrence of other, complicating processes which probably involve reactions of the carbon monoxide used to inhibit the enzyme.

Low Temperature Oxidation of ca. Three-Fourths Reduced Cytochrome c Oxidase. The role played by the fourth electron in the reaction of cytochrome oxidase with dioxygen may be investigated in low temperature kinetic experiments using enzyme samples which are reduced by fewer than four equivalents. The results of such an experiment are displayed in Figure 7, which plots the intensities of the $Cu_A$, $Fe_a$, and unusual $Cu_B$ EPR signals observed during incubation at 181K of a sample initially reduced by only 3.4 equivalents. In this situation, most of the enzyme molecules contain only 3 electrons at the beginning of the reaction. The important observations are: First, $Fe_a$ oxidation during this initial reaction step takes place to a much greater extent and at a slower apparent rate as compared to the situation in the fully reduced enzyme (compare with Figure 1), and second, the unusual $Cu_B$ signal shows no early decay phase (compare with Figure 2).

The next step of the reaction, namely, the decay of the unusual $Cu_B$ signal, was investigated by incubating the sample at 205K. The unusual $Cu_B$ signal decays to near completion at a rate which is in agreement with rates measured with the fully reduced enzyme (Figure 8). This observation confirms that the transfer of the fourth electron to the dioxygen reduction site is not required for the elimination of the unusual $Cu_B$ signal, since most of the oxidase molecules do not contain a fourth electron.

Solvent Dependence. The solvent dependence of the low-temperature dioxygen reduction reaction was examined by conducting some experiments in 50% glycerol rather than in 40% ethylene glycol. The results of these experiments may be summarized as follows: The first reaction step, which involves the oxidation of $Fe_a$ or $Cu_A$ to produce the intermediate which exhibits the unusual copper EPR signal, was not substantially affected by the

change in solvent. The unusual copper EPR signal was identical in appearance and was produced in similar yield. By contrast, the next reaction step, which involves the decay of the unusual copper signal, was significantly affected: In 50% glycerol, this process was approximately 100 times slower than in 40% ethylene glycol, requiring incubation temperatures some 15 degrees higher to achieve comparable rates.

Figure 7. Intensities of the $Cu_A$, $Fe_a$, and unusual $Cu_B$ EPR signals during incubation of a partially (ca. 3.4 equivalents) reduced cytochrome c oxidase sample at 181K. The lines through the data points are drawn to guide the eye. Conditions were as noted in the legends to Figures 1 and 2. This figure should be compared with Figures 1 and 2, which depict an experiment which is identical except that it employs fully reduced enzyme.

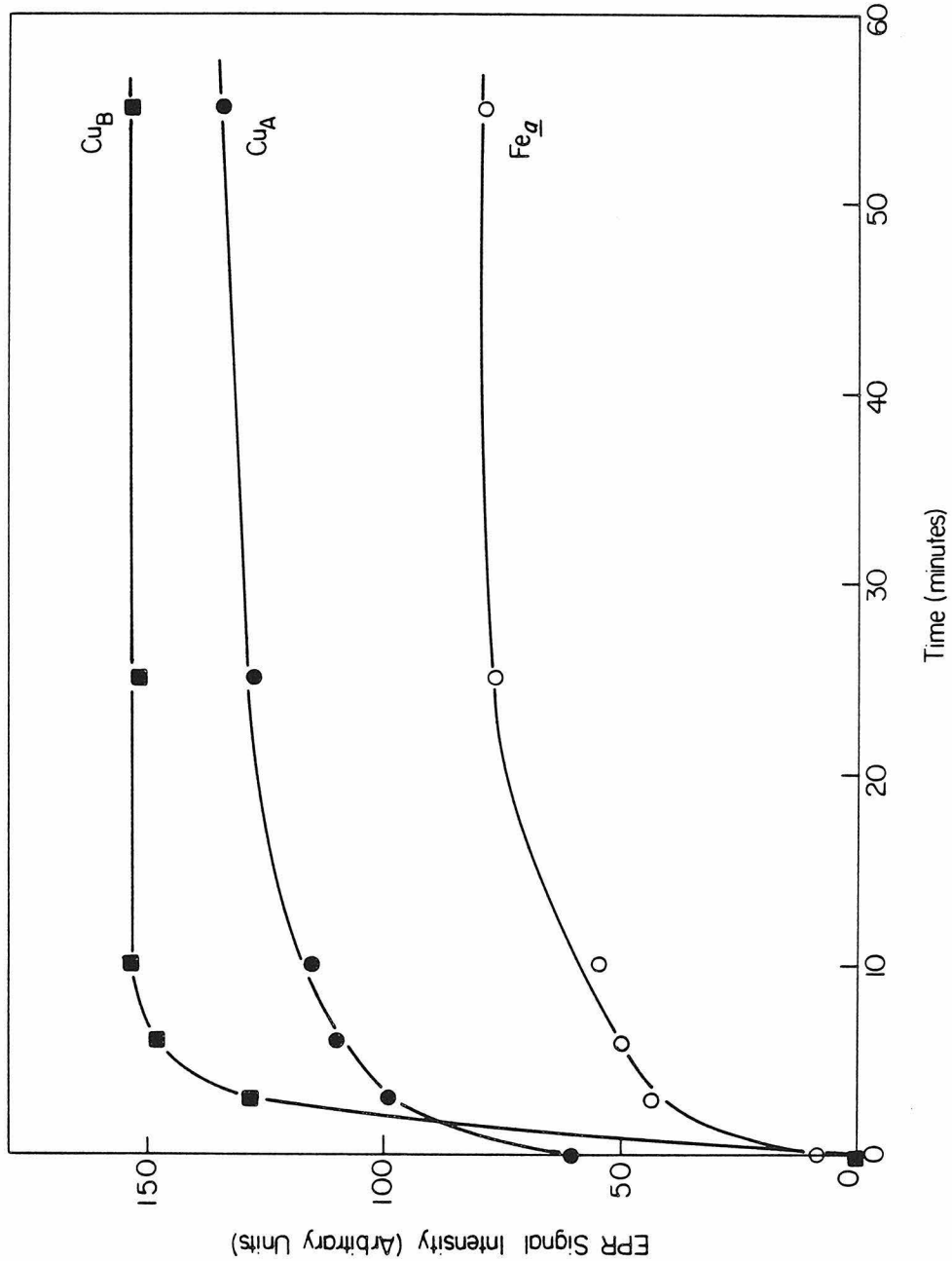
EPR Signal Intensity (Arbitrary Units)
150
100
50
0
0
10
20
30
40
50
60
Time (minutes)
$Cu_B$
$Cu_A$
$Fe_a$

Figure 8. Decay of the unusual $Cu_B$ EPR signal during 205K incubation of a cytochrome *c* oxidase sample initially reduced by 3.4 equivalents. The sample was preincubated at 181K for 55 minutes to generate the unusual $Cu_B$ signal. Conditions of EPR spectroscopy were as described in the legends to Figures 1 and 2.

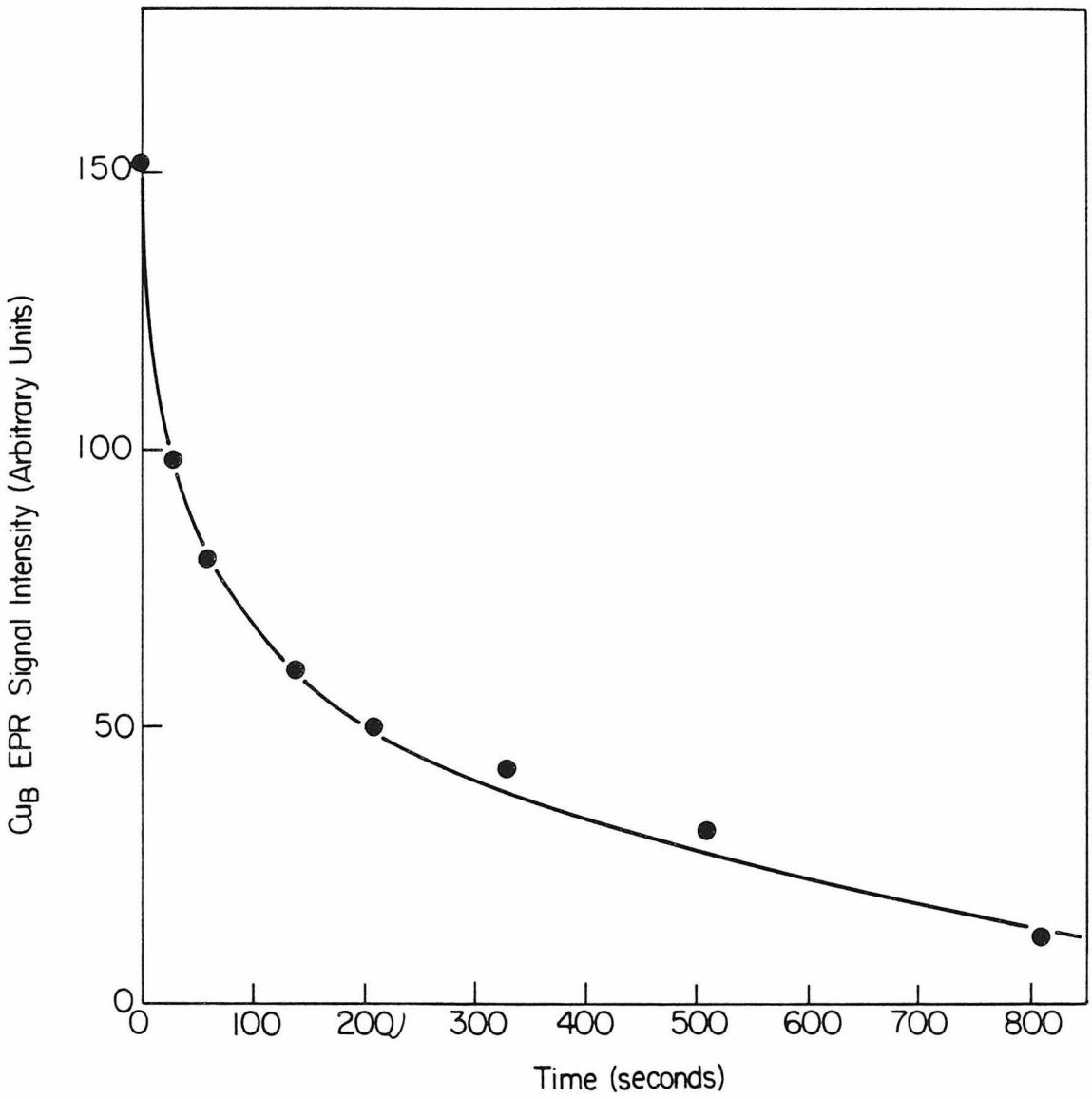
150
100
50
0
0
100
200
300
400
500
600
700
800
Time (seconds)
$Cu_B$ EPR Signal Intensity (Arbitrary Units)

## DISCUSSION

The Initial Reaction Steps. The overall reaction scheme which best accounts for the initial electron transfer events is shown above in Scheme 1, and is essentially identical to that deduced by Clore et al (8). This scheme involves first the transfer of an electron from either $Cu_A$ or $Fe_a$, with similar apparent rates, to produce an intermediate at the $Fe_{a_3}/Cu_B$ site which is formally at the 3-electron level of dioxygen reduction. This 3-electron intermediate gives rise to the unusual $Cu_B$ EPR signal which exhibits only the features associated with one g-value and which is unusually resistant to power saturation. At 181K, both of these electron transfer processes have an apparent first-order rate constant of ca. $4.4 \times 10^{-3}$ $s^{-1}$. Approximately 30% of $Fe_a$ and 70% of $Cu_A$ are oxidized in this step. The reduced $Cu_A$ which remains is oxidized in a somewhat slower process ($k$ = ca. $1 \times 10^{-3}$ $s^{-1}$). At 181K, $Fe_a$ is still about 70% reduced after 2 hrs. Thus, after 2 hrs. at 181K, 70% of the $Fe_{a_3}/Cu_B$ sites are at the 3-electron level of dioxygen reduction and exhibit the unusual $Cu_B$ EPR signal, while the remaining 30% are at the 4-electron (formally, water) level.

The evidence for this reaction scheme consists of the following observations: (1) The careful kinetic analysis of Clore et al. showed convincingly that $Fe_a$ is oxidized in a single first-order step during incubation at a comparable temperature (173K), and that $Cu_A$ oxidation is well fitted by the expression appropriate to the two-step mechanism in Scheme 1. All of the present data on the oxidations of $Fe_a$ and $Cu_A$ are consistent with this scheme: In numerous experiments at 181K, the overall time course of $Cu_A$ oxidation was not well fitted by a single exponential, and the time course of $Fe_a$ oxidation did not parallel that of $Cu_A$. After 2 hrs. of incubation at 181K, integration of the $Cu_A$ and $Fe_a$ signals shows that the amount of oxidized $Fe_a$ corresponds to much less than (approximately 30% of) the amount of oxidized $Cu_A$. (2) After subsequent incubation for 30 minutes at 203K, the $Fe_a$ signal increases to approximately 80% of $Cu_A$. This indicates that a

substantial percentage of the $Fe_{a_3}/Cu_B$ sites were in fact still at the 3-electron level of dioxygen reduction after the incubation at 181K, as required by Scheme 1. At the same time, the $Cu_A$ signal does not increase appreciably, indicating that the oxidation of this site was very nearly complete at the lower temperature. (3) The $Cu_B$ signal, which is associated with an intermediate of dioxygen reduction at the 3-electron level, shows a small but reproducible decrease at times between 5 and 10 minutes of incubation at 181K. In the present reaction scheme, this decrease is caused by the elimination of some 3-electron intermediate by the transfer of the fourth electron from $Cu_A$ to the $Fe_{a_3}/Cu_B$ site (the conversion from intermediate IIA to intermediate III). In samples initially reduced by only 3.4 electrons, in which the transfer of the fourth electron may not take place in most of the enzyme molecules, this early phase of $Cu_B$ decay was not observed.

The causes underlying the branched reaction scheme are in part revealed by the experiments using partially (ca. 3.4 equivalent) reduced enzyme samples. In the ca. 3.4-equivalent reduced samples, $Fe_a$ is approximately 10% oxidized and $Cu_A$ is approximately 50% oxidized at the beginning of the experiment. In these samples, $Fe_a$ is oxidized to a much greater extent, approaching 80%, in the first electron transfer step. This step is analogous to the conversion from intermediate I to intermediate IIA in Scheme 1, differing only in that $Cu_A$ is already largely oxidized. In the partially reduced samples, the $Fe_a$ oxidation exhibits an apparent 1st-order rate constant which is approximately 2-fold smaller than that observed in the fully reduced samples. These observations are readily interpreted in terms of Scheme 1. In the initial electron transfer step of this scheme, the apparent rate constants for $Fe_a$ or $Cu_A$ oxidation in the case of the fully reduced enzyme will be the sum of the rate constants for the oxidations of these sites (29), whereas in the case of the three electron-reduced enzyme the apparent rate constants will be the same as the actual rate constants. The more extensive oxidation of $Fe_a$ in the ca. 3 equivalent-reduced enzyme indicates that the electron transfer from

$Fe_a$ is relatively fast if the electron is the third electron to be transferred to dioxygen, but slow if it is the fourth. In the fully reduced enzyme, $Fe_a$ must compete with $Cu_A$ to be the donor of this third electron. It was previously suggested (8) that the trapping of the fourth electron in $Fe_a$ is due to an $Fe_a$-$Cu_A$ interaction, in which the oxidation of $Cu_A$ blocks the $Fe_a$ to $Cu_B/Fe_{a_3}$ electron transfer. The experiment using three electron reduction shows that the contrary is the case: The presence of initially oxidized $Cu_A$ <u>increases</u> the amount of $Fe_a$ oxidation.

The first electron transfer from $Cu_A$ was examined over a range of temperatures between 166 and 186K. The rate was estimated using the slope of the early portion of the $Cu_A$ oxidation data, since at later times the curve is complicated by the second electron transfer step (the conversion from intermediate IIA to intermediate III), in which some 30% of the $Cu_A$ oxidizes more slowly to yield the 4-electron product at the $Fe_{a_3}/Cu_B$ site. The activation parameters deduced for the first electron transfer from $Cu_A$ are $\Delta H^{\ddagger}$ = 13.2 +/- 1.4 kcal $mol^{-1}$ and $\Delta S^{\ddagger}$ = 2.8 +/- 7.7 cal $mol^{-1}$ $K^{-1}$ (in a 40% ethylene glycol glass). This electron transfer step showed only a weak dependence upon the nature of the medium: In a 50% glycerol glass, the rate was not markedly different from that in 40% ethylene glycol.

<u>The Nature of the First Reaction Step</u>. While the initial processes which were monitored, namely the oxidations of $Fe_a$ or $Cu_A$, must involve electron transfer from $Fe_a$ or $Cu_A$ to the dioxygen reduction site, it does not necessarily follow that the rates which are observed reflect the intrinsic rates of these electron transfers. It is possible that an event at the dioxygen reduction site must take place before the electron transfer step may occur. If the electron transfers are rapid relative to this event, then the observed rate will be that of the process occurring at the dioxygen reduction site. In a recent low temperature infrared absorption study, Fiamingo et al. (26) have shown that CO is not completely dissociated from the dioxygen reduction site by low temperature photolysis. The CO molecules which are photolyzed

from $Fe_{a_3}$ first bind to $Cu_B$ and then (in the absence of oxygen) recombine with $Fe_{a_3}$ in a second, slower step. Comparison with the present measurements on the initial electron transfer step reveals that at 181K the rate of CO recombination is comparable to that of $Cu_A$ oxidation while the activation enthalpies for these processes are significantly different. The correspondence is close enough to suggest that the first process under examination in these experiments may in fact be the dissociation of CO from $Cu_B$, followed by relatively rapid reaction with iron-bound dioxygen to generate a peroxy intermediate and enable electron transfer from $Cu_A$ or $Fe_a$:

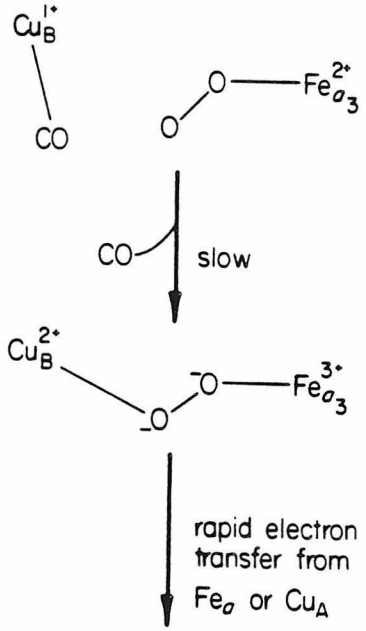


Scheme 2

It should be noted that the infrared absorption study was carried out in mitochondria suspended in 100% glycerol while the bulk of the present studies were done with detergent solubilized enzyme in 40% ethylene glycol. The difference in activation enthalpies may be related to the different reaction media employed

or to the fact that the process monitored by Fiamingo et al., namely, the simple reassociation of CO with $Fe_{a_3}$ in the absence of dioxygen, is different from that in the first step in Scheme 2. Further studies of the medium dependence of this step and complementary studies of the dioxygen reaction by FT-IR would test the validity of Scheme 2.

An examination of the first electron transfer step in the light of long distance electron transfer theory lends some support to the idea that CO dissociation, and not electron transfer per se, is rate-limiting in the first oxidation step. An activation enthalpy as large as 13 kcal $mol^{-1}$ would imply that large structural rearrangements accompany the electron transfer. According to current electron transfer theories (30-32), the observed rate is surprisingly large given this large activation enthalpy and the intersite distances of ca. 15 Å which are implied by magnetic data (33-35). However, if the rate limiting factor is CO dissociation, then the actual activation enthalpy for the electron transfer process may be much less than 13.2 kcal $mol^{-1}$ and electron transfer rates which are well in excess of the observed overall rate (as required by scheme 2) would then be possible at intersite distances greater than 15 Å.

If Scheme 2 is correct, then the first intermediate in the low temperature dioxygen reaction (probably a dioxygen adduct of ferrous $Fe_{a_3}$ (8)) may differ from the physiologically relevant intermediate due to the involvement of the CO molecule bound to $Cu_B$. In the absence of CO, such an intermediate may never be formed or may have a very short lifetime. This possibility emphasizes the need to devise kinetic experiments, both at low- and physiological temperatures, in which inhibitory ligands are not present.

The Second Reaction Step. As noted above, an unusual EPR signal from $Cu_B$ appears in concert with the early oxidation of $Cu_A$ and $Fe_a$. Subsequent electron transfer from $Cu_A$ in the subpopulation of molecules which underwent initial oxidation at $Fe_a$ causes a portion of this signal to disappear, but most of the unusual $Cu_B$ signal, which is assigned to intermediate IIB in Scheme

1, remains after 1 hour at 181K. The next distinct reaction step which is observed, after prolonged incubation at 181K or much shorter incubation at temperatures ca. 10 degrees higher, is the disappearance of this unusual $Cu_B$ signal. During this process, very little further oxidation of $Cu_A$ or $Fe_a$ takes place, and the time courses of $Cu_A$ and $Fe_a$ oxidation do not parallel the disappearance of the unusual $Cu_B$ signal. In samples which are initially reduced by only ca. 3.4 equivalents, the unusual $Cu_B$ signal disappears to near completion and at the same rate as observed in fully reduced samples, indicating that the transfer of a fourth electron is not required for elimination of the three electron intermediate which gives rise to the unusual $Cu_B$ signal. These observations imply that there are <u>two</u> intermediates at the 3-electron level of dioxygen reduction, the first EPR-detectable and the second EPR-undetectable under the conditions of these experiments.

The conversion from the first to the second 3-electron intermediate was characterized in considerable detail. This process exhibits markedly nonexponential behavior, which is attributed to the existence of multiple conformations which have different activation enthalpies for this step and which interconvert only slowly at these low temperatures. Analogous behavior has been observed in the recombination of CO with myoglobin (22) or with cytochrome oxidase (26) following photolysis. The progress of these reactions was satisfactorily fitted by the power law expression (Materials and Methods) which is appropriate to a distribution of activation enthalpies. The power law also gives a good fit to the conversion between the two 3-electron intermediates. The power law analysis was used in conjunction with examination of this process over a range of temperatures to estimate the most probable activation enthalpy. The value deduced is 18.1 kcal $mol^{-1}$. The corresponding activation entropy is 21.4 cal $mol^{-1}$ $K^{-1}$ (assuming a prefactor of $10^{13}$ $s^{-1}$, which is probably an overestimate). These activation parameters thus indicate that this reaction step is entropically promoted to a substantial degree: An activation entropy of 21 cal $mol^{-1}$ $K^{-1}$ corresponds to a rate enhancement of

approximately $4 \times 10^4$.

This reaction step was also examined by conducting some experiments in 50% glycerol rather than in 40% ethylene glycol. In the glycerol glass, this step was much (ca. 100-fold) slower, taking place at an appreciable rate only at temperatures some 15 degrees higher than the reactions in ethylene glycol. This result may reflect a change in the conformation of the enzyme, or its conformational flexibility, in the glycerol glass. The intensity and position of the $Cu_B$ signal are the same in the glycerol and ethylene glycol glasses, which suggests that the structure of the dioxygen reduction site is not substantially different. If the rate difference is caused by a difference in conformational flexibility, this would suggest that a significant protein conformational change is involved in this step.

The two 3-electron intermediates are at the same formal oxidation level, but they must be structurally different since one exhibits an unusual copper EPR signal while the other does not. Various structures which contain the correct number of electrons may be envisaged, depending upon the state of the dioxygen bond and the extent of protonation. The activation parameters for the conversion process and the sensitivity of the process to conformation (which is implied by its distributed activation enthalpy) suggest that this process corresponds to the breaking of the dioxygen bond. The first of the 3-electron intermediates would then contain a peroxidic adduct of ferrous $Fe_{a_3}$, while the second would contain a ferryl ion (Scheme 3). Adopting the hypothesis in Scheme 3, we may say that the breaking of the oxygen-oxygen bond is promoted largely by a positive entropy change. Such a favorable entropy of activation could be achieved through ordering of the reactant state, in which hydroperoxide is coordinated to both the copper and the iron. If the intermetal distance is appropriate, the metals may act as a "rack" (36) on which the hydroperoxide is stretched and thereby ordered. Conversely, the hydroperoxide binding is expected to constrain the intermetal distance, thus decreasing the motional freedom of the surrounding protein.

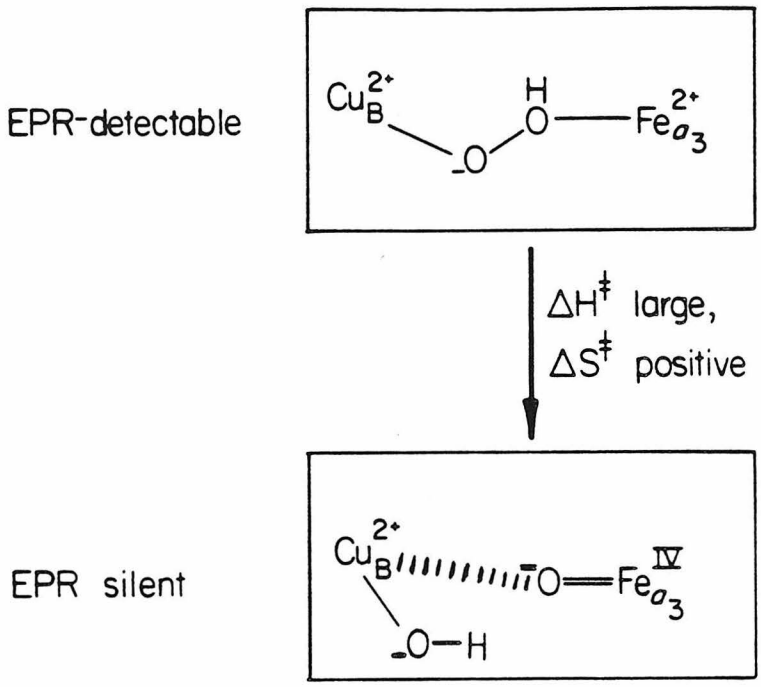


Scheme 3

**The description shown in Scheme 3 applies to intermediate IIB only, since intermediate IIA is eliminated by a different pathway which involves the transfer of a fourth electron to the dioxygen reduction site. Following this electron transfer, the oxygen-oxygen bond may be broken, via a mechanism which is different from that in Scheme 3, or it may remain intact until the temperature is raised further. Since intermediate III is EPR-silent, other approaches will be required to study this alternate pathway. We only note here that the highly activated character of the reaction step in Scheme 3 makes it very likely that this path, which proceeds via two 3-electron intermediates, will be the dominant one at physiological temperature, since the postulated bond-breaking step is predicted to**

be very rapid ($10^6$ - $10^8$ $s^{-1}$) at 37 °C (by extrapolation of the Arrhenius plot in Figure 5).

The Nature of the Unusual $Cu_B$ EPR Signal. If Scheme 3 is correct, it must somehow account for the unusual EPR spectroscopic properties of the two 3-electron intermediates. With regard to the first intermediate, we must explain why only a small portion of the copper EPR spectrum is observed and why this signal is very difficult to saturate relative to magnetically isolated copper species. Previously, in the absence of evidence for two different 3-electron intermediates, this unusual $Cu_B$ EPR signal was proposed to arise from a cupric ion in proximity to a ferryl ion (the second 3-electron intermediate in the present reaction scheme). Additionally, it was proposed that a hydroxide ion coordinated to the copper is hydrogen bonded to the ferryl oxygen, facilitating a superexchange interaction between the copper and iron spins (14). The rapid relaxation of the copper spin and the absence of $g_x$ and $g_y$ features were ascribed to dipolar and/or superexchange coupling to the S=1 (low-spin) ferryl ion, which is expected to relax fairly rapidly (13,15,37).

In the present reaction scheme, the unusual $Cu_B$ signal is proposed to arise from a hydroperoxide-bridged cupric/ferrous intermediate. In this intermediate, the hydroperoxide coordination to copper may be stronger than its coordination to iron; consequently, it is proposed that the ferrous iron is high spin (S=2) or intermediate spin (S=1). Neither of these spin states would be surprising given that the hydroperoxide coordination to copper could substantially weaken its coordination to iron. The peroxidic bridge between the copper and iron ions will facilitate a superexchange coupling between the ions. If the superexchange coupling parameter J is small relative to the axial zero field splitting D of the high-spin ferrous heme, then perturbation theory may be used to calculate the g-values of the coupled cupric/ferrous spin system. This perturbation treatment shows that the superexchange coupling affects $g_x$ and $g_y$ to first order in J/D, but $g_z$ only to second order. The shape and intensity of the resolvable portion of the spectrum

at $g_z$ is consistent with values for $g_x$ and $g_y$ less than or equal to 1.3 (13). Assuming an axial zero field splitting of 20 $cm^{-1}$ and iron g-values of 2.0, the superexchange coupling required to give $g_x$- and $g_y$-values of 1.3 is calculated to be 3.5 $cm^{-1}$ if the iron is intermediate spin, or 1.1 $cm^{-1}$ if the iron is high spin. Using these value for J, the value of $g_z$ (which is perturbed only to second order in J/D) is predicted to be typical for copper, even if the g-values of the iron are quite anisotropic (e.g., $g_z$(Fe) = 3.0), which is itself unlikely. Similarly, the copper hyperfine coupling parameter $A_z$(eff) will not be significantly reduced relative to the isolated copper ion.

The absence of observable inflections near g = 1.3 could be caused by inhomogeneous broadening of the resonance, either by g-anisotropy in the iron (which would cause $g_y$ to be $> 1.3$ and $g_x$ to be $< 1.3$) and/or "J-strain," a distribution in the value of the superexchange coupling parameter J caused by conformational heterogeneity. The resistance of the unusual $Cu_B$ EPR signal to power saturation also follows as a consequence of weak superexchange coupling to the iron ion. The presence of nearby higher-lying states in the iron spin manifold, which are admixed with the copper spin states, will facilitate the relaxation of the copper spin via the Orbach mechanism (38). The temperature dependence of the $Cu_B$ relaxation rate is consistent with relaxation via an Orbach mechanism which involves spin excited states ca. 20 $cm^{-1}$ higher in energy (39). Thus, all of the properties of the unusual $Cu_B$ signal are accounted for by adopting the structure proposed in Scheme 3 and postulating a fairly weak (1.1 or 3.5 $cm^{-1}$, depending on the iron spin-state) superexchange interaction between the copper and the high-spin iron.

With regard to the second intermediate at the 3-electron level of dioxygen reduction, which is suggested to be in the cupric/ferryl oxidation state, we must explain why no EPR spectrum assignable to this intermediate is observed. The perturbation treatment described above, as well as an analogous treatment in which a very strong superexchange interaction is assumed and the zero field splitting is

treated as a perturbation, indicate that in the limits of very strong or very weak coupling, the superexchange interaction cannot make the expected resonance so anisotropic or so inhomogeneously broadened that all of its spectral features, particularly those at $g_z$, are undetectable. However, at intermediate strengths of the superexchange coupling (which would require a higher-order calculation for quantitative characterization), it is possible that the $g_x$- and $g_y$-values could be lowered, shifting these resonances to much higher field so that even the resonance at $g_z$ became very weak. Using the formulas of Aasa and Vanngard (21), it may be calculated that a shift in $g_x$ and $g_y$ from 1.3 to ca. 0.5 would result in a 10-fold reduction in the area of the peak at $g_z$. In the S(Fe) = 1, S(Cu) = 1/2 system, this would require a superexchange coupling of 8 $cm^{-1}$, using the above perturbation treatment. (However, since J/D = 0.4 in this case, this calculation must be considered approximate.) If there is even a weak direct bond between the ferryl oxygen and the copper ion, the superexchange coupling between the metals could be much stronger in the ferryl-containing intermediate than in the hydroperoxide-bridged intermediate, and possibly as strong as 8 $cm^{-1}$. Another possible explanation for the absence of an EPR signal from the second 3-electron intermediate is that spin relaxation in this cupric/ferryl system is very rapid ($1/T_2 > 10^{10}$ $s^{-1}$), so that the spectral features are broadened beyond detection.

The Third Reaction Step. In the third step of the reaction, an additional fraction of $Fe_a$ is oxidized. This takes place at conveniently monitored rates at temperatures near 203K. At ca. 193K, $Fe_a$ oxidation takes place much more slowly, so this step is rather highly activated. Precise measurement of the activation enthalpy was not made. As discussed above, the slowness of this oxidation is related to the fact that the electron in $Fe_a$ at this step is the fourth electron to take part in the dioxygen reaction; when it is the third electron, the transfer occurs more rapidly. This indicates that the different electron transfers which take

place during the dioxygen reduction reaction can have significantly different rates, even when the electron donor is the same. This is not surprising in view of the changes which are necessarily taking place at the dioxygen reduction site during the reaction cycle.

Electron Transfer Pathways. Scheme 1 has important implications for the mechanisms of electron transfer within the oxidase. This scheme involves the partitioning of the oxidase molecules into two distinct populations by transfer of the first electron from either $Fe_a$ or $Cu_A$. The occurrence of this partitioning indicates that both $Cu_A$-to-$Fe_{a_3}/Cu_B$ site and $Fe_a$-to-$Fe_{a_3}/Cu_B$ site electron transfer pathways are approximately equally competent at these temperatures. The similarity of the rates via the two paths indicates that one is not very much better than the other with respect to the distance of the transfer or the suitability of the intervening material (30). The existence of two competent electron pathways to the dioxygen-reduction site would have implications for the mechanisms of energy conservation by the oxidase. It is now well established that the cytochrome oxidase-catalyzed transfer of electrons from cytochrome c to dioxygen is coupled to the active transport of protons across the mitochondrial membrane (4), and it appears most likely that either $Fe_a$ or $Cu_A$ is involved in this proton pumping function. If, for example, $Cu_A$ were the proton pump, then the $Fe_a$-to-$Fe_{a_3}/Cu_B$ electron transfer path would bypass the pump. Such a bypass mechanism might be important at steps in dioxygen reduction where the $Cu_A$-to-$Fe_{a_3}/Cu_B$ transfer, which is linked to proton pumping, is relatively slow because these steps are not sufficiently exothermic. Some of the observations described above constitute evidence that electron transfer to the dioxygen reduction site is slower at some steps than at others; the existence of two competent electron transfer pathways to the dioxygen-reduction site may reflect the need to uncouple electron transfer from proton pumping at the slow steps.

REFERENCES

1. Wikstrom, M. (1982). Current Topics in Membranes and Transport 16 pp. 303-321.

2. Vik, S.B., and Capaldi, R.A. (1980). Biochem. Biophys. Res. Comm. 94 348-354.

3. Merle, P., and Kadenbach, B. (1980). Eur. J. Biochem. 105, 499-507.

4. Wikstrom, M., Krab, K., and Saraste, M. (1981). Cytochrome Oxidase--A Synthesis, Academic Press, London.

5. Chance, B., and Leigh, J. S. Jr. (1977). Proc. Nat. Acad. Sci. USA 74, 4777-4780.

6. Clore, G.M., and Chance, E.M. (1978). Biochem. J. 173, 811-820.

7. Clore, G.M., and Chance, E.M. (1978). Biochem. J. 175, 709-725.

8. Clore, G.M., Andreasson, L.E., Karlsson, B., Aasa, R., and Malmstrom, B.G. (1980). Biochem. J. 185, 139-154.

9. Gibson, Q.H., and Greenwood, C. (1963). Biochem. J. 86, 541-554.

10. Greenwood, C., and Gibson, Q.H. (1967). J. Biol. Chem. 242, 1782-1787.

11. Chance, B., Saronio, C., and Leigh, J.S. Jr. (1975). J. Biol. Chem. 250, 9226-9237.

12. Babcock, G.T., Jean, J.M., Johnston, L.N., Palmer, G., and Woodruff, W.H. (1984). J. Am. Chem. Soc. 106, 8305-8306.

13. Karlsson, B., Aasa, R., Vanngard, T., and Malmstrom, B.G. (1981). FEBS Letters 131, 186-188.

14. Hansson, O., Karlsson, B., Aasa, R., Vanngard, T., and Malmstrom, B.G. (1982). EMBO J. 1, 1295-1297.

15. Theorell, H., and Ehrenberg, A. (1952). Arch. Biochem. Biophys. 41, 442-461.

16. Schulz, C., Chiang, R., and Debrunner, P.G. (1979). J. Physique 40, C2-534-536.

17. Change to an S=1 reference.Karlsson, B., and Andreasson, L.E. (1981). Biochim. Biophys. Acta 635, 73-80.

18. Hartzell, C.R., and Beinert, H. (1974). Biochim. Biophys. Acta 368, 318-338.

19. Laboratory Methods in Porphyrin and Metalloporphyrin Research (1975). Fuhrop, J.-H., and Smith, K.M., eds. Elsevier.

20. Markwell, M.A.K., Haas, S.M., Bieber, L.L., and Tolbert, N.E. (1978). Anal. Biochem. 87, 206-210.

21. Aasa, R., and Vanngard, T. (1975). J. Mag. Res. 19, 308-315.

22. Austin, R.H., Beeson, K., Eisenstein, L., Frauenfelder, H., Gunsalus, I.C., and Marshall, V.P. (1974). Phys. Rev. Lett. 32, 403-405.

23. Austin, R.H., Beeson, K.W., Eisenstein, L., Frauenfelder, H., and Gunsalus, I.C. (1975). Biochemistry 14, 5355-5373.

24. Agmon, N., and Hopfield, J.J. (1983). J. Chem. Phys. 79, 2042-2053.

25. At 200K, the Eyring prefactor kT/h is approximately 0.4x10**13 s-1, so 1.0x10**13 is likely to be an overestimate. Also, the transmission coefficient K has been taken to be 1.0, the maximum possible. The effect of these assumptions, which probably overestimate the effective frequency prefactor, will be to underestimate the activation entropy.

26. Fiamingo, F.G., Altschuld, R.A., Moh, P.P., and Alben, J.O. (1982). J. Biol. Chem. 257, 1639-1650.

27. Lanne, B., Malmstrom, B.G., and Vanngard, T. (1979). Biochim. Biophys. Acta 545, 205-214.

28. Tang, S.C., Koch, S., Papaefthymiou, G.C., Foner, S., Frankel, R.B., Ibers, J.A., and Holm, R.H. (1976). J. Am. Chem. Soc. 98, 2414-2434.

29. Espenson, J.H. (1981). In Chemical Kinetics and Reaction Mechanisms, McGraw Hill, p. 55.

30. Hopfield, J.J. (1974). Proc. Nat. Acad. Sci. USA 71, 3640-3644.

31. Marcus, R.A., and Sutin, N. (1985). Biochim. Biophys. Acta Reviews in Bioenergetics (in press).

32. Hopfield, J.J. (1977). In Electrical Phenomena at the Biological Membrane Level, Roux, E., ed. Elsevier, pp. 471-492.

33. Brudvig, G.W., Blair, D.F., and Chan, S.I. (1984). J. Biol. Chem. 259, 11001-11009.

34. Mascarenhas, R., Wei, Y.-H., Scholes, C.P., and King, T.E. (1983). J. Biol. Chem. 258, 5348-5351.

35. Ohnishi, T., LoBrutto, R., Salerno, J.C., Bruckner, R.C., and Frey, T.G. (1982). J. Biol. Chem. 257, 14821-14825.

36. Lumry, R., and Eyring, H. (1954). J. Phys. Chem. 58, 110-120.

37. Schulz, C.E., Rutter, R., Sage, J.T., Debrunner, P.G., and Hager, L.P. (1984). Biochemistry 23, 4743-4754.

38. Orbach, R. (1961). Proc. R. Soc. Lond. Ser. A264, 458-484.

39. Malmstrom, B.G., unpublished results.

40. Nicholls, P., and Chanady, G.A. (1981). Biochim. Biophys. Acta 634, 256-265.

41. Bickar, D., Bonaventura, C., and Bonaventura, J. (1984). J. Biol. Chem. 259, 10777-10783.

# CHAPTER VI. STEADY-STATE KINETIC ANALYSIS OF REDOX-LINKED PROTON PUMPING: THE IMPORTANCE OF ELECTRON GATING

## INTRODUCTION

In recent years, it has become widely accepted that at least one of the members of the respiratory chain, cytochrome c oxidase, functions as a redox-linked proton pump. In this enzyme, the flow of electrons from cytochrome c at the cytosol (outer) side of the inner mitochondrial membrane to dioxygen and to protons derived from the matrix (inner) side is coupled to the electrogenic pumping of protons from the matrix to the cytosol (1). The protons so pumped contribute to the maintenance of a proton electrochemical potential (electrically negative inside) across the inner mitochondrial membrane. This proton electrochemical potential is used to drive the synthesis of ATP from ADP and inorganic phosphate which is catalyzed by another transmembranous mitochondrial enzyme, the ATP synthase (2). The directionality of the coupled electron and proton flows in cytochrome c oxidase makes the mechanism of proton translocation by this enzyme fundamentally different from the "redox loop" mechanism proposed by Mitchell (3) for the coupling sites in the respiratory chain. In the redox loop model, electron movements across the mitochondrial membrane from the cytosol to the matrix alternate with simultaneous, electroneutral movements of electrons and protons in the opposite direction. Because of the persuasive demonstration (4) of proton pumping in cytochrome c oxidase, and because of the possibility that other proton translocating elements in the respiratory chain are also electron transfer-driven proton pumps, it is important to understand the molecular mechanisms by which electron transfer reactions can be coupled to vectorial proton translocation.

This chapter explores the theoretical question of how redox processes can be coupled to vectorial proton transport at a proton-pumping site involving a single redox center within a respiratory enzyme. In particular, it investigates the role of electron gating (i.e., the control of electron transfer into and out of the coupling site) in such coupling. The steady-state rate

equations appropriate to a some models of proton pumping have been solved and the solutions used to calculate the rate of electron transfer through the pumping site and the efficiency of proton pumping. In this way, a systematic study has been made of the relationship between the various parameters which describe the pumping site ($pK_a$s, reduction potentials, relative electron transfer rates, etc.) and the resultant performance of the pump. The examination has revealed that some of the predictions of simple models of proton pumping (5,6), for example, a strongly pH-dependent reduction potential of the redox center associated with pumping, are based upon implicit assumptions which are not necessarily valid in a more complete treatment.

The present theoretical investigation makes predictions regarding the likely mechanisms of proton pumping in cytochrome c oxidase. Additionally, the analysis of a simple model transducer should be of general use in the quantitative study of other biological energy transducers with which a formal analogy can be made. The present analysis is particularly useful in predicting the effects of "slippage" (partial uncoupling) on the important properties of the transducer (for example, its maximum power output and the corresponding membrane potential, its minimum rate of heat generation and the corresponding membrane potential, and the maximum membrane potential which can be generated). This predictive ability should lead to the design of more effective experiments for clarifying the mechanisms of proton pumping in cytochrome oxidase and other enzymes.

## SIMPLE MODELS OF REDOX-LINKED PROTON PUMPING: $pK_a$ CONTROL

Current models for redox-linked proton pumping frequently involve, with minor variations, the four-state paradigm shown in Figure 1 (5,7). P refers to the pumping site, including whatever molecular components are necessary to the pumping action; these components include both a center which can undergo reversible

Figure 1. Schematic for a four-state redox-linked proton pump. Clockwise passage among the four states leads to proton pumping. P refers to the pump site, including all elements (e.g., proton-conducting channels) required for pumping action; the subscripts ox and red refer to the oxidation state. Proton subscripts M and C signify the mitochondrial matrix and cytosol, respectively.

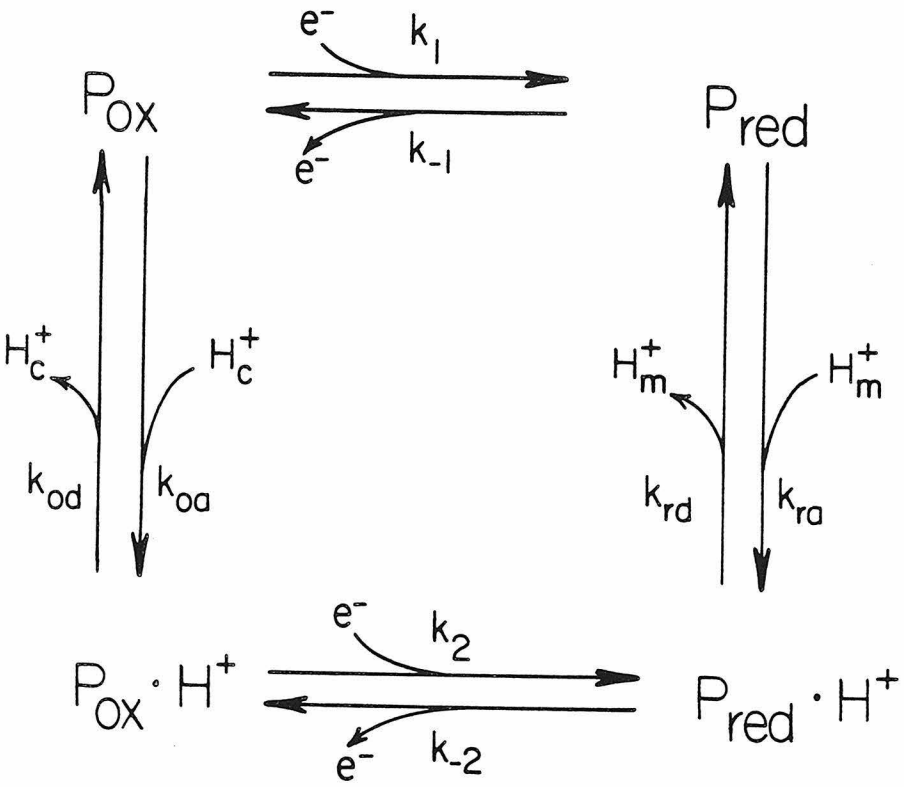
e⁻
k1
P_ox
P_red
e⁻
k-1
H_c⁺
H_c⁺
H_m⁺
H_m⁺
k_od
k_oa
k_rd
k_ra
e⁻
k2
P_ox · H⁺
P_red · H⁺
e⁻
k-2

oxido-reduction and a group which can reversibly bind a proton. The four states shown correspond to the four possible conditions of oxidation/reduction and protonation/deprotonation. The specific sequence of states drawn is not essential to the paradigm or to the ideas to be developed. For example, protonation could equally well occur upon oxidation and deprotonation upon reduction. In the scheme in Figure 1, each turnover cycle involves the transfer of one electron and the pumping of a single proton from the matrix to the cytosol, so in this model the maximum possible $H^+/e^-$ stoichiometry is 1.

The features which are important to the scheme of Figure 1 and which have been particularly stressed by other authors include the following: First, it has been noted that an efficient pump based on this four-state cycle is likely to involve some thermodynamic linkage between oxido-reduction and protolysis (a redox Bohr effect) (8,9). This means that in the cycle drawn, reduction of the pumping site causes protonation to be favored relative to that in the oxidized state; i.e., $pK_a(red)$ is greater than $pK_a(ox)$. In this way, the affinity of the site for protons is varied cyclically during the operation of the pump. Equivalently, the pump may be considered as alternating between a state with relatively high affinity for an electron (a higher reduction potential) and a state with a lower affinity for an electron (a lower reduction potential), depending upon whether it is protonated or not. In this way, one state of the pump is matched to conditions on the electronic and protonic input sides, namely, low solution redox potential and high solution pH, while the other state is matched to the conditions of high redox potential and low pH found on the output sides.

A feature that is essential to the operation of any real pump derived from the model in Figure 1 is the gating of protons (9). In the cycle drawn, proton gating is necessary to ensure that protonation of the reduced state of the pump occurs only from the matrix side of the mitochondrial membrane, while deprotonation of the oxidized state occurs only to the cytosol side. It has been suggested (9,10) that proton-conducting channels leading to and from

the pumping site are also likely to be important, and various molecular mechanisms for proton channeling and gating have been proposed (11,12). There is also a requirement for an analogous gating of electron flow. This requirement has been noted previously (13,14), but it has not previously been discussed in detail.

The emphasis which has been given to the first two points above, namely, the thermodynamic linkage of oxido-reduction to protolysis, and proton gating, has led the authors of some proton pump models to assume implicitly that it is primarily or exclusively these two factors which control the proton pumping cycle (5,6). In this kind of proton pump model, which could be called a "$pK_a$-controlled" pump, thermodynamic linkage together with proton gating cause the site to alternate between a state which is mostly protonated from the matrix side, and a state which is mostly deprotonated to the cytosol side. Alternation between the two states so defined would, in fact, lead to proton pumping. However, the mechanism of alternation between these states, which involves electron transfers to and from the pumping site, is obscured by this way of looking at the proton pumping cycle. Specifically, this viewpoint overlooks the importance of the relative rates of the electron transfers to and from the pump in its various states. The rates of electron transfer are likely to depend upon whether the site is protonated or not, because electron transfer rates are dependent upon the structures and reduction potentials of the electron transfer partners (15-17). Hence, it is important to consider the probable nature of this effect and its consequences for the design of an efficient proton pump.

The simple kind of model under discussion, in which thermodynamic linkage and proton gating are paramount, makes a clear prediction regarding reduction potentials. Since reduction leads to substantial protonation ($pK_a$(red) is higher than the pertinent solution pH) and oxidation leads to substantial deprotonation ($pK_a$(ox) is lower than the pertinent solution pH), the pumping site should exhibit a reduction potential which is strongly (ca. 60 mV/pH unit) dependent upon pH in the physiological range (18) (Figure 2). A site

Figure 2. The dependence of reduction potential upon pH for a redox couple in which reduction is strongly linked to protonation. In the pH range between $pK_a$(red) and $pK_a$(ox), the reduction potential exhibits a steep pH dependence (ca. -60 mV/pH unit for a one-electron, one-proton acceptor at 303K). This would be the behavior anticipated for a proton pump in which $pK_a$ changes were of greatest importance in defining the most probable reaction path; i.e., in which $pK_a$(ox) < 7 and $pK_a$(red) > 7.

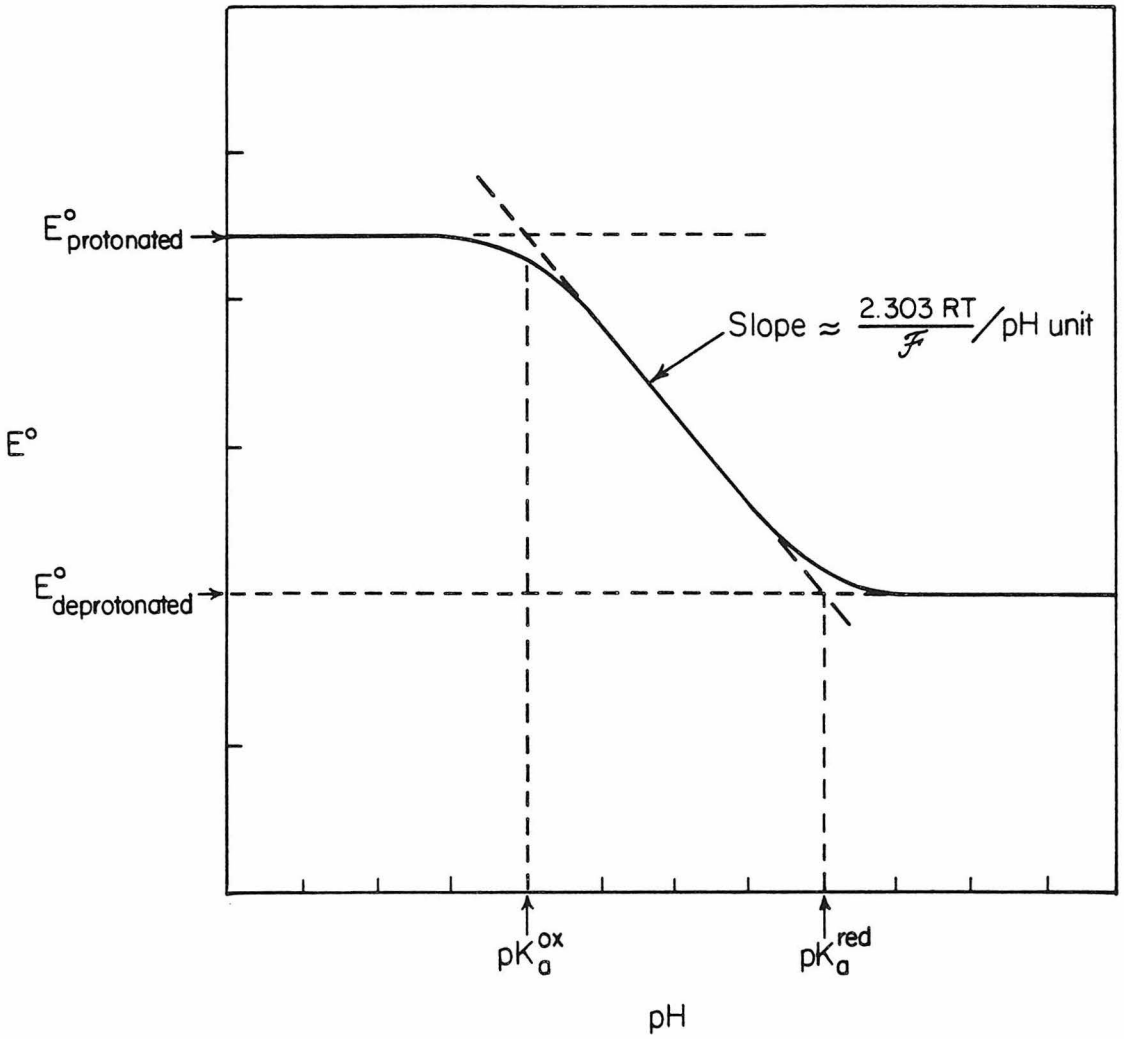
$E^\circ_{protonated}$
Slope $\approx \frac{2.303\,RT}{\mathcal{F}}$ / pH unit
$E^\circ$
$E^\circ_{deprotonated}$
$pK_a^{ox}$
$pK_a^{red}$
pH

which has a pH-dependent reduction potential would then appear more likely to be the proton pump than one which does not. This reasoning has been used to implicate one site in particular ($Fe_a$) in the proton pumping function of cytochrome *c* oxidase. This point will be considered again below, following the development of a more complete conceptual model for proton pumping.

## A DIFFERENT PERSPECTIVE: THE IMPORTANCE OF ELECTRON GATING

An examination of Figure 1 reveals that models of the kind depicted are symmetrical with respect to electron and proton movements, so that electrons and protons play analogous roles during the pumping cycle when they are viewed formally as ligands to the pumping site. There is therefore no fundamental reason to emphasize proton gating more than electron gating; in fact, efficient electron gating may be more difficult to achieve because of the delocalized character of electrons and their associated capacity for tunneling. Nevertheless, the importance and possible mechanisms of electron gating have received less attention in the literature of mitochondrial energy transduction.

The importance of electron gating and the nature of electron gating mechanisms may be fruitfully explored within the framework of electron transfer rate theory. To this end, it is helpful to outline briefly some of the central concepts of this theory as elaborated, for example, by Marcus (19) or Hopfield (15). It should be emphasized that this area is currently a very active field of investigation and that many of the ideas are only beginning to be systematically tested in protein model systems (20–22), which are the most relevant to the present discussion.

At least four factors are important in determining the rate of an electron transfer reaction. The first of these is the reaction exothermicity. Under all but extraordinary conditions, a more exothermic electron transfer reaction is expected to proceed more rapidly than a less exothermic (but otherwise identical) reaction

(15,19). This factor will always operate against energy conservation, since uncoupled (i.e., those in which electron transfer through the pump is not accompanied by proton pumping) processes are more exothermic than coupled ones. In many cases, probably including the present one, a change in the reaction free energy will be manifested as a change in the activation energy for the reaction which is about one-half as large (19,23). This approximation will be used below in the kinetic treatment of proton pump models.

A second factor which influences electron transfer rates is the so-called rearrangement energy associated with the electron transfer. This refers to the amount of energy involved in the structural rearrangements which accompany the oxidation of the electron donor and the reduction of the electron acceptor. For reactions which are not extremely exothermic, including those of mitochondrial electron transport, a smaller rearrangement energy will lead to more rapid electron transfer. Since the rearrangement energy involves the details of the coordination geometry of the electron transfer partners, it should be possible to effect significant changes in it by changing the coordination geometry, for example, by protonating a ligand, or exchanging one ligand for another, at the pumping site.

A third factor influencing electron transfer rate is the distance between the electron donor and acceptor. Electron transfer over long distances involves the weak overlap of the tails of the donor and acceptor orbitals. These tails are expected to fall off rapidly with distance in a protein and in the reduction potential range relevant to mitochondrial electron transfer. If other factors remain fixed, it is expected that the electron transfer rate will drop by ca. 100-fold for every 3 Å increase in distance (15). Conformational changes which change the intersite distances by even a few Angstroms will thus have a significant electron-gating effect.

A final factor, which is related to the distance, is the nature of the intersite material. The donor and acceptor orbital amplitudes will decrease with distance more rapidly in a saturated

hydrocarbon environment or in a vacuum than in regions containing aromatic groups or other pi-systems, assuming that the aromatic orbitals have the proper symmetry to interact with the donor and acceptor orbitals. Particular alignments of hemes, coordinated or non-coordinated histidyl imidazoles, or other aromatic amino acid side chains could therefore enhance the rate of electron transfer. The probable magnitude of this effect is currently under investigation (24,25), but it is likely to be substantial. Owing to symmetry restrictions on orbital overlaps in the intervening medium, it is possible that fairly minor conformational changes, which involve, for example, rotations of aromatic groups, could have a significant impact on electron transfer rates.

The role of electron gating in redox-linked proton pumping is depicted in Figure 3. The reaction cycle drawn is an elaborated version of the four state scheme in Figure 1; the electron donor and acceptor are explicitly identified and the electron transfer pathways which can uncouple electron transport from proton pumping (the "electron leaks") are shown. The electron leaks shown are expected to be significantly exothermic, so the reverse processes, which would be much slower, have been ignored. A rate constant is assigned to each of the various electron- and proton-transfer processes. Proton gating is recognized as before by the proton subscripts M and C, and this proton gating will be assumed to be perfect. Perfect proton gating means that the reduced pump site is in protonic contact with only the matrix, and the oxidized pump site in protonic contact with only the cytosol. Uncoupling processes involving protonation/deprotonation (the vertical legs of the cycle in Scheme 2) may therefore be ignored. The generalization to imperfect proton gating is not difficult but would obscure some of the central points of the present analysis. We note that even with perfect <u>proton</u> gating, the pumping site may nevertheless exhibit less than perfect pumping efficiency, and even net proton leakage, because of the presence of the <u>electron</u> leaks.

The importance of effective electron gates is readily appreciated if one considers the following reasoning, as applied to

Figure 3. Four state redox-linked proton pumping cycle which includes electron leak pathways. The electron donor and acceptor are signified by D and A, respectively. The uncoupled electron transfers are assigned primed rate constants; the reverse of the uncoupled processes are not included since they are expected to be much slower. Other symbols are the same as those used in Figure 1.

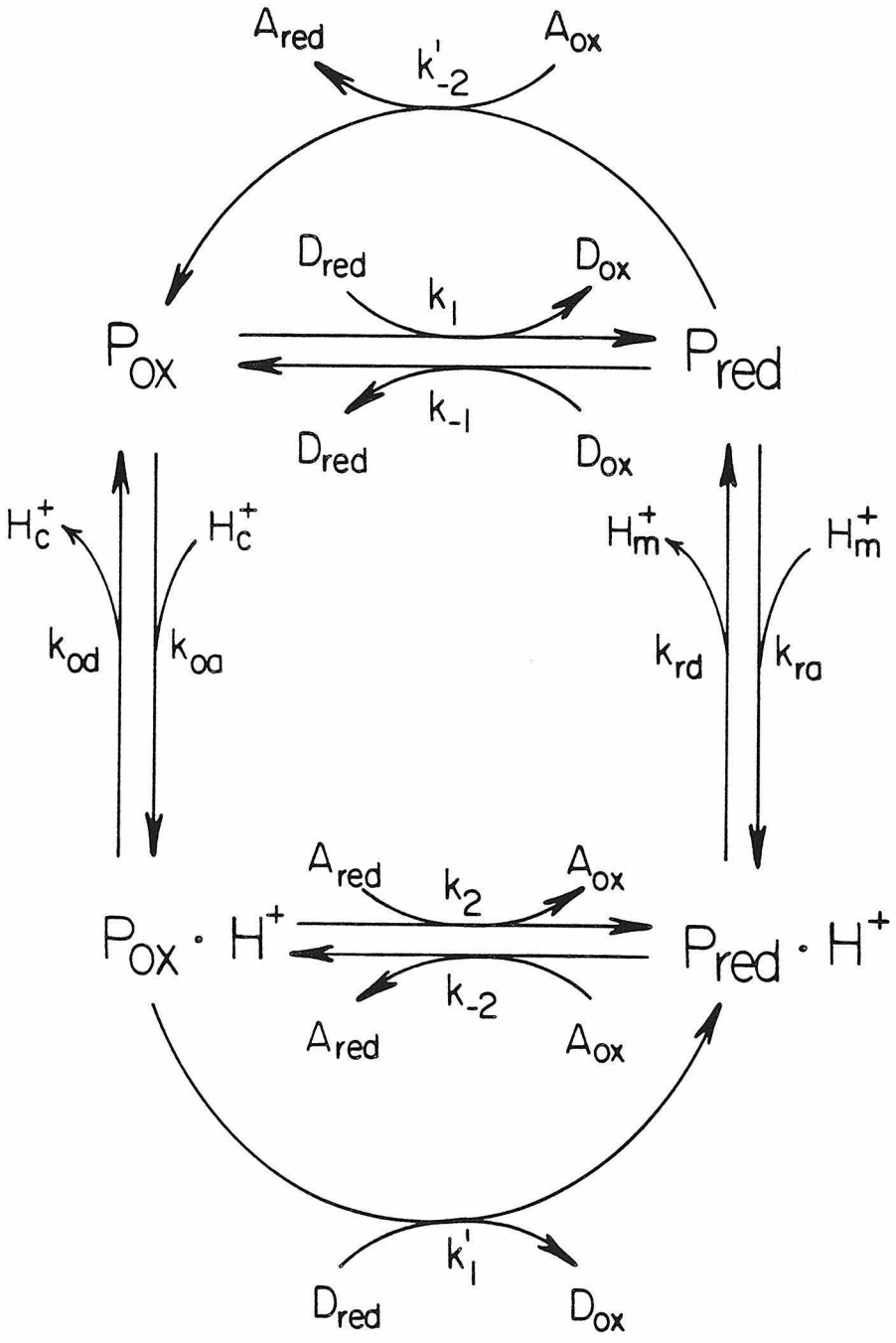
A red
A ox
k'-2
D red
D ox
k1
P ox
P red
k-1
D red
D ox
H+c
H+c
H+m
H+m
kod
koa
krd
kra
A red
k2
A ox
P ox · H+
P red · H+
k-2
A red
A ox
k'1
D red
D ox

the scheme of Figure 3: As described above, $pK_a$-controlled proton pumps are based upon a thermodynamic linkage between oxido-reduction and protolysis. The $pK_a$ of the reduced pump will therefore be different from (in a scheme like Figure 3, greater than) the $pK_a$ of the oxidized pump, and the reduction potential of the protonated site will be greater than that of the deprotonated site. Hence, the uncoupled process k1' in Figure 3 will be more exothermic than the coupled process k1, by an amount equal to the thermodynamic linkage. The same is true of the uncoupled process k2' relative to the coupled process k2. Without special provisions for directing the electron transfers, the rate constants for the more exothermic, uncoupled processes will be greater, as indicated above, and efficient proton pumping will not occur.

Having recognized the importance of both proton- and electron-gating, we may envisage proton pumps which might be designated "kinetically controlled" pumps. In their most extreme form, kinetically controlled pumps would involve no thermodynamic linkage (no $pK_a$ control) but would rely exclusively upon proton- and electron-gating effects. In a less extreme form, kinetic control would play a significant role in the pumping cycle, and thermodynamic linkage would assume a correspondingly diminished role. As the foregoing discussion suggests, a substantial degree of kinetic control is essential. It should be emphasized that electron leaks are a problem that should be considered in any type of model for a redox-linked proton pump, because they can be a significant constraint on the overall efficiency of a real pump, and because any real pump must incorporate mechanisms for minimizing them.

## KINETIC ANALYSIS OF A REDOX-LINKED PROTON PUMP WHICH INCLUDES SLIPPAGE PATHWAYS

### 1. Solution of the Steady-State Rate Equations

In this section, a quantitative investigation will be undertaken of the importance of electron gating, the role of

thermodynamic linkage, and other issues involved in redox-linked proton pumping. The approach is based upon the solution of the steady-state rate equations which describe the pump, and is in some respects similar to the work of Lauger (26), who considered an analogous case but with perfect gating. The initial analysis is based upon the four-state reaction scheme given in Figure 3. The important assumptions implicit in this reaction scheme have been noted above.

The present analysis addresses the steady state rather than the equilibrium condition of a proton pump, so it reveals some of the important kinetic properties of the pump. Any real proton pump must operate at a nonzero rate to be useful, which will entail some irreversibility in the reaction cycle and an accompanying departure from maximum efficiency. It is interesting to inquire at what level of efficiency (and hence rate) a real proton pump is likely to operate, and how this level of operating efficiency is related to the magnitude of the electron or proton leaks which are present. The answer to this question must involve the relationship of the efficiency of the pump to its turnover rate, and the relationship of both to the electron or proton leaks. These relationships are readily predicted using the steady-state analysis. This steady-state analysis is probably applicable to mitochondria which are in a particular steady state of respiration, i.e., with a defined membrane potential. However, it is not directly applicable to the transient behavior which is observed in measurements of proton pumping stoichiometry in cytochrome c oxidase (27), which typically involve a pulse of reductant or oxygen. In these experiments, the membrane potential is initially zero and rapidly increases as protons are pumped.

Previous theoretical treatments (28) of the kinetics of mitochondrial energy transduction have been more purely phenomenological, using the formalism of irreversible thermodynamics under the assumptions of linear flow-force relationships and Eyring reciprocity. The present approach is complementary in that it begins with a particular molecular model for transduction and makes

predictions which can be compared with those of irreversible thermodynamics. The assumptions of the irreversible thermodynamic treatment may therefore be critically evaluated for particular molecular models of interest, and the parameter domains for which they are valid established. The occurrence of slippage, which is incorporated phenomenologically in some of the irreversible thermodynamic analyses, is given precise meaning in terms of kinetic constants in the present analysis.

A depiction of the four state pumping cycle which emphasizes the irreversibility of the reaction is given in Figure 4. In this figure, the electron and proton free energy changes at each reaction step are given in terms of the various reduction potentials and $pK_a$s which describe the pump. This figure thus introduces some of the symbols (reduction potentials and $pK_a$s) which are important in later discussion, and facilitates the visualization of the corresponding quantities.

The electron and proton free energies shown in Figure 4 reflect the energetic scheme most commonly assumed for a "$pK_a$- controlled" proton pump; i.e., protonation from the matrix is somewhat exothermic in the reduced state and deprotonation to the cytosol is somewhat exothermic in the oxidized state. Also, the reduction of the deprotonated pump by the donor and the oxidation of the protonated pump by the acceptor are both slightly exothermic. This is in accordance with the presumed requirement, noted above, for matching of the input and output states of the pump to input and output potentials. While the figure is drawn to reflect particularly this conventional type of pump, the analysis which follows will extend to a range of pump "designs," some of which will have state energies that do not resemble those in Figure 4.

The initial state $P_{ox} + H^+_M$ and the final state $P_{ox} + H^+_C$ (Figure 4B) differ in protonic free energy by the magnitude of the proton electrochemical potential across the membrane. In an energized mitochondrion, this potential corresponds to a protonmotive force (see Ref.3) close to 200 mV (29,30). With respect to electronic standard free energy (Figure 4A), the initial

Figure 4. Electronic (A), protonic (B), and total (C) standard free energy changes which occur in the four state proton pumping cycle of Figure 3. The expressions for free energy changes for the electron transfer reactions assume that the donor and acceptor are 50% reduced, so that the operating potentials equal the standard potentials. The symbols used are: $E^o_D$, the standard reduction potential of the electron donor to the pump; $E^o_A$, the standard reduction potential of the electron acceptor; $E^o_L$, the standard reduction potential of the deprotonated state of the pump; $E^o_H$, the standard reduction potential of the protonated state of the pump; $pK_{red}$, the $pK_a$ of the reduced pump; $pK_{ox}$, the $pK_a$ of the oxidized pump. For the purpose of illustrating the standard free energy changes accompanying proton transfers to and from the aqueous phases, in this figure the solvent is represented by protonatable donor and acceptor groups with $pK_a$s $pK_a^D$ and $pK_a^A$ equal to the matrix and cytosol pH respectively. Actual (as opposed to standard) free energy changes of proton transfer to the bulk solvent were incorporated in the calculations described in the text. Note that the pump is considered as having two different reduction potentials, $E^o_H$ or $E^o_L$, depending upon whether it is protonated or not. In this formal convention, the coupling between protonic and electronic energies occurs at the 2nd step drawn, namely, the protonation of the reduced pump. This step thus involves the simultaneous stabilization of the electron and destabilization of the proton, with the former process making the overall process slightly exothermic.

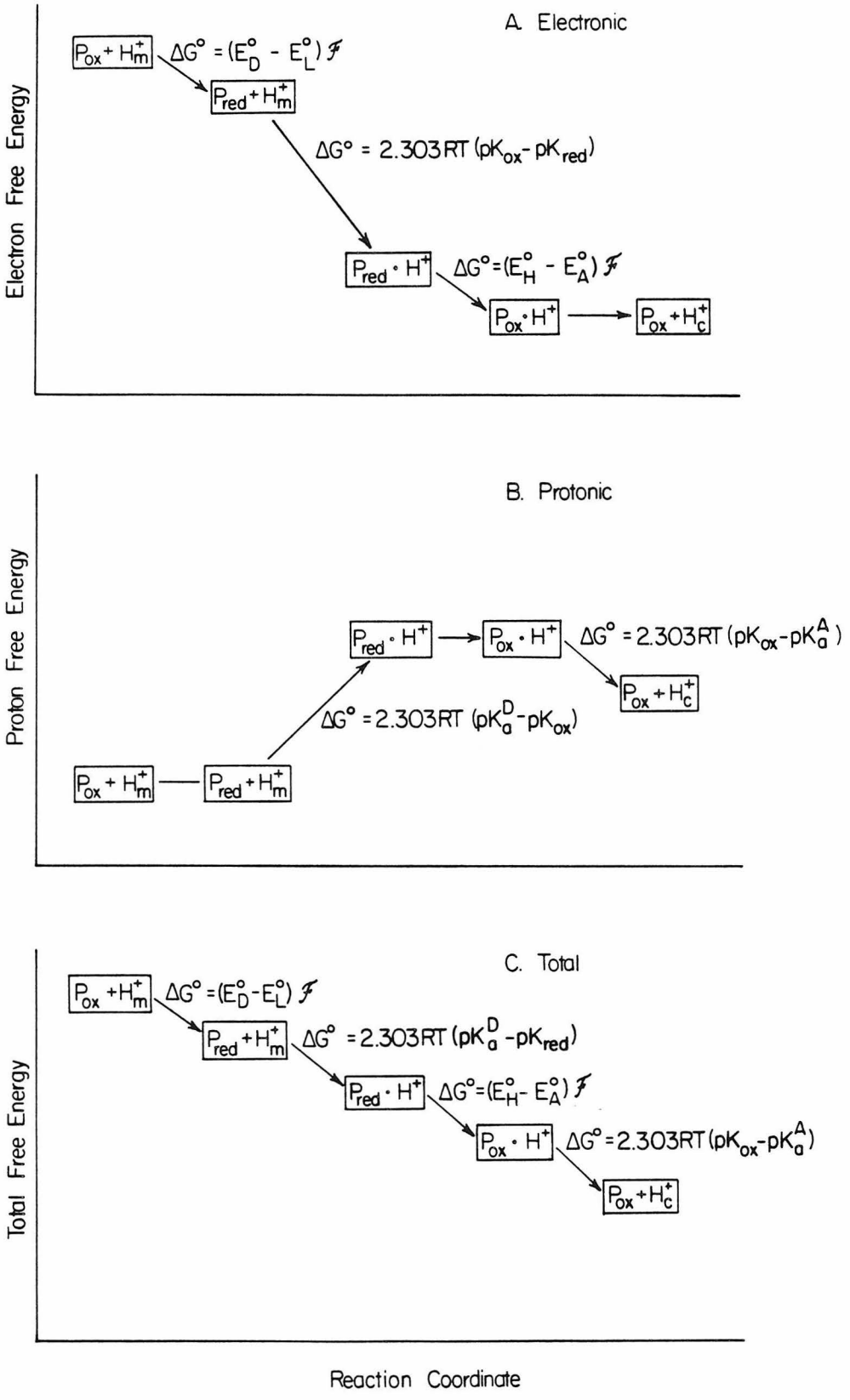
A. Electronic
Electron Free Energy
$P_{ox} + H_m^+$
$\Delta G^\circ = (E_D^\circ - E_L^\circ)\mathcal{F}$
$P_{red} + H_m^+$
$\Delta G^\circ = 2.303RT\,(pK_{ox} - pK_{red})$
$P_{red} \cdot H^+$
$\Delta G^\circ = (E_H^\circ - E_A^\circ)\mathcal{F}$
$P_{ox} \cdot H^+$
$P_{ox} + H_c^+$
B. Protonic
Proton Free Energy
$P_{red} \cdot H^+$
$P_{ox} \cdot H^+$
$\Delta G^\circ = 2.303RT\,(pK_{ox} - pK_a^A)$
$P_{ox} + H_c^+$
$\Delta G^\circ = 2.303RT\,(pK_a^D - pK_{ox})$
$P_{ox} + H_m^+$
$P_{red} + H_m^+$
C. Total
Total Free Energy
$P_{ox} + H_m^+$
$\Delta G^\circ = (E_D^\circ - E_L^\circ)\mathcal{F}$
$P_{red} + H_m^+$
$\Delta G^\circ = 2.303RT\,(pK_a^D - pK_{red})$
$P_{red} \cdot H^+$
$\Delta G^\circ = (E_H^\circ - E_A^\circ)\mathcal{F}$
$P_{ox} \cdot H^+$
$\Delta G^\circ = 2.303RT\,(pK_{ox} - pK_a^A)$
$P_{ox} + H_c^+$
Reaction Coordinate

and final states will differ by the difference between the standard reduction potentials of the electron donor and acceptor. In the case of cytochrome c oxidase, for example, this will be approximately 550 mV (for the average of the four different electron transfers required to reduce dioxygen to water), of which only about half will be available for proton pumping, since the electron transfers to dioxygen are themselves electrogenic (4).

The rate of proton pumping in the reaction scheme of Figure 3 is given by:

$$R_{H^+} = k_{ra} \left[H^+_M\right] \left[P_{red}\right] - k_{rd} \left[P_{red} \cdot H^+\right] . \qquad (1)$$

The rate of electron transfer is:

$$R_{e^-} = k_1 \left[D_{red}\right] \left[P_{ox}\right] + k_1' \left[D_{red}\right] \left[P_{ox} \cdot H^+\right] - k_{-1} \left[D_{ox}\right] \left[P_{red}\right]. \qquad (2)$$

Defining the stoichiometric efficiency of proton pumping by $Eff = R_{H^+} / R_{e^-}$, the overall energetic efficiency of the pump is then

$$\varepsilon = Eff \ (\Delta\tilde{\mu}_{H^+} / \Delta G) \qquad (3)$$

where $\Delta\tilde{\mu}H+$ is the proton electrochemical potential across the membrane, and $\Delta G$ is the total free energy available for proton pumping. The other symbols are defined by reference to Figure 3.

The equations which describe the steady-state condition of the pump of Figure 3 are solved in the Appendix. The resulting

expressions for the steady-state concentration of each of the four species were used in equations 1 and 2 to derive the following expressions for the rate of electron transfer through the pump and the stoichiometric efficiency of proton pumping:

$$R_{e^-} = A / B \tag{4}$$

$$Eff = C / A \ , \tag{5}$$

where

$$\begin{aligned} A = {} & k_1[D_r] \{k_{rd}k'_{-2}[A_0] (k_{od} + k_2[A_r] + k_i'[D_r]) \\ & + k_{od}k_{-2}[A_0] (k'_{-2}[A_0] + k_{ra}[H_m^+])\} \\ & + k_i'[D_r] \{k_{rd}k_{oa}[H_c^+]k'_{-2}[A_0] + k_{ra}[H_m^+]k_1[D_r]k_{-2}[A_0] \\ & + k_{oa}[H_c^+]k_{-2}[A_0] (k'_{-2}[A_0] + k_{-1}[D_o] + k_{ra}[H_m^+])\} \\ & - k_{-1}[D_0]k_2[A_r]k_{0a}[H_c^+]k_{rd} \end{aligned}$$

$$\begin{aligned} B = {} & \{k_{-2}[A_0] (k_{od} + k_{oa}[H_c^+]) + k_{oa}[H_c^+] (k_2[A_r] + k_i'[D_r])\} \\ & \{k'_{-2}[A_0] + k_{-1}[D_o] + k_{ra}[H_m^+]\} \\ & + \{k_{rd}(k'_{-2}[A_0] + k_{-1}[D_o] + k_1[D_r]) + k_{ra}[H_m^+]k_1[D_r]\} \\ & \{k_{od} + k_2[A_r] + k_i'[D_r]\} \\ & + k_{oa}[H_c^+]k_{rd} (k_2[A_r] + k_i'[D_r] + k'_{-2}[A_0] + k_{-1}[D_o]) \\ & + k_1[D_r]k_{-2}[A_0] (k_{ra}[H_m^+] + k_{od}) \end{aligned}$$

$$\begin{aligned} C = {} & k_{ra}[H_m^+]k_{-2}[A_0]k_1[D_r]k_{od} - k_{oa}[H_c^+]k_{rd} (k'_{-2}[A_0] + k_{-1}[D_o]) \\ & (k_2[A_r] + k_i'[D_r]) \end{aligned}$$

and the various symbols are defined in Table I and Fig. 3. These expressions were employed to calculate electron transfer rates and

proton pumping efficiencies, using various values for the kinetic parameters which describe the pump. A description of the input parameters is given in Table 1; the available driving force and input/output potentials were chosen to roughly approximate cytochrome oxidase. Rates and efficiencies were calculated for transmembrane proton electrochemical potentials ranging from zero to a potential equal to the driving force available to the pump from the electron transfer reactions. This membrane potential is the maximum attainable at steady state and can occur only in the case of perfect pumping efficiency. The following assumptions were made regarding the mitochondrial electrochemical proton gradient: First, the pH on the cytosol side of the membrane was assumed not to vary, since it involves a volume and a buffering capacity which is large relative to the interior of the mitochondrion. The cytosol pH was fixed at 7.0 (which is a reasonable estimate of intracellular pH), so that, for example, a transmembrane ΔpH of 3 units (typical of an energized mitochondrion) would correspond to a matrix pH of 10.0. For the initial analysis, the electrochemical proton potential was treated as consisting only of a pH difference, with no electrostatic component. Calculations which explicitly incorporate an electrostatic component in the membrane potential (not shown) demonstrate that this simplification has no influence upon the principal conclusions to be drawn from the analysis. Membrane potentials are therefore expressed as the corresponding ΔpH. The proton electrochemical potential difference associated with a pH gradient (ΔpH) is given by the equation $\Delta\mu H^+ = 2.303\ RT\ \Delta pH/F$. For simplicity, a temperature of 30° was assumed so that one pH unit corresponds to 60 mV.

## 2. Pump Rates and Efficiencies: Effects of Membrane Potential and Electron Leaks

Both the rate of electron transfer through a proton pumping site and the efficiency of the proton pumping are expected to depend

upon the magnitude of the membrane potential. In Figure 5, the predicted energetic efficiency of the proton pump (calculated according to equations (3) and (5)) is plotted as a function of the magnitude of the membrane potential for 4 different values of the electron leak rates. The other parameters were selected to preserve symmetry (with respect to the relationship of the pump $pK_a$s to the pH gradient across the membrane, and the relationship of the pump reduction potentials to the donor and acceptor reduction potentials) for simplicity, and to attain a near optimum in kinetic performance. In all cases examined below, the rate of protonation has been assumed to be fast relative to the electron transfer rates. This is in accordance with the present emphasis on electron transfer and electron gating. The assumption that protonation is fast relative to electron transfer is also in accordance with what is known about the intersite distances in cytochrome c oxidase. The $Fe_a$ and $Cu_A$ sites are a considerable distance, probably 15 Å or more, away from the $Fe_{a_3}/Cu_B$ site (31). It is expected that the rate of electron transfer over such a large distance can not be much greater than the overall turnover rate which the enzyme can achieve under uncoupled conditions (ca. 400 $s^{-1}$ (32)), even if the other factors which influence the electron transfer rate are optimal (15). On the other hand, protonation/deprotonation could be considerably faster than this if the proton transfers are catalyzed by suitably situated acid/base groups (32), so long as the $pK_a$s of these groups are not extreme.

The rates of electron leakage are expressed as the ratio of the uncoupled and the coupled electron transfer rates. The electron transfer rates are expected to depend upon the electron transfer exothermicities, and this correlation has been explicitly incorporated into the kinetic analysis. Because of this correlation between exothermicity and rate, the uncoupled and coupled electron transfer rates were standardized to zero exothermicity, and these isoergonic electron transfer rates were used in calculating the uncoupled:coupled rate ratios. The electron transfer rates standardized to zero exothermicity will be called the "standard"

electron transfer rates (see footnote to Table 1). The standard electron transfer rate thus reflects all of the factors besides exothermicity which influence the electron transfer rate, including the intersite distance, the nature of the intervening material, and the rearrangement energies. It is these factors which can be manipulated to achieve electron gating, so the uncoupled:coupled standard electron transfer rate ratio thus measures the effectiveness of these gating mechanisms.

It is evident from Figure 5 that the rate of electron leakage has a dramatic effect on the efficiency of the pump. When the ratio of the uncoupled and coupled standard electron transfer rates is zero (perfect electron gating), the efficiency attains a value of 1.0 when the membrane proton electrochemical potential equals the available free energy (this occurs at pH = 5 for the parameters used in Figure 5). When the uncoupled:coupled ratio is .0001, the maximum attainable efficiency is 0.76, and when this ratio is increased to .001, the maximum efficiency drops to 0.57. At a ratio of 0.01, which still involves significant gating, the maximum efficiency is only 0.31. At a ratio of 1.0, corresponding to no gating at all, the efficiency is zero at zero membrane potential and negative (i.e., cycling causes discharge of the membrane potential) for all nonzero membrane potentials (data not plotted).

Figure 5 indicates that in the presence of electron leaks there is a membrane potential which is optimal for the efficiency of the pump. However, in all cases which were investigated the efficiency does not drop off very steeply away from this optimum, so that relatively efficient operation is possible over a substantial (plus or minus ca. 20%) range of membrane potential.

In respiring mitochondria and in vesicle-reconstituted cytochrome c oxidase, the rate of electron transfer decreases as the membrane potential increases (34,35). This phenomenon is a manifestation of "respiratory control," and the ratio of the electron transfer rate in phosphorylating (State 3) mitochondria (in which the membrane potential is partially discharged by the ATP synthase) to the rate in fully membrane-energized (State 4)

TABLE 1. PARAMETERS USED IN THE CALCULATION OF RATES AND EFFICIENCIES OF THE FOUR STATE REDOX LINKED PROTON PUMP.

| PARAMETER | DESCRIPTION | VALUE USED IN INITIAL ANALYSIS |
|---|---|---|
| $E^o_D$ | Reduction potential of the electron donor to the pump | 250 mV |
| $E^o_A$ | Reduction potential of the electron acceptor | 550 mV |
| $D_r$ | Concentration of the reduced form of the donor relative to that of the pump | 0.5 |
| $D_o$ | Concentration of the oxidized form of the donor relative to that of the pump | 0.5 |
| $A_r$ | Concentration of the reduced form of the acceptor relative to that of the pump | 0.5 |
| $A_o$ | Concentration of the oxidized form of the acceptor relative to that of the pump | 0.5 |
| $E^o_L$ | reduction potential of the deprotonated pumping site (Fig. 3, upper redox equilibrium) | 310 mV |
| $E^o_H$ | reduction potential of the protonated pumping site (Fig. 3, lower redox equilibrium) | 490 mV |

(Table I, cont.)

| | | |
|---|---|---|
| $pK_a^{red}$ | $pK_a$ of the reduced pump site | 10.0 |
| $pK_a^{ox}$ | $pK_a$ of the oxidized pump site | 7.0 |
| $PP_i$ | Product of the rates of protonation and deprotonation on the input (matrix) side of the pump. This quantity is related to the height of the barrier to protonation/ deprotonation, and thus describes the kinetics of proton movements. | $1x10^{15}(s-2)$ |
| $PP_o$ | product of the rates of protonation and deprotonation on the output (cytosol) side of the pump | $1x10^{15}(s-2)$ |
| $EP_i$ | product of the forward and backward rates of electron transfer on the input side of the pump. The electron transfer analog of $PP_i$ | $1x10^4$ (s-2) |
| $EP_o$ | product of the forward and backward rates of electron transfer on the output side of the pump. | $1x10^4$ (s-2) |
| $KL_i$ | standardized* rate of the electron leak involving the electron donor | |
| $KL_o$ | standardized* rate of the electron leak involving the electron acceptor | |

(Table I, cont.)

*By "standardized," it is meant that these rate constants apply for the electron transfers in question when the processes are isoergonic. To obtain actual rate constants, the standard rates were adjusted under the assumption that changes in $\Delta G^{o}$ are manifested as changes in $\Delta G^{\ddagger}$ which are one-half as large, consistent with the discussion (see text) of the factors that influence electron transfer rates. In this way, the anticipated effect of changes in $E^{o}_{L}$ or $E^{o}_{H}$ upon the rates of electron leakage are automatically taken into account. Note that the standard rates for the coupled electron inputs and outputs are given just by the square roots of $EP_{i}$ and $EP_{o}$.

Figure 5. Energy efficiency of the proton pump model (Fig.3) as a function of the mitochondrial membrane pH gradient, for five different values of the electron leak rate. The electron leak rate is expressed in the figure as the ratio of the "standard" uncoupled and coupled electron transfer rates (for an explanation of the term "standard," see the text and the footnote to table I). The values of the parameters which describe the pump (see Table I) are as follows: $E^{o}_{D}$ = 250 mV; $E^{o}_{A}$ = 550 mV; $E^{o}_{L}$ = 310 mV; $E^{o}_{H}$ = 490 mV; $FD_{red}$ = 0.5; $FA_{red}$ = 0.5, [D] = [A] = 1.0; $pK_a$(red) = 10.0 ($pK_a$(ox) thus equals 7.0); $PP_i = PP_o = 10^{15}\ s^{-2}$; $EP_i = EP_o = 10^4\ s^{-2}$. Since $EP_i$ and $EP_o$ are $10^4\ s^{-2}$, the standard <u>coupled</u> electron transfer rate is the square root of $10^4$, or 100 $s^{-1}$. Note that these parameters are symmetric with respect to the input and output sides of the pump; i.e., $PP_i=PP_o$, $EP_i=EP_o$, $(E^{o}_{L}-E^{o}_{D})=(E^{o}_{A}-E^{o}_{H})$, etc.

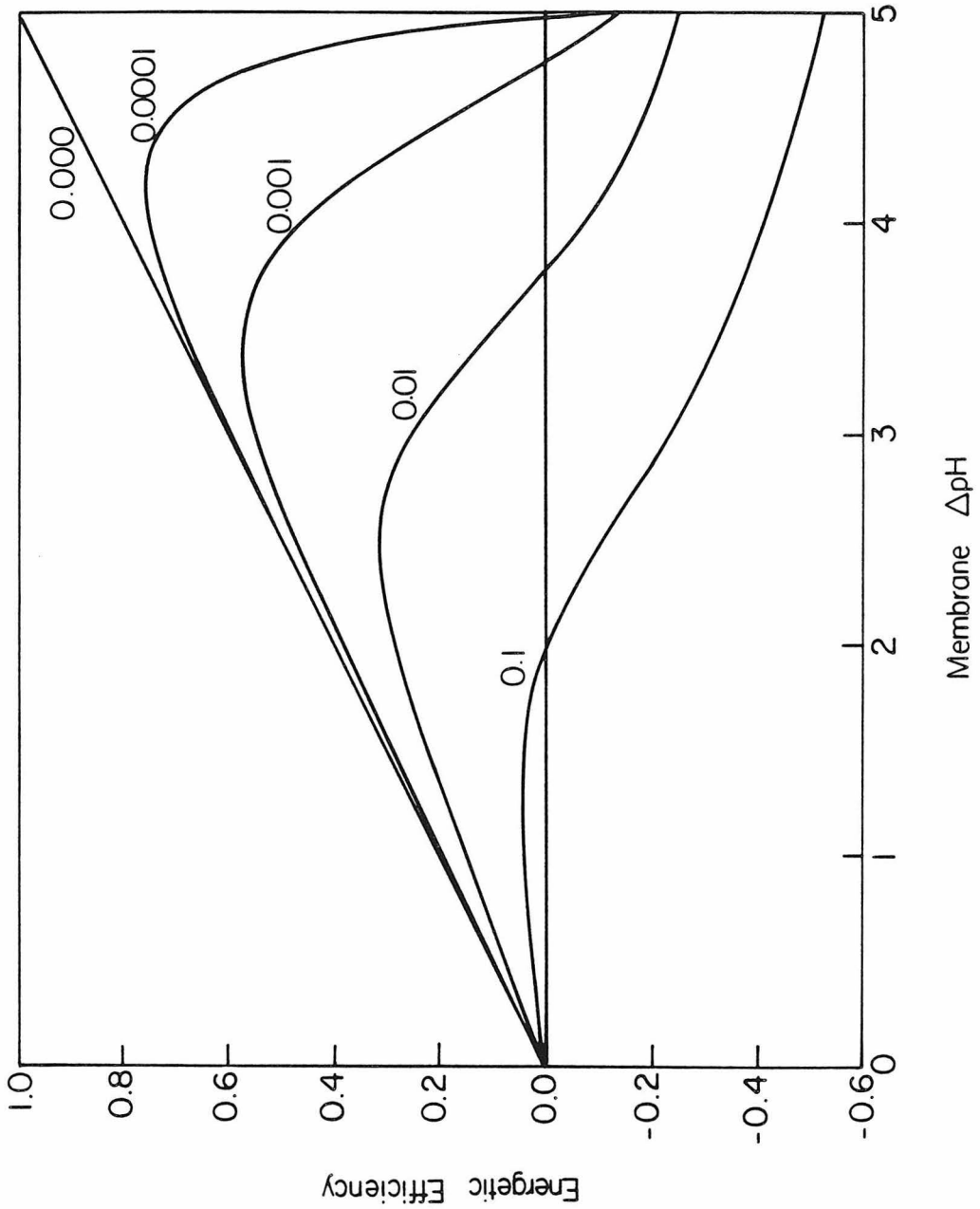
0.000
0.0001
0.001
0.01
0.1
1.0
0.8
0.6
0.4
0.2
0.0
-0.2
-0.4
-0.6
0
1
2
3
4
5
Energetic Efficiency
Membrane ΔpH

Figure 6. Electron transfer rate ($s^{-1}$) for the proton pump model (fig. 3) as a function of the mitochondrial membrane pH gradient, for four different values of the electron leak rates. The parameters describing the pump are the same as those used in Figure 4; the electron leak rates, again expressed as the ratio of standard uncoupled and coupled electron transfer rates, are shown in the figure. As noted in the caption to Figure 5, the standard coupled electron transfer rate for this parameter set is 100 $s^{-1}$.

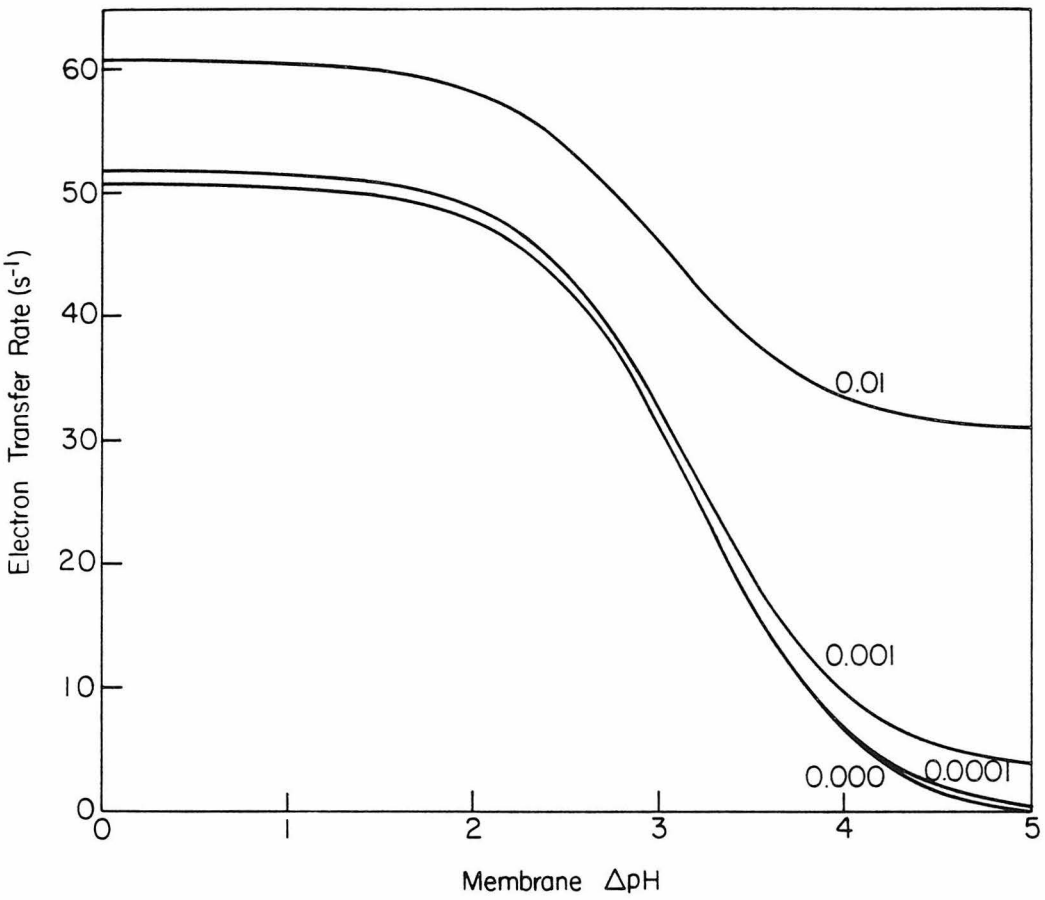
Electron Transfer Rate ($s^{-1}$)
60
50
40
30
20
10
0
0
1
2
3
4
5
Membrane ΔpH
0.01
0.001
0.000
0.0001

Figure 7. Energy efficiency vs. electron transfer rate for the four-state pump of Figure 3, for four different electron leak rates. For a given leak rate, the position on the curve at which the pump actually operates is fixed by the applied membrane potential.

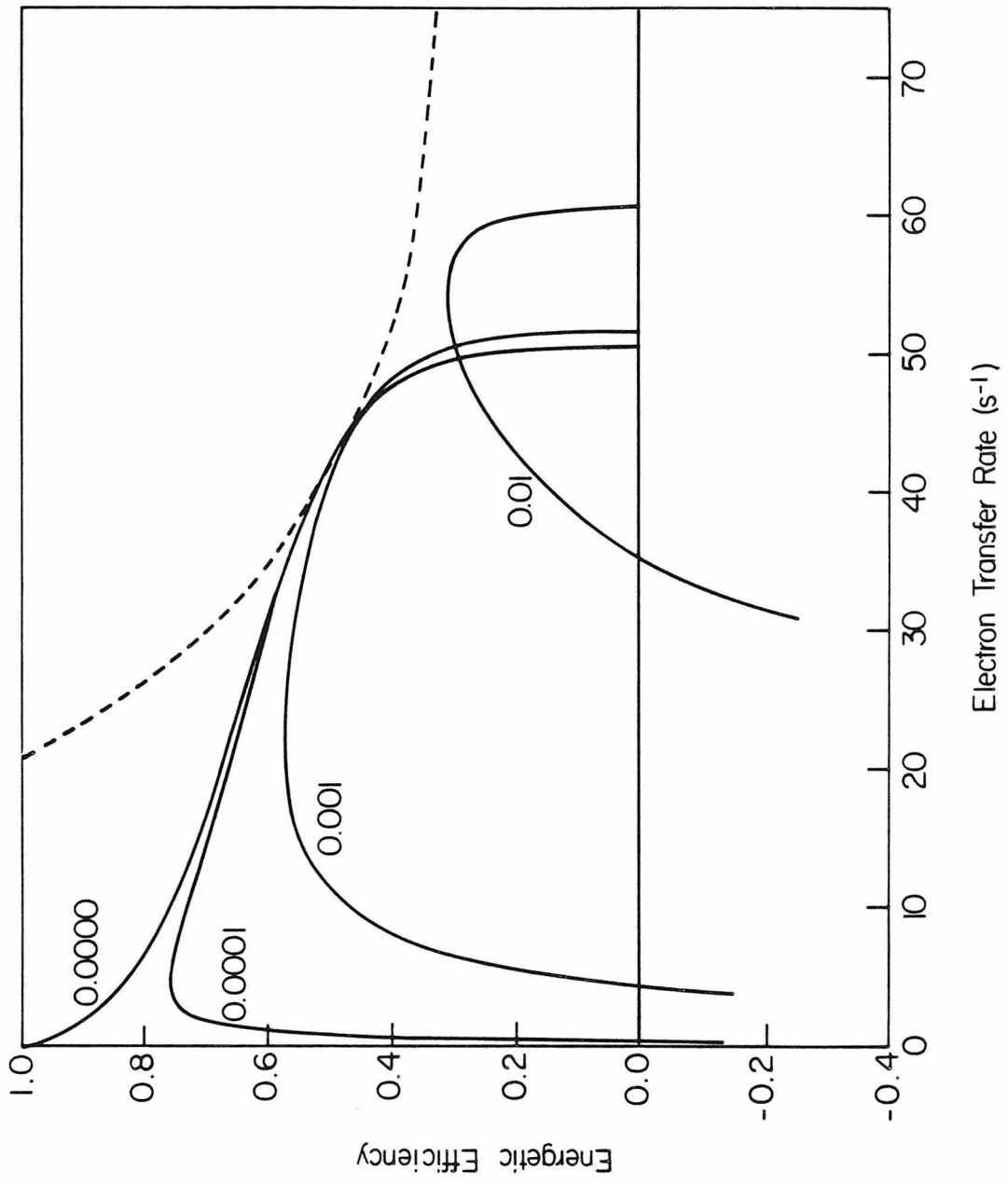
Energetic Efficiency
1.0
0.8
0.6
0.4
0.2
0.0
-0.2
-0.4
0
10
20
30
40
50
60
70
Electron Transfer Rate (s-1)
0.0000
0.0001
0.001
0.01

mitochondria is called the "respiratory control ratio" (36). This kind of behavior is illustrated in Figure 6, which plots the rate of electron transfer through the pump as a function of the membrane potential (for the same parameters used in Figure 5). The electron transfer rate decreases sigmoidally with increasing membrane potential, and in the case of perfect gating the rate becomes zero when the applied potential equals the available free energy ($\Delta pH$= 5.0), as expected. As gating is made less efficient, the drop in rate with increasing potential becomes less severe. When the uncoupled:coupled rate constant ratio is .01, the electron transfer rate is still at ca. 50% of its maximum value when $\Delta pH = 5$. With uncoupled:coupled ratios 10-fold or more larger than this, an increase in electron transfer rate with increasing membrane potential is predicted, because the pump is then so inefficient that it functions mostly as an uncoupled electron leak.

In Figure 7, the rate and efficiency data of Figures 5 and 6 are correlated at various membrane potentials. As one would expect, there is a tradeoff between the efficiency and the rate. However, there is a wide range of rates over which the efficiency does not decrease very steeply, indicating that in these ranges a substantial gain in rate can be realized with relatively small sacrifice of efficiency. This is particularly true for the cases with nonzero electron leaks, and suggests that a real pump operating according to the schematic of Figure 2 will ordinarily not operate at very high ($> 0.75$) efficiency, because of the large loss in rate which this would entail.

## 3. Optimization of $pK_a$s

Figures 5-7 describe the effects of uncoupling processes and variations in membrane potential upon the performance of a proton pump which is otherwise optimized. The same type of analysis may be used to examine the effect of changes in the pump parameters, e.g., $pK_a$s and reduction potentials, away from their optimum values. In

Figure 8, the relationship between the $pK_a$s of the pump and the rate of its turnover is displayed. In all cases, the thermodynamic linkage parameter $\Delta pK_a$ ($pK_a$(red) - $pK_a$(ox)) has been constrained to 3.0 units. Because the rate of turnover is closely related to the efficiency of pumping, the efficiency has been constrained to particular levels by appropriate selection of the membrane potential. Three curves corresponding to three different efficiency levels (0.4, 0.6, and 0.8) are drawn. It is evident that operation of the pump at near maximal rates depends rather critically upon appropriate selection of the $pK_a$s and that the optimal values for the pump $pK_a$s are determined by the efficiency which is demanded of the pump. This is because the membrane $\Delta pH$ depends upon the chosen efficiency/rate combination. Close examination of the calculations reveals that the maximum rate is achieved when the $pK_a$s are symmetrically disposed relative to the steady-state pH values on the two sides of the membrane (recall that the cytosol pH has been fixed at 7.0 and only the matrix pH allowed to vary). This is strictly a consequence of the symmetric character of the input and output states of the pump, which has been preserved by appropriate selection of the other input and output parameters.

The effect of asymmetric gating parameters is illustrated in Figure 9, which uses the same parameters as Figure 8 except that electron leaks have been introduced. In one case, the input and output "gating ratios" (the uncoupled: coupled rate ratios) have both been made equal to .001, preserving input/output symmetry. In a second case the input gating ratio is .0001 and the output gating ratio is .01, introducing a 100-fold asymmetry in the efficiency of electron gating. These latter parameters would describe a situation in which the enzyme is more successful in regulating electron flow on one side of the pump than on the other. The maximum attainable efficiency is plotted as a function of the $pK_a$s of the pump for both sets of leak parameters. In the case of asymmetric leaks, we find that the maximum attainable efficiency is greater when the $pK_a$s are <u>not</u> symmetrically placed with respect to the matrix and cytoplasm pH values. The corresponding analysis of electron transfer rate

Figure 8. The electron transfer rate through the four-state proton pump as a function of the $pK_a$s of the pump, at three different levels of operating efficiency (0.8, 0.6, and 0.4). The parameters are the same as those used above in Figures 5, 6, and 7, with a zero electron leak rate, except that $pK_a$(red) and $pK_a$(ox) have been varied while maintaining their difference constant.

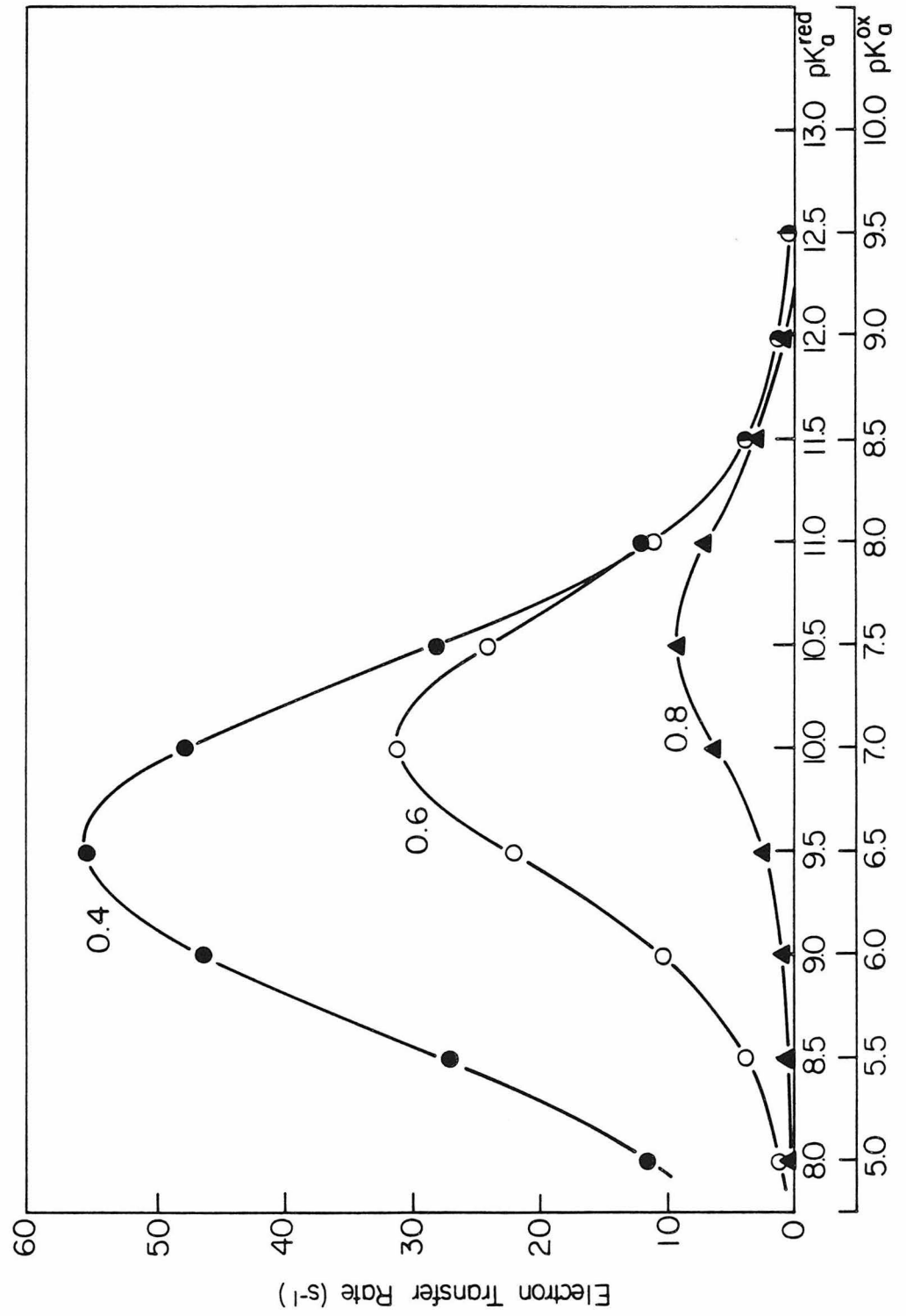
Electron Transfer Rate (s-1)
60
50
40
30
20
10
0
0.4
0.6
0.8
5.0
5.5
6.0
6.5
7.0
7.5
8.0
8.5
9.0
9.5
10.0
10.5
11.0
11.5
12.0
12.5
13.0
pKared
pKox

Figure 9. The maximum attainable efficiency of the four-state proton pump as a function of the $pK_a$s of the pump, for two different sets of electron leak parameters (for leaks equal to zero, the maximum attainable efficiency is always 1.0). Parameters are the same as in Figure 7, except that two sets of electron leaks have been introduced: a symmetric case where input and output leak ratios are both equal to .001 (closed circles), and an asymmetric case where input and output leak ratios are equal to .0001 and .01, respectively (open circles).

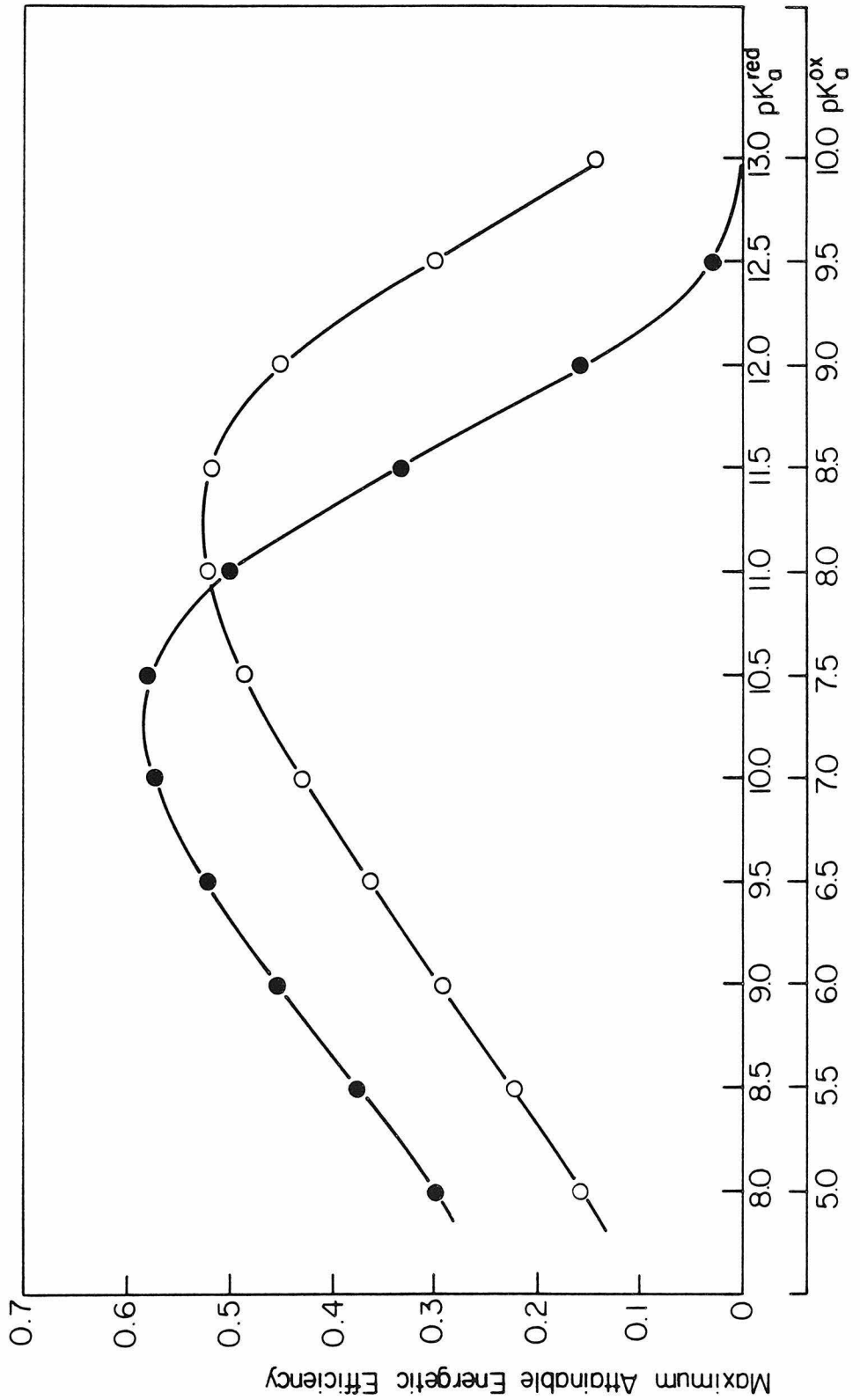
Maximum Attainable Energetic Efficiency
0.7
0.6
0.5
0.4
0.3
0.2
0.1
0
5.0
5.5
8.0
8.5
6.0
9.0
6.5
9.5
7.0
10.0
7.5
10.5
8.0
11.0
8.5
11.5
9.0
12.0
9.5
12.5
10.0
13.0
pK$_a^{red}$
pK$_a^{ox}$

vs. $pK_a$ (plot not shown) indicates that the turnover rate still peaks near a symmetric $pK_a$ disposition and drops off ca. 10-fold when the $pK_a$s are more than 1.5 units removed from this. Nevertheless, the possibility that some asymmetry in gating efficiency exists suggests that the $pK_a$s of the pump may be biased to values which would otherwise seem surprisingly high or low. In the present example, $pK_a$s of 8.5 and 11.5 would be optimal for efficiency, but electrochemical titrations in the pH range between 6.0 and 8.0 (i.e., below the pump $pK_a$s) would not reveal a pronounced pH dependence of the pump's reduction potential (see Figure 2).

## 4. The Role of Thermodynamic Linkage

Finally, it is instructive to examine the importance of thermodynamic linkage between oxido-reduction and protolysis, as measured by the quantity $\Delta pK_a$ ($pK_a(red) - pK_a(ox)$). Conventionally, it has been supposed that significant (comparable in magnitude to the membrane potential) linkage of this kind is essential to achieve the necessary rapid turnover rates (9). In Figure 10, rate vs. efficiency plots are given for several different values of $\Delta pK_a$, for a pump driven by an available free energy corresponding to a membrane $\Delta pH = 5$. Two cases are presented: perfect gating (Figure 10A) and gating ratios of 0.001 (Figure 10B). It is seen in Figure 10A that for a given electron transfer rate only a small (10-15%) loss in efficiency accompanies the decrease in thermodynamic linkage from $\Delta pK_a = 4$ to $\Delta pK_a = 2$. In the efficiency range around 0.7, which as noted above may be the optimal range of operation, the decrease in thermodynamic linkage from 4.0 units to 2.0 units causes only a ca. 3-fold decrease in electron transfer rate. Further decreasing the linkage to only 1.0 units decreases the efficiency by an additional ca. 15%, or the rate by an additional factor of 3. In Figure 10B, where electron leaks have been introduced, even more striking behavior is observed: A decrease in thermodynamic linkage

Figure 10. Energy efficiency vs. rate plots for four-state proton pumps with different degrees of thermodynamic linkage, measured as the difference between the $pK_a$s of the oxidized and reduced pumps. Parameters are the same as in Figures 4, 5, and 6, except that $pK_a(ox)$ was fixed at 7.0, and $E^o_H$, $E^o_L$, and $pK_a(red)$ have been varied in the following manner: $\Delta pK_a = 4$, $pK_a(red) = 11$, $E^o_H = 520$ mV, $E^o_L = 280$ mV; $\Delta pK_a = 3$, $pK_a(red) = 10$, $E^o_H = 490$ mV, $E^o_L = 310$ mV; $\Delta pK_a = 2$, $pK_a(red) = 9$, $E^o_H = 460$ mV, $E^o_L = 340$ mV; $\Delta pK_a = 1$, $pK_a(red) = 8$, $E^o_H = 430$ mV, $E^o_L = 370$ mV; $\Delta pK_a = 0$, $pK_a(red) = 7$, $E^o_H = E^o_L = 400$ mV. Two different electron leak situations are shown: no leaks (Figure 9A) and input and output leak ratios of .001 (Figure 9B).

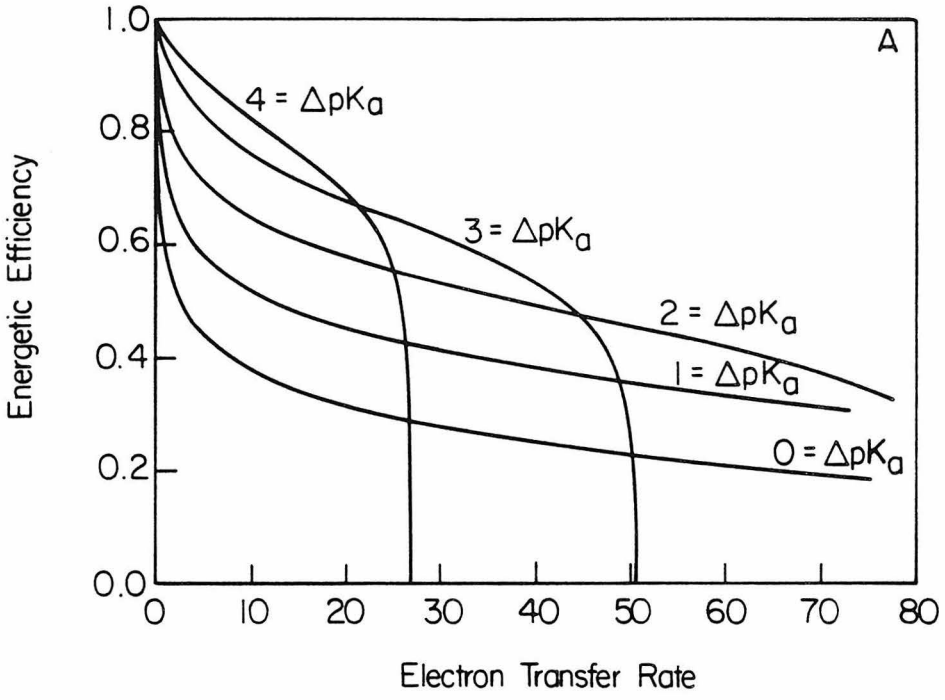
A
4 = ΔpKa
3 = ΔpKa
2 = ΔpKa
1 = ΔpKa
0 = ΔpKa
Energetic Efficiency
Electron Transfer Rate
1.0
0.8
0.6
0.4
0.2
0.0
0
10
20
30
40
50
60
70
80

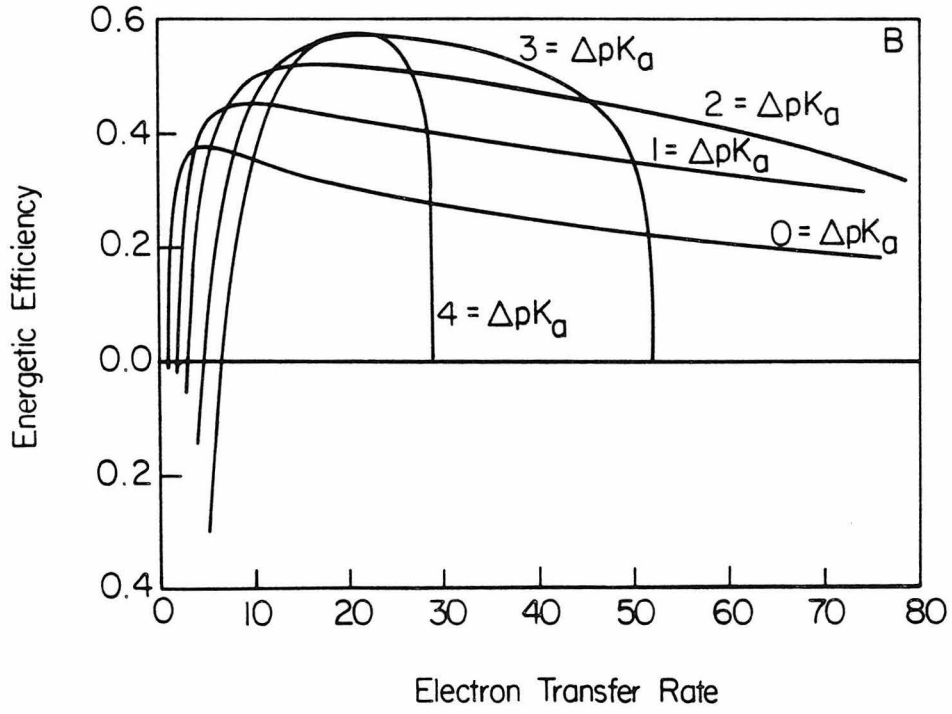
B
3 = ΔpKa
2 = ΔpKa
1 = ΔpKa
0 = ΔpKa
4 = ΔpKa
Energetic Efficiency
Electron Transfer Rate
0.6
0.4
0.2
0.0
0.2
0.4
0
10
20
30
40
50
60
70
80

**Figure 11. The effect of changing the degree of thermodynamic linkage upon the various electron transfer exothermicities. The uncoupled electron transfers (k1′ and k2′) are always more exothermic than the coupled ones (k1 and k2); as the thermodynamic linkage increases, this difference in exothermicities increases.**

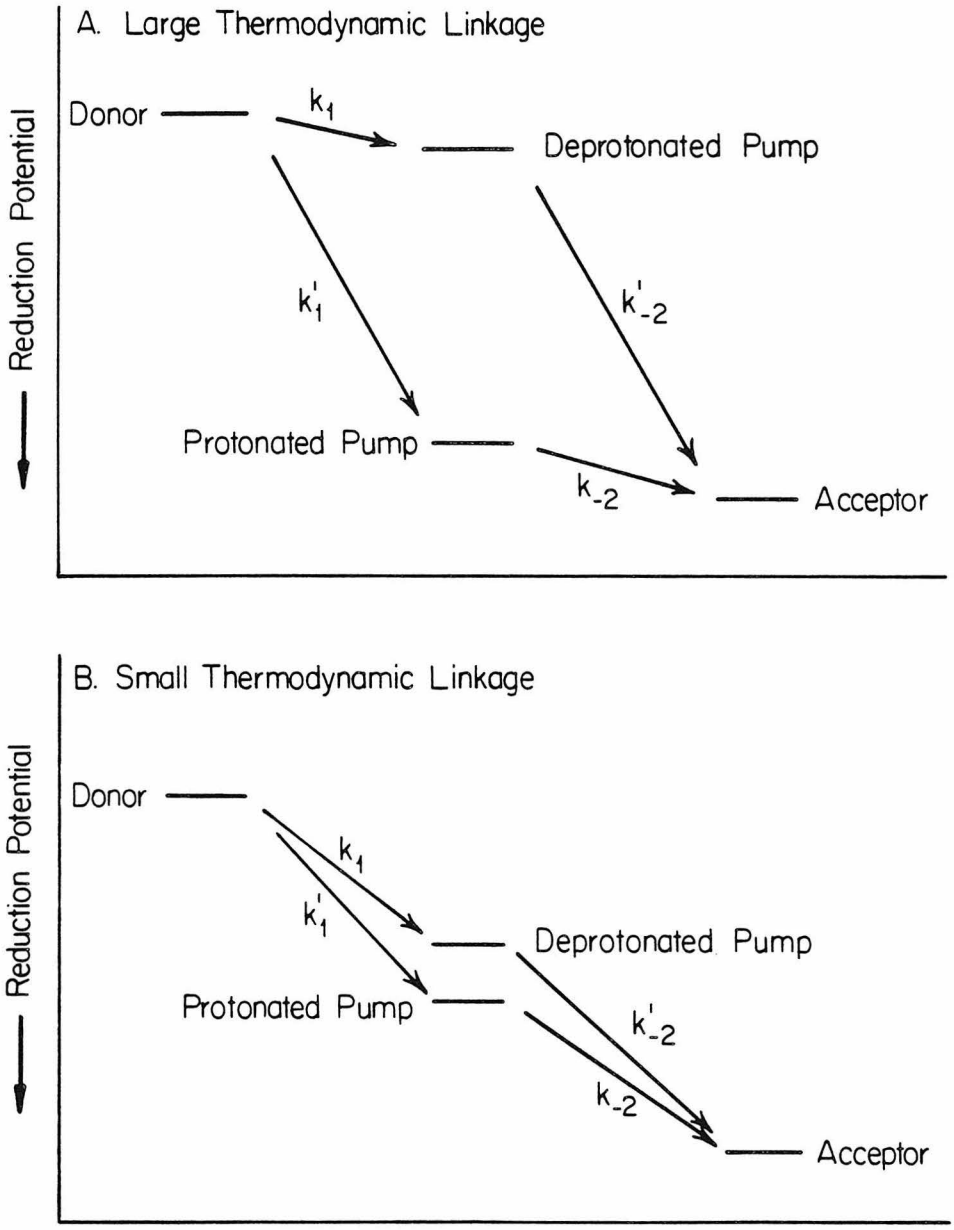
A. Large Thermodynamic Linkage
Reduction Potential
Donor
$k_1$
Deprotonated Pump
$k'_1$
$k'_{-2}$
Protonated Pump
$k_{-2}$
Acceptor
B. Small Thermodynamic Linkage
Reduction Potential
Donor
$k_1$
$k'_1$
Deprotonated Pump
Protonated Pump
$k'_{-2}$
$k_{-2}$
Acceptor

from 4.0 units to 2.0 units decreases peak efficiency by only ca. 8% while actually increasing the rate of electron transfer at many efficiency values. Thus the pump with less thermodynamic linkage exhibits greater flexibility with respect to the range of rates which it can achieve.

The most important reason for these results is the connection between electron transfer rate and electron transfer exothermicity which has been incorporated in the analysis. While a decrease in thermodynamic linkage causes the $pK_a$s of the pump to be less closely matched to the proton input and output environments, it also causes the rate constants for the desired (coupled) electron transfers to increase because these processes become more exothermic and the rate constants for the uncoupled processes to decrease because these processes become less exothermic (Figure 11). As described earlier, these effects must be considered, because a correlation of electron transfer rate and exothermicity is anticipated on the basis of both theory (19) and experiment (17). As the thermodynamic linkage parameter $\Delta pK_a$ is made smaller, the observed pH dependence of the reduction potential of the pump will also decrease, especially if the $pK_a$s of the pump are not symmetrically disposed about 7.0. For example, with $pK_a$s of 8.0 and 9.0, only a very weak pH dependence would be observed below pH 8. A pump with these $pK_a$s, while not optimal, nevertheless appears an acceptable compromise given the occurrence of some electron leakage.

## 5. Summary of the Steady-State Analysis

The analysis of the simple four-state model shows that the consideration of electron leak processes leads to some novel conclusions. It reveals at least two plausible mechanisms whereby a pump of this type may not exhibit a pronounced pH dependence of its reduction potential. These are: First, asymmetrical disposition of the pump $pK_a$s, which is required for optimal efficiency in situations having an asymmetry in the input/output electron gating

efficiencies; and second, a smaller thermodynamic linkage than would otherwise be expected, which still leads to performance which is comparable to a pump with greater linkage because the electron transfer rates correlate with reaction exothermicities.

A second important conclusion arising from the steady-state analysis is that efficient operation of a redox-linked proton pump of this kind requires efficient electron gating. Specifically, for a pump described by the parameters in Figure 3, which are intended to approximate cytochrome c oxidase, a gating ratio of .001 or smaller (measured as the ratio of the uncoupled and coupled standard electron transfer rates) would be desirable. The standard electron transfer rates depend upon intersite distance, the nature of the intervening material, and the rearrangement energies; changing any one of these must necessarily involve some structural change at or near the pump site (for example, a 1000-fold enhancement of electron transfer rate would require a ca. 5Å decrease in intersite distance, according to one estimate (15)).

## IMPLICATIONS FOR MITOCHONDRIAL OXIDATIVE PHOSPHORYLATION

The possibility of molecular "slippage" (uncoupling of transduction at the molecular level, for example, by electron leakage of the kind described above) in mitochondrial electron transport has been noted before (9,28), but the implications of such slippage have not been thoroughly explored in terms of its consequences for the molecular mechanisms of transduction. In some treatments of the proton pump problem (1), the occurrence of significant slippage has been dismissed as unlikely. This neglect of slippage would be justified if it could be shown that mitochondrial energy transduction is nearly 100% efficient in State 4 (the fully membrane-energized state), as is sometimes supposed (37,38). In order to establish that molecular-level slippage may in fact be important in oxidative phosphorylation, some of the evidence behind

the supposition of very high efficiency will be critically examined, and some evidence to the contrary will be described. Additionally, the probable nature of the various mitochondrial steady states will be considered in the light of the steady-state model transducer analysis.

The transduction efficiency of respiring mitochondria has been estimated by combining measurements of the operating potentials of the electron transport components and the maximum attainable phosphorylation potential in resting (State 4) mitochondria (37) with measurements of the number of ATP molecules synthesized per oxygen atom consumed (the P/O ratio) in phosphorylating (State 3) mitochondria (39,40). On this basis, it has been claimed (37,38) that the electron transfer reactions are very nearly at thermodynamic equilibrium with the phosphorylation reactions, so that $\Delta G$ for the coupled reactions approaches zero, implying close to 100% energy conservation efficiency. The use of this method assumes that the P/O ratio is unchanged on going from State 3 to State 4. However, measurements of the P/O ratio under a range of conditions intermediate between States 3 and 4 (41) show that the P/O ratio decreases by approximately twofold as State 4 is approached. This decrease was attributed (41) to the dissipation of energy by other reactions, for example, calcium transport, which can efficiently compete with ATP synthesis when phosphorylation is made slow. A complete accounting of energy utilization by other reactions has not been made, so the decrease in P/O ratio may be interpreted as well in terms of molecular slippage, which leads to leakage of some electrons through the electron transport chain without concomitant transport of a stoichiometric number of protons.

Estimates of the efficiency of cytochrome *c* oxidase are especially complicated because the various intermediates of dioxygen reduction produced at the $Fe_{a_3}/Cu_B$ site of this enzyme may each have different effective reduction potentials. In the estimates of the operating potentials of electron transport components mentioned above (37), a single potential was assumed for $Fe_{a_3}$ and it was estimated to be 600 mV vs. NHE. Since the potential of the $O_2/H_2O$

couple is close to 800 mV under the conditions used, this causes a substantial underestimation of the total free energy which is available from the electron transfers to dioxygen, and a corresponding overestimate of the efficiency. In a more recent consideration of energy conservation by cytochrome c oxidase (1), the appropriate potential of the $O_2/H_2O$ couple was used, and an efficiency estimate of 90% was obtained, based on the assumption that one proton is pumped per electron transferred (i.e., that no slippage occurs) under highly membrane-energized (State 4) conditions. The stoichiometry of one proton pumped per electron transferred is based upon measurements of proton pumping in mitochondria (42) or in vesicles (27) in which the proton electrochemical potential was mostly discharged by uncoupling agents. Hence this efficiency estimate suffers from the same difficulty described above, namely, the use of stoichiometries measured under one set of conditions in combination with thermodynamic quantities measured under different conditions.

It has been stated that it is hard to visualize an energy transducer that is designed to lose energy as heat via molecular-level slippage (1). In the case of redox-driven proton translocation, slippage paths are readily envisioned, and in fact such slippage may not be so much a consequence of design as of difficulty in achieving the very efficient electron gating which is required to avoid it. In the case of cytochrome c oxidase, it appears possible that some slippage, of the kind described above or via complete bypass of the proton pumping site (43,44), may be advantageous at steps in dioxygen reduction which would otherwise be slow, either because they are less exothermic or because they involve large rearrangement energies. The kinetic study described in Chapter V furnishes evidence that some of the cytochrome oxidase electron transfers are significantly more rapid than others.

The occurrence of slippage would have important implications for the measurements of P/O ratios. In State 4 mitochondria, a significant fraction of the (relatively slow) electron transport rate may be due to slippage, rather than to other energy-dissipating

reactions or passive leakage of protons across the membrane. Significant slippage would imply that one or more of the transducers is operating at close to its maximum attainable membrane potential (the point at which the energy efficiency curve crosses zero in Figure 5). The transition to State 3, which involves a decrease in membrane potential of ca. 0.5-1 pH unit (29,30), would cause a dramatic increase in the efficiency of the transducer (note the steepness of the efficiency vs. potential curves near the zero crossing in Figure 5, especially for the more tightly coupled pumps). Hence, the energy of electron transfer will be more efficiently conserved, on the average, in State 3 than in State 4. The slow oxygen consumption observed in State 4 should therefore not be simply subtracted from the oxygen consumption rate in State 3 (as is usually done) to obtain the net rate of phosphorylation-coupled electron transport.

Examination of the efficiency vs. rate curves in Figure 7 allows specification of the conditions which would pertain (for the simple model transducer) in particular situations of interest. For example, the maximum power output of this transducer will occur where the efficiency vs. rate curves are tangent to a hyperbola defined by the equation: Rate*Eff = P, where P is the maximum power output. The minimum rate of heat production will occur where the efficiency vs. rate curves are tangent to a hyperbola (not shown) defined by: Rate*(1 - Eff) = Q, where Q is the minimum rate of heat production. The curves in Figure 7 indicate that for a fairly broad range of electron leak rates, including all of the situations in which a reasonable maximum efficiency is attainable, the condition for maximum power output corresponds to an energy conservation efficiency in the neighborhood of 50% and a rate which is approximately 80% of the uncoupled rate. This suggests that under conditions where maximum power generation is required, a transducer of this sort will dissipate ca. 50% of its available free energy as heat. The occurrence of some slippage will not have a significant effect on the performance of the transducer under these conditions, because most of the heat is lost not to slippage (i.e., electron

leakage) but to the kinetically advantageous net driving force for the coupled reactions. On the other hand, the minimum rate of heat generation, and the corresponding conditions, depend strongly upon the electron leak rates. Thus, avoiding slippage is most important under resting conditions. Ideally, the condition for maximum efficiency (the maximum in the efficiency vs. rate curves, which is more or less broad depending upon the extent of slippage) should correspond to the relatively slow rate of respiration required to sustain the basal metabolic processes of the cell.

The conditions for maximum power output and minimum heat production deserve particular consideration because they might roughly correspond to the mitochondrial States 3 and 4, respectively. Measurements of the overall efficiency of mitochondria respiring in State 3, which take careful account of the pertinent time-dependent phosphorylation potential (rather than using the maximum attainable phosphorylation potential), and a comparison of State 3 electron transport rates to rates in fully uncoupled mitochondria, would furnish an interesting test of this proposition. The nature of State 4 would be clarified substantially if the respiration rate in this state could be resolved into components due to slippage, to passive proton leakage through the membrane, and to utilization of energy by various cellular processes.

## CYTOCHROME c OXIDASE

Proton pumping by cytochrome c oxidase has been the subject of several investigations (4), involving both measurement of the proton/electron stoichiometry (27) and the measurement of thermodynamic (45,46) or spectroscopic (47) properties which might bear on the mechanism of proton pumping. In particular, a moderate pH dependence of the reduction potential of $Fe_a$ has been observed (48, Chapter IV). This observation has been cited as evidence that $Fe_a$ performs the proton pumping function (9). In the light of the

above discussion, it is clear that a pH-dependent reduction potential is not required for reasonably efficient proton pumping. Furthermore, the observed dependence at $Fe_a$ is maximally only 30 mV/pH unit (Chapter IV), which is not consistent with a simple "pK-controlled" mechanism of proton pumping in which $pK_a$(ox) is well below 7 and $pK_a$(red) is well above 7 (cf. figure 2); this kind of model predicts a ca. 60 mV/pH unit dependence. If the intrinsic pH-dependence of the $Fe_a$ reduction potential is even less than this (-9 mV/pH unit), as measured in the CO-inhibited enzyme (Chapter III, 49), then protonation is not very tightly coupled to oxido-reduction of $Fe_a$. The evident influence of the $Fe_{a_3}/Cu_B$ site upon the pH dependence of the $Fe_a$ reduction potential (Chapter IV) might even reflect the involvement a protonatable site which is relatively remote from the iron center. The pH dependence of the $Fe_a$ reduction potential is therefore not a sound basis for concluding that $Fe_a$ is the proton pump. The other site which has been considered as a possible proton pump is $Cu_A$ (7). The reduction potential of this site is weakly if at all pH-dependent (45); the present analysis has shown that this observation is not inconsistent with a proton pumping function, as has sometimes been supposed.

The importance of efficient electron gating has been demonstrated above. Gating is likely to involve significant structural changes at the pumping site. It is noteworthy that localized molecular mechanisms for coupling protonation to electron gating, such as ligand protonation, ligand exchange, and metal ion movement, are more readily envisioned occurring at a metalloprotein copper center than at a heme iron. The axial ligands of $Fe_a$ are almost certainly neutral histidyl imidazoles in both the oxidized and reduced states of the iron (51,52), and the coordination geometry changes accompanying the reduction of $Fe_a$ are expected to be small, since the iron is low-spin in both redox states. In contrast, there is no evidence against a change in the identity or geometry of the coordinating ligands upon reduction of $Cu_A$. Substantial changes in the coordination geometry of $Cu_A$ upon reduction would not be surprising, since copper exhibits very

different preferred geometries in its cuprous and cupric states (53). The electron transfers into and out of $Fe_a$ are likely to take place via the heme macrocycle (54,55), which is not expected to undergo large movements in relation to the protein as a whole. Hence, electron gating through $Fe_a$ would probably have to involve conformational changes at the formyl (5) and/or vinyl groups on the periphery of the macrocycle, or more gross protein conformational changes (consistent with the large negative entropy of reduction of $Fe_a$) which change the alignment of electron-conducting groups between the heme and its electron transfer partners. The efficiency of gating by these mechanisms cannot be assessed precisely with presently available theory, but it would be limited by the occurrence of electron transfer from more than one locus on the heme edge.

In summary, the present analysis weakens the traditional arguments which implicate $Fe_a$ as the proton pump in cytochrome oxidase, while introducing new considerations which suggest that pumping mechanisms involving $Cu_A$ and which explicitly incorporate electron gating can be formulated readily. However, no compelling arguments for one or the other site may be advanced on the basis of these theoretical considerations alone, and reliable selection between the alternatives must await more information from experiment. Studies on the structure of the reduced $Cu_A$ and $Fe_a$ sites and a fairly detailed elucidation of the nature of the steady state (with respect to the levels of $Fe_a$ and $Cu_A$ reduction) and its response to membrane energization would be helpful in this regard.

REFERENCES

1. Wikstrom, M., and K. Krab. (1980). In Current Topics in Bioenergetics 10. Academic Press (New York) 51-101.

2. Maloney, P.C. (1982). J. Memb. Biol. 67, 1-12.

3. Mitchell, P. (1961). Nature 191, 144-148.

4. Wikstrom, M., and K. Krab. (1979). Biochim. Biophys. Acta 549, 177-222.

5. Babcock, G.T., and P.M. Callahan. (1983). Biochemistry 22, 2314-2319.

6. Wikstrom, M., K. Krab, and M. Saraste. (1981). Ann. Rev. Biochem. 50, 623-655.

7. Chan, S.I., D.F. Bocian, G.W. Brudvig, R.H. Morse, and T.H. Stevens. (1979). In Cytochrome Oxidase, T.E. King et al. Eds. Elsevier/North-Holland Biomedical Press, Amsterdam, pp. 177-188.

8. Papa, S. (1976). Biochim. Biophys. Acta. 456:39-84.

9. Wikstrom, M., K. Krab, and M. Saraste. (1981). Cytochrome Oxidase: A Synthesis. Academic Press, London.

10. Casey, R.P, M. Thelen, and A. Azzi. (1980). J. Biol. Chem. 255, 3994-4000.

11. Nagle, J.F., and M. Mille. (1981). J. Chem. Phys. 74, 1367-1372.

12. Hoppe, J., and W. Sebald. (1984). Biochim. Biophys. Acta

768, 1-27.

13. DeVault, D. (1971). Biochim. Biophys. Acta 225, 193-199.

14. Hopfield, J.J. (1982). In Oxidases and Related Systems, T.E. King et al., Eds. Pergamon, Oxford, 35-49.

15. Hopfield, J.J. (1974). Proc. Natl. Acad. Sci. U.S.A. 71, 3640-3644.

16. Marcus, R.A., and N. Sutin. (1985). Biochim. Biophys. Acta Reviews in Bioenergetics (in press)

17. Meyer, T.E., C.T. Przysiecki, J.A. Watkins, A. Bhattacharyya, R.P. Simondsen, M.A. Cusanovich, and G. Tollin. (1983). Proc. Natl. Acad. Sci. U.S.A. 80, 6740-6784.

18. Dutton, P.L. (1978). Methods in Enzymology, Vol. LIV, 411-435.

19. Marcus, R.A. (1979). In Light-Induced Charge Separation in Biology and Chemistry, H. Gerischer and J.J. Katz, Eds. Weinheim, New York, pp. 15-43.

20. Winkler, J.R., D.G. Nocera, K.M. Yocom, E. Bordignon, and H.B. Gray. (1982). J. Am. Chem. Soc. 104, 5798-5800.

21. Margalit, R., N.M. Kostic, C.-M. Che, D.F. Blair, H.-j. Chiang, I. Pecht, J.B. Shelton, J.R. Shelton, W.A. Schroeder, and H.B. Gray. (1984). Proc. Natl. Acad. Sci. U.S.A. 81, 6554-6558.

22. Peterson-Kennedy, S.E., J.L. McGourty, and B.M. Hoffman. (1984). J. Am. Chem. Soc. 106, 5010-5012.

23. Marcus, R.A., and N. Sutin. (1975). Inorganic Chemistry 14,

213-216.

24. Siders, P., R.J. Cave, and R.A. Marcus. (1984). J. Chem. Phys. 81, 5613-5624.

25. Beratan, D.N., and J.N. Onuchic. (1985). J. Am. Chem. Soc., submitted for publication.

26. Lauger, P. (1979). Biochim. Biophys. Acta. 552, 143-161.

27. Thelen, M., P.S. O'Shea, and A. Azzi. (1985). Biochem. J. 227, 163-167.

28. Rottenberg, H. (1979). Biochim. Biophys. Acta 529, 225-253.

29. Mitchell, P. and J. Moyle. (1969). Eur. J. Biochem. 7, 471-484.

30. Nicholls, D.G. 1974. Eur. J. Biochem. 50, 305-315.

31. Brudvig, G.W., D.F. Blair, and S.I. Chan. (1984). J. Biol. Chem. 259, 11001-11009.

32. Vik, S.B., and R.A. Capaldi. (1980). Biochem. Biophys. Res. Comm. 94, 348-354.

33. (a) Scheiner, S. (1981). Ann. N.Y. Acad. Sci. 367, 493-509. (b) de la Vega, J.R. (1982). Acc. Chem. Res. 15, 185-191.

34. Hansford, R.G. 1980. In Current Topics in Bioenergetics 10. Academic Press, New York, pp. 217-278.

35. Hunter, D.R., and R.A. Capaldi. 1974. Biochem. Biophys. Res. Comm. 56, 623-628.

36. Chance, B., and G.R. Williams. 1956. Adv. Enzymol. 17,

65-134.

37. Wilson, D.F., M. Erecinska, C.S. Owen, and L. Mela. (1974). In Dynamics of Energy-Transducing Membranes, L. Ernster, R.W. Estabrook, and E.C. Slater, Eds. Elsevier, Amsterdam, pp. 221-231.

38. Slater, E.C., J. Rosing and A. Mol. (1973). Biochim. Biophys. Acta 92, 534-553.

39. Chance, B., and G.R. Williams. (1955). J. Biol. Chem. 217, 383-393.

40. Copenhaver, J.H.Jr., and H.A. Lardy. (1952). J. Biol. Chem. 195, 225-238.

41. Ernster, L. and K. Nordenbrand. (1974). In Dynamics of Energy-Transducing Membranes, L. Ernster, R.W. Estabrook, and E.C. Slater, Eds. Elsevier, Amsterdam, pp. 283-288.

42. Wikstrom, M.K.F. (1977). Nature 266, 271-273.

43. Gelles, J. and S.I. Chan. (1985). Biochemistry (in press)

44. Blair, D.F., S.N. Witt and S.I. Chan. 1985. J. Am. Chem. Soc. (in press)

45. van Gelder, B.F., J.L.M.L. vanRijn, G.J.A. Schilder and J. Wilms. (1977). In Structure and Function of Energy-Transducing Membranes, K. van Dam and B.F. van Gelder, Eds., Elsevier/North Holland, Amsterdam, pp. 61-68.

46. Nakao, K., and G. Palmer. (1983). J. Biol. Chem. 258, 14908-14913.

47. M.K.F. Wikstrom. (1974). Ann. N. Y. Acad. Sci. 227, 146-158.

48. Artzatbanov, V.Y, A.A. Konstantinov, and V.P. Skulachev. (1978). FEBS Lett. 87, 180-185.

49. Ellis, W.R., D.F. Blair, H. Wang, H.B. Gray, and S.I. Chan. (1985). Biochemistry, in press.

50. Babcock, G.T., P.M. Callahan, M.R. Ondrias, and I. Salmeen. (1981). Biochemistry 20, 959-966.

51. Martin, C.T., C.P. Scholes, and S.I. Chan. (1985). J. Biol. Chem. 260, 2857-2861.

52. Diaddario, L.C.Jr., E.R. Dockal, M.D. Glick, L.A. Ochrymowycz, and D.B. Rorabachev. (1985). Inorg. Chem. 24, 356-363.

53. Makinen, M.W., S.A. Schichman, S.C. Hill, and H.B. Gray. (1983). Science 222, 929-931.

54. Poulos, T.L., and J. Kraut. (1980). J. Biol. Chem. 255, 10322-10330.

# CHAPTER VII. CONCLUSIONS

The redox thermodynamic properties of cytochrome oxidase must be considered remarkable with regard to both the large negative reduction entropies of cytochrome *a* and $Cu_A$ and the complex assortment of anticooperative intersite interactions. A conceptually simple means of uniting many of the observations was noted briefly above, and it will be re-emphasized here: It is suggested that a fairly large protein conformational change is linked to the reduction of cytochrome *a*, and that this conformational change influences the reduction potentials of the other metal sites in the protein via perturbations to their structures. The link between cytochrome *a* reduction and the kinetics of cyanide binding, the $Cu_A$ EPR lineshape, the volume of the protein, and the reduction potentials of all three other sites, as well as the large negative entropy of reduction of cytochrome *a*, may all be rationalized in terms of this conformational change.

The mechanistic significance, if any, of a large conformational change linked to cytochrome *a* reduction remains to be demonstrated. It was suggested above (Chapter VI) that significant structural changes are likely to be involved in redox-linked proton pumping, in order to achieve efficient control over electron flow. In the case of proton pumping by cytochrome *a*, it was suggested that these structural changes might be global in character. The suggested conformational change may therefore play a role in redox-linked proton pumping by cytochrome *a*. The standard entropy of reduction of $Cu_A$ is also comparatively large and negative (although less strikingly so than that of cytochrome *a*), so by this criterion a model postulating proton pumping by $Cu_A$ is also attractive. The question of which site pumps protons must be settled by more direct biochemical experiments. Such experiments are already under way, and rapid resolution of this question may be anticipated. The present studies furnish insights, and measurements of fundamental chemical quantities, which should contribute to a detailed mechanistic understanding of proton pumping whichever site is proven responsible for this fascinating activity.

The examination of the reaction of the enzyme with dioxygen at low temperature provides additional experimental support for earlier suggestions that electrons are transferred through the oxidase via more than one pathway. Additionally, it was shown that the thermal activation of the two pathways is similar, so that at physiological temperature neither is expected to become much more important than the other. While this suggestion relies on extrapolation over a considerable temperature and thus should be regarded with caution, it nevertheless merits further investigation in view of its profound implications for the mechanisms of energy conservation by the enzyme.

The demonstration of two distinct intermediates of dioxygen reduction at the three-electron level of dioxygen reduction is the first experimental suggestion that the bond cleavage actually takes place at this reaction step. While a variety of data find their most ready explanation in this model, it must be remembered that the present evidence is circumstantial, and that more direct spectroscopic and chemical characterization of the relevant intermediates is called for. Again, the insights made available in the present studies will be helpful in understanding the mechanisms which are eventually proven, regardless of the precise identities of the various reaction intermediates. The relevance of the low temperature kinetic results to the mechanism at physiological temperature has been briefly considered above. We point out here that the putative bond-breaking step is predicted, by extrapolation of the Arrhenius plots, to be significantly faster than the preceding reaction step and hence difficult to observe at physiological temperature. The low temperature approach may therefore be best suited to the characterization of this reaction step. Of immediate practical value, the present studies provide recipes for the high-yield preparation of intermediates of interest for detailed characterization at low temperature, as well as the suggestion that future experiments be conducted with an awareness of the potential effects of carbon monoxide.

Chapter VI was motivated by a desire to establish a quantitative foundation for statements regarding the mechanisms of redox-linked proton pumping. The roles played by thermodynamic linkage and the optimum placement of the pump $pK_a$s are of particular interest in the context of the present experimental results. The absence of pronounced pH dependences in the reduction potential of either of the candidate proton pump sites is easier to rationalize in the light of the kinetic analysis. At the same time, the analysis underscores the importance of other, kinetically manifested linkages.

While not presented in Chapter VI, an analogous treatment of a more complex six-state model was also developed, and with respect to the important conclusions to emerge from the analysis it was not significantly different. This similarity suggests that many of the conclusions of the analysis will not be very sensitive to the details of the postulated mechanism, and hence that the present analysis could be of some value in understanding a wide variety of models of transduction. It is possible, for example, to make a formal analogy between the present analysis and the more classical redox loop steps in mitochondrial electron transport. The effects of membrane potential, the relevant $pK_a$s, etc., upon these electron transfer steps could therefore be examined in a closely analogous fashion.

APPENDIX. Solution of the Steady-State Rate Equations for the Four-State Proton Pump.

We require the steady-state concentrations of each of the four pump species in the reaction scheme given in Figure 3. First, the various species concentrations are defined:

$[D_{red}] = r_1$ $\quad [P_{ox}] = P_o$ $\quad [H_m^+] = H_m^+$

$[D_{ox}] = o_1$ $\quad [P_{red}] = P_r$ $\quad [H_c^+] = H_c^+$

$(A_{red}] = r_2$ $\quad [P_{ox}\cdot H^+] = P_o\cdot H^+$

$[A_{ox}] = o_2$ $\quad [P_{red}\cdot H^+] = P_r\cdot H^+$

Total concentration of pumping sites = $P_T$.

The steady-state rate equations are

$$P_O + P_R + P_O\cdot H^+ + P_R\cdot H^+ = P_T \tag{A1}$$

$$(k_{oa}H_c^+ + k_1 r_1)P_o - (k'_{-2}o_2 + k_{-1}o_1)P_R - (k_{od})P_o\cdot H^+ = 0 \tag{A2}$$

$$-(k_1 r_1)P_o + (k'_{-2}o_2 + k_{-1}o_1 + k_{ra}H_m^+)P_R - (k_{rd})P_R\cdot H^+ = 0 \tag{A3}$$

$$-(k_{oa}H_c^+)P_o + (k_{od} + k_2 r_2 + k'_1 r_1)\, P_o\cdot H^+ - (k_{-2}o_2)P_R\cdot H^+ = 0 \tag{A4}$$

These four equations are used to define the matrix equation

$$\begin{bmatrix} C_{11} & C_{12} & C_{13} & C_{14} \\ C_{21} & C_{22} & C_{23} & 0 \\ C_{31} & C_{32} & 0 & C_{34} \\ C_{41} & 0 & C_{43} & C_{44} \end{bmatrix} \begin{bmatrix} P_o \\ P_R \\ P_o\cdot H^+ \\ P_R\cdot H^+ \end{bmatrix} = \begin{bmatrix} P_T \\ 0 \\ 0 \\ 0 \end{bmatrix}$$

thereby defining the $c_{nm}$ s.

Rows 2-4 of the matrix may be manipulated to give all species concentrations relative to $P_o$. The results of these manipulations are

$$P_R \cdot H^+ = \frac{C_{21}C_{32}C_{43} - C_{31}C_{22}C_{43} - C_{23}C_{41}C_{32}}{C_{43}C_{22}C_{34} + C_{44}C_{32}C_{23}} \cdot P_o \qquad (A5)$$

$$P_o \cdot H^+ = \frac{C_{31}C_{44}C_{22} - C_{34}C_{41}C_{22} - C_{32}C_{21}C_{44}}{C_{43}C_{22}C_{34} + C_{44}C_{32}C_{23}} \cdot P_o \qquad (A6)$$

$$P_R = \frac{C_{41}C_{23}C_{34} - C_{43}C_{21}C_{34} - C_{44}C_{31}C_{23}}{C_{43}C_{22}C_{34} + C_{44}C_{32}C_{23}} \cdot P_o \; . \qquad (A7)$$

Inserting these expressions into the expressions for the rates of proton pumping and electron transfer (Equations 1 and 2), we obtain

$$R_{H^+} = \left\{ K_{ra} H_m^+ \left( \frac{C_{41}C_{23}C_{34} - C_{43}C_{21}C_{34} - C_{44}C_{31}C_{23}}{C_{43}C_{22}C_{34} + C_{44}C_{32}C_{23}} \right) \right.$$

$$\left. - k_{rd} \left( \frac{C_{21}C_{32}C_{43} - C_{31}C_{22}C_{43} - C_{23}C_{41}C_{32}}{C_{43}C_{22}C_{34} + C_{44}C_{32}C_{23}} \right) \right\} \cdot P_o \qquad (A8)$$

and

$$R_{e^-} = \left\{ k_1 r_1 + k_1' r_1 \left( \frac{C_{31}C_{44}C_{22} - C_{34}C_{41}C_{22} - C_{32}C_{21}C_{44}}{C_{43}C_{22}C_{34} + C_{44}C_{32}C_{23}} \right) \right.$$

$$\left. - k_{-1} o_1 \left( \frac{C_{41}C_{23}C_{34} - C_{43}C_{21}C_{34} - C_{44}C_{31}C_{23}}{C_{43}C_{22}C_{34} + C_{44}C_{32}C_{23}} \right) \right\} \cdot P_o \; . \qquad (A9)$$

The quotient of these is the stoichiometric efficiency (the $H^+/e^-$ ratio):

$$Eff = \frac{k_{ra}H_m^+(C_{41}C_{23}C_{34}-C_{43}C_{21}C_{34}-C_{44}C_{31}C_{23})-k_{rd}(C_{21}C_{32}C_{43}-C_{31}C_{22}C_{43}-C_{23}C_{41}C_{32})}{\{k_1r_1(C_{34}C_{43}C_{22}+C_{32}C_{23}C_{44})+k_1'r_1(C_{31}C_{44}C_{22}-C_{34}C_{41}C_{22}-C_{32}C_{21}C_{44}) -k_{-1}o_1(C_{41}C_{23}C_{34}-C_{43}C_{21}C_{34}-C_{44}C_{31}C_{23})\}.} \quad (A10)$$

After replacement of the $c_{nm}$ s by the appropriate rate constants and simplication, this becomes

$$Eff = \frac{k_{ra}H_m^+k_{-2}o_2k_1r_1k_{od}-k_{rd}k_{oa}H_c^+(k_{-2}'o_2+k_{-1}o_1)(k_2r_2+k_1'r_1)}{\{k_1r_1[k_{rd}k_{-2}'o_2(k_{od}+k_2r_2+k_1'r_1)+k_{od}k_{-2}o_2(k_{-2}'o_2+k_{ra}H_m^+)]-k_{-1}o_1k_2r_2k_{oa}H_c^+k_{rd} +k_1'r_1[k_{rd}k_{oa}H_c^+k_{-2}'o_2+k_{ra}H_m^+k_1r_1k_{-2}o_2+(k_{-2}'o_2+k_{-1}o_1+k_{ra}H_m^+)(k_{oa}H_c^+k_{-2}o_2)]\}.} \quad (A11)$$

This expression is equivalent to equation (5).

The other important quantity is the electron transfer rate per pump site, $R_e\text{-}/P_T$. This is obtained from equation A9 above by inserting the appropriate rate constants in place of the $c_{nm}$'s. The resulting equation is:

$$\frac{R_e'}{P_T} = \frac{\{k_1r_1[k_{rd}k_{-2}'o_2(k_{od}+k_2r_2+k_1'r_1)+k_{od}k_{-2}o_2(k_{-2}'o_2+k_{ra}H_m^+)]-k_{-1}o_1k_2r_2k_{oa}H_c^+k_{rd} +k_1'r_1[k_{rd}k_{oa}H_c^+k_{-2}'o_2+k_{ra}H_m^+k_1r_1k_{-2}o_2+(k_{-2}'o_2+k_{-1}o_1+k_{ra}H_m^+)(k_{oa}H_c^+k_{-2}o_2)]\}}{\{[(k_{od}+k_{oa}H_c^+)k_{-2}o_2+(k_2r_2+k_1'r_1)k_{oa}H_c^+](k_{-2}'o_2+k_{-1}o_1+k_{ra}H_m^+) +[k_{rd}(k_{-2}'o_2+k_{-1}o_1+k_1r_1)+k_{ra}H_m^+k_1r_1](k_{od}+k_2r_2+k_1'r_1) +k_{oa}H_c^+k_{rd}(k_2r_2+k_1'r_1+k_{-2}'o_2+k_{-1}o_1)+k_1r_1k_{-2}o_2(k_{ra}H_m^++k_{od})\}.} \quad (A12)$$

This expression is equivalent to equation (4).

The overall energetic efficiency of the pump was calculated from the stoichiometric efficiency and the membrane potential according to equation (3) in the text.

For all calculations performed by computer, it was assumed that $\frac{RT}{F}$ = 60 mV, for simplicity. (This is used in relating membrane potentials given in pH units to reduction potentials in mV; e.g., a membrane potential of 5 pH units corresponds to a potential difference of 300 mV.)

An important element in the computer simulations of proton pump performance is the incorporation of a connection between electron transfer exothermicity and rate. In accordance with the considerations outlined in the text, electron transfer rate constants were adjusted according to

$$k = k_{standard}(e^{-\Delta G°/2RT})$$

where $k_{standard}$ is a so-called "standard" electron transfer rate, which is either specified directly (in the case of the "leaks") or fixed by the electron transfer rate products EP1 and EP2 (the products of the forward and backward rate constants), and $\Delta G°$ is the standard free-energy charge of the electron transfer reaction.